



<https://theses.gla.ac.uk/>

Theses Digitisation:

<https://www.gla.ac.uk/myglasgow/research/enlighten/theses/digitisation/>

This is a digitised version of the original print thesis.

Copyright and moral rights for this work are retained by the author

A copy can be downloaded for personal non-commercial research or study, without prior permission or charge

This work cannot be reproduced or quoted extensively from without first obtaining permission in writing from the author

The content must not be changed in any way or sold commercially in any format or medium without the formal permission of the author

When referring to this work, full bibliographic details including the author, title, awarding institution and date of the thesis must be given

Enlighten: Theses

<https://theses.gla.ac.uk/>
research-enlighten@glasgow.ac.uk

Formation of Higher Alcohols from Synthesis Gas

Simon Andrew Moore, B.Sc. (Hons)

Thesis submitted to the University of Glasgow for the
Degree of Doctor of Philosophy.

© Simon Moore, May 2000.

ProQuest Number: 10390849

All rights reserved

INFORMATION TO ALL USERS

The quality of this reproduction is dependent upon the quality of the copy submitted.

In the unlikely event that the author did not send a complete manuscript and there are missing pages, these will be noted. Also, if material had to be removed, a note will indicate the deletion.



ProQuest 10390849

Published by ProQuest LLC (2017). Copyright of the Dissertation is held by the Author.

All rights reserved.

This work is protected against unauthorized copying under Title 17, United States Code
Microform Edition © ProQuest LLC.

ProQuest LLC.
789 East Eisenhower Parkway
P.O. Box 1346
Ann Arbor, MI 48106 – 1346

GLASGOW
UNIVERSITY
LIBRARY

11939 (copy 1)

“Raise the Pressure”
Breathe, Prodigy, 1997.

© 1997 Prodigy
All rights reserved.

Acknowledgements

I would like to thank my supervisor Professor Geoffrey Webb of the University of Glasgow for the support, guidance, assistance and opportunities he has given to me throughout my studies.

I would like to acknowledge my funding body, the EPSRC and Kvaerner Process Technology for the CASE award funding and the time and experience gained by talking to the many staff when working at the Technology Centre in Thornaby.

I would also thank the following people, whose help and encouragement has been essential throughout the course of this study.

- The technical staff, past and present in the Chemistry and Earth Sciences departments
- Drs. Diane Stirling and Philip Landon
- and the lads and lasses in the department especially Pete, Bernie, Graham, Dave and Malky who made my life a little more bearable during those lonely evenings!!. Not forgetting Janice.

A special thank you goes to my family for the encouragement, patience and support they gave me throughout my education.

Summary

This study investigates the selective formation of higher oxygenates from a synthesis gas mixture using a variety of copper-based heterogeneous catalysts.

The catalysts are prepared by co-precipitation. Full characterisation of the catalysts, both before and after use, is achieved using primarily by spectroscopy, thermogravimetric and X-ray analysis and BET and copper surface area measurements.

The catalytic activities and selectivities of the products are determined from the reaction of synthesis gas mixtures ($H_2/CO/CO_2$) in a self-built continuous flow microreactor, equipped with on-line gas chromatographic analysis, operating at moderate temperature and pressure.

The activity is measured in terms of conversion from reactants and the conversion and product distribution of all products formed determine the selectivity of higher alcohols. These factors can be determined by variation in the reactor gasfeed composition, the pressure, the temperature and the gas hourly space velocity. The effect on selectivity of production by the addition of lower alcohol (methanol or ethanol) to the reactant mixture has also been examined. The variation in microreactor parameters can be related to possible correlations between catalyst structure and catalyst activity and selectivity.

Preparation of the initial catalyst, Cu/Cr_2O_3 , formed preferentially methanol; hydrocarbons and dimethyl ether were also produced. Substitution of chromium for aluminium and magnesium caused changes in product distribution; the aluminium for increasing activity and the magnesium to decrease the acidity.

However, the initial preparation conditions for the Cu/MgO/Al₂O₃ (50/10/40) catalyst resulted in incomplete co-precipitation and a consequential decrease in activity such that no alcohols were produced. Methane was the primary product for this catalyst.

Binary catalysts of Cu/MgO and Cu/Al₂O₃ were prepared to optimise the preparation condition to give complete co-precipitation. A main emphasis has been to establish preparation conditions, which have been shown to lead to reproducibility in catalyst structure and catalytic activity.

The magnesium concentration was initially fixed at 2 % of the total metal content; however, this still resulted in the production of hydrocarbons and dimethyl ether. The magnesium concentration was gradually increased through 5 % to 7 % with respect to the copper and aluminium components. This increase in magnesium concentration resulted in a precursor with increased crystallinity and a catalyst, which gave a higher yield of higher alcohols. However, methanol was still the predominant alcohol in the total alcohol yield. At this increased magnesium concentration, hydrocarbons and dimethyl ether were still being produced.

On the basis that the inhibiting step is the C₁-C₂ chain growth step, it has been found that this can be overcome by K-promotion of the Cu/Mg/Al₂O₃ (60/7/35) catalysts with the K⁺ ion at 0.005 wt %. This was especially noticeable with the catalyst prepared at pH = 8 and aged in the mother liquor for 30 mins, as a large production of ethanal was observed. Under the conditions used unlike unpromoted catalysts, no induction period in the formation of oxygenates was observed with these catalysts. However, the overall activity as measured by the consumption of the reactants was lower than that observed with unpromoted catalysts. No DME was formed with the K-promoted catalysts.

Contents

	<u>Page Number</u>
List of Tables	xvi
List of Figures	xxiv
1 Introduction	1
1.1 Background	1
1.2 Modified Methanol Synthesis catalysts	4
1.2.1 Modified Low Temperature Methanol synthesis catalysts	5
1.2.2 Modified High Temperature Methanol synthesis catalysts	8
1.2.3 Modified Fischer-Tropsch and Group VIII metal-based catalysts	9
1.2.4 Others Catalysts based on Rh, MoS ₂ and Cu/Mg/CeO ₂	13
1.3 Theoretical Considerations and Physical Parameters	15
1.3.1 Kinetic and Thermodynamic Factors	15
1.3.2 Effects of the Operating Variables	16
1.4 Mechanism for Higher Alcohol Synthesis	19
1.4.1 Proposed Mechanisms for the Modified LT Methanol synthesis catalysts	19
1.4.2 Proposed Mechanisms for the Modified HT Methanol Catalysts	24

1.4.3	Proposed Mechanisms for the Modified Fischer-Tropsch and Group VIII metal-based catalysts	25
1.4.4	Proposed Mechanisms for other catalysts	27
1.5	Other Reactions	29
1.5.1	Water Gas Shift Reaction	29
1.5.2	The Water Gas Shift Mechanism	29
1.5.3	Ethers	31
1.5.4	Aldehydes and Ketones	32
1.6	Precursor and Catalyst Form	33
1.7	Poisoning and Deactivation	38
2	Aims and Objectives	40
3	Experimental	42
3.1	Introduction	42
3.2	Materials	42
3.2.1	Gases	42
3.2.2	Liquids and Solids	43
3.3	Precursor Preparation	43
3.3.1	Cu/Cr ₂ O ₃ (50/50) (Cu _{Cr})	44
3.3.2	Cu/MgO/Al ₂ O ₃ (50/10/40) (Cu _{Mg(10)Al})	44
3.3.3	Cu/MgO (60/40) (Cu _{Mg})	45
3.3.4	Cu/Al ₂ O ₃ (60/40) (Cu _{Al})	45
3.3.5	Cu/MgO/Al ₂ O ₃ (60/2/38) (Cu _{Mg(2)Al})	46
3.3.6	Cu/MgO/Al ₂ O ₃ (60/5/35) (Cu _{Mg(5)Al})	46
3.3.7	Cu/MgO/Al ₂ O ₃ (60/7/35) (Cu _{Mg(7)Al})	46

3.3.8	K/Cu/MgO/Al ₂ O ₃ (K60/7/35) (Cu _{MgAlK})	46
3.4	Sample Preparation	48
3.4.1	Differential Thermal Analysis (DTA)	48
3.4.2	X-ray Powder Diffraction (XRD)	48
3.4.3	X-ray Fluorescence (XRF)	48
3.4.4	Flame Atomic Absorption Spectroscopy (AAS)	49
3.4.5	Temperature Programmed Reduction (TPR)	50
3.4.6	Nitrous Oxide chemisorption and Copper Surface Area measurements	50
3.4.7	Elemental Analysis (EA)	53
3.4.8	Titrometry	54
3.4.9	BET Surface Area measurements	54
3.5	Catalyst Testing	57
3.5.1	Introduction	57
3.5.2	The Feed system	57
3.5.2.1	Synthesis Gases	57
3.5.2.2	Methanol and Ethanol Vapourisation	58
3.5.3	The Reactor System	58
3.5.3.1	Reactor Pressure Control	58
3.5.3.2	Reactor and Furnace	59
3.5.4	The Analytical system	60
3.5.4.1	The Gas Sample Valve (GSV)	60
3.5.4.2	Gas Chromatographic Analysis	60
3.5.4.2a	Thermal Conductivity Detector (TCD)	61
3.5.4.2b	Flame Ionised Detector (FID)	61

	3.5.4.3 Gas Chromatograph Calibrations	62
4	Preparation and Characterisation of Catalyst Precursors	63
4.1	Cu/Cr ₂ O ₃ (50/50) (Cu _{Cr})	63
4.1.1	Preparation	63
4.1.2	Differential Thermal Analysis	63
4.1.3	X-ray Diffraction	64
4.1.4	X-ray Fluorescence	64
4.1.5	Atomic Absorption Spectroscopy	65
4.1.6	Temperature Programmed Reduction	65
4.1.7	Nitrous Oxide Experiments and Copper Surface	66
	Area measurements	
4.1.8	Elemental Analysis	67
4.1.9	BET Surface Area measurements	68
4.1.10	Summary	68
4.2	Cu/MgO/Al ₂ O ₃ (50/10/40) (Cu _{Mg(10)Al})	69
4.2.1	Preparation	69
4.2.2	Differential Thermal Analysis	70
4.2.3	X-ray Diffraction	70
4.2.4	X-ray Fluorescence	72
4.2.5	Atomic Absorption Spectroscopy	73
4.2.6	Temperature Programmed Reduction	74
4.2.7	Nitrous Oxide Experiments and Copper Surface	75
	Area measurements	
4.2.8	Elemental Analysis	76
4.2.9	BET Surface Area measurements	76

4.2.10	Summary	77
4.3	Binary Catalysts	78
4.3.1	Cu/MgO (60/40) (Cu_{Mg})	78
4.3.1.1	Preparation	78
4.3.1.2	Differential Thermal Analysis	79
4.3.1.3	X-ray Diffraction	79
4.3.1.4	X-ray Fluorescence	80
4.3.1.5	Atomic Absorption Spectroscopy	81
4.3.1.6	Temperature Programmed Reduction	82
4.3.1.7	Nitrous Oxide Chemisorption and Copper	83
	Surface Area measurements	
4.3.1.8	Elemental Analysis	84
4.3.1.9	BET Surface Area measurements	85
4.3.2	Cu/Al ₂ O ₃ (60/40) (Cu_{Al})	86
4.3.2.1	Preparation	86
4.3.2.2	Differential Thermal Analysis	87
4.3.2.3	X-ray Diffraction	87
4.3.2.4	X-ray Fluorescence	88
4.3.2.5	Atomic Absorption Spectroscopy	89
4.3.2.5	Temperature Programmed Reduction	90
4.3.2.7	Nitrous Oxide chemisorption and Copper	91
	Surface Area measurements	
4.3.2.8	Elemental Analysis	92
4.3.2.9	BET Surface Area measurements	93
4.3.3	Summary	94

4.4	Cu/MgO/Al ₂ O ₃ (60/2/38) (Cu _{Mg(2)Al})	95
4.4.1	Preparation	95
4.4.2	Differential Thermal Analysis	95
4.4.3	X-ray Diffraction	96
4.4.4	X-ray Fluorescence	97
4.4.5	Atomic Absorption Spectroscopy	98
4.4.6	Temperature Programmed Reduction	99
4.4.7	Nitrous Oxide Chemisorption and Copper Surface	100
	Area measurements	
4.4.8	Elemental Analysis	101
4.4.9	BET Surface Area measurements	102
4.4.10	Summary	102
4.5	Cu/MgO/Al ₂ O ₃ (60/5/35) (Cu _{Mg(5)Al})	104
4.5.1	Preparation	104
4.5.2	Differential Thermal Analysis	105
4.5.3	X-ray Diffraction	105
4.5.4	X-ray Fluorescence	106
4.5.5	Atomic Absorption Spectroscopy	107
4.5.6	Temperature Programmed Reduction	107
4.5.7	Nitrous Oxide chemisorption and Copper Surface	108
	Area measurements	
4.5.8	Elemental Analysis	109
4.5.9	BET Surface Area measurements	110
4.5.10	Summary	111

4.6	Cu/MgO/Al ₂ O ₃ (60/7/35) (Cu _{Mg(7)Al})	112
4.6.1	Preparation	112
4.6.2	Differential Thermal Analysis	112
4.6.3	X-ray Diffraction	113
4.6.4	X-ray Fluorescence	113
4.6.5	Atomic Absorption Spectroscopy	114
4.6.6	Temperature Programmed Reduction	115
4.6.7	Nitrous Oxide Chemisorption and Copper Surface	115
	Area measurements	
4.6.8	Elemental Analysis	116
4.6.9	BET Surface Area measurements	118
4.6.10	Summary	118
4.7	K/Cu/MgO/Al ₂ O ₃ (K60/7/35) (Cu _{MgAlK})	119
4.7.1	Preparation	119
4.7.2	Differential Thermal Analysis	119
4.7.3	X-ray Diffraction	119
4.7.4	X-ray Fluorescence	119
4.7.5	Atomic Absorption Spectroscopy	120
4.7.6	Temperature Programmed Reduction	121
4.7.7	Nitrous Oxide Chemisorption and Copper Surface	122
	Area measurements	
4.7.8	Elemental Analysis	123
4.7.9	BET Surface Area measurements	124
4.7.10	Summary	125

5	Microreactor Experiments	126
5.1	Treatment of Microreactor Results	126
5.2	Cu/Cr ₂ O ₃ (50/50) (Cu _{Cr})	127
5.2.1	Effect of changes in Temperature	127
5.2.2	Effect of changes in Gas Hourly Space Velocity	128
5.2.3	Effect of changes in Gasfeed Composition	129
5.2.4	Effect of changes in Methanol Addition	129
5.2.5	Summary	130
5.3	Cu/MgO/Al ₂ O ₃ (50/10/40) (Cu _{Mg(10)Al})	131
5.3.1	Effect of changes in Gas Hourly Space Velocity	131
5.3.2	Summary	131
5.4	Cu/MgO/Al ₂ O ₃ (60/2/38) (Cu _{Mg(2)Al})	132
5.4.1	Effect of changes in Temperature	133
5.4.2	Effect of changes in Gasfeed Composition	134
5.4.3	Effect of changes in Methanol Addition	135
5.4.4	Summary	136
5.5	Cu/MgO/Al ₂ O ₃ (60/5/35) (Cu _{Mg(5)Al})	137
5.5.1	Effect of changes in Temperature	138
5.5.2	Effect of changes in Gas Hourly Space Velocity	139
5.5.3	Effect of changes in Gasfeed Composition	141
5.5.4	Effect of changes in Methanol Addition	142
5.5.5	Summary	142
5.6	Cu/MgO/Al ₂ O ₃ (60/7/35) (Cu _{Mg(7)Al})	143
5.6.1	Effect of changes in Temperature	145
5.6.2	Effect of changes in Gas Hourly Space Velocity	145

5.6.3	Effect of changes in Gasfeed Composition	146
5.6.4	Summary	149
5.7	K/Cu/MgO/Al ₂ O ₃ (K60/7/35) (Cu _{MgAlK})	150
5.7.1	Effect of changes in Temperature	151
5.7.2	Effect of changes in Gas Hourly Space Velocity	152
5.7.3	Effect of changes in Gasfeed Composition	154
5.7.4	Summary	155
6	Characterisation of Used Catalysts	156
6.1	Cu/Cr ₂ O ₃ (50/50) (Cu _{Cr})	156
6.1.1	Elemental Analysis	156
6.1.2	Summary	156
6.2	Cu/MgO/Al ₂ O ₃ (60/2/38) (Cu _{Mg(2)Al})	157
6.2.1	Titrometry	157
6.2.2	Summary	157
6.3	Cu/MgO/Al ₂ O ₃ (60/5/35) (Cu _{Mg(5)Al})	158
6.3.1	X-ray Fluorescence	158
6.3.2	Elemental Analysis	158
6.3.3	BET surface area measurements	160
6.3.4	Titrometry	160
6.3.5	Summary	161
6.4	Cu/MgO/Al ₂ O ₃ (60/7/35) (Cu _{Mg(7)Al})	162
6.4.1	X-ray Fluorescence	162
6.4.2	Elemental Analysis	162
6.4.3	BET surface area measurements	164

6.4.4	Titrometry	165
6.4.5	Summary	165
6.5	K/Cu/MgO/Al ₂ O ₃ (K60/7/35) (Cu _{MgAlK})	166
6.5.1	Elemental Analysis	166
6.5.2	BET surface area measurements	167
6.5.3	Summary	168
7	Discussion	169
7.1	Preparation and Characterisation of Catalyst Precursors	169
7.2	Microreactor Experiments	174
7.2.1	Cu/Cr ₂ O ₃ (50/50) (Cu _{Cr})	174
7.2.2	Cu/MgO/Al ₂ O ₃ (50/10/40) (Cu _{Mg(10)Al})	177
7.2.3	Cu/MgO/Al ₂ O ₃ (60/2/38) (Cu _{Mg(2)Al})	179
7.2.4	Cu/MgO/Al ₂ O ₃ (60/5/35) (Cu _{Mg(5)Al})	183
7.2.5	Cu/MgO/Al ₂ O ₃ (60/7/35) (Cu _{Mg(7)Al})	190
7.2.6	K/Cu/MgO/Al ₂ O ₃ (K60/7/35) (Cu _{MgAlK})	195
8	Conclusions	202
9	References	205
10	Appendix	223
10.1	Atomic Absorption Spectroscopy	223
10.2	Nitrous Oxide Chemisorption (Derivation of Copper density constant)	223
10.3	Errors from Results	223
10.4	Conversion of Units	224

List of Tables

- Table 3.5.1. TCD Gas Chromatograph Calibrations.
- Table 3.5.2. Selected FID Gas Chromatograph Calibrations.
-
- Table 4.1.1. XRD d-spacing values (Å) for the Cu_{Cr} catalyst, with intensities in parentheses.
- Table 4.1.2. AAS results for the Cu_{Cr} catalyst.
- Table 4.1.3. Nitrous oxide chemisorption results for the Cu_{Cr} catalyst.
- Table 4.1.4. Copper surface reduction temperatures for the Cu_{Cr} catalyst.
- Table 4.1.5. Elemental Analysis results for the Cu_{Cr} precursor and calcined samples.
- Table 4.1.6. BET surface area measurements for the Cu_{Cr} catalyst.
- Table 4.2.1. XRD d-spacing values (Å) for the $^{7}_{30}\text{Cu}_{\text{Mg}(10)\text{Al}}$ precursor, with intensities presented in parentheses.
- Table 4.2.2. XRD d-spacing values (Å) for the $^{7}_{30}\text{Cu}_{\text{Mg}(10)\text{Al}}$ catalyst, with intensities presented in parentheses.
- Table 4.2.3. Percentage of copper co-precipitated (wt / wt) for the $\text{Cu}_{\text{Mg}(10)\text{Al}}$ catalysts with variation in preparation conditions.
- Table 4.2.4. Metal composition for the $^{7}_{30}\text{Cu}_{\text{Mg}(10)\text{Al}}$ catalyst.
- Table 4.2.5. Nitrous oxide chemisorption results for the $^{7}_{30}\text{Cu}_{\text{Mg}(10)\text{Al}}$ with variation in calcination temperature.
- Table 4.2.6. Copper surface reduction for the $^{7}_{30}\text{Cu}_{\text{Mg}(10)\text{Al}}$ catalysts temperatures with variation in calcination temperature.

- Table 4.2.7. Elemental Analysis results for the $\text{Cu}_{\text{Mg}(10)\text{Al}}$ precursors with variation in pH.
- Table 4.2.8. Elemental Analysis results for the $^{7}_{30}\text{Cu}_{\text{Mg}(10)\text{Al}}$ catalysts with variation in calcination temperature.
- Table 4.2.9. BET surface area measurements for the $^{7}_{30}\text{Cu}_{\text{Mg}(10)\text{Al}}$ catalysts with variation in calcination temperature.
- Table 4.3.1. XRD d-spacing values (\AA) for the $^{8}_{70}\text{Cu}_{\text{Mg}}$ precursor, with intensities presented in parentheses.
- Table 4.3.2. Percentage of magnesium co-precipitated (wt / wt) for the Cu_{Mg} catalysts with variation in preparation conditions.
- Table 4.3.3. Copper metal ratio for the Cu_{Mg} catalysts with variation in preparation conditions.
- Table 4.3.4. Magnesium metal ratio for the Cu_{Mg} catalysts with variation in preparation conditions.
- Table 4.3.5. Nitrous oxide chemisorption results for the Cu_{Mg} catalysts with variation in preparation conditions.
- Table 4.3.6. Copper surface reduction temperatures for the Cu_{Mg} catalysts with variation in preparation conditions.
- Table 4.3.7. Elemental Analysis results for the $^{8}_{70}\text{Cu}_{\text{Mg}}$ precursors with variation in preparation conditions.
- Table 4.3.8. Elemental Analysis results for the Cu_{Mg} catalysts with variation in preparation conditions.
- Table 4.3.9. BET surface area measurements for various Cu_{Mg} catalysts with variation in preparation conditions.

- Table 4.3.10. Percentage of copper co-precipitated (wt / wt) for the Cu_{Al} catalysts with variation in preparation conditions.
- Table 4.3.11. Percentage of aluminium precipitated (wt / wt) for the Cu_{Al} catalysts with variation in preparation conditions.
- Table 4.3.12. Copper metal ratio for the Cu_{Al} catalysts with variation in preparation conditions.
- Table 4.3.13. Aluminium metal ratio for the Cu_{Al} catalysts with variation in preparation conditions.
- Table 4.3.14. Nitrous oxide chemisorption results for the Cu_{Al} catalysts with variation in preparation conditions.
- Table 4.3.15. Copper surface reduction temperatures for the Cu_{Al} catalysts with variation in preparation conditions.
- Table 4.3.16. Elemental Analysis results for the Cu_{Al} precursors with variation in preparation conditions.
- Table 4.3.17. Elemental Analysis results for the Cu_{Al} catalysts with variation in preparation conditions.
- Table 4.3.18. BET surface area measurements for the Cu_{Al} catalysts with variation in preparation conditions.
- Table 4.4.1. XRD d-spacing values (\AA) for the $^8_{140}\text{Cu}_{\text{Mg}(2)\text{Al}}$ precursor, with intensities presented in parentheses.
- Table 4.4.2. Percentage of copper, magnesium and aluminium co-precipitated (wt/wt) for the $\text{Cu}_{\text{Mg}(2)\text{Al}}$ catalysts with variation in ageing time.
- Table 4.4.3. Metal ratios of copper, magnesium and aluminium for the $\text{Cu}_{\text{Mg}(2)\text{Al}}$ catalysts with variation in ageing time.

- Table 4.4.4. Nitrous oxide chemisorption results for the $\text{Cu}_{\text{Mg}(2)\text{Al}}$ catalysts with variation in ageing time.
- Table 4.4.5. Copper surface reduction temperatures for the $\text{Cu}_{\text{Mg}(2)\text{Al}}$ catalysts with variation in ageing time.
- Table 4.4.6. Elemental Analysis results for the $\text{Cu}_{\text{Mg}(2)\text{Al}}$ precursors with variation in preparation conditions.
- Table 4.4.7. Elemental Analysis results for the $\text{Cu}_{\text{Mg}(2)\text{Al}}$ catalysts with variation in ageing time.
- Table 4.4.8. BET surface area measurements for the $\text{Cu}_{\text{Mg}(2)\text{Al}}$ catalysts with variation in ageing time.
- Table 4.5.1. Percentage of copper, magnesium and aluminium co-precipitated (wt / wt) for the $\text{Cu}_{\text{Mg}(5)\text{Al}}$ catalysts with variation in ageing time.
- Table 4.5.2. Metal ratios of copper, magnesium and aluminium for the $\text{Cu}_{\text{Mg}(5)\text{Al}}$ catalysts with variation in ageing time.
- Table 4.5.3. Nitrous oxide chemisorption results for the $\text{Cu}_{\text{Mg}(5)\text{Al}}$ catalysts with variation in ageing time.
- Table 4.5.4. Copper surface reduction temperatures for the $\text{Cu}_{\text{Mg}(5)\text{Al}}$ catalysts with variation in ageing time.
- Table 4.5.5. Elemental Analysis results for the $\text{Cu}_{\text{Mg}(5)\text{Al}}$ precursors with variation in preparation conditions.
- Table 4.5.6. Elemental Analysis results for the $\text{Cu}_{\text{Mg}(5)\text{Al}}$ catalysts with variation in preparation conditions.
- Table 4.5.7. BET surface area measurements for the $\text{Cu}_{\text{Mg}(5)\text{Al}}$ catalysts with variation in ageing time.

- Table 4.6.1. Percentage of copper, magnesium and aluminium co-precipitated (wt / wt) for the $\text{Cu}_{\text{Mg}(7)\text{Al}}$ catalysts with variation preparation conditions.
- Table 4.6.2. Metal ratios of copper, magnesium and aluminium for the $\text{Cu}_{\text{Mg}(7)\text{Al}}$ catalysts with variation in preparation conditions.
- Table 4.6.3. Nitrous oxide chemisorption results for the $\text{Cu}_{\text{Mg}(7)\text{Al}}$ catalysts with variation in preparation conditions.
- Table 4.6.4. Copper surface reduction temperatures for the $\text{Cu}_{\text{Mg}(7)\text{Al}}$ catalysts with variation in preparation conditions.
- Table 4.6.5. Elemental Analysis results for the $\text{Cu}_{\text{Mg}(7)\text{Al}}$ precursors with variation in preparation conditions.
- Table 4.6.6. Elemental Analysis results for the $\text{Cu}_{\text{Mg}(7)\text{Al}}$ catalysts with variation in preparation conditions.
- Table 4.6.7. BET surface area measurements for the $\text{Cu}_{\text{Mg}(7)\text{Al}}$ catalysts with variation in preparation conditions.
- Table 4.7.1. Percentage of wet-impregnated potassium (wt / wt) for the Cu_{MgAlK} catalysts with variation in preparation conditions.
- Table 4.7.2. Metal ratios of copper, magnesium, aluminium and potassium for the Cu_{MgAlK} catalysts with variation in preparation conditions.
- Table 4.7.3. Nitrous oxide chemisorption results for the Cu_{MgAlK} catalysts with variation in preparation conditions.
- Table 4.7.4. Copper surface reduction temperatures for the Cu_{MgAlK} catalysts with variation in preparation conditions.
- Table 4.7.5. Elemental Analysis results for the Cu_{MgAlK} precursors with variation in preparation conditions.

- Table 4.7.6. Elemental Analysis results for the Cu_{MgAlK} catalysts with variation in preparation conditions.
- Table 4.7.7. BET surface area measurements for the Cu_{MgAlK} catalysts with variation in preparation conditions and the pH = 8 30 mins precursor.
- Table 5.2.1. Product distribution for the Cu_{Cr} catalyst with variation in temperature (expressed as a conversion).
- Table 5.2.2. Product distribution for the Cu_{Cr} catalyst with variation in gas hourly space velocity (expressed as a conversion).
- Table 5.2.3. Product distribution for the Cu_{Cr} catalyst with variation in gasfeed composition (expressed as selectivity).
- Table 5.2.4. Product distribution for the Cu_{Cr} catalyst with variation in gasfeed composition (expressed as selectivity).
- Table 5.3.1. Product distribution for the $^{73}\text{Cu}_{\text{Mg(10)Al}}$ catalyst with variation in gas hourly space velocity (expressed as conversion).
- Table 5.4.1. Product distribution for the $\text{Cu}_{\text{Mg(2)Al}}$ catalysts with variation in ageing time (expressed as a conversion).
- Table 5.4.2. Product distribution for the $^{87}\text{Cu}_{\text{Mg(2)Al}}$ catalyst with variation in temperature (expressed as a conversion).
- Table 5.4.3. Product distribution for the $^{81}\text{Cu}_{\text{Mg(2)Al}}$ catalyst with variation in gasfeed composition (expressed as a conversion).
- Table 5.4.4. Product distribution for the $^{81}\text{Cu}_{\text{Mg(2)Al}}$ catalyst with variation in gasfeed composition (expressed as a conversion).
- Table 5.5.1. Product distribution for the $\text{Cu}_{\text{Mg(5)Al}}$ catalyst with variation in ageing time (expressed as a conversion).

- Table 5.5.2. Product distribution for the ${}^8_{30}\text{Cu}_{\text{Mg}(5)\text{Al}}$ catalyst with variation in temperature (expressed as a conversion).
- Table 5.5.3. Product distribution for the ${}^8_{70}\text{Cu}_{\text{Mg}(5)\text{Al}}$ catalyst with variation in temperature (expressed as a conversion).
- Table 5.5.4. Product distribution for the ${}^8_{30}\text{Cu}_{\text{Mg}(5)\text{Al}}$ catalyst with variation in gas hourly space velocity (expressed as a conversion).
- Table 5.5.5. Product distribution for the ${}^8_{140}\text{Cu}_{\text{Mg}(5)\text{Al}}$ catalyst with variation in gas hourly space velocity (expressed as a conversion).
- Table 5.5.6. Product distribution for the ${}^8_{70}\text{Cu}_{\text{Mg}(5)\text{Al}}$ catalyst with variation in gasfeed composition (expressed as a conversion).
- Table 5.6.1. Product distribution for the ${}^8_{140}\text{Cu}_{\text{Mg}(7)\text{Al}}$ catalyst with variation in temperature (expressed as a conversion).
- Table 5.6.2. Product Distribution for the ${}^8_{70}\text{Cu}_{\text{Mg}(7)\text{Al}}$ catalyst with variation in gas hourly space velocity (expressed as selectivity).
- Table 5.6.3. Product Distribution for the ${}^8_{30}\text{Cu}_{\text{Mg}(7)\text{Al}}$ catalyst with variation in gasfeed composition (expressed as selectivity).
- Table 5.7.1. Product distribution for the Cu_{MgAlK} catalyst with variation in preparation conditions (expressed as a conversion).
- Table 5.7.2. Product distribution for the ${}^8_{140}\text{Cu}_{\text{MgAlK}}$ catalyst with variation in temperature (expressed as a conversion).
- Table 5.7.3. Product distribution for the ${}^8_{70}\text{Cu}_{\text{MgAlK}}$ catalyst with variation in gas hourly space velocity (expressed as a conversion).
- Table 5.7.4. Product distribution for the ${}^8_{70}\text{Cu}_{\text{MgAlK}}$ catalyst with variation in gasfeed composition (expressed as a conversion).

- Table 6.1.1. Elemental Analysis result for the post-microreactor Cu_{Cr} catalyst.
- Table 6.2.1. Conversion of reaction number to conditions for Karl Fischer Titrometry for the $\text{Cu}_{\text{Mg}(2)\text{Al}}$ catalysts with variation in ageing time.
- Table 6.3.1. Elemental Analysis results for the $\text{Cu}_{\text{Mg}(5)\text{Al}}$ post reaction catalysts with variation in ageing time.
- Table 6.3.2. Conversion of reaction reference to conditions for the $\text{Cu}_{\text{Mg}(5)\text{Al}}$ catalysts.
- Table 6.3.3. BET surface area measurements for the $\text{Cu}_{\text{Mg}(5)\text{Al}}$ post reaction catalysts with variation in ageing time.
- Table 6.3.4. Conversion of reaction number to conditions for Karl Fischer Titrometry for the $\text{Cu}_{\text{Mg}(5)\text{Al}}$ catalysts with variation in ageing time.
- Table 6.4.1. Elemental Analysis results for the $\text{Cu}_{\text{Mg}(7)\text{Al}}$ post reaction catalysts with variation in preparation conditions.
- Table 6.4.2. Conversion of reaction reference to conditions for the $\text{Cu}_{\text{Mg}(7)\text{Al}}$ catalysts.
- Table 6.4.3. BET surface area measurements for the $\text{Cu}_{\text{Mg}(7)\text{Al}}$ post reaction catalysts with variation in preparation conditions.
- Table 6.4.4. Conversion of reaction number to conditions for Karl Fischer Titrometry for the $\text{Cu}_{\text{Mg}(7)\text{Al}}$ catalysts with variation in preparation conditions.
- Table 6.5.1. Elemental Analysis results for the Cu_{MgAlK} post reaction catalysts with variation in preparation conditions.
- Table 6.5.2. Conversion of reaction reference to conditions for Cu_{MgAlK} catalysts.
- Table 6.5.3. BET surface area measurements for the Cu_{MgAlK} post reaction catalysts with variation in preparation conditions.

List of Figures

- Figure 1.1.1. Formation of alcohols with the simultaneous formation of hydrocarbons, aldehydes, esters and DME.
- Figure 1.4.1. Smith and Anderson [98] proposed reaction network.
- Figure 1.4.2. The proposed reaction mechanism on Cu/Co based catalysts [143].
- Figure 1.6.1. Hydrotalcite structure.
-
- Figure 3.3.1. Co-precipitation Apparatus.
- Figure 3.3.2. Calcination Reactor Set-up.
- Figure 3.3.3. Calcination Rig.
- Figure 3.3.4. Reduction Procedure.
- Figure 3.4.1. DTA cell.
- Figure 3.4.2. N₂O chemisorption / TPR line.
- Figure 3.4.3. TPR vessel.
- Figure 3.4.4. Water analysis / Titrometry.
- Figure 3.5.1. The Schematic of the Microreactor System.
- Figure 3.5.2. Vapourisation unit.
- Figure 3.5.3. Furnace.
- Figure 3.5.4. Gas Sample Valve.
-
- Figure 4.1.1. DTA profile for the Cu_{Cr} precursor.
- Figure 4.1.2. XRF spectrum for the Cu_{Cr} precursor.
- Figure 4.1.3. XRF spectrum for the filtered Cu_{Cr} catalyst.
- Figure 4.1.4. TPR profile for the Cu_{Cr} catalyst.

- Figure 4.2.1. DTA profiles for various $\text{Cu}_{\text{Mg}(10)\text{Al}}$ precursors.
- Figure 4.2.2. XRD patterns for the $^{7}_{30}\text{Cu}_{\text{Mg}(10)\text{Al}}$ precursors.
- Figure 4.2.3. XRD patterns for the $\text{Cu}_{\text{Mg}(10)\text{Al}}$ precursors with variation in pH.
- Figure 4.2.4. XRD patterns for the $\text{Cu}_{\text{Mg}(10)\text{Al}}$ catalysts with variation in preparation conditions and calcination temperature (K).
- Figure 4.2.5. XRF spectrum for the $^{7}_{30}\text{Cu}_{\text{Mg}(10)\text{Al}}$ precursor.
- Figure 4.2.6. XRF spectrum for the $^{9.5}_{30}\text{Cu}_{\text{Mg}(10)\text{Al}}$ precursor.
- Figure 4.2.7. XRF spectrum for the calcined 623 K $^{7}_{30}\text{Cu}_{\text{Mg}(10)\text{Al}}$ catalyst.
- Figure 4.2.8. XRF spectrum for the calcined 873 K $^{7}_{30}\text{Cu}_{\text{Mg}(10)\text{Al}}$ catalyst.
- Figure 4.2.9. TPR profiles for the $\text{Cu}_{\text{Mg}(10)\text{Al}}$ catalysts with variation in calcination temperature (K).
- Figure 4.3.1. DTA profiles for the $^8\text{Cu}_{\text{Mg}}$ precursors with variation in ageing time.
- Figure 4.3.2. XRD patterns for the Cu_{Mg} precursors with variation in pH (30 mins ageing time).
- Figure 4.3.3. XRD patterns for the $^8\text{Cu}_{\text{Mg}}$ precursors with variation in ageing time.
- Figure 4.3.3. XRD patterns for the $^8\text{Cu}_{\text{Mg}}$ precursors with variation in ageing time.
- Figure 4.3.4. XRD patterns for the Cu_{Mg} catalysts with variation in pH (30 mins ageing time).
- Figure 4.3.5. XRD patterns for the $^8\text{Cu}_{\text{Mg}}$ catalysts with variation in ageing time.
- Figure 4.3.6. XRD patterns for the $^9_{140}\text{Cu}_{\text{Mg}}$ precursor and catalyst.
- Figure 4.3.7. XRF spectrum for the $^8_{70}\text{Cu}_{\text{Mg}}$ precursor.
- Figure 4.3.8. XRF spectrum for the $^8_{30}\text{Cu}_{\text{Mg}}$ catalyst.
- Figure 4.3.9. XRF spectrum for the $^8_{140}\text{Cu}_{\text{Mg}}$ catalyst.
- Figure 4.3.10. TPR profiles for the Cu_{Mg} catalysts with variation in preparation conditions.

Figure 4.3.11. DTA profiles for the Cu_{Al} precursors with variation in preparation conditions.

Figure 4.3.12. XRD patterns for the Cu_{Al} precursors with variation in pH (30 mins ageing time).

Figure 4.3.13. XRD patterns for the $^8\text{Cu}_{\text{Al}}$ precursors with variation in ageing time.

Figure 4.3.14. XRD patterns for the Cu_{Al} catalysts with variation in pH (30 mins ageing time).

Figure 4.3.15. XRD patterns for the $^8\text{Cu}_{\text{Al}}$ catalysts with variation in ageing time.

Figure 4.3.16. XRD patterns for the $^9_{140}\text{Cu}_{\text{Al}}$ precursor and catalyst.

Figure 4.3.17. XRF spectrum for the $^7_{30}\text{Cu}_{\text{Al}}$ precursor.

Figure 4.3.18. XRF spectrum for the $^{10}_{30}\text{Cu}_{\text{Al}}$ precursor.

Figure 4.3.19. XRF spectrum for the $^8_{70}\text{Cu}_{\text{Al}}$ catalyst.

Figure 4.3.20. XRF spectrum for the filtered $^8_{70}\text{Cu}_{\text{Al}}$ catalyst.

Figure 4.3.21. TPR profiles for the Cu_{Al} catalysts with variation in preparation conditions.

Figure 4.4.1. DTA profiles for the $^8\text{Cu}_{\text{Mg}(2)\text{Al}}$ precursors with variation in ageing time.

Figure 4.4.2. DTA profiles for the $^9\text{Cu}_{\text{Mg}(2)\text{Al}}$ precursors with variation in ageing time.

Figure 4.4.3. XRD patterns for the $^8\text{Cu}_{\text{Mg}(2)\text{Al}}$ precursors with variation in ageing time.

Figure 4.4.4. XRD pattern for the $^9\text{Cu}_{\text{Mg}(2)\text{Al}}$ precursors with variation in ageing time.

Figure 4.4.5. XRD patterns for the $^8\text{Cu}_{\text{Mg}(2)\text{Al}}$ catalysts with variation in ageing time.

Figure 4.4.6. XRF spectrum for the $^8_{30}\text{Cu}_{\text{Mg}(2)\text{Al}}$ precursor.

Figure 4.4.7. XRF spectrum for the $^9_{30}\text{Cu}_{\text{Mg}(2)\text{Al}}$ precursor.

- Figure 4.4.8. XRF spectrum for the $^8\text{Cu}_{\text{Mg}(2)\text{Al}}$ catalyst.
- Figure 4.4.9. XRF spectrum for the $^8\text{Cu}_{\text{Mg}(2)\text{Al}}$ catalyst.
- Figure 4.4.10. TPR profiles for the $^8\text{Cu}_{\text{Mg}(2)\text{Al}}$ catalysts with variation in ageing time.
- Figure 4.5.1. DTA profiles for the $\text{Cu}_{\text{Mg}(5)\text{Al}}$ precursors with variation in preparation conditions.
- Figure 4.5.2. XRD patterns for the $\text{Cu}_{\text{Mg}(5)\text{Al}}$ precursors with variation in preparation conditions.
- Figure 4.5.3. XRD pPatterns for the $\text{Cu}_{\text{Mg}(5)\text{Al}}$ catalysts with variation in preparation conditions.
- Figure 4.5.4. XRF spectrum for the $^8\text{Cu}_{140\text{Mg}(5)\text{Al}}$ precursor.
- Figure 4.5.5. XRF spectrum for the filtered $^9\text{Cu}_{\text{Mg}(5)\text{Al}}$ precursor.
- Figure 4.5.6. XRF spectrum for the $^8\text{Cu}_{\text{Mg}(5)\text{Al}}$ catalyst.
- Figure 4.5.7. XRF spectrum for the filtered $^8\text{Cu}_{140\text{Mg}(5)\text{Al}}$ catalyst.
- Figure 4.5.8. TPR profiles for the $^8\text{Cu}_{\text{Mg}(5)\text{Al}}$ catalysts with variation in ageing time.
- Figure 4.6.1. DTA profiles for the $\text{Cu}_{\text{Mg}(7)\text{Al}}$ precursors with variation in preparation conditions.
- Figure 4.6.2. XRD patterns for the $\text{Cu}_{\text{Mg}(7)\text{Al}}$ precursors with variation in preparation conditions.
- Figure 4.6.3. XRD patterns for the $\text{Cu}_{\text{Mg}(7)\text{Al}}$ catalysts with variation in preparation conditions.
- Figure 4.6.4. XRF spectrum for the $^8\text{Cu}_{\text{Mg}(7)\text{Al}}$ precursor.
- Figure 4.6.5. XRF spectrum for the filtered $^8\text{Cu}_{\text{Mg}(7)\text{Al}}$ precursor.
- Figure 4.6.6. XRF spectrum for the $^8\text{Cu}_{\text{Mg}(7)\text{Al}}$ catalyst.
- Figure 4.6.7. XRF spectrum for the filtered $^8\text{Cu}_{\text{Mg}(7)\text{Al}}$ catalyst.

- Figure 4.6.8. TPR profiles for the $\text{Cu}_{\text{Mg}(7)\text{Al}}$ catalysts with variation in preparation conditions.
- Figure 4.7.1. DTA profiles for the Cu_{MgAlK} precursors with variation in preparation conditions.
- Figure 4.7.2. XRD patterns for the Cu_{MgAlK} precursors with variation in preparation conditions.
- Figure 4.7.3. XRD patterns for the Cu_{MgAlK} catalysts with variation in preparation conditions.
- Figure 4.7.4. XRF spectrum for the $^8_{30}\text{Cu}_{\text{MgAlK}}$ precursor.
- Figure 4.7.5. XRF spectrum for the $^8_{70}\text{Cu}_{\text{MgAlK}}$ catalyst.
- Figure 4.7.6. TPR profiles for the Cu_{MgAlK} catalysts with variation in preparation conditions.
-
- Figure 5.2.1. Product distribution for the Cu_{Cr} catalyst.
- Figure 5.2.2. Product distribution for the Cu_{Cr} catalyst.
- Figure 5.2.3. Product distribution for the Cu_{Cr} catalyst.
- Figure 5.4.1. Product distribution for the $^8_{30}\text{Cu}_{\text{Mg}(2)\text{Al}}$ catalyst.
- Figure 5.4.2. Product distribution for the $^8_{70}\text{Cu}_{\text{Mg}(2)\text{Al}}$ catalyst.
- Figure 5.4.3. Product distribution for the $^8_{140}\text{Cu}_{\text{Mg}(2)\text{Al}}$ catalyst.
- Figure 5.5.1. Product distribution for the $^8_{70}\text{Cu}_{\text{Mg}(5)\text{Al}}$ catalyst.
- Figure 5.5.2. Product distribution for the $^8_{140}\text{Cu}_{\text{Mg}(5)\text{Al}}$ catalyst.
- Figure 5.5.3. Product distribution for the $^8_{70}\text{Cu}_{\text{Mg}(5)\text{Al}}$ catalyst.
- Figure 5.6.1. Product distribution for the $^8_{30}\text{Cu}_{\text{Mg}(7)\text{Al}}$ catalyst.
- Figure 5.6.2. Product distribution for the $^8_{70}\text{Cu}_{\text{Mg}(7)\text{Al}}$ catalyst.
- Figure 5.6.3. Product distribution for the $^8_{140}\text{Cu}_{\text{Mg}(7)\text{Al}}$ catalyst.

Figure 5.6.4. Product distribution for the ${}^9_{30}\text{Cu}_{\text{Mg}(7)\text{Al}}$ catalyst.

Figure 5.6.5. Product distribution for the ${}^8_{30}\text{Cu}_{\text{Mg}(7)\text{Al}}$ catalyst.

Figure 5.6.6. Product distribution for the ${}^8_{30}\text{Cu}_{\text{Mg}(7)\text{Al}}$ catalyst.

Figure 5.6.7. Product distribution for the ${}^9_{30}\text{Cu}_{\text{Mg}(7)\text{Al}}$ catalyst.

Figure 5.6.8. Product distribution for the ${}^8_{70}\text{Cu}_{\text{Mg}(7)\text{Al}}$ catalyst.

Figure 5.7.1. Product distribution for the ${}^8_{30}\text{Cu}_{\text{MgAlK}}$ catalyst.

Figure 5.7.2. Product distribution for the ${}^8_{70}\text{Cu}_{\text{MgAlK}}$ catalyst.

Figure 5.7.3. Product distribution for the ${}^8_{140}\text{Cu}_{\text{MgAlK}}$ catalyst.

Figure 5.7.4. Product distribution for the ${}^8_{70}\text{Cu}_{\text{MgAlK}}$ catalyst.

Figure 5.7.5. Product distribution for the ${}^8_{30}\text{Cu}_{\text{MgAlK}}$ catalyst.

Figure 6.3.1. XRF spectrum for a ${}^8_{70}\text{Cu}_{\text{Mg}(5)\text{Al}}$ post reaction catalyst.

Figure 6.3.2. XRF spectrum for a ${}^8_{70}\text{Cu}_{\text{Mg}(5)\text{Al}}$ post reaction catalyst.

Figure 6.4.1. XRF spectrum for a ${}^8_{30}\text{Cu}_{\text{Mg}(7)\text{Al}}$ post reaction catalyst.

Figure 6.4.2. XRF spectrum for a ${}^9_{30}\text{Cu}_{\text{Mg}(7)\text{Al}}$ post reaction catalyst.

Figure 6.4.3. XRF spectrum for a ${}^8_{70}\text{Cu}_{\text{Mg}(7)\text{Al}}$ post reaction catalyst.

1 Introduction

1.1 Background

In 1836, J.J. Berzelius [1] recognised a single concept when changes in composition of numerous substances came in contact with small amounts of various “ferment”, liquids or solids and from this idea coined the phrase “catalysis”. It was Ostwald [2] 60 yrs later, who conceived the modern idea of catalysis by pronouncing that a catalyst is a substance, which changes the rate of a chemical reaction without itself appearing in the products. Since this original conception, catalyst technology has expanded exponentially.

The first commercial catalytic process for hydrogenation of CO to methanol was developed by BASF in 1923 [3] with by-products of C₂₊ alcohols, CO₂, and water. By 1936, selective higher alcohol mixtures were being commercially produced using alkalised iron catalysts but were discontinued in 1947 [3]. The renewed incentive to form higher alcohols in the 1970's was mainly to reduce oil dependency by producing synthetic components for gasoline blends. However, in the late 1980's oil prices dropped and such research was uneconomic [4].

In 1989, the Clean Fuel act in the U.S.A. was introduced banning the use of lead containing antiknock agents, thus bringing additional incentives for producing alcohols as substitute octane boosters [5]. However by 1990, pure alcohols or alcohol blends had almost disappeared from the gasoline pool and ethers (mainly methyl-tetra-butylether (MTBE)) prevailed. However, the future demand is expected to exceed the traditional feedstock supply and alternative sources are still highly desirable [5].

Alcohol fuels have already been used in U.S.A. and Germany for automobiles (ca. 3-5 vol %) [6].

Alcohol synthesis is a favourable way to upgrade syngas because of favourable thermodynamics, low yield of by-products and economics.

	ΔH_{298}° kJ mol ⁻¹	ΔH_{298}° kJ mol ⁻¹ (for 1 / n mol C _n OH)
CH ₃ OH	-90.47	-90.47
CH ₃ CH ₂ OH	-254.98	-127.49
n-C ₃ OH	-408.09	-136.03
n-C ₄ OH	-572.37	-143.09
CH ₄	-205.95	-205.95

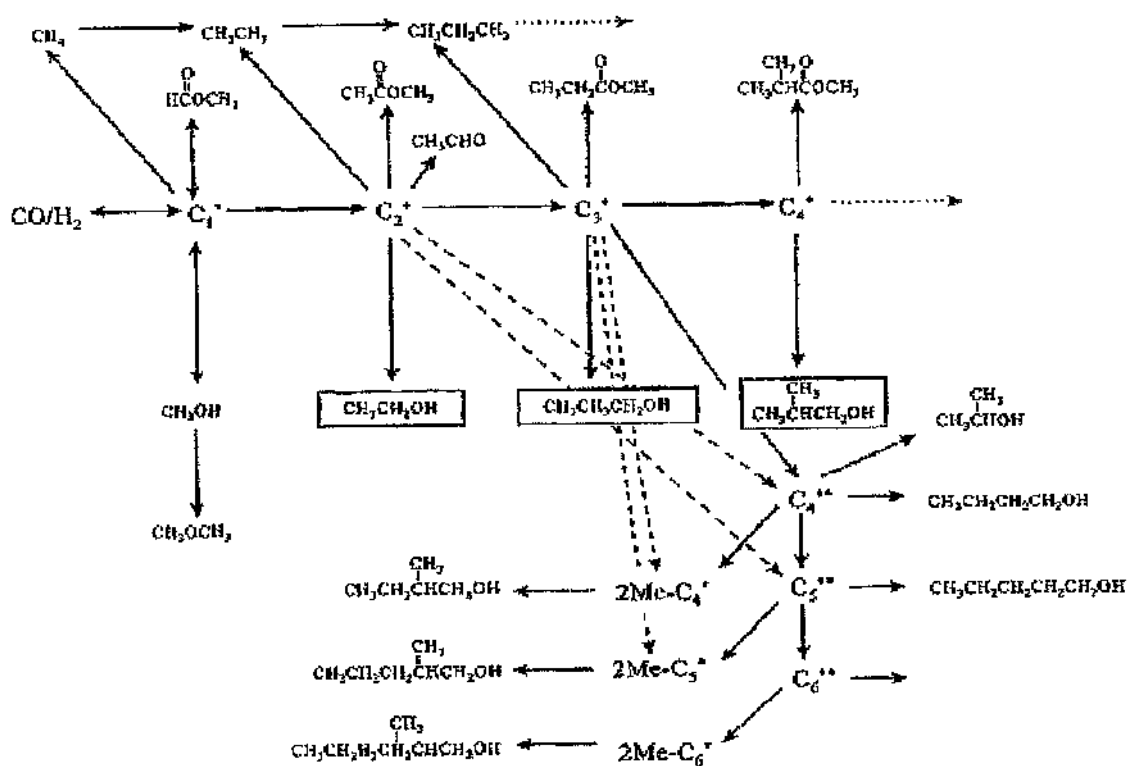
These considerations have resulted in a continuation of the investigation of higher alcohol synthesis from CO and hydrogen, both by academic researches and by the chemical and petroleum industrial companies. There is a joint venture between Enichem, Snamprogetti and Haldor Topsøe using a Na promoted Zn/Cr catalyst. IFP and Idemitsi Kosan have also collaborated to develop a process for the co-production of methanol and 35-45 wt % of light C₂₊ alcohols [7,8] using a Cu/Co-based catalyst [5].

However, higher alcohol synthesis (HAS) involves a complex set of numerous reactions (Figure 1.1.1) and its investigation requires an integrated approach where consideration must be given to catalytic behaviour and physico-chemical characterisation of catalysts, as well as to kinetic and thermodynamic aspects.

Catalysts for HAS can be divided into the following classes:

- 1) Either Low Temperature (Cu/ZnO) or High Temperature (ZnO/Cr₂O₃) methanol synthesis catalysts usually modified with an alkali metal.
- 2) Modified Fischer-Tropsch and Group VIII metal-based catalysts.
- 3) Others Catalysts based on Rh, MoS₂ and Cu/Mg/CeO₂.

Figure 1.1.1. Formation of alcohols with the simultaneous formation of hydrocarbons, aldehydes, esters and dimethyl ether (DME).



1.2. Modified Methanol Synthesis catalysts

Higher alcohols, principally ethanol, propanols and butanols are produced as by-products in the industrial methanol process, however, the relative high hydrogen partial pressure used under normal methanol synthesis conditions tends to limit their formation. Aldehydes, secondary alcohols, ketones and esters, usually methyl ester are formed in minor quantities [9]. Higher quantities of methyl esters are formed in the low temperature (LT) methanol synthesis process than in the modified high temperature (HT) methanol process, this is due to thermodynamic considerations [4,6].

The formation of water and CO_2 are unavoidable by-products, the latter being favoured at low $\text{H}_2:\text{CO}$ ratios and under CO_2 removal conditions due to the occurrence of the Water Gas Shift (WGS) reaction [4].

Addition of alkali or alkaline-earth elements to both the low temperature (LT) and high temperature (HT) methanol synthesis catalysts can produce larger quantities of higher alcohols [10]. In the 1940's, Dupont used an alkalisied Mn/Cr catalyst [11] to produce methanol and higher alcohols on a commercial scale at 800 atm and with a $\text{H}_2:\text{CO}$ ratio of 12:1 [4].

The addition of alkali metals is used to increase productivity by accelerating the slow $\text{C}_1\text{-C}_2$ step and the $\text{C}_2\text{-C}_3$ step. The distribution of higher alcohols is not notably modified apart from the ethanol/propanol ratio. The promoting effect of the added compounds is probably related to the basicity of the compound added which, for convenience is normally a potassium compound [6]. Also, the addition of alkali metals is very effective in reducing the selectivity to ethers [4].

Several workers have investigated non-alkalisied and alkalisied systems.

1.2.1 Modified Low Temperature Methanol synthesis catalysts

In 1966, ICI introduced a low temperature (523 K) and pressure system (50-100 bar) for the formation of methanol using the typical syngas containing 2-8 vol % CO₂ from a H₂:CO:CO₂ mixture in H₂ rich syngas with a new catalyst, Cu/ZnO/Al₂O₃ with selectivities of > 99.5 % [3]. This moved away from the old ZnO/Cr₂O₃ (HT) methanol catalyst, which required increased running costs due to an elevated temperature of 623 K and higher pressure of 250-350 bar [12]. The new process used a gas hourly space velocity (GHSV) of between 5000 and 60,000 hr⁻¹ but the conversion is limited to 25 % due to the chemical equilibrium [3]. The catalyst composition typically contains 20-39 % Cu, 45-55 % ZnO and 13 % Al₂O₃ [13].

Copper is acknowledged as the active phase for the methanol synthesis [14]. Copper metal being the important catalyst constituent [3], as during activation surface Cu ions are effectively reduced to the metal during activation [15] and are solely present post reaction at 523 K [15]. This is further confirmed by evidence on Raney copper [16], copper single crystals [17] and recent experimental and modelling evidence [18,19]. However, debate is still apparent for the active copper active site [9,20,21].

The synthesis activity is proportional to copper metal area over a range of supports and copper areas [22] and, therefore, it is a structure sensitive reaction [17] but deviations are observed in the literature [23]. Burch *et al* [24] think the deviations are due to the wide range of experimental conditions used and, therefore, difficult to transpose the activities to standard conditions but another suggestion has been presented by Joyner [25]. Joyner suggested that when Cu⁰ is a source of H_{ads}, it

migrates to the active centres on the support or promoter, the synthesis activity would be proportional both to the number of active centres and to the Cu metal surface area.

Zinc oxide is incorporated into the catalyst, as early workers [26] ascribed the uniquely high activity as a special "synergy" between the copper and zinc oxide as the activity was greatly improved when compared to pure copper. The synergy has been later discounted, as oxides as diverse as SiO₂ or MgO, with the latter having a similar Brønsted activity as ZnO, are both equally active [22,27]. Other possible explanations have been proposed to account for this increase in activity ranging from the quantity of anionic vacancies [28], the ability to generate active hydrogen species [29], α -brass formation [30,31] to gas phase transport of hydrogen atoms or possible carriers [32-34].

Andrew [35] originally believed that copper was the lone active species, however, Herman *et al* [36] have proposed that ZnO activates H₂ with Cu⁺ present as a "solution" in ZnO. Zinc oxide has various functions [37].

- i) hinders agglomeration of the copper particles.
- ii) acts a poison sink especially for sulfur and chlorine compounds.
- iii) reacts with and thus neutralises the latent surface acidity with the alumina.

Chromia was initially used instead of alumina as the refractory support but the latter has a greater stabilising effect [38]. Alumina is mainly a structural promoter putting the catalyst into a suitable morphological form by stabilising the active Cu/ZnO phase with the paracrystallinity [9], but not significantly influencing the activity [39]. The active copper species found in Cu/ZnO catalyst is considered to be essentially the same as that in alumina promoted catalysts [26]. Zinc aluminate is also included to further increase catalyst stability with respect to deactivation and prevent sintering of copper particles [40].

The synthesis yields over a Cu/ZnO/Al₂O₃ catalyst preferentially form primary C₂ to C₄ alcohols, but methanol is by far the most abundant oxygenated product.

The productivity to higher alcohols is favoured by operating at a low H₂:CO ratio (< 2) with a CO₂ feed content of < 1 % and a low GHSV value (2000-4000 hr⁻¹) compared to the industrial LT methanol formation conditions. Higher reaction temperatures (543-583 K) are required, but they must not shorten the life of the catalyst due to copper sintering [4]. Pressures greater than the LT methanol synthesis conditions are also required [6].

Elliott [41] observed the formation of alcohols over a Cu/ZnO/Al₂O₃ catalyst with 4 % CO₂ in the feedgas stream. This catalyst formed methanol with a 70 % selectivity and ethanol, 6 %. When methanol was substituted for carbon dioxide, this resulted in a decrease in the methanol selectivity, but did not proportionately increase the ethanol production (8 %).

Calafat and Laine [42] produced a selectivity of 59.1 % to methanol, 15.6 % of iso-C₃-C₆ alcohols, 7.7 % of ketones, 6.1 % n-C₂-C₆ alcohols with 7 % hydrocarbons and unidentified products. Cobalt, when added in concentrations of up to 5 % to the tertiary catalyst increased the chain growth and decreased the methanol concentration. However, the promoted Cu/ZnO/Cr₂O₃ catalyst deactivated quicker than the unpromoted catalyst. Methanol inclusion in the gasfeed primarily increased the hydrocarbon, ethanol and the n-butanol yield.

Smith and Anderson [43] promoted a 46:46:8 Cu/ZnO/Al₂O₃ catalyst with K₂CO₃, a maximum butanol selectivity of 23 % was observed with 0.5 % addition and a maximum conversion at 1 % K₂CO₃, which was about twice the selectivity of the unpromoted catalyst. However, later work involving Smith [44] using a Cu/Zn/Cr₂O₃ catalyst gave little indication of conversion or the formation of other products formed.

Campos-Martín *et al* [45] used a Cu/ZnO/Cr₂O₃ catalyst producing a selectivity of 20.5 % C₂₊ alcohols and 47 % methanol but 25.8 % of the products were hydrocarbons and 1.4 % were ethers. Other work by Campos-Martín [46] from a H₂:CO mixture decreased the C₂₊ alcohol selectivity. Co-feeding with methanol produced an ethanol selectivity of 3.7 % but 85 % were CO₂ and ethers. Ethanol was utilised instead of methanol in enhancing the propanol and isobutanol yields. Promoting with caesium increased higher alcohols yields but CO₂ production was also increased.

Metal acetylides (CaC₂, Na₂C₂, LaC₂ and CeC₂) have also been used in conjunction with a Cu/ZnO catalyst [47]. Isobutanol was the predominant higher alcohol formed. However, the fraction of higher alcohols was typically < 2 % and had fallen to 0.2 % after 36 hrs on stream.

1.2.2 Modified High Temperature Methanol synthesis catalysts

The higher alcohols that are formed are preferentially primary branched alcohols, isobutanol is the main component with little ethanol and propan-1-ol being obtained. Aldehydes are formed in greater amounts over HT modified methanol catalysts, when compared to the LT process, this is due to thermodynamic considerations [48]. Hydrocarbons and trace amounts of ethers are also formed along with large quantities of CO₂ [4].

The formation of HAS is maximised by operating at low H₂:CO and under CO₂ removal conditions [49]. Higher reaction temperatures and lower gas hourly space velocities than those used in the industrial HT methanol synthesis process are also helpful [4].

Süd Chemie [50] claimed a total CO conversion of between 21-28.8 mole % with a catalyst promoted with 1.7-2.5 wt % of K_2O . The selectivity for alcohols was 66.1-78.5 %, while that for C_{2+} alcohols was 29.0-44.7 % and CO_2 , 17.4-24.9 %. Other promoter elements used were Cr, Ce, La, Mn or Th alone or in combination making a homogeneous catalyst a possible problem.

Forzatti [4] also used manganese as a promoter as it increased the ethanol production [6]. Keim and Falter [51] used both Zn/Cr and Mn/Cr based catalysts with a Zn/Cr atomic ratio of 1 being the optimum. The Zn/Cr catalyst formed the following products in descending quantity:- methanol > isobutanol > C_2 hydrocarbons > C_{2+} hydrocarbons > methane > propan-1-ol [52]. Other work by the same group [4], promoting a Zn/Cr catalyst with Na resulted in the production of 68-72 % methanol, 2-3 % ethanol, 3-5 % C_3 alcohols, 10-15 % C_4 alcohols and 7-12 % C_5 alcohols.

1.2.3 Modified Fischer-Tropsch and Group VIII metal-based catalysts

In 1922, Fischer and Tropsch [53] obtained a large amount of oxygenated products from syngas using iron and other catalysts; they called the product "Synthol". Subsequently, by 1926, Fischer and Tropsch [54] synthesised higher hydrocarbons using Fe, Ni and Co at 1 atm; these results led to the initiation of studies of the Fischer-Tropsch synthesis (FTS) in various countries. The first commercial process began operation in 1935 [3]. Similar impurities to those found in the industrial methanol process are also produced, aldehydes, alcohols, ether, ketones, acids, CO_2 and water. Oxygenated compounds are formed at all temperatures with the reactivity towards alcohols being less on iron than on cobalt [55]. Regardless of temperature, the most abundant single oxygenated compound is ethanol [56]. At 493 K, over iron,

the main oxygenated compounds are, in decreasing order, ethanol, acetic acid, acetone and n-propanol.

Primarily iron (promoted with K_2O) is used commercially to make hydrocarbons with the purified syngas composition being preferably a ratio of about $H_2:CO$ (1.9-2.2:1) [57]. Carbon dioxide has no apparent influence over iron but the activity decreases with increasing water vapour pressure [58]. Cobalt (supported on SiO_2 or Al_2O_3 [58]) is intrinsically more active than iron for the FTS, it also gives rise to more favourable kinetics and has a greater resistance to oxidation by water vapour [56]. The iron catalyst is also active for the Water Gas Shift reaction, which is near equilibrium at these operating conditions for the high temperature process of 603-623 K and an operating pressure of around 25 bar [57]. However, iron has the advantage of increasing the probability of chain growth due to the higher basicity, is less susceptible to sulfur poisoning and is primarily, more economic [56]. Sasol use a fused iron oxide catalyst for the HT FTS [59] and a precipitated iron catalyst for the LT FTS [60]. The low temperature iron process occurs at about 493 K and a pressure of 45 bar [56]. Both processes have similar gas hourly space velocities [58]. Cobalt would only be considered for the LT process, as at the higher temperatures this metal produces mainly methane. The production of methane is also consistent with iron. The carbon deposition rate on both catalysts also increases with increasing temperature [56].

Cobalt activity is support dependent, decreasing in the order $TiO_2 > SiO_2 > Al_2O_3 > C, MgO$ [61], with dispersion decreasing for each support with increasing cobalt concentration. However, Iglesia *et al* [58] concluded that chain growth rates depended only weakly on the Co dispersion and the type of support. However, according to Sic [62], the rate of Fischer-Tropsch (FT) reaction is inversely

proportional to catalyst particle size and is proportional to the partial pressure of hydrogen multiplied by the proportion of the "reduced" state Fe catalyst particle [63]. The reaction is insensitive to surface structure for the synthesis of light hydrocarbons [64].

Most of the HAS work has been conducted with cobalt rather than iron. The cobalt catalysts are usually modified with the incorporation of copper and, occasionally, an alkali metal. The usual ratio of Cu/CoO/Cr₂O₃ catalyst that is used is $1 < \text{Cu/Co} < 3$ and $\text{Co/Cr} > 0.5$ [65].

Alcohols are mainly saturated straight chain terminal alcohols [6] e.g. FT-like activity [5]. A decrease in methanol yield is observed usually with a gain in the yield of hydrocarbons [66]. The catalysts usually also have an active WGS reaction [67]. The product distributions obtained are, therefore, different from those produced by modified methanol catalysts.

The Cu/Co-based catalysts are preparation dependent, to begin with CoO has a low solubility in CuO [68], they are calcination temperature dependent [69] and the start-up procedure alters the selectivity [70,71]. Cobalt requires a reduction temperature exceeding 673 K [72] but according to Baker *et al* [73], little cobalt reduction occurs below 873 K. Copper sinters at this temperature resulting in CuO segregation [65].

Even with these preparation problems, attempts have been made to higher alcohols. The most successful being the joint IFP and Idemitsu Kosan process being sponsored by the Japanese ministry of international trade and industry. An initial demonstration unit was constructed in Japan producing 6000 barrels per day [6]. By the 4th generation, the temperature and pressure ranges were narrowed to 583-588 K and between 60-80 atm [5]. Selectivity is now between 90-95 % for the productivity

of alcohols, which are mainly saturated straight chain terminal alcohols with primarily methane, the remainder [6]. However the activity especially for higher alcohols is still very low [8]. The Anderson-Schulz-Flory (ASF) distribution is followed for both higher alcohol and hydrocarbons synthesis [74]. The main components claimed [75] in the IFP-Idemitsu Kosan process are Na-Cu/Co/Zn(B)/Al(C) with a typical example $\text{Na-Cu}_{0.6}\text{Co}_{0.4}\text{Zn}_{0.5}\text{Al}_{1.2}$ ($M^{2+}/M^{3+} = 1.58$). Zinc can be replaced (wholly or partially) by Cd or Mn^{2+} , Al by metals including Cr, Mn^{3+} or Ti and M stands for group VIII noble metals consisting of preferably 0.02-0.8 wt % of Ru, Rh, Pd, Os, Ir and Pt of which Rh, Pd, and Pt are preferred. Obviously, with such a variable array of elements, homogeneity of the catalyst and precursor is important, which is stressed in the reference [67]. Other problems connected with their long-term stable activity and selectivity might be a major obstacle, as after the initial start up, a slow deactivation is observed [6]; higher alcohol synthesis decreased by 50 %, methane by 60 % and methanol by 20 % over 1000 hrs [76]. Deactivation was reported [65] to be caused by the formation of surface carbides, Co carbonyls and separation of Co from the Co and Cu phases resulting in the loss of active species, possibly due to the destruction of the spinel structure, leading to sintering of Cu and Co [77]. However, the cobalt sintering problems do not appear to affect the chain growth and the average particle size [65].

Sheffer and King [69] conducted work on a Cu/CoO/Cr₂O₃ catalyst with 58 % selectivity for alcohols, but hydrocarbons constituted 40 % of the product and aldehydes, 9 %.

It is apparent that the selectivity to mixed alcohols over modified Group VIII metal-based catalysts is always low due to the difficulty in suppressing the hydrogenation function of the metals [4].

1.2.4 Others Catalysts based on Rh, MoS₂ and Cu/Mg/CeO₂

Precious metals have been studied for the production of alcohols and other oxygenated compounds from synthesis gas but generally suffer from poor selectivity, as yields of methanol formation are high.

Ichikawa *et al* [78] reported a Rh-based catalyst system containing Rh, Ir and a 3rd metal M, which was selected from Mn, Ti, Zr and Fe. This produced selectivity for C₂-oxygenates of about 50 %. Hydrocarbon selectivity primarily constituted the remainder and the general activity was very low. Further work by Ichikawa [79] showed the effects of substrates. For ethanol or C₂₊ oxygenate activity, the best substrates were the basic or mildly basic oxides, the more acidic oxides producing methane together with some higher hydrocarbons, resulting in the selectivity to methanol and other oxygenated products being significantly diminished. The product distribution was dependent on the stability of the oxygenated intermediates.

Union Carbide catalysts [80] are Rh/SiO₂-based and promoted by Fe, Mn, Mo, W, Th, U or etc. Iron was identified as being the most selective for C₂ oxygenates with the best result produced from 2.5 wt % Rh and 0.05 wt % Fe; however, selectivity for hydrocarbons was 52.5 %.

A dual-bed bench-scale system with a 4.5 wt % Rh/SiO₂ catalyst [81] on the upper section of the reactor catalyst promoted with Mn and Li, and Ir and Fe on the bottom catalyst section of the reactor gave an ethanol selectivity of 63.1 % (based on CO consumed). Cerium and other lanthanides supported on Rh/SiO₂ can also increase the ethanol yield [82].

The rhodium-based catalysts are especially selective for C₂ oxygenates. However, rhodium is scarce and its price is high. Besides, the catalysts are easily

poisoned by CO₂ even though formation is generally low and normally the methane selectivity is high (50 %) [76].

Dow Chemical claimed to have developed an alkalisied agglomerated molybdenum sulfides catalyst system capable of making C₂-C₅ alcohols [83]. The catalysts were then suitably supported e.g. MoS₂/SiO₂-K [84]. Variations using W or Re, instead of Mo were also used. Total selectivity to alcohols is 70-80 % with a CO₂ free mixture [83]. However, methanol comprises of more than 50 % of the liquid product and hydrocarbon yields are in the range of 15-30 % [83]. The product mixture consists of linear alcohols and hydrocarbons, both of which exhibit an ASF distribution [4]. Carbon dioxide is formed in large quantities due to the WGS reaction [4]. However, these catalysts had to be free of Fe, Co, Cu, Zn, Rh, Ru, Ti, V, Ce, Th, U, Ir, Pd, Pt, Ag, Cd and halogens [76] making preparation difficult.

Apesteuguía *et al* [85] carried out work using K-Cu/MgO/CeO₂ and K-Cu/MgO/NdO/CeO₂ catalysts, the latter produced a 93 % total selectivity towards alcohols with 8 % selectivity towards isobutanol, but 83 % was methanol. On a similar catalyst, an overall increase in C₂-C₃ to 3.2 % and isobutanol to 7.2 % was observed at the expense of methanol. Up to 4.8 % DME and methane were produced.

Hilmen *et al* [86] used a similar K-Cu/MgO/CeO₂ catalyst. This produced a 10-15 % CO conversion with 12 % selectivity to C₂₊ alcohols, but 75 % formed was methanol and 4+ % were paraffins. Isobutanol rates are higher with a higher Cu content, but the increased copper content decreased selectivity. Little change in selectivity was observed with variation in gas hourly space velocity. Further experiments [87] produced a 15 % isobutanol product selectivity, 5 % propanol, 5 % ethanol and a decrease to 45 % in methanol production.

1.3 Theoretical Considerations and Physical Parameters

1.3.1 Kinetic and Thermodynamic Factors

Thermodynamical ΔG° values (at 523 K) decrease in the class of reaction, methanol, HAS, FTS [6]. Therefore, under normal HAS operating conditions, saturated hydrocarbons are more favoured than alcohols [6]. Low temperatures and high pressures preferentially favour alcohol formation rather than hydrocarbons [5]. Branched alcohols are slightly more stable than linear ones and, therefore, a driving force exists towards branched alcohols where the catalysed pathways permit their formation [4,10]. Isobutanol is the preferred alcohol species between 473 and 773 K [88]. The apparent stoichiometry of alcohol formation is dependent on the extent to which the WGS reaction takes place [88].

A strict correspondence is always observed between primary alcohols and aldehydes and between secondary alcohols and ketones as they are related through hydrogenation equilibria [89]. Operating at lower temperatures and higher hydrogen partial pressures can reduce the aldehyde content of the reaction products [6]. Ester formation especially methyl formate is limited by thermodynamics [6].

The theoretical limitation of alcohol conversion is partly thermodynamic, but the most important one is heat removal from the reactor [90]. However, Tronconi *et al* [48,89] found that the extent of chain growth is kinetic controlled over both LT and HT modified methanol catalysts.

It should be also noted that apart from methanol synthesis and WGS reactions, the main and secondary reactions are not thermodynamically limited under usual operating conditions (523-623 K) and water and CO₂ appear as symmetrical by-products due to the WGS reaction equilibrium [5].

1.3.2 Effects of the Operating Variables

Higher alcohol selectivity multiplies sharply with increasing temperature at the expense of methanol [4] making it a key parameter. The production of branched species continually increase with temperature, whereas those of linear species go through a distinct maximum [4]. However, higher temperature also enhances the formation of hydrocarbons. The rate of formation of CO_2 is seen to parallel essentially that of higher alcohols and/or hydrocarbon selectivity [4], however, the increase in concentration of CO_2 tends to favour the formation of low molecular weight products (MW) i.e. methanol [4]. Therefore, CO_2 is an inhibitor for the formation of C_{2+} oxygenates [89]. The more basic the catalyst, the more CO_2 inhibition is caused [86]. Carbon dioxide has been named as a "fatal" by-product of the HAS [91] on modified methanol catalysts. This effect is explained by assuming that water is the true inhibitor of the HAS instead of CO_2 [92] because of its competition with C_1 -oxygenated intermediates for adsorption on the catalyst active sites [4,49,93] and can even cause irreversible deactivation [49].

Above 723 K, some oxygenates will not be stable enough and will decompose, which sets an upper temperature limit to the synthesis of alcohols [10], even though the productivity is enhanced. The energy costs for the reaction become higher and the deactivation of the catalysts will also be faster at a higher reaction temperature. Catalyst deactivation due to sintering of copper crystallites limits the maximum temperature of Cu-based systems to 593 K [4,43].

At low temperatures, the currently available catalysts show high methanol selectivities because the methanol equilibrium is closely approached during HAS [89]. Temperatures in the range 560-583 K is adequate for obtaining high production

of C₂-C₃ alcohols. Also, in this temperature range the formation of undesired side-products primarily, hydrocarbons is minimised.

The concentration of methanol in the products grows quadratically with total pressure due to its equilibrium, while the concentration of higher alcohols exhibit a weaker dependence resulting from the kinetics of the HAS reaction [94]. High pressure is beneficial for a higher alcohol-to-hydrocarbon ratio since the productivity to hydrocarbons increases to a lesser extent than that of higher alcohols. The thermal stability of various oxygenates also increases with pressure [6].

Higher gas hourly space velocity means a shorter contact time. It is a common observation that lowering the gas hourly space velocity can enhance the selectivity to higher alcohols. Although an increase of gas hourly space velocity increases the selectivity, the conversion may be lowered [4]. This has been interpreted as an indication that the formation of alcohols takes place consecutively beyond the formation of methanol. This indicates that methanol formation is fast compared to HAS [6].

Decreasing the H₂:CO ratio below the stoichiometric value 2:1 [43,49] will favour CO insertion and C-C chain growth. This leads to increased production of higher alcohols and/or hydrocarbons but it also increases coke formation [6] and can diminish the activity [69].

Carbon dioxide in the gasfeed causes greater amounts of water to be produced due to the equilibrium of the reverse WGS reaction [4]. Carbon dioxide inhibits CO hydrogenation [95] and water inhibits CO₂ hydrogenation [96]. Steady state conditions experiments at 45 bar and 473 to 573 K revealed that CO and H₂O are the only products present when CO₂ and H₂ were fed on an ICI Cu/ZnO/Al₂O₃ catalyst [97].

Alcohols have been added to the feedgas and resulted in significant increases in the yields of some alcohols [98]. In general it was found that C_n addition increased C_{n+1} and some C_{n+2} yields. It is possible that the lower alcohols maybe recycled in an industrial situation, thus increasing subsequent higher alcohol yields. Ester injection into the $H_2:CO$ feed stream produced results parallel to those obtained upon injection of the corresponding alcohols [92]. Isopropylamine in the feedgas reduces the formation of alcohols whilst unaffected the hydrocarbon activity [99].

1.4. Mechanism for Higher Alcohol Synthesis

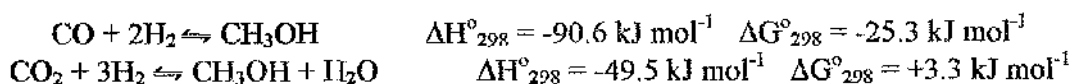
Early mechanistic ideas were based on HT methanol-based catalysts. Frohlich and Cryder [100] and Graves [101] ascribed the formation of higher alcohols to the condensation of lower alcohols. Morgan [102] went into greater detail describing the formation of alcohols through a series of aldol condensation reactions starting with methanal condensing to glycoaldehyde and proceeding through successive condensation, dehydration and hydrogenation reactions to higher alcohols. Almost 30 yrs later, Natta *et al* [10] proposed a series of reactions involving CO insertion into an alkali alkoxide species to give the next higher carboxylate, which is then reduced to the alcohol.

1.4.1 Proposed Mechanisms for the Modified LT Methanol synthesis catalysts

The first significant mechanism involved the hydrogenation of CO into methanol via a formyl or formate and methoxy intermediate species [10,103]. Klier *et al* [36] assumed that the role of CO₂ was that of an oxidant, maintaining the active centre in the Cu⁺ state, which agreed with results by Apai *et al* [104]. Increasing the carbon dioxide concentration to 10 %, it was viewed as a retardant [105].

In 1987, Chinchin *et al* [106] corrected the dismissal of early Russian work [107-109] by conducting radio-labelled experiments under realistic industrial conditions and concluded that the carbon source from the methanol came from CO₂ instead of CO as originally thought. This hypothesis continues down to parts per million (ppm) levels of carbon dioxide [106]. A distinct maximum of carbon to methanol conversion is observed at about 2 % CO₂ in the make-up gas [105].

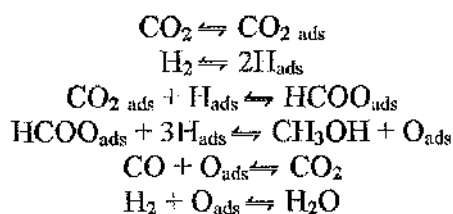
Western scientists had dismissed the Russian work [107-109] as it appeared to be too energetically costly to break the $\sim 116 \text{ kJ mol}^{-1}$ C-O bond in CO₂.



The carbon dioxide itself promotes the change in copper surface by being responsible for the extent of the partially covered adsorbed oxygen surface [110,111]. The extent of coverage is determined by the CO:CO₂ ratio in the reacting gas mixture [22,110,112] with an average of 0.3 of adsorbed oxygen present on the surface of a typical industrial catalyst under steady state conditions [113]. In pulse flow microreactor experiments conducted by Jackson and Brandreth [114], steady state production was not achieved until at least 1 hr after start-up with a considerable delay of between 15-25 mins before a significant production of methanol was observed.

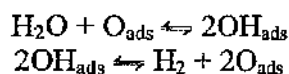
Gaseous hydrogen reacts with the copper surface to attain adsorbed hydrogen atoms, with carbon dioxide being coadsorbed [115]. These react to form a bidentate formate intermediate species on the preferential copper metal surface [116]. The symmetrical [117] and inclined [118] formate species is the most stable and the longest lived intermediate species on the copper surface [115]. This reaction takes place on the copper rather than the support, as the rate of hydrogenation is faster due to the lower energy pathway [119]. The reaction continues by the hydrogenolysis of the formate intermediate to methanol, with the addition of the first hydrogen being the rate-determining step of the reaction [116].

A simplified schematic of the reaction is shown below



This sequence goes through hydrogenation steps of dioxymethane and methoxy species [28,116] but with hydrogen activated on a site different to metallic copper [120]. The mechanism on ZnO proceeds through a similar formate species, as formed on copper, from a carbon dioxide containing feedstock [116].

The formation of methanol from carbon dioxide leaves an extra adsorbed oxygen on the surface, which can either be removed or reacts with hydrogen and completes the WGS reaction. Single crystal studies have shown [113] that the adsorbed oxygen can facilitate water dissociation to surface hydroxyls, which then dissociate to give hydrogen and adsorbed oxygen.

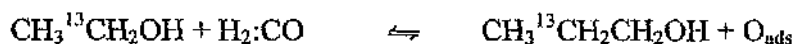


Carbon monoxide must be converted by the WGS reaction [121] to carbon dioxide with any adsorbed oxygen before it can produce methanol when carbon dioxide is included in the feedstock with no carbon-containing surface intermediate common to the methanol synthesis and WGS reaction [106]. Carbon monoxide also maintains the copper in the more highly reduced (more active) state [22] than could be achieved by hydrogen alone. Although methanol can be synthesised from a H₂:CO feedstock on Cu/ZnO/Al₂O₃, the reaction rate is about 100 times slower in absence of CO₂ and also the catalyst deactivates more rapidly [3].

The most widely accepted and acknowledged mechanism for the inherently slow C₁-C₂ step was proposed by Nunan *et al* [122-124]. On Cu/ZnO/Al₂O₃ and Cs/Cu-ZnO catalysts, they showed that linear growth is assumed to lead to the formation of ethanol from a C₁ species. They proposed a nucleophilic attack of a formyl species, not methyl formate, on the electropositive carbon of adsorbed formaldehyde or methanol. A similar mechanism is stipulated for promoted catalysts [123].

Independently, Elliott [41] concluded a similar hypothesis to Nunan *et al* [122-124]. Further work by Elliott [125] concluded that there must be a common intermediate, which leads to the formation of both methanol and ethanol with ethanol being produced directly from both methanol and CO [126]. Smith *et al* [127] added that the reaction proceeds via an S_N2 reaction between formaldehyde and an alcohol (not an aldehyde as in aldol condensation) in which the OH group of the alcohol is the leaving group.

Two mechanistic routes dominate the formation of C₂₊ alcohols. Over an unpromoted Cu/ZnO catalyst, the dominant carbon chain growth process is by a linear insertion chain growth mechanism [123].



However, carbon chain growth over a Cs-promoted Cu/ZnO catalyst is dominated by β-carbon addition wherein the adding C₁ intermediate retains its oxygen [123].



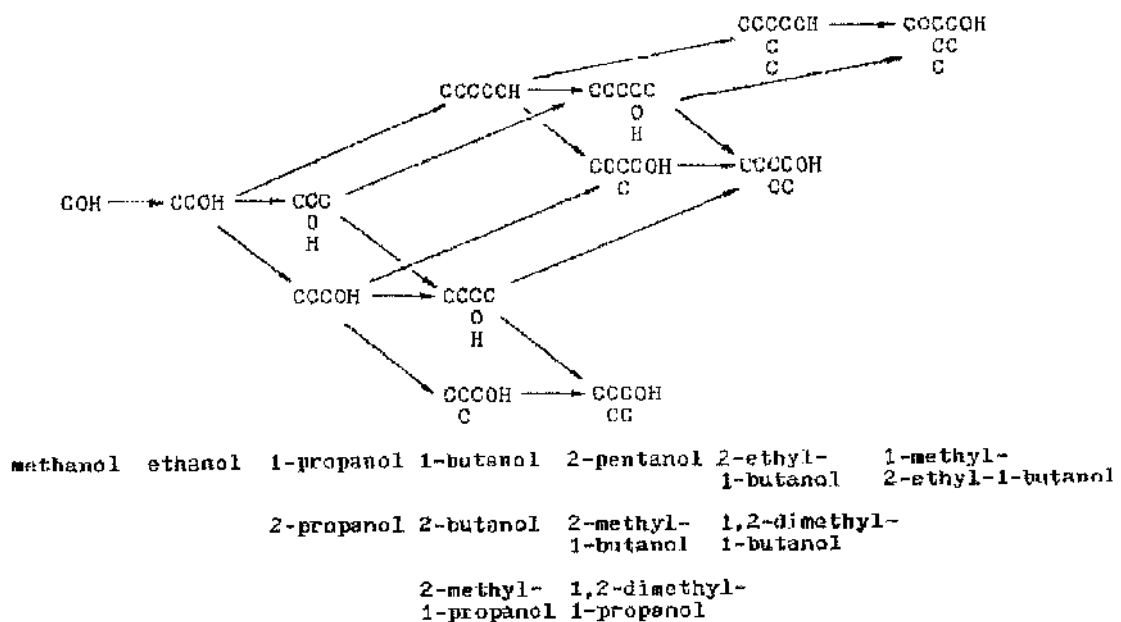
This mechanism was termed “aldol coupling with oxygen retention reversal” [123]. The term “oxygen retention reversal” is to indicate that the oxygen of the formaldehyde remains in the final product, whereas the oxygen of the growing intermediate in the normal aldol condensation reaction remains in the final product. This reaction is apparently specific to the presence of a caesium salt dopant [4]. The key to the selectivity to the products of the reverse or normal pathway is to be sought in a mechanism for removal of one of the two oxygens of the 1,3-ketoalkoxide intermediate [128,129].

The normal aldol condensation reaction appears faster than the reverse step when proceeding from a C₃ species to a C₄ species on both unpromoted and promoted types of catalysts [130].

Smith *et al* [127] later extended the mechanism. 2-methyl-branched primary alcohols are formed by an aldol condensation in which an oxygenated C_1 species adds to the β -position of an aldehydic C_n (β) and subsequent dehydration and hydrogenation. These authors suggest that β -addition is faster than linear growth; they consider that the addition of a C_1 species to the α -position of a growing alcohol is unimportant, as this will lead to secondary alcohols.

Due to the complexity of the higher alcohol synthesis, Smith and Anderson [43,98] further examined the synthesis of alcohol mixtures and they proposed the reaction network shown in Figure 1.4.1. This scheme was based on an earlier mechanism suggested by Graves [101], which depended on the following ideas:- i) two lower alcohols condense to give a higher alcohol, thereby losing H at either the α - or β - position, the loss of H at the β -carbon being faster, ii) the rate of loss of hydrogen from methanol is slower than that from a β -carbon position and iii) secondary alcohols react by losing OH instead of H.

Figure 1.4.1. Smith and Anderson [98] proposed reaction network.



Smith and Anderson [43,98] added the following proposals, iv) addition does not take place at a CH group, v) the species added consist of 1 or 2 C-atoms, vi) an intermediate containing 2 C-atoms does not add to the α -position of a growing chain, vii) the chain growth reactions are irreversible and have rate constants which are independent of the chain length of the growing intermediate and viii) the reactions are first order in the concentration of the growing intermediate.

Further proposals to the reaction scheme were added by Klier *et al* [127], ix) further growth of 2-methyl branched alcohols by linear growth will either be slow or cannot occur, an assumption also made by Mazanec [131], x) the reaction rates are dependent on the chain length of the growing chain and xi) β -addition of a species containing 3-C atoms may also occur.

1.4.2 Proposed Mechanisms for the Modified HT Methanol Catalysts

A mechanism involving aldol condensation over copper-free unpromoted and promoted catalysts has been adopted for the C_1 - C_2 step by other authors [94,132]. Riva *et al* [132] suggested that the adsorption of methyl formate might give rise to the formation of the C_1 species involved in chain growth; methyl formate might also rearrange to give acetic acid, which upon reduction by hydrogen leads to ethanol.

Riva *et al* [132] found that for subsequent chain growth (C_{2+} step) takes place through insertion of a C_2 unit in the β -position of a C_n unit as methanol and methanal were added to the $H_2:CO$ mixture resulted in no significant change in the product distribution. The presence of common carboxylate intermediates was also found for the formation of methyl esters as well as alcohols.

Berretta *et al* [133] found that not only do condensation of linear precursors with a C₁ intermediate occur, they also form via normal aldol condensations with C₂₊ chain growth. They also found with C₃₊ reactions, that the following reactions occurred:- reversal and normal aldol condensations, ketonisation reactions, and reversal and normal α -additions. According to Lietti *et al* [134-137], the mechanism of chain growth leading to C₃₊ primary alcohols involves a series of crossed aldolic condensations of aldehydic molecules.

The chemistry involved in the higher alcohol synthesis over LT and HT modified methanol catalysts appear to be basically the same.

1.4.3 Proposed Mechanisms for the Modified Fischer-Tropsch and Group VIII metal-based catalysts

Since the 1970's, the predominant opinions [138,139] regarded the FT mechanism as involving surface methylene/carbene (CH₂) units with CO insertion accounting for the formation of oxygenates [139].

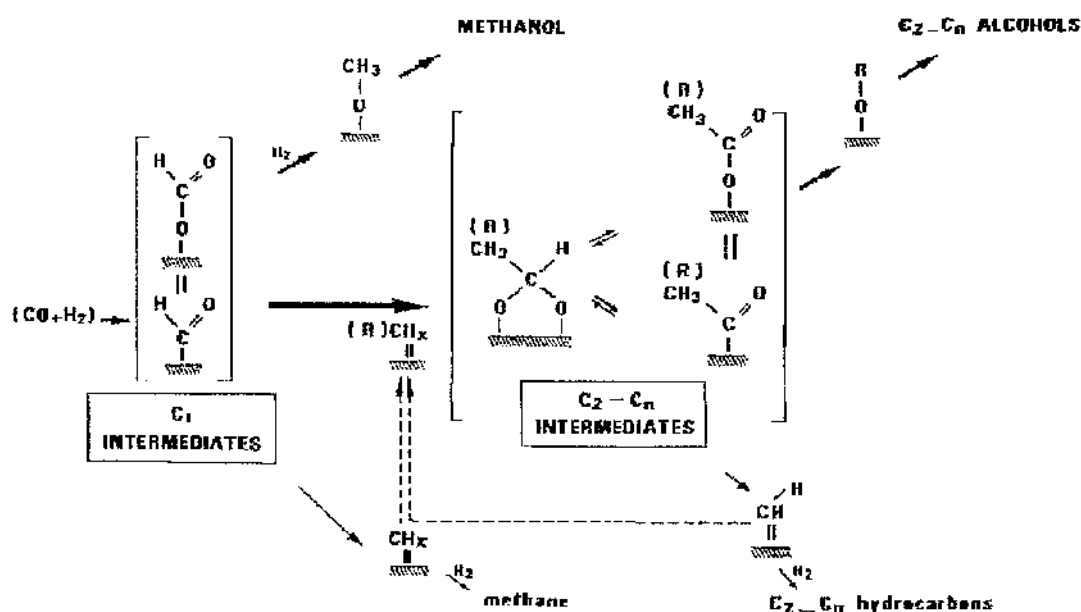


where * is a vacant surface site. The comprehensive mechanism was published in 1993 [140]. The first step in chain initiation is the chemisorption of CO, followed by "initial" chain growth by formation of chemisorbed ethylene or metallacyclopropane. The next CH₂ addition at either of the 2 equivalent C-M bonds results in cyclobutane, which arranges to the metallacyclopropane structure.

In many cases, high CO and water concentrations during FTS inhibit secondary reactions of hydrocarbons into alcohols [141] with secondary hydrogenation of α -alkenes often competing effectively with readsorption and chain initiation.

For higher alcohol formation, Kiennemann *et al* [142] confirmed the earlier mechanisms [138,139] concerning the initial slow C_1 - C_2 step and found that the alcohols are formed through the reaction of a hydrocarbonated species and a C_1 oxygenate entity (formyl or CO). This can be formed on the copper surface with a carbene (or hydrocarbon) entity located on Co or at the Co/Cu interface. The mechanism is shown in Figure 1.4.2 [143]. It is apparent that the higher alcohol synthesis mechanism is intrinsically different from the mechanism of the FT reaction [144].

Figure 1.4.2. The proposed reaction mechanism on Cu/Co based catalysts [143].



Subsequent C_2 oxygenates are not involved in the formation of higher primary oxygenates as it seems that the formation of alcohols is the result of a coupling reaction of C_xH_y group with a C_1 oxygenated intermediate (CO or formyl) with acyls as possible reaction intermediates. Others oxygenates are by various chain termination reactions or CO insertion into the proposed metallocyclopropane

intermediates to yield aldehydes, alcohols or methyl ketones. Carboxylates do not take part in the chain growth [142].

Net termination to oxygenates depends only weakly on carbon number and are independent of bed residence times [58]. ASF selectivities and kinetics govern product distribution and choosing process conditions can vary the molecular weight and/or catalyst to achieve a given amount of chain growth but a wide distribution of products other than methane is inherent [3]. The maximum wt % of C₂-C₄'s is 56 %, 47 % C₅-C₁₁'s and 40 % C₁₂-C₁₇'s. Most attempts to circumvent the selectivity limitations have met with failure [145].

1.4.4 Proposed Mechanisms for other catalysts

Ichikawa *et al* [146] proposed that C₂ oxygenates such as ethanol, acetaldehyde and acetates over Rh-based catalysts come from acetyl species (CH₃CO), formed by a subsequent CO insertion with surface methyl/methylene (CH₃/CH₂), which were derived from CO dissociation.

Both Mazanec [131] and Santiesteban *et al* [147] showed that, on unpromoted and promoted catalysts, the formation of ethanol over MoS₂-based catalysts occurs through CO insertion into a methyl intermediate bound to the surface to form an acyl precursor, which can be hydrogenated to produce ethanol. The methyl intermediate over these catalysts is derived from an oxygenated species. The mechanism of chain growth to form C₃ and C₄ alcohols is similar to that of ethanol synthesis.

For Cu/MgO/CeO₂ based catalysts, pathways involving coupling reactions of surface formate and methyl formate formed directly from CO account for the formation of the initial C-C bond in ethanol from H₂:CO on K-Cu/MgO/CeO₂. Methyl acetate is a likely precursor to ethanol [148].

One pathway for ethanol to propan-1-ol chain growth involves carbonylation of ethanol by CO [148] without requiring the intermediate formation of acetaldehyde [129]. Subsequent chain growth occurs by both normal and oxygen retention reversal types of aldol condensation occurring on K-Cu/MgO/CeO₂ catalysts. These pathways are unavailable for ethanol formation from two methanol molecules, because methanol lacks the two α -hydrogens required for aldol-type condensation pathways. Mixtures of alcohol dehydrogenation and condensation reactions are involved in isobutanol formation [129].

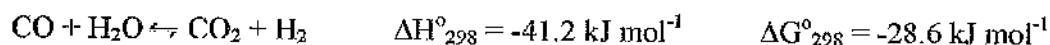
On ZnO and ThO₂ catalysts, C-C bond formation is by CO insertion into metal-carbon bonds in adsorbed formaldehyde species [131].

A reaction scheme proposed by Falter [149] over a Zr-Zn-Mn-Li-Pd-K catalyst includes an aldol-type growth, with the formation of ethanol being formed from methanol via DME. The mechanism proposed over carbides (CaC₂, Na₂C₂, CeC₂ and LaC₂) involved coupling with the carbide and a C₁-aldehydic intermediate [150].

1.5 Other Reactions

1.5.1 Water Gas Shift Reaction

Industrially, two different catalysts are used for the WGS reaction, both with dissimilar working conditions.



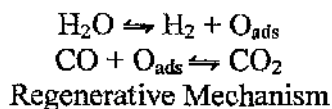
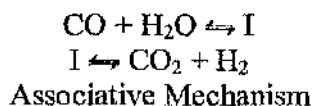
The LT shift reaction takes place on a Cu/ZnO/Al₂O₃ catalyst with a ratio of 33:34:33, a temperature of 483-513 K [151], 25-35 bar pressure and a GHSV of 3600 hr⁻¹ [152].

The operating conditions and catalyst are similar to those found for the LT methanol synthesis. As a consequence of this similarity, considerable work has been published on the morphology, composition and the oxidation state of the individual components. However, the exact catalyst phases used during the reaction remain controversial and also still a matter for debate, akin the methanol synthesis, with similar arguments being proposed.

The HT shift reaction, Fe₃O₄/Cr₂O₃ (90-95 % Fe₃O₄) is used with working conditions of 583-723 K using a pressure of 25-35 bar [153] with feed gas containing 3-75 % of CO [154] and a GHSV of 400-1200 hr⁻¹ [155]. The optimum chromium concentration is 14 wt % [156] but this is reduced industrially to 8-10 wt % to increase the catalyst stability, as the main purpose of the chromium is to retard sintering and maintain the active surface area of the supported iron oxide.

1.5.2 The Water Gas Shift Mechanism

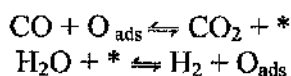
Two contrasting mechanistic pathways have been proposed based on either (a) an associative mechanism where I is an intermediate or (b) a regenerative mechanism.



Recent mechanisms have been proposed for both the HT [157] and LT [113,158] WGS reactions with both processes occurring by a regenerative mechanism. The concept of a regenerative mechanism was first proposed by Kul'kova and Temkin [159] and also fits experimental data obtained by Boreskov *et al* [160].

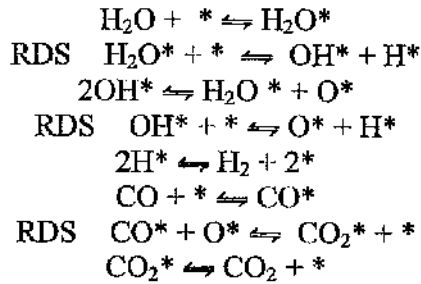
An associated mechanism for copper-based catalysts was originally proposed by proposed van Herwijnen *et al* [161,162], the reaction occurring via a surface formate. They dismiss a regenerative mechanism on the basis that neither CuO nor Cu₂O could be formed under reaction conditions from copper metal and steam, which is used in the reduction process [163].

The recent regenerative mechanism for the LT shift reaction [113] consists of adsorbed oxygen, which acts a promoter as well as a reaction intermediate, which facilitates the chemisorption and subsequent dissociation of both water (via hydroxyls) and carbon dioxide.



where * is a vacant surface site. The probable rate determining steps under most reaction conditions are the dissociation reactions [106,164,165]. No common carbon intermediate for both methanol synthesis and WGS reaction are observed [106].

Nakamura *et al* [164] claim to provide strong evidence for a surface redox mechanism involving oxygen adatoms with a revised and more detailed mechanism given below [166] but stipulates that this may only occur on copper.



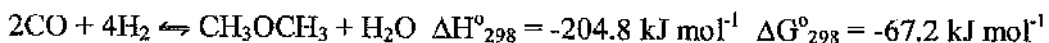
where RDS are the rate determining steps. Au and Roberts [167] showed that water dissociation into hydroxyls is promoted by adsorbed oxygen on copper but on clean Cu(110) and Cu(111) facets dissociation did not occur.

The reverse water gas shift (RWGS) reaction according to Nakamura *et al* [162] occurs mainly over metallic copper with Cu(110) rather than Cu(111) facets [17], suggesting a structure sensitive reaction, which agrees with early Chinchén and Spencer [168] work. However, there is disagreement with this theory [169], although the method by Ginés *et al* [169] were at ambient pressure and with a different reactor mixture than those used under industrial conditions.

Decades later after the first mechanisms were proposed a wholly satisfactory and universally accepted mechanistic description of the WGS reaction fails to exist. The reaction appears to be considerably pressure dependent, which diminishes the significance of results and assumptions based on non-industrial conditions.

1.5.3 Ethers

Ethers production usually occurs in the presence of an added acid catalyst.



Dawood [170] found DME to be a product of methanol decomposition over a Cu/ZnO/Al₂O₃ catalyst. Therefore, any acidity of normal methanol synthesis catalysts, perhaps due to trace impurities or acidic support material would be expected

to produce some DME. Over the commercial ICI methanol catalyst, any acidic sites on alumina containing phases are neutralised, probably by ZnO [37].

Matulewicz [171] formed DME from a $H_2:CO$ mixture via a reaction intermediate in common with the formation of methanol with the initial rates being linearly dependent on methanol concentration and the contact time. Carbon dioxide greatly suppressed the rate of DME formation. However, the alumina content in the catalyst was 76 %, which probably explains the unusually high DME quantities produced.

1.5.4 Aldehydes and Ketones

Aldehydes and ketones are formed by incomplete hydrogenation of straight and branch alcohols respectively.

Aldehydes and ketones proceed in both the normal and the reverse crossed aldolic-type condensations modes [172]. Higher aldehydes are produced in the first case and ketones are produced in the latter during condensations of 2 aldehydes; condensations involving ketones always result in the formation of higher ketones. Ketones showing lower reactivity than aldehydes.

Elliott and Pennella [173] confirmed that $2n$ ketones are produced by aldol-type condensation, with the $2n-1$ ketones being generated by aldol condensation of the aldehyde via a surface carboxylate.

to produce some DME. Over the commercial ICI methanol catalyst, any acidic sites on alumina containing phases are neutralised, probably by ZnO [37].

Matulewicz [171] formed DME from a $H_2:CO$ mixture via a reaction intermediate in common with the formation of methanol with the initial rates being linearly dependent on methanol concentration and the contact time. Carbon dioxide greatly suppressed the rate of DME formation. However, the alumina content in the catalyst was 76 %, which probably explains the unusually high DME quantities produced.

1.5.4 Aldehydes and Ketones

Aldehydes and ketones are formed by incomplete hydrogenation of straight and branch alcohols respectively.

Aldehydes and ketones proceed in both the normal and the reverse crossed aldolic-type condensations modes [172]. Higher aldehydes are produced in the first case and ketones are produced in the latter during condensations of 2 aldehydes; condensations involving ketones always result in the formation of higher ketones. Ketones showing lower reactivity than aldehydes.

Elliott and Pennella [173] confirmed that $2n$ ketones are produced by aldol-type condensation, with the $2n-1$ ketones being generated by aldol condensation of the aldehyde via a surface carboxylate.

1.6 Precursor and Catalyst Form

Most of the catalyst precursors formed in this study are based on a hydrotalcite (HTlc) template. Hydrotalcite ($Mg_6Al_2(OH)_{16}CO_3 \cdot 4H_2O$) belongs to a class of anionic clays and is the generic name for many other isostructural compounds, which are both natural and synthetic in origin. These hydrotalcite-like or double sheet compounds have the general formula, $M(II)M(III)A-HT=[M(II)_{8-x}M(III)_x(OH)_{16}]^{x+}(A^{n-})_{x/n} \cdot mH_2O$, where M(II) and M(III) represent metal 2+ and 3+ ions respectively, A represents an anion.

Structurally hydrotalcite materials consist of brucite-like ($Mg(OH)_2$) metal hydroxide layers [174]; where octahedra of M^{2+} ions (6-fold co-ordinated to -OH) share edges and form infinite sheets (Figure 1.6.1). In hydrotalcite materials, M^{2+} ions are isomorphously and randomly substituted by M^{3+} ion generating a positive charge in the hydroxylated sheet. To achieve electric neutrality the net positive charge is compensated and balanced by CO_3^{2-} anions, which lie in the interlayer region between 2 adjacent brucite-like sheets. The hydroxylated sheets are stacked on top of each other and are held together by hydrogen bonding [175] as in gibbsite ($Al(OH)_3$) [176]. According to the literature, pure hydrotalcite structures can be synthesised when x, the mole ratio of M^{3+} ions, falls in the range $0.1 < x < 0.5$ [177,178], although other research [175] restricts this range further $0.19 < x < 0.34$.

Aluminium containing HTlc and HTlc-like structures have rhombohedral symmetry with 3 metal hydroxide sheets in the unit cell [179]. The unit cell parameters may be described by; a, b and c^1 , where a and b are independent of anion nature and $c = 3c'$, where c' is the thickness of one brucite-like sheet and the interlayer between two adjacent brucite-like sheets. This variable distance, c' , is

¹ Rhombohedral system, $a \neq b \neq c$, $\alpha = \beta = \gamma = 90^\circ$, Hexagonal system; $a = b \neq c$, $\alpha = \beta = \gamma = 90^\circ$.

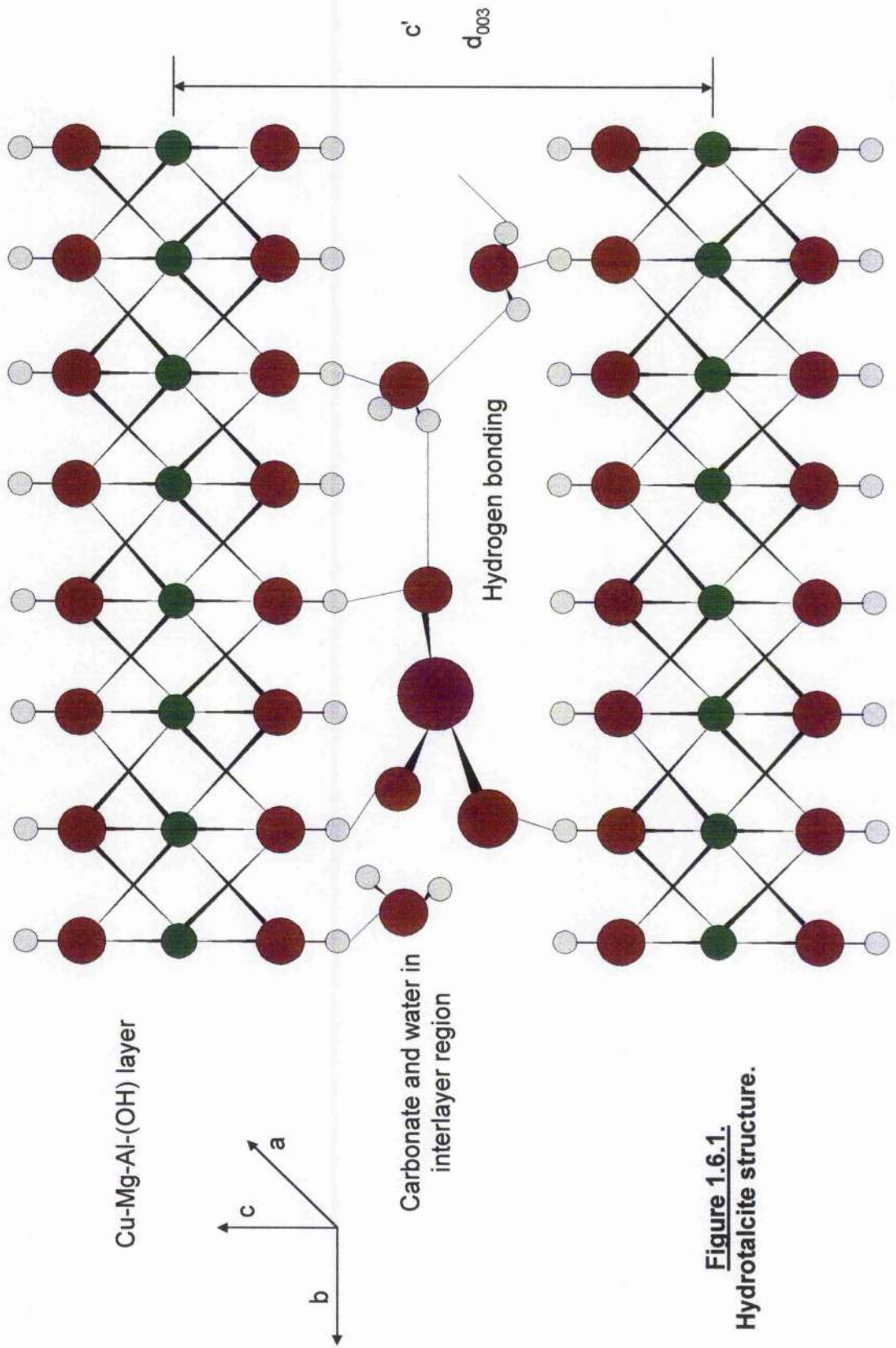


Figure 1.6.1.
Hydrotalcite structure.

dependent on anion size [180], the x value [181] and on the degree of hydration of some anions [182] and for one metal composition, in this case, hydrotalcite itself (Mg:Al 3:1), the c-axis length has been found to vary in the range of 7.6-11.1 Å [183] depending on the anions included in the interlayer.

A hexagonal hydrotalcite structure can also occur and is thought to be the high temperature version of the rhombohedral hydrotalcite. The compound is harder to synthesis than the more common rhombohedral and is favoured by transition metals other than copper [184].

For x values lower than 0.33 in Mg and Al hydrotalcites, the Al octahedra are not neighbouring [185] due to Columbic forces, however, this leads to a high density of Mg octahedra in the brucite-like sheet, acting as nuclei for the formation of Mg(OH)₂. For higher values of x, the increased number of neighbouring Al octahedra leads to the formation of Al(OH)₃ [179].

In copper containing HTlc-like structures when the Cu²⁺/M(II) ratio is ≤ 1, the Cu²⁺ cations in the brucite sheet are separate from one another, and copper arranges in an undistorted octahedral co-ordination typical of the brucite structure. When the ratio is > 1, the Cu²⁺ ions can be situated in near-lying octahedra, and the formation of a copper compound with distorted octahedra (Jahn-Teller distortion) is prepared [186]. Copper containing HTlc-like structures require another bivalent cation species present to form a HTlc structure [187], as copper preferentially forms malachite [184] and other mono and binary compounds [188].

The easily exchangeable anions and water molecules are randomly located in the interlayer region with their respective oxygen atoms closely around the central symmetry, which passes through the hydroxyl groups of the adjacent brucite-like sheet [189]. These hydroxyl groups are bonded to the CO₃²⁻ groups directly or via

intermediate H_2O through hydrogen bridges: $\text{OH}-\text{CO}_3-\text{OH}$ or $\text{OH}-\text{H}_2\text{O}-\text{CO}_3-\text{H}_2\text{O}$ [190].

In each case, since the oxygen positions are so near together, only one site is occupied. Three oxygen atoms from three adjacent sets of sites form a carbonate group, with the carbon atom placed in the central position. The interlayer arrangement of hydroxide, nitrate, chloride and carbonate HTlc-like materials is similar [191]. Anion stability decreases in the following order $\text{OH}^- > \text{F}^- > \text{Cl}^- > \text{Br}^- > \text{NO}_3^- > \text{I}^- > \text{CO}_3^{2-} > \text{SO}_4^{2-}$ [192]. Strong hydrogen bonds occur in the carbonate- and hydroxide- containing hydrotalcites [191]. There is essentially no practical limit of anion exchange in the interlayer.

Water molecules are localised in the interlayer region in sites, which are not occupied by the anions. The molecule can assume a tetrahedral configuration by forming hydrogen bonds to other oxygen atoms in nearby sets of oxygen sites, or to OH groups in adjacent brucite-like sheets. Natural hydrotalcite has four water molecules, however, direct measurements of synthetic products usually gives values lower than four, as approximately one third of the interlayer water in carbonate and nitrate hydrotalcites can be lost between room temperature and 373 K [182]. Miyata [192] considers the weight loss below 373 K as due only to physisorbed water. The temperature at which interlayer water is lost is shifted towards lower temperatures as the value of the mole ratio of $x (\text{M}^{3+})$, decreases [192,193]. Water like interlayer anions can be eliminated without destroying the structure.

Preparation of the HTlc structures can be done by several methods 1) co-precipitation or precipitation by increasing pH, 2) hydrothermal synthesis and treatments or 3) exchange methods. The main preparation technique is co-precipitation as it is simple and inexpensive but problems may arise as different

ageing times or hydrothermal treatments of a precipitate can give rise to dissolution of metal cations. The following order of importance has been observed for the preparation of dry (co-precipitated) precursors : ageing of precipitate > precipitation temperature > pH > total metal ion concentration > drying temperature [194]. The pH is the most common variable for preparation but it is necessary to precipitate at higher than, or equal to, the pH at which the more soluble hydroxide precipitates. Preparation at low supersaturation, which is involved in the study described in this thesis, is at constant pH, and is controlled by the slow addition of base (KOH, NaOH, NaHCO₃) to the appropriate metal containing solution. At low supersaturation conditions, the rate of crystal growth is lower than the rate of nucleation, as a result, the precipitates are more crystalline compared to high supersaturation. At a very alkaline pH and at elevated temperature, the HTlc-like structure decomposes forming CuO [40] and can also influence the aluminium solubility [187].

During calcination, exiting steam and carbon dioxide escape through holes in the crystal surface, which then appear as small, fairly regular spaced craters [195]. It appears that the interlamellar forces in HTlc structures are sufficiently strong, even during heating, so that interstitial venting through the metal oxide layers is not possible. As a result of this, the sample becomes more basic, the surface area values increase and changes in the crystal morphology take place. The sample forms a homogeneous mixture of oxides with very small crystal size. The interaction among the elements in the anionic precursor determines the CuO crystal sizes after calcination [184].

The “memory effect” allows the reconstruction of the original layered structure. This can occur after mild calcination conditions of the precursor by contact with a water solution containing and subsequent adsorption of various anions [180] or

simply upon exposure to the air [196]. This property is strongly dependent on the heating temperature ($T < 723\text{-}823\text{ K}$) [197] and may be interpreted by taking account of the mechanism of thermal decomposition of HTlc precursors [180]. Above 1273 K, most hydrotalcites form a spinel structural phase [198].

Heterogeneous catalysis can utilise the properties of calcined HTlc structures in industrial processes, for example, industrial LT methanol synthesis [14,36,199] and higher alcohol synthesis [200].

1.7 Poisoning and Deactivation

Decrease in catalytic activity occurs usually by either chemical or thermal means. The two most common chemical means is by either poison adsorption or coking. Sintering is a thermal effect, which results in the loss of surface area. Copper is very susceptible to both of these problems, both of which are well known with the industrial LT methanol synthesis catalyst [37].

Poisoning reduces the reactive copper surface area either pore or site blockage thus lowering the activity. Copper-based catalysts can be easily poisoned by S [201], Cl [202], Ni and Fe carbonyl compounds [3,203].

Sulfur and chlorine poisoning on a metal surface during CO hydrogenation results in first, the strongly adsorbed poison physically blocking sites on the metal surface. By virtue of its strong chemical bond, it electronically modifies its nearest neighbour and perhaps its next nearest metal atoms, thereby modifying the surface atoms abilities to adsorb and/or dissociate reactant molecules. A further effect may be surface restructuring, possibly causing dramatic changes in catalytic properties, especially for a reaction sensitive to surface structure. In addition, the adsorbed poison blocks access of adsorbed reactants to each other and finally prevents or slows surface diffusion of adsorbed reactants [204].

The poisoning by sulfur is avoided by purification of the synthesis gas, as it is harmful down to ppm levels [37]. Chlorine compounds are purified to an acceptable level of 5 ppb (parts per billion) [205]. The presence of Ni and Fe metals can promote exothermic CO hydrogenation to methane and heavier hydrocarbons respectively. Carbon steel and rust in the feed system are especially to be avoided, since in contact with high pressure CO they readily form iron carbonyls [206] but a K-doped

γ -alumina trap maintained at 523 K is used to decompose iron carbonyls [207].

Regular purging of the catalyst can reduce these problems.

Deactivation is the result of the decrease in catalyst activity for reasons connected with the catalyst itself, normally as a result of sintering. Sintering can occur by causing 1) loss of catalytic surface due to crystallite growth on the catalytic phase, 2) loss of support area due to collapse and of catalytic surface due to pore collapse on metal crystallites or 3) transformations of catalytic phases to non-catalytic phases [208]. These affects can be generally accelerated by the presence of water vapour [209].

Catalytic deactivation has been extensively studies elsewhere [14,26,210].

2 Aims and Objectives

The main purpose of this study is to investigate the selective formation of higher oxygenates from a synthesis gas mixture using a variety of copper-based heterogeneous catalysts, the latter being chosen as the potential of the production of alcohols, which has previously been reported.

Mono- and bimetallic alumina-supported copper-based catalysts, in particular alkali/alkaline earth-promoted copper-alumina catalysts will be prepared by a co-precipitation method, with the emphasis on establishing preparation conditions which lead to reproducibility in catalyst structure and hence, hopefully, in catalytic activity. Full characterisation of the catalysts, both before and after use, will be achieved using thermogravimetric analysis, powder X-ray diffraction, spectroscopy, total surface area measurement by the BET method and copper surface area determinations using nitrous oxide chemisorption/decomposition methods.

Catalytic activities and selectivities will be determined for the reaction of synthesis gas mixtures ($H_2/CO/CO_2$) in a continuous flow microreactor, equipped with on-line gas chromatographic analysis, operating at moderate temperature and pressure with the following objectives:

1. To determine the overall activity of each of the catalysts in terms of conversion of the reactants.
2. To determine the product distribution and hence the selectivity of the catalysts for the formation of higher oxygenate products.
3. To determine the effects of variations in reactor pressure and temperature on both the activity and the product distribution.

4. To examine the effects of additions of methanol to the reactant mixture on the activity and selectivity to higher oxygenate formation.
5. To seek the possible existence of correlations between catalyst structure, activity and selectivity.
6. To determine the influence of the reaction mechanism on the product distribution and selectivity.

3 Experimental

3.1 Introduction

Several catalysts were prepared during this study, all initially by co-precipitation. They were subsequently characterised and tested for activity in the synthesis of higher alcohols.

Various methods of characterisation were utilised for samples in the liquid, solid and gaseous states. Differential Thermal analysis (DTA), Atomic Absorption Spectroscopy (AAS), Temperature Programmed Reduction (TPR), nitrous oxide chemisorption, X-ray powder diffraction (XRD) and BET surface area measurements were conducted at Glasgow. Elemental analysis, X-ray Fluorescence (XRF) and Titrimetry were carried out at Kvaerner Process Technology, Thornaby. Several DTA samples were conducted at the University of Edinburgh on a Stanton Redcroft machine. Three XRF samples were conducted on the Energy Dispersive X-ray (EDX) machine connected to the Electron microscope at the University of Glasgow.

Catalytic testing was investigated using a purpose built gas phase high pressure microreactor with on line gas chromatographic capabilities.

3.2 Materials

3.2.1 Gases

Three gases were used in catalytic testing experiments: carbon monoxide, carbon dioxide and hydrogen (all B.O.C.) with purities exceeding 99.9 %. Nitrogen (B.O.C.) was used as back pressure for the microreactor experiments. Air and helium (B.O.C.) were used for gas chromatography. The nitrogen, air and helium gases were not purified further.

3.2.2 Liquids and Solids

The chromium (III) oxide (98 %) standard and methanol (99 %) for the microreactor experiments were both supplied by Sigma-Aldrich Chemical Company. Ethanol (99.9 %) was supplied by BDH AnalaR. Copper (II) oxide (97.5 %) and magnesia (97 %) standards were supplied by BDH AnalaR. Aluminium oxide 'C' (99 %) was supplied by Degussa.

3.3 Precursor Preparation

Ranges of precursors were prepared with different metal ratios from 1 mol dm⁻³ nitrate solutions. The metal solutions were copper (II) nitrate hemipentahydrate (98 %, Sigma-Aldrich Chemical Co.), chromium (III) nitrate nonahydrate (99 %, Sigma-Aldrich Chemical Co.), magnesium (II) nitrate hexahydrate (98 %, Avocado) and aluminium (III) nitrate nonahydrate (99 %, Sigma-Aldrich Chemical Co.). These precursors were formed by a low supersaturation co-precipitation technique using various predetermined pH values. The experimental apparatus for precursor preparation is shown in Figure 3.3.1. Mixed metal nitrate solutions and an equimolar solution of sodium hydroxide (99 %, Fisher Scientific) and sodium bicarbonate (99 %, Prolabo (Rhône-Poulenc)) solutions were driven simultaneously by means of peristaltic pumps into a glass vessel at a temperature of 333 K. On completion, the stirred precipitate was aged in the mother liquor for a period of 30, 70 or 140 mins. The suspension was then filtered immediately using 2 L of warm distilled water. Thereafter, the precursors were dried overnight in an oven at a temperature of 378 K. The precursors were placed in the calcination reactor vessel (Figure 3.3.2). Calcination conditions were precursor dependent but all used flowing air at

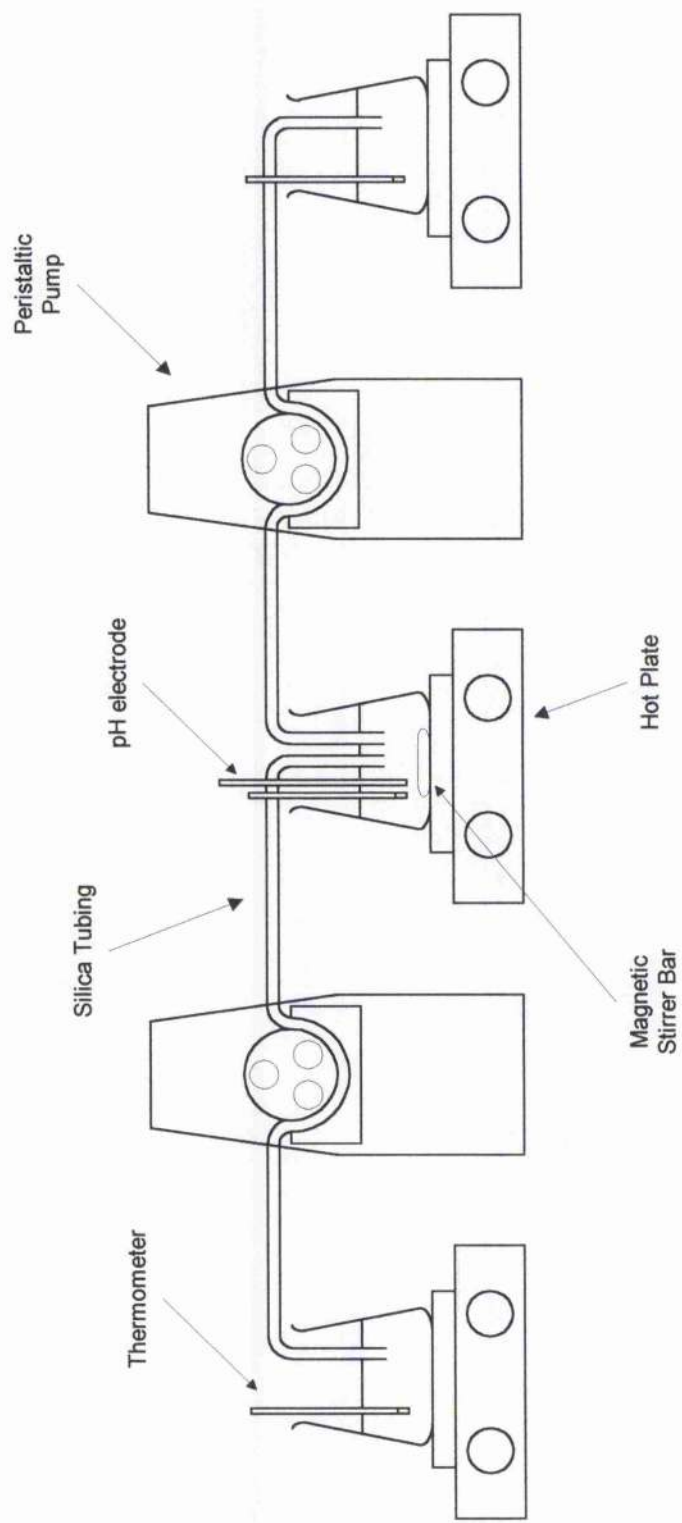


Figure 3.3.1. Co-precipitation Apparatus.

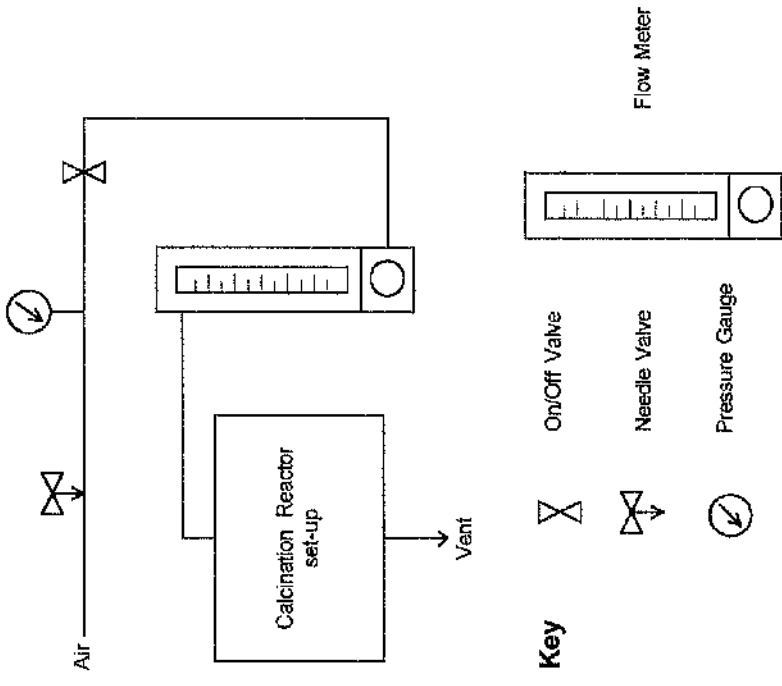


Figure 3.3.3.
Calcination Rig.

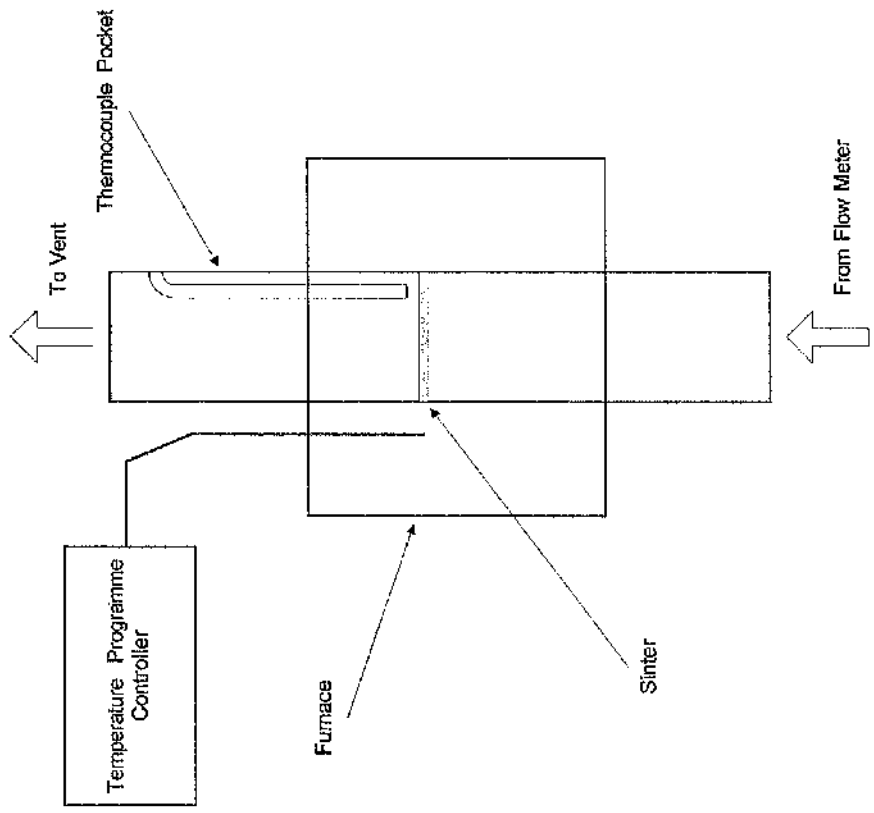


Figure 3.3.2.
Calcination Reactor Set-Up.

30 ml min⁻¹, regulated by the flow meter (Figure 3.3.3). A temperature programmed controller was used for the initial temperature ramp rate of 5 K min⁻¹, and the duration of the calcination at the elevated temperature.

The resultant powder was crushed and sieved into 3 different sizes, between 1000-350 μm, 350-180 μm and below 180 μm. The *in situ* reduction was performed using a gradual temperature increase of 1 K min⁻¹ with every 30 K rise being maintained for 30 mins until 523 K (Figure 3.3.4). At 523 K, the temperature was held stationary for 1 hr before being increased further to the required reaction temperature. A gas composition of 6 % H₂/N₂ at 30 ml min⁻¹ was employed.

These were used as the standard preparation and activation procedures unless stated otherwise.

3.3.1 Cu/Cr₂O₃ (50/50) (Cu_{Cr})

The Cu/Cr₂O₃ catalyst was prepared using equimolar equivalents of 0.1 mol dm⁻³ solutions of copper and chromium containing solutions and an equimolar equivalent of ammonia (99 %, BDH AnalaR) and ammonium carbonate (99 %, Fluka Chemie) as the basic solution [211]. For this catalyst, a pH of 6.2 and an ageing time of 30 mins were used [211]. Calcination was performed at 573 K for 4 hrs. The resultant powder was crushed and sieved into 2 sizes, between 1000-350 μm and below 350 μm. The *in situ* reduction was performed at 583 K for 20 hrs with a gas flow of 18 ml min⁻¹.

3.3.2 Cu/MgO/Al₂O₃ (50/10/40) (Cu_{Mg(10)Al})

A Cu/MgO/Al₂O₃ (50/10/40) catalyst was prepared using appropriate equivalents of copper, magnesium and aluminium containing solutions and an equimolar equivalent of ammonia (99 %, Sigma-Aldrich Chemical Co.) and ammonium carbonate (99 %,

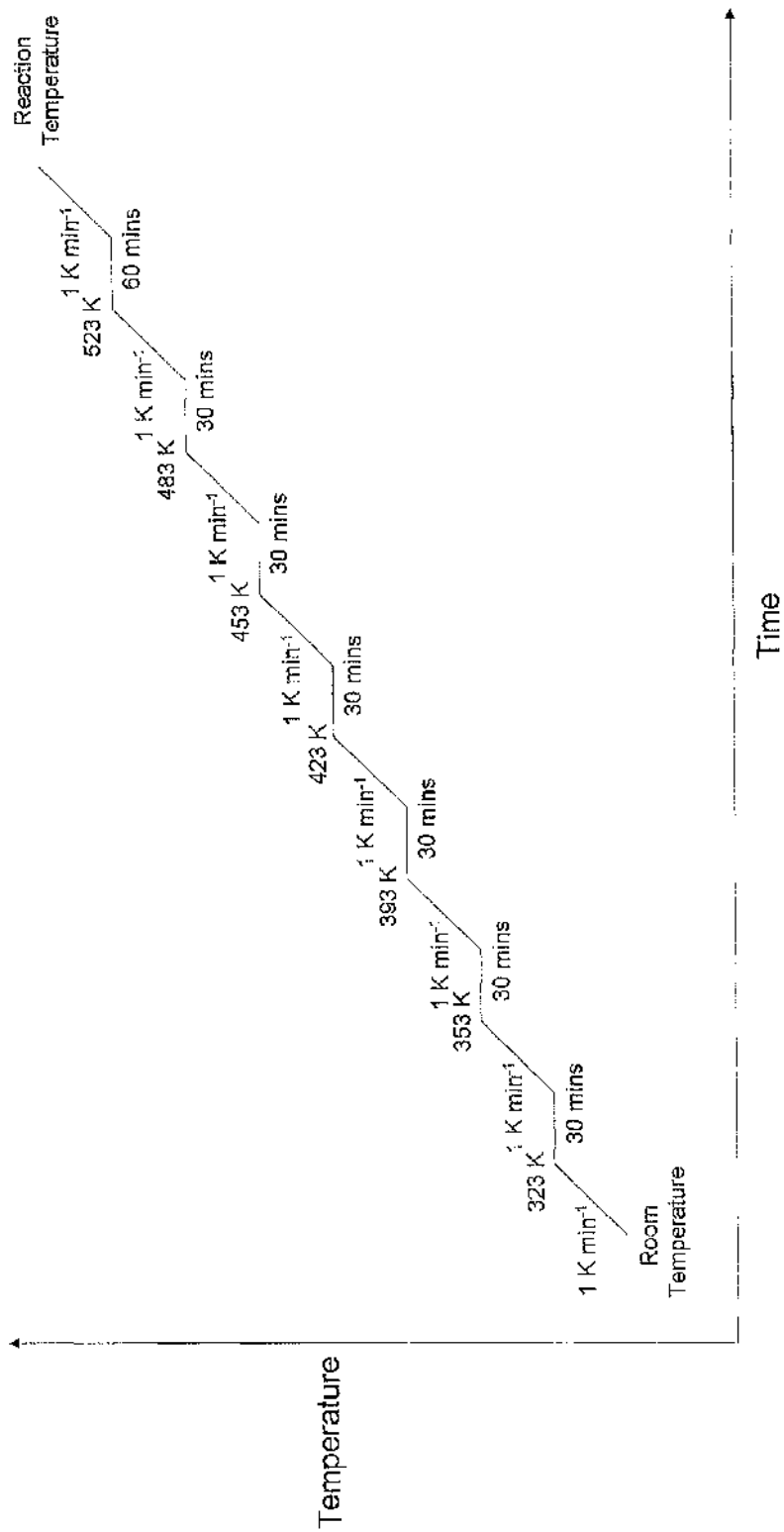


Figure 3.3.4. Reduction Procedure.

Sigma-Aldrich Chemical Co.) as the basic solution at a pH of 7. The mother liquor was aged for 30 mins. Various calcination temperatures ranging from 523 K to 1023 K in 50 K increments were used. These were coupled with lengthening calcination times of 4 to 20 hrs. Two temperatures were decided upon, 623 K and 873 K, both calcined for 12 hrs. For the *in situ* reduction and subsequent reaction, two reduction procedures were applied, initially, 623 K for 12 hrs but this was later substituted by the standard calcination procedure (Section 3.3).

A second preparation under identical pH = 7 conditions was conducted. This was followed by subsequent preparations at a pH of 7.5, 8.25 and 9.5. The second preparation at pH = 7 was calcined at 623 K for 12 hrs.

3.3.3 Cu/MgO (60/40) (Cu_{Mg})

The Cu/MgO samples were prepared using appropriate equivalents of copper and magnesium containing solutions with ageing times of either 30, 70 and 140 mins for the pH = 8 and 9 samples. The preparations at pH = 7 and 10 were subject to an ageing time of 30 mins. A calcination temperature of 623 K for 12 hrs was applied.

3.3.4 Cu/Al₂O₃ (60/40) (Cu_{Al})

Cu/Al₂O₃ catalysts were prepared using appropriate equivalents of copper and aluminium containing solutions at pH = 7, 8, 9 and 10. Ageing times of 30, 70 or 140 mins for the pH = 8 and 9 samples and 30 mins for pH = 7 and 10 samples were applied. A calcination temperature of 623 K for 12 hrs was employed.

Due to the problems of co-precipitation and precursor stability of this catalyst series and the Cu/MgO (60/40) catalyst series, pH values of 8 and 9 were used for later preparations.

3.3.5 Cu/MgO/Al₂O₃ (60/2/38) (Cu_{Mg(2)Al})

Cu/MgO/Al₂O₃ catalysts were prepared using appropriate equivalents of copper, magnesium and aluminium containing solutions at pH = 8 and 9 and aged for 30, 70 or 140 mins. A calcination temperature of 623 K for 12 hrs was employed.

3.3.6 Cu/MgO/Al₂O₃ (60/5/35) (Cu_{Mg(5)Al})

Cu/MgO/Al₂O₃ samples were prepared using appropriate equivalents of copper, magnesium and aluminium solutions for either 30, 70 or 140 mins ageing times at pH = 8 and 30 mins for pH = 9. A calcination temperature of 623 K was tried to stay consistent with the conditions used for previous catalysts but the samples showed no signs of decomposition even after extending the duration of calcination from 12 to 24 hrs. A calcination temperature of 673 K for 12 hrs proved successful.

3.3.7 Cu/MgO/Al₂O₃ (60/7/35) (Cu_{Mg(7)Al})

Due to the problem of incomplete magnesium co-precipitation, the initial concentration of magnesium was increased with respect to the other components. Cu/MgO/Al₂O₃ catalysts were prepared using appropriate equivalents of copper, magnesium and aluminium containing solutions at pH = 8 and 9. The pH = 8 samples were aged for 30, 70 or 140 mins and at pH = 9 for 30 mins only. A calcination temperature of 673 K for 12 hrs was employed.

3.3.8 K/Cu/MgO/Al₂O₃ (K60/7/35) (Cu_{MgAlK})

This catalyst was prepared using the "wet-impregnation" technique and the Cu/MgO/Al₂O₃ (60/7/35) catalyst as a template, a potassium carbonate (99 %, FSA

Laboratory Supplies) solution, 0.005 M, was added to the calcined catalyst. This was then rotary evaporated leaving a free flowing powder. This was further dried and calcined at 573 K for 30 mins.

3.4 Sample Preparation

3.4.1 Differential Thermal Analysis

The data was collected on a Du Pont 932 series DTA apparatus with the deflection (mV) being recorded on the 900 series thermal analyser. The sample, ca. 9 mg, was placed in a silica glass vial, which was positioned in the reactor furnace (Figure 3.4.1) under an air (B.O.C.) flow rate of 30 ml min⁻¹. The temperature was increased from room temperature to 823 K at 10 K min⁻¹.

3.4.2 X-ray Powder Diffraction

The data was collected on a Philips PW 1050/35 X-ray diffractometer with a vertical goniometer between 2 θ values of 4 ° and 80 ° at a rate of 2 ° min⁻¹ (Ni-filtered Co-K α radiation, $\lambda_D = 0.1790$ nm). The samples were ground in a pestle and mortar with a small volume of acetone, to make a fine paste, which was poured onto a glass slide. The acetone gradually evaporated providing a "smear mount" for analysis. In each case the data were compared with literature values held in the X-ray Powder Diffraction files, Joint Committee on Powder Diffraction Standards (JCPDS).

3.4.3 X-ray Fluorescence

The XRF machine was a Link Analytical XR 200 energy dispersive X-ray Fluorescence spectrometer with a Si(Li) type X-ray detector.

The solid samples were ground in a pestle and mortar to obtain a fine powder, which was then placed in a 1.25 " diameter polypropylene cup with a Prolene film window. A 10 mm collimator was situated in the impending X-ray beam before placing the sample cup in position. A vacuum was applied to increase the resolution at lower atomic number. The tube voltage and current was then controlled to give a

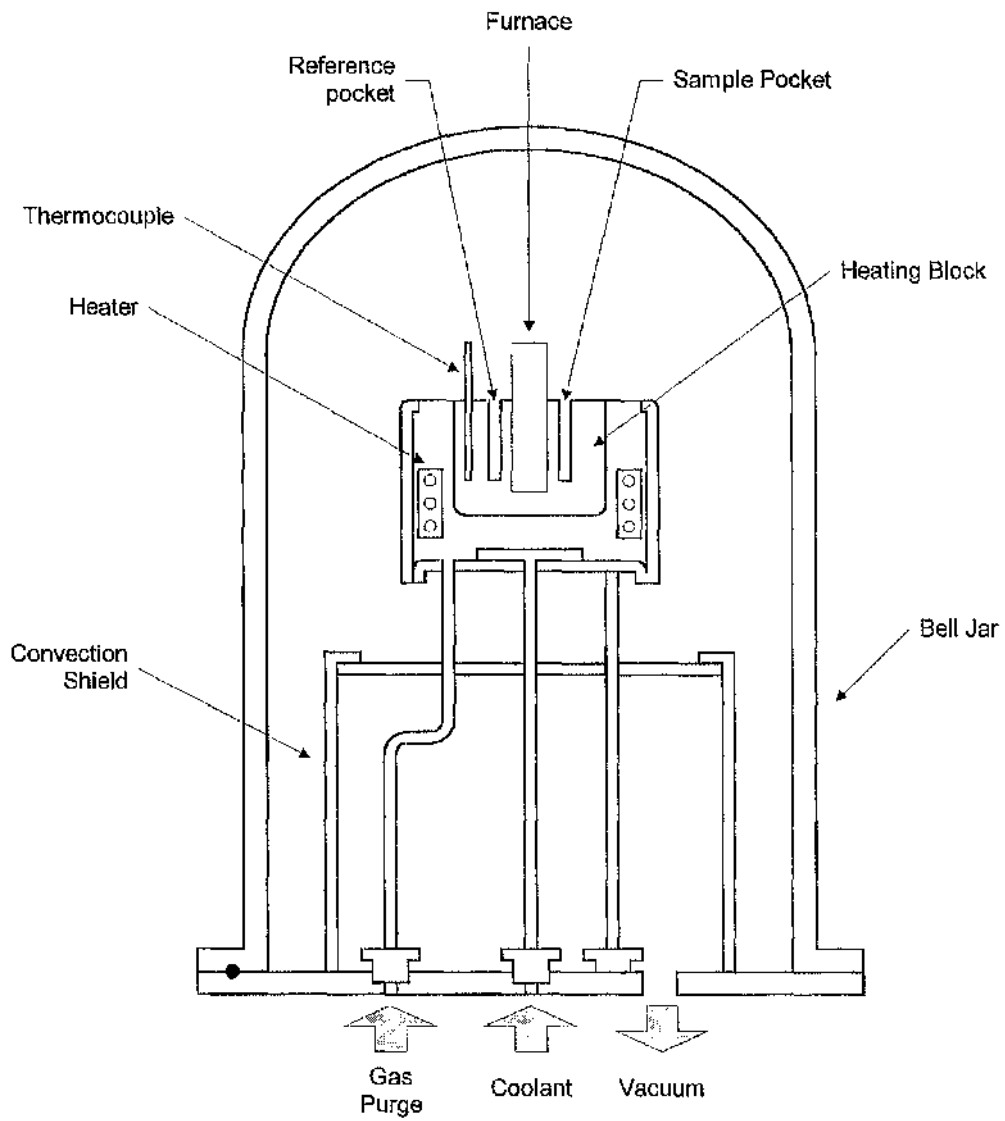


Figure 3.4.1. DTA Cell.

45-50 % dead time through the Be tube window and Rh tube target. The Rh tube target produces Rh L-lines, which were always found at 2.70 keV. This falls between Cl and Ar K-line peaks and can mask these elements. Spectra determination was repeated using a 1mm chromium filter with the 10 mm collimator in place to eliminate any irregularity arising from this problem. The filtered spectra experiments were conducted for 90 seconds and the initial spectra for 180 seconds.

Sum peaks at keV < 10 can often be seen when large quantities of an element are present. These peaks arise from the summation of appropriate emission lines e.g. for iron, the K_{α} line is at 6.40 keV and gives a sum peak at 12.8 keV. Any peaks below 1.0 keV can be ignored as these are classified as escape peaks.

3.4.4 Flame Atomic Absorption Spectroscopy

The quantity of each element in the calcined catalyst was determined using a Perkin Elmer 1100B Spectrophotometer fitted with a Cathodean Ltd. hollow cathode lamp. The lamp is element dependent.

Copper, aluminium magnesium, chromium and potassium standard 1000 ppm solutions were diluted to the following concentrations (see Appendix 10.1).

Copper	1, 2, 3, 4 & 5 ppm
Aluminium	10, 25, 50, 75 & 100 ppm
Magnesium	0.1, 0.25, 0.5, 0.75 & 1 ppm
Chromium	1, 2, 3, 4 & 5 ppm
Potassium	0.2, 0.5, 1.0, 1.5 & 2.0 ppm

A calibration curve was constructed from the dilutions.

Sample solutions were prepared using a known weight, ca. 0.1 g of catalyst, which had been digested in 10 % concentrated nitric acid solution. After filtration, the

resultant solution was diluted to produce a final concentration within the linear region of the calibration curve.

3.4.5 Temperature Programmed Reduction

Temperature programmed reduction experiments were performed using the apparatus in Figure 3.4.2 with the sample, ca. 20 mg, placed inside the TPR vessel (Figure 3.4.3) on top of the sinter.

The gases were first flowed through a Pd/WO₃ oxygen trap and 5 Å molecular sieves to remove oxygen and water contained in the reductive and carrier gases. The flow stream proceeded through the reference side of the thermal conductivity detector, which utilised a Wheatstone Bridge to detect changes in gas composition. The gas mixture was either flowed through the bypass or the reactor. A 3-way tap decided the direction of the flow. A dry ice/acetone trap was incorporated post-reactor to remove any water and potential harmful reduction products from the gas effluent stream. Following this, the gas stream was vented. The TCD was connected to an amplifier the output from which was fed to an integrator.

Samples were first purged with flowing helium at 40 ml min⁻¹ before introducing the reducing gas mixture. The 6 % H₂/N₂ mixture was flowed at 30 ml min⁻¹ and then temperature increased at a linear ramping rate of 5 K min⁻¹ using a temperature programmer. After sample reduction, helium at a flow rate of 30 ml min⁻¹ was used to purge the reduction gases whilst the sample was cooled to room temperature.

3.4.6 Nitrous Oxide chemisorption and Copper Surface Area measurements

Nitrous oxide chemisorption has been found to be effective in determining the total copper surface area of a reduced sample [212]. Both carbon monoxide and hydrogen

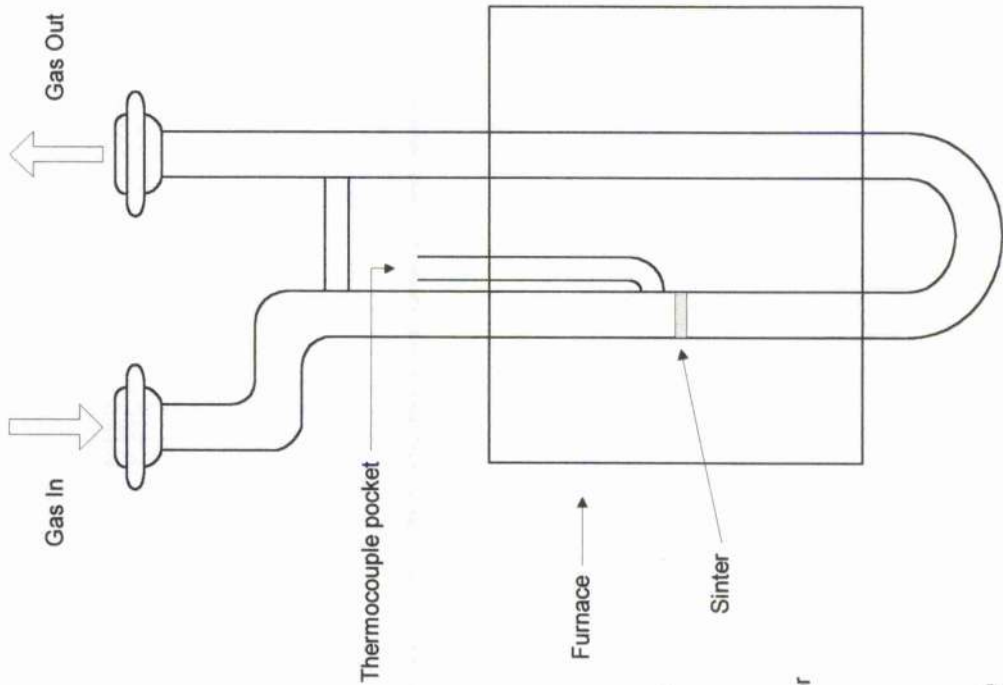


Figure 3.4.3. TPR vessel.

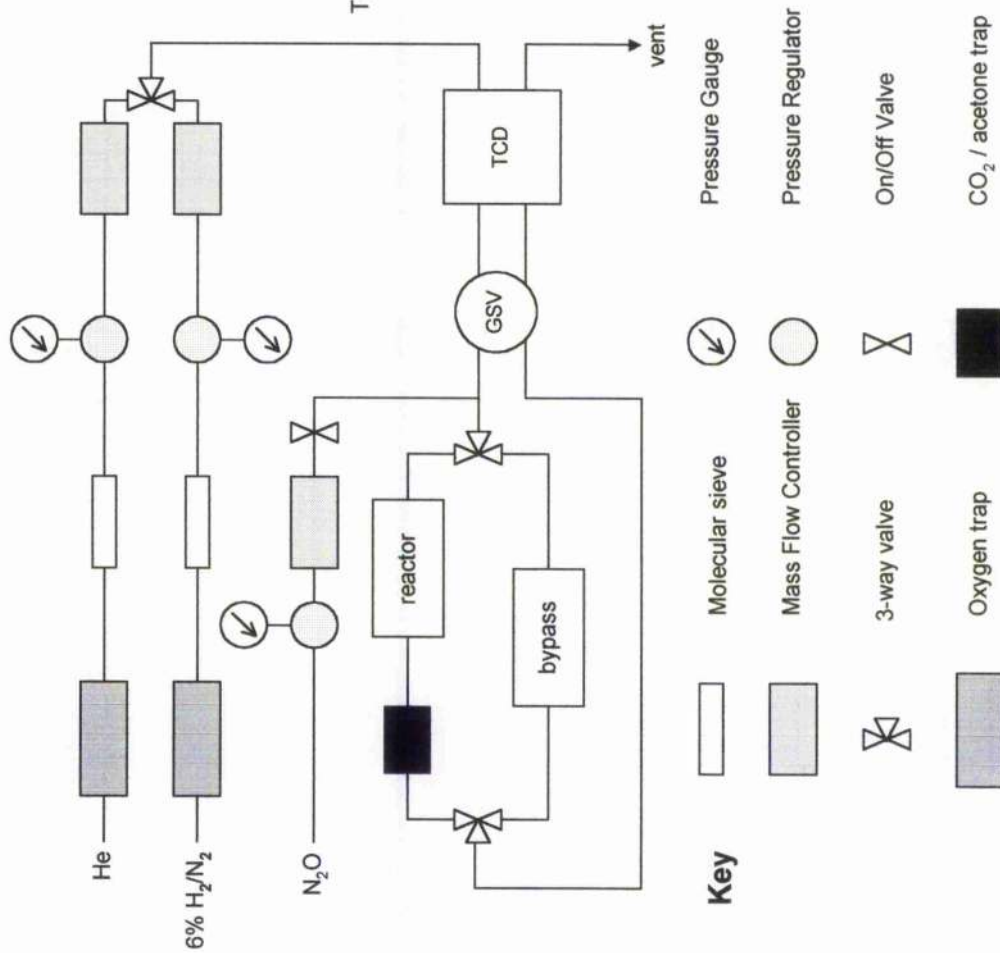


Figure 3.4.2. N₂O chemisorption / TPR line.

have been attempted but neither adsorbate is thought to provide accurate results [213]. Nitrous oxide reacts by the decomposition on the copper surface of one nitrogen molecule and an adsorbed 2-way bridged oxygen atom.



From ultra violet photoelectron spectroscopy (UPS) studies [214], it has been shown that the surface reoxidation of copper by nitrous oxide is unreactive enough to only go to Cu(I) at temperature below 373 K.

Two recent methods of copper particle size determination were by Chinchén *et al* [215] and Bond and Namijo [212]. In the former, Chinchén *et al* [215] entitled their technique reactive frontal chromatography, where the chart speed of the integrator is important to quantify nitrogen consumption from a katharometer calibration using various volumes. Bond and Namijo [212] use a two-stage method by calculating the extent of N_2O chemisorption in the following manner. This method was conducted during this work.

The dispersion is measured by the ratio of the total number of exposed atoms (N_s) over the total number of copper atoms (N_T).

$$\text{Dispersion (\%)} = \frac{N_s}{N_T} \times 100$$

This can be calculated either from a ratio of the integrator peaks areas of the bulk and surface reduction or from a hydrogen consumption calibration as



It is assumed that the copper is present as Cu(II)O therefore stoichiometric. From this the number of copper atoms present in the sample can be calculated when dividing by Avogadro's constant. This value can be checked against the ratio of bulk and surface reduction peak areas displayed on the integrator.

The particle size can also be determined by dividing 104 by the dispersion.

$$\text{Average Particle Size (nm)} = \frac{104}{\text{Dispersion (\%)}}$$

where 104 is a constant derived from the density of copper atoms (see Appendix 10.2).

The total surface area can be calculated if the number of metals atoms per unit area is known. It is assumed that the catalyst surface of equal proportions of the main low index crystal planes. The concentration of surface atoms of copper per unit area is defined as being equal to 1.47×10^{19} atoms m^{-2} [216].

$$\text{Copper Surface Area (m}^2 \text{ g}^{-1}\text{)} = \text{no. of Cu}_{(s)} \text{ atoms} \times \frac{1 \text{ m}^2}{1.47 \times 10^{19}} \times \frac{1}{\text{sample weight (g)}}$$

The same apparatus as used for TPR experiments was utilised for N_2O chemisorption (Figure 3.4.2 & 3.4.3). The sample was initially reduced using a 6 % H_2/N_2 gas mixture and at a temperature ramp rate of 5 K min^{-1} until initial reduction had been completed. The sample was subsequently cooled to and then maintained at 323 K under a 30 ml min^{-1} helium flow.

Nitrous oxide (B.O.C.) was then introduced by means of a Brooks mass flow controller, a 2-way tap (Whitey SS-41XS2) and a 3-way union. A 5 % $\text{N}_2\text{O}/\text{He}$ gas composition at 30 ml min^{-1} was initially flowed through the bypass to sustain a constant current output from the TCD. The stream was then passed over the sample to be re-oxidised. This was continued until no N_2 was produced from the N_2O , which could be determined from the response on the TCD detector. The sample was then

re-reduced under identical conditions before finally being purged under a helium flow whilst cooling.

3.4.7 Elemental Analysis

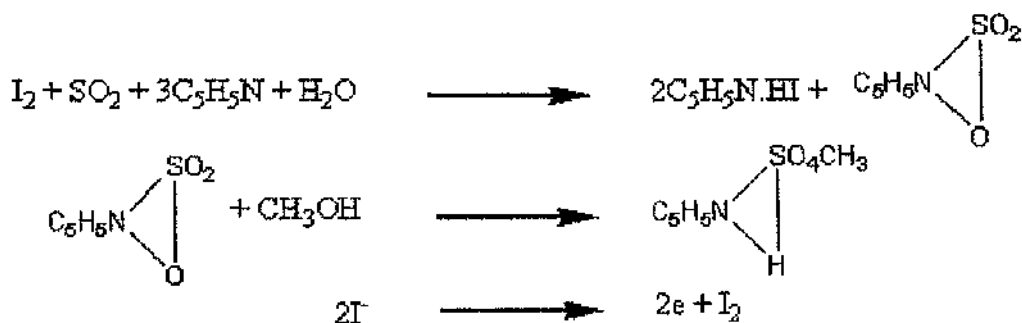
Analysis was conducted on a LECO CHNS-932 machine. Samples of between 1.8 and 2.2 mg were weighed into silver vials and crimped in a special designated vice. The sample is placed in the sample loading chamber and held there until a dose of oxygen had been released by the pressure system. The sample was then dropped into the furnace simultaneous to the arrival of the oxygen, whereupon it was combusted by the heated oxygen rich environment (1273 K). Under combustion the silver was melted and the C, H, N and S were converted into CO₂, H₂O, N₂ and SO_x respectively. Thereupon all gases were transported by a He carrier gas through an oxidation tube to complete the conversion of SO_x to SO₂. The gas mixture was flowed through a non-dispersive infra-red (IR) absorption detection system, which detected H₂O, and was subsequently removed by an Anhydrone® packed tube. The gas stream continued through individual SO₂ and CO₂ IR detection systems. A packed tube of Lecosorb® then removed these gases, leaving only the N₂ and the He carrier gas. A thermal conductivity detector set at 318 K measured the N₂. Adjustments for blank calibration and weight were applied to the final integrated signal and the answers were displayed as weight percent of C, H, N and S.

The IR detector cell fitted with CaF₂ windows was operated at a temperature of 1023 K with the detector responding to energy changes between the carrier gas and measure gas to measure concentration.

3.4.8 Titrimetry

The water present in the sample is coulometrically titrated to a predefined end point at which there is a minute excess of free iodine present. Stoichiometrically, 1 mol of water reacts with 1 mol of iodine and from this the magnitude of the electrolysis current can be calculated.

It reacts under the reaction.



Results are displayed on weight/weight (wt / wt) basis.

$$\text{Results (\%)} = \frac{\text{microgram count of I}_2}{\text{weight of sample (g)}}$$

Water analysis was conducted on post-reaction samples on a GRS2000 Coulometric Karl Fischer Titrator machine. Pre-weighed liquid samples of varying volumes of between 0 and 300 μl were injected into the anode reagent (Figure 3.4.4), with the titrimetry machine measuring the electrolysis current produced.

3.4.9 BET Surface Area measurements

Measurement of surface areas involves the principles of physical adsorption. Langmuir [217] first developed the idea, however, the method is only valid at low pressures monolayer formation ($p/p^\circ < 0.1$) as multilayer condensation becomes extensive. To overcome this problem the Brunauer, Emmett and Teller (BET) equation (below)

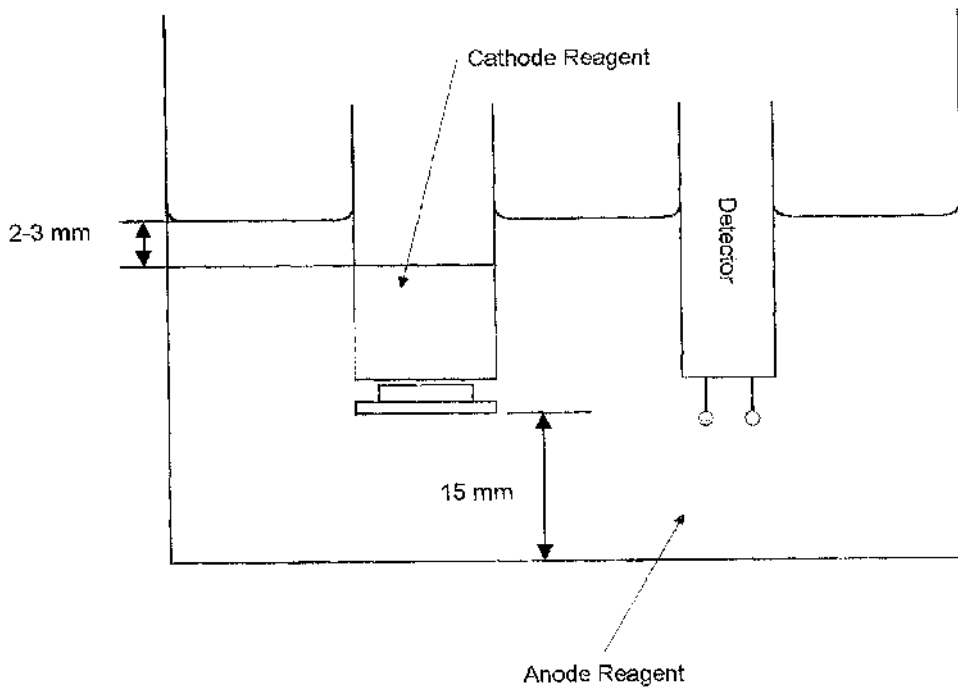


Figure 3.4.4.
Water Analysis / Titrimetry.

[218] was derived to successfully account for multilayer physical adsorption but still basing the equation on Langmuir's principle assumptions.

$$\frac{v}{v_m} = \frac{cp/p^0}{(1-p/p^0)[1+(c-1)p/p^0]}$$

where v is the quantity of gas adsorbed at an equilibrium pressure p , p^0 , the vapour pressure of the adsorbate in the condensed state at the adsorption temperature. v_m is the value v at monolayer coverage, and finally c is a temperature dependent constant related to the heat of adsorption into the first layer and the heat of condensation of the adsorbate and has values less than 100.

It may be rewritten so a straight line results when $p/(p^0-p)v$ is plotted against the relative pressure p/p^0 . The value of v_m can be obtained from the slope, which equals $(c-1)/cv_m$ and the intercept equals $1/v_m c$ (below).

$$\frac{p}{v(p^0-p)} = \frac{1}{v_m c} + \frac{(c-1)p}{(v_m c)p^0}$$

However, this equation is only valid up to $p/p^0 = 0.3$ as above this vapour pressure p/p^0 tends towards unity, liquefaction begins in the micropores and progresses through to mesopores.

The important assumptions for the BET theory are that adsorbed species in the first layer serve as site of adsorption for the 2nd layer and the rate of adsorption on the base surface is equal to the rate of desorption from the monolayer.

Analysis was conducted on a Micromeritics Gemini III 2375 surface area analyser. Samples of known weight (ca. 100 mg) were first placed in a sample tube and outgassed overnight at 383 K under a N₂ flow to remove any moisture. The

pressure of an empty vessel/reference and an empty sample tube were calculated; these were both evacuated and cooled to 77 K. The empty sample tube was then replaced with the catalytic sample and evacuated. At 77 K, the real sample was dosed with helium to determine the free space volume. Thereafter the sample chamber was evacuated of helium. Under varying pressure doses of nitrogen, the BET surface area was calculated.

3.5 Catalyst Testing

3.5.1 Introduction

Experiments to determine catalytic activity, selectivity and stability were performed in a high pressure microreactor system (Figure 3.5.1). The system was constructed of stainless steel and was capable of operating at temperatures of up to 823 K and pressures up to 40 barg (see Appendix 10.4).

The high pressure system was designed for continuous flow studies and consisted of three sections :-

- (i) the feed system;
- (ii) the reactor system;
- (iii) the analytical system.

The reactant gases were blended prior to contact with the catalyst at the desired reaction temperature and pressure. The gaseous reaction products were vented to atmospheric pressure and the liquid products diverted into a collection vessel.

The reaction products were sampled at regular intervals by means of a heated gas sampling valve situated downstream of the reactor. The sampled products were then analysed by two gas chromatographs (GC).

3.5.2 The Feed system

The feed system incorporated essentially two different parts, the vapourisation of the liquid and the regulation of the synthesis gases.

3.5.2.1 Synthesis Gases

The reactant gases were introduced to the system by means of a APO GA400 cylinder regulator equipped with 0.25 " o.d. thick walled copper piping, which changed to

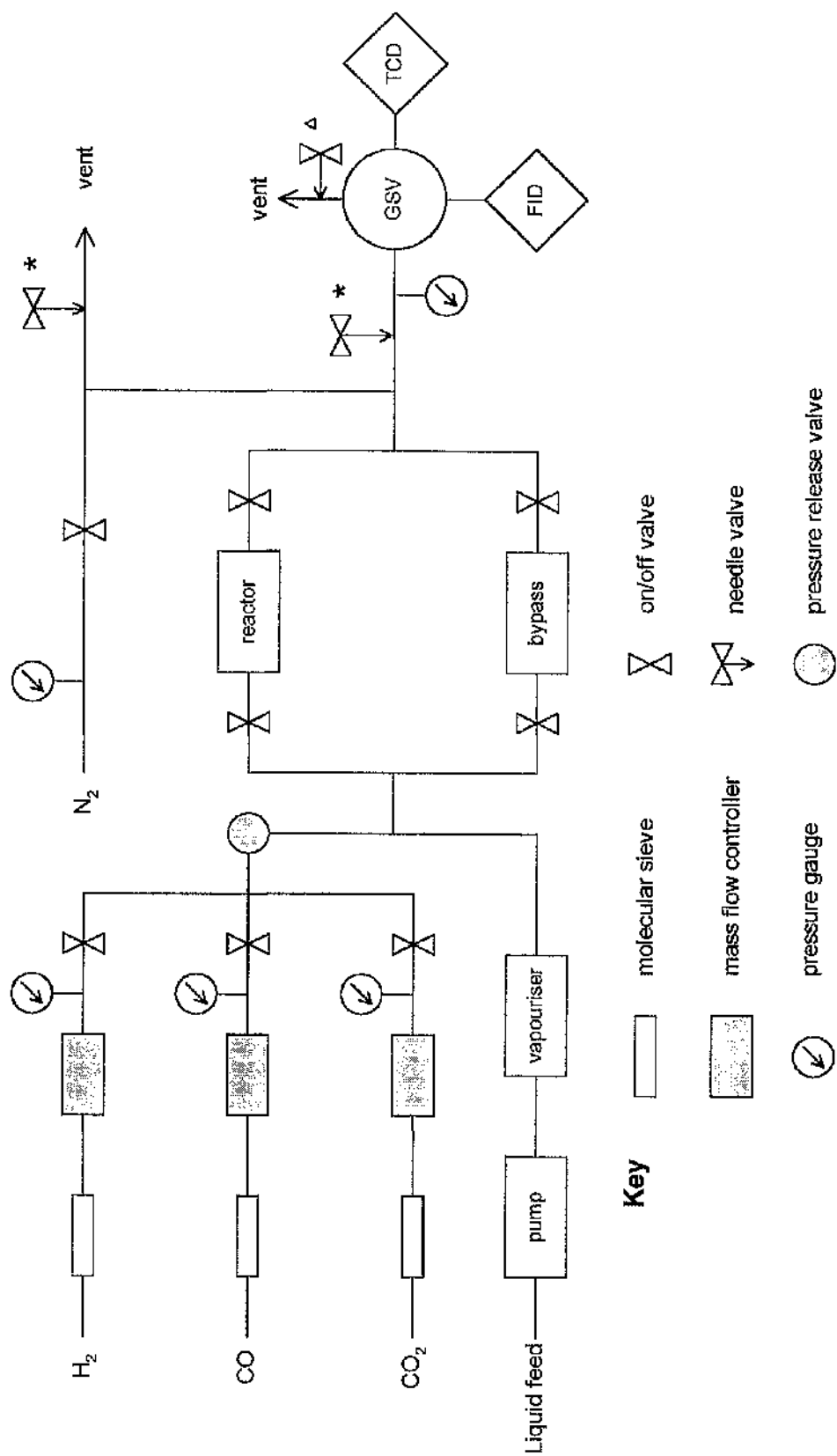


Figure 3.5.1. The Schematic of the Microreactor System.

0.125 " o.d. upon reaching the 5 Å molecular sieves (Figure 3.5.1). The gases were then introduced to the system through individual Hoke valves.

Before reaching individual Whitey on/off valves (model no. SS-41S2), the flow rates were monitored by Brooks 5850E mass flow controllers, which were connected to a mass flow meter (Brooks Instruments Ltd., model 5878) with the pressure being monitored by Budenberg 0-600 lb in⁻² Type 316SS Tube pressure gauges. From this, the individual synthesis gases were combined into one gas stream using T pieces, which flowed through a pressure release valve (Nupro SS-4R3-A).

3.5.2.2 Methanol and Ethanol Vapourisation

Methanol and ethanol are liquids at room temperature, therefore they require vapourisation before reaching the catalyst. The vapourisation unit was conducted in a device illustrated in Figure 3.5.2. This was heated using Zenith variac with respective heating element. The temperature was maintained at 383-393 K by monitoring with a Cr/Al thermocouple. A Labatron LDP-20 pump and a Mettler PJ-3600 balance controlled the liquid flow.

3.5.3 The Reactor System

The reactor system incorporated several different parts, the reactor pressure control, the reactor itself and the furnace.

3.5.3.1 Reactor Pressure Control

After regulating the synthesis gases, these were allowed to flow through the reactor. The gas stream was then split by means of a T piece (Figure 3.5.1). The nitrogen was connected to the reactor system after this T junction. The elevated pressure inside the

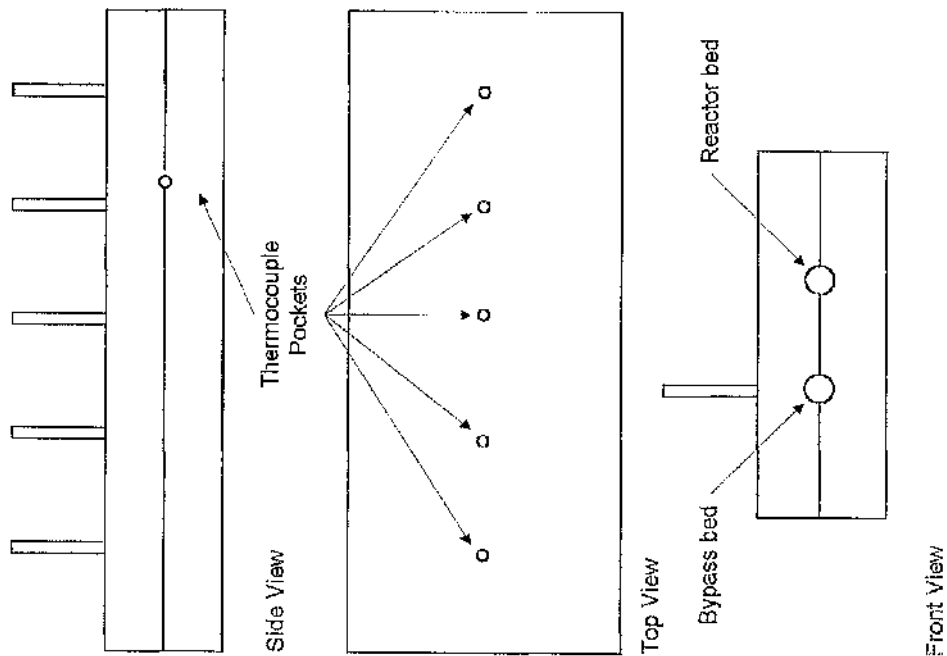


Figure 3.5.3. Furnace.

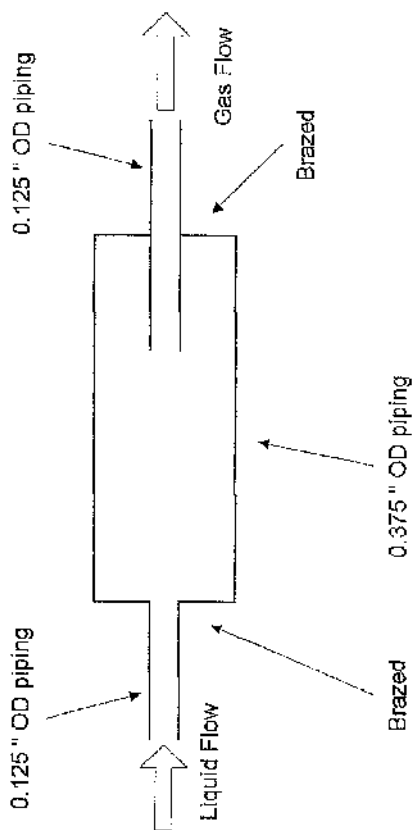


Figure 3.5.2. Vapourisation Unit.

reactor was controlled by the output pressure on the nitrogen regulator (GA400) and was displayed by a further Budenburg pressure gauge. The sole purpose of the nitrogen gas was as back pressure.

Flow restriction to the vent was achieved by using two needle valves (indicated with a star) situated downstream of the reactor bed (Figure 3.5.1). These needle valves had a secondary purpose of fine adjustments to the internal pressure of the system.

3.5.3.2 Reactor and Furnace

The reactor, the vapourisation unit and the relevant valves (Whitey SS-3NBS4-G) were all contained in the reactor box, which had internal measurements of 11 " x 7.1 " x 18.7 " and was built from Tufnol. The inside walls and lid were lined with 0.25" thick Duratech, whilst the base was protected by 1.25 " thick ceramic tiles.

The furnace (Figure 3.5.3) had dimensions of 15.2 cm x 7.6 cm x 4.5 cm and was heated using 8 x 100 W heating cartridges, which were connected to a F.G.II. temperature programmer (Model no. K-P200) in conjunction with a 10 A solid state relay and a Cr/Al thermocouple controlling the furnace temperature. To ensure an isothermal heat distribution, a further Cr/Al thermocouple monitored the temperature and was connected to a six channel digital thermometer (Gulton Europe Ltd, Type 4F4LH/120AF). This thermometer was also used with the vapourisation unit.

Blank experiments were performed using the reactor, as this gave an indication of any residual activity in the reactor, which was conducted in the bypass tube. The bypass tube was situated parallel to the reactor and was identical to the reactor tube in all aspects except that it contains no catalyst.

3.5.4 The Analytical system

The analytical system incorporated two different parts, the gas sample valve and the gas chromatographic analysis.

3.5.4.1 The Gas Sample Valve (GSV)

The gas sample valve (Perkin Elmer L419 111 10 -port) was situated downstream of the reactor in between two needle valves (Nupro "S" series). The needle valve situated just after the gas sample valve (indicated with a triangle) regulated the pressure of gas flowing into the GC to ensure optimum operating conditions (Figure 3.5.1). A Budenburg pressure gauge fitted adjacent to the GSV monitored the pressure.

The temperature of the GSV was maintained at 383 K by using a Pye series 104 chromatograph to stop condensation of products occurring. The temperature was checked with the use of another Cr/Al thermocouple connected to the Gulton thermometer described previously.

Various sample loop sizes were attached to the GSV for the use with the flame ionised detector (FID) and the thermal conductivity detector (TCD). A schematic diagram of the gas sampling valve is shown in Figure 3.5.4. The vent line was also lagged by high temperature heating tape and maintained at elevated temperatures by a Zenith variac.

3.5.4.2 Gas Chromatographic Analysis

The GSV was arranged so dual analysis of both thermal conductivity and flame ionised detection could be achieved. The helium gas was only required for the carrier gas into the GC via the gas sample valve, consequently, a Helium 2-stage regulator providing a

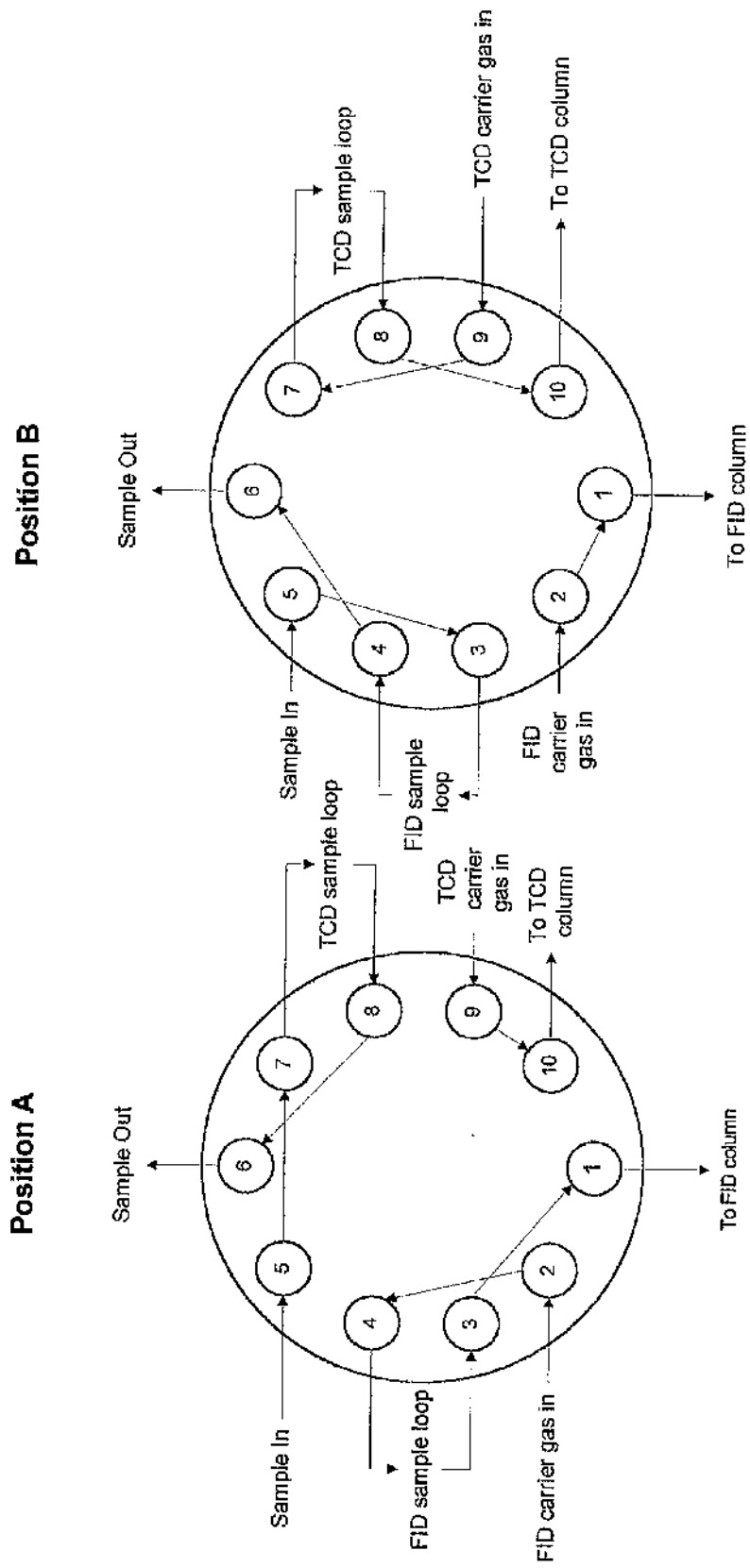


Figure 3.5.4. Gas Sample Valve.

maximum output pressure of 4 barg was used. The air cylinder was fitted with a regulator providing a maximum output pressure of 5 barg.

3.5.4.2a Thermal Conductivity Detector

The Gas Chromatograph comprised of a Perkin Elmer oven and Gow-Mac Instruments (Power supply, model 40-202) amplifier fitted with a packed column of 2 m in length and 0.125 " o.d. piping using silica 80-100 mesh as the stationary phase. The operating conditions use a flow of Helium at 20 ml min⁻¹ and an oven temperature of 298 K.

The interconnecting metal piping from the GSV was cooled in an acetone/dry ice trap to condense liquid products. The output was calibrated using the same Hewlett Packard 3395 Integrator as the FID system.

3.5.4.2b Flame Ionised Detector

The Gas Chromatograph was a Carlo Erba 4200 fitted with a packed column of 1 m in length and 0.25 " o.d. using Chromosorb 101 as the stationary phase.

The optimum operating conditions were found to be:-

30 ml min ⁻¹	Helium and Hydrogen flow
200 ml min ⁻¹	Air flow
403 K	Injection port temperature
413 K	Column temperature
423 K	Detector temperature

The interconnecting metal piping from the GSV was lagged by using high temperature heating tape and maintained at 423 K by a Zenith variac to prevent condensation of products. The output was calibrated using a Hewlett Packard 3395 integrator.

3.5.4.3 Gas Chromatograph Calibrations

A wide variety of products may be formed using syngas reactions so several calibrations were conducted using standard procedures. A selection of product calibrations is displayed in Tables 3.5.1 and 3.5.2.

Table 3.5.1. TCD Gas Chromatograph Calibrations.

Product Name	Response Factor ($\times 10^{11}$)	Retention Time (mins)
Carbon Monoxide	1.85	5.2
Carbon Dioxide	2.29	22.8

Table 3.5.2. Selected FID Gas Chromatograph Calibrations.

Product Name	Response Factor ($\times 10^{11}$)	Retention Time (mins)
Methanol	5.87	3.2
Ethanol	7.11	4.8
Propan-1-ol	12.5	7.8
Propan-2-ol	11.3	6.6
Dimethyl Ether	9.0	2.8
Methanal	0.665	2.2

4 Preparation and Characterisation of Catalyst Precursors

4.1 Cu/Cr₂O₃ (50/50) (Cu_{Cr})

4.1.1 Preparation

During preparation, the mother liquor was dark turquoise in colour. Filtration resulted in a similar coloured filtrate as the mother liquor. These colours were indicative of a mixture of Cu²⁺ and Cr³⁺ ions. The dried precursor was dark green in colour, which decomposed on calcination to a very dark brown precipitate. This suggested that the copper precursor has decomposed.

4.1.2 Differential Thermal Analysis

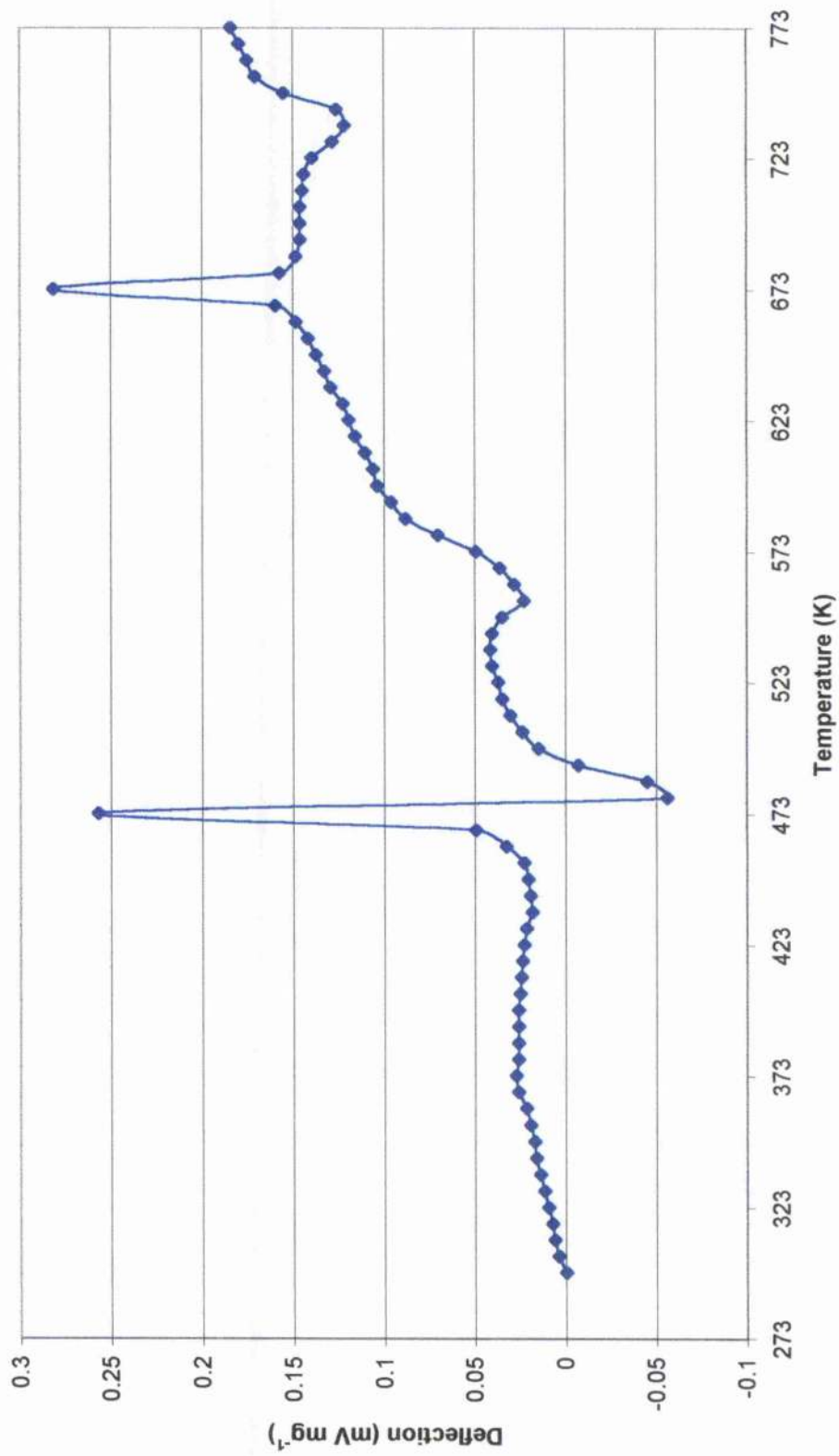
The DTA profile shows (Figure 4.1.1) a slight increase in the heat capacitance until ca. 373 K whereupon the profile decreases marginally until a large exothermic peak occurs at 473 K. The decrease in the profile was possibly the initialisation of an endothermic peak, which was hidden by the exothermic peak. The endothermic and exothermic peak was due to simultaneous dehydration from the lattice accompanied by a phase change.

At 553 K, a second endothermic peak was shown but was smaller in magnitude than the former endothermic peak. This was due to further decomposition of the precursor with the loss of hydroxide groups. A second exothermic peak was present at 673 K, which was due a further phase change within the potential spinel structure.

Increasing the temperature resulted in a third endothermic peak present at 748 K. This was similar in size to the second endothermic peak and was due to decarboxylation from the structure.

Bulk copper (II) oxide showed a very small exothermic peak centred on 523 K.

Figure 4.1.1. DTA profile for the Cu_{Cr} precursor.



4.1.3 X-ray Diffraction

The precursor XRD pattern gave a very poorly crystalline background with no long-range order being present. Calcination gave small peaks of $\text{CuCr}_2\text{O}_7 \cdot 2\text{H}_2\text{O}$ [219] at 2 θ angles of 28.1 °, 29.1 °, 40.0 ° and 42.0 ° (Table 4.1.1). The file numbers for the data of the relevant standard compounds have been given as references.

Table 4.1.1. XRD d-spacing values (Å) for the Cu_{Cr} catalyst, with intensities in parentheses.

Cu_{Cr}	$\text{CuCr}_2\text{O}_7 \cdot 2\text{H}_2\text{O}$ [219]
3.68(95)	3.67(83)
3.56(98)	3.55(100)
2.62(99)	2.61(83)
2.49(100)	2.48(100)

4.1.4 X-ray Fluorescence

Copper and Chromium peaks were present both in the precursor (Figure 4.1.2) and in the catalyst. The copper K_{α} -line was present at 8.041 keV and is approximately five times larger than K_{β} -line at 8.907 keV, which was due to the difference in probability of the two processes occurring. The chromium peaks, K_{α} -line (5.411 keV) and K_{β} -line (5.947 keV) are present in the same ratio. Calcium (K_{α} -line 3.69 keV) was present as an impurity both in the precursor and the catalyst. No calcium K_{β} -lines were distinguishable from the background, therefore this element was only present in minor quantities. The calcium was from the ammonium base used in the preparation. The slightly smaller peak present around at 6.375 keV was iron (K_{α} -line, 6.400 keV). The iron was from the copper precursor salt used in the preparation as it had the largest concentration of any transition metal contaminant of < 0.005 %.

Figure 4.1.2. XRF spectrum for the Cu_Cr precursor.

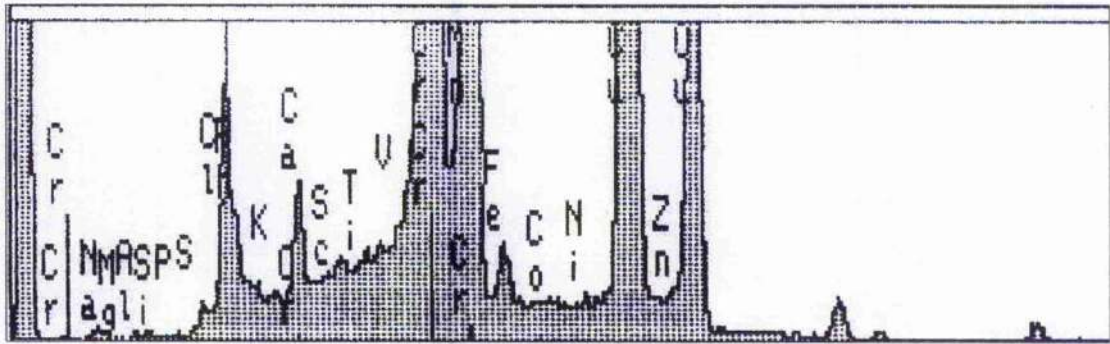
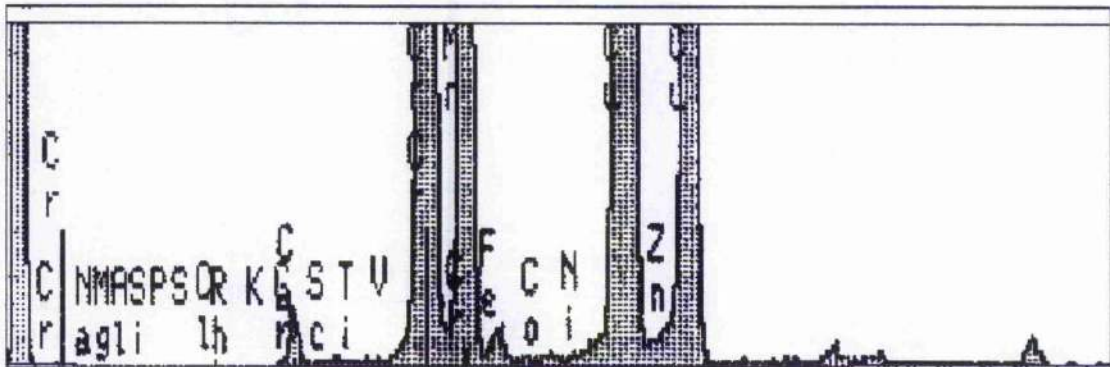


Figure 4.1.3. XRF spectrum for the filtered Cu_Cr catalyst.



A chromium filter was introduced to reduce background noise but primarily to remove the rhodium interference lines. As a result, it was found that no chlorine was present as an impurity in the catalyst (Figure 4.1.3).

4.1.5 Atomic Absorption Spectroscopy

Atomic absorption spectroscopy analysis proved that only 77.3 % of the copper and 82.6 % of the chromium had co-precipitated from the mother liquor (Table 4.1.2). This confirmed the coloration of the filtrate during preparation.

Although incomplete co-precipitation did occur, the metal ratio was 48.3:51.7 copper:chromium, this being within experiment error of the desired 50:50 metal ratio. From the quantified metal ratio, it can be assumed that the incomplete co-precipitation occurred equally.

Table 4.1.2. AAS results for the Cu_{Cr} catalyst.

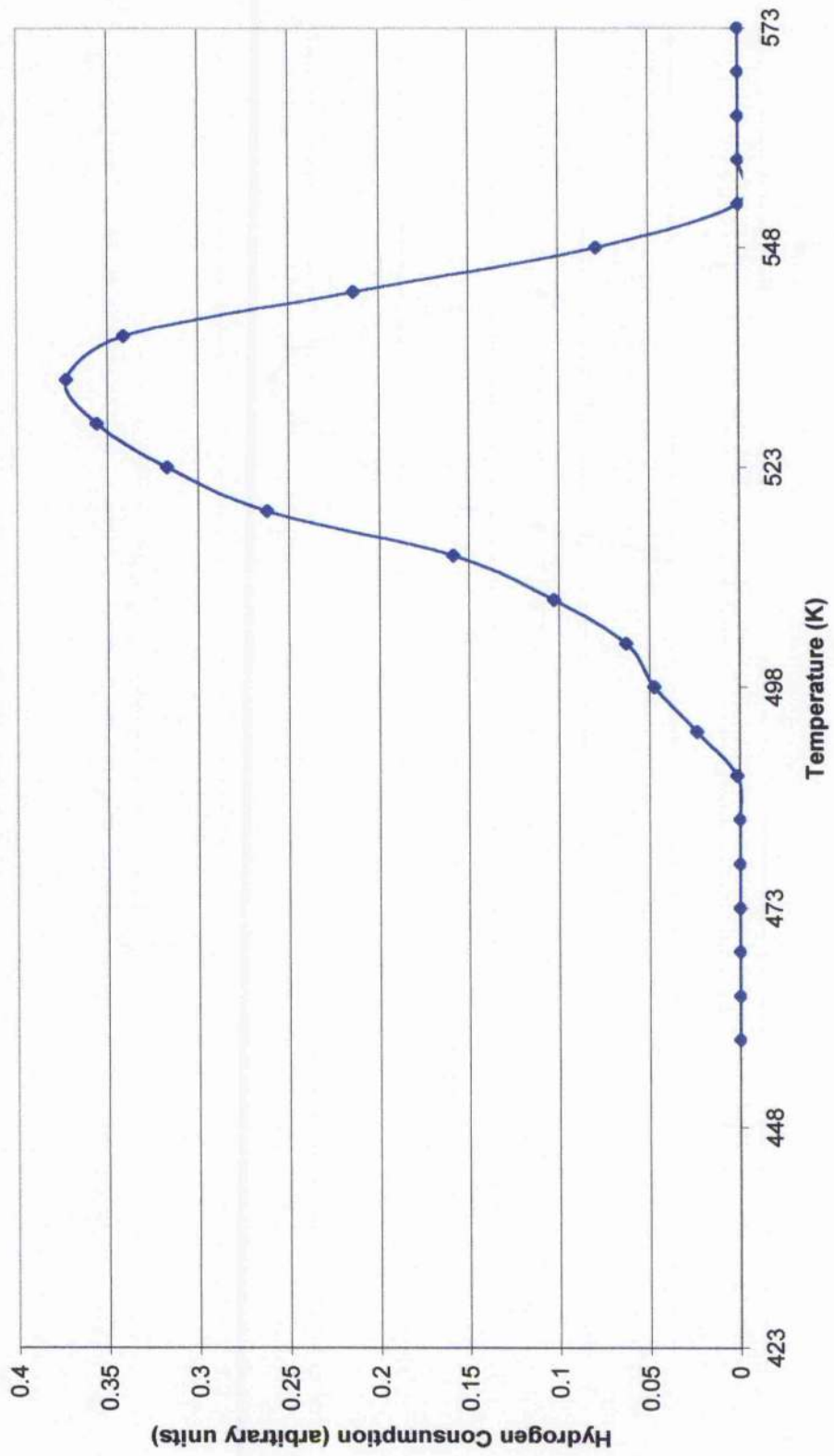
Element	Copper	Chromium
Percentage co-precipitated (wt / wt)	77.3	82.6
Metal Ratio	48.3	51.7

4.1.6 Temperature Programmed Reduction

The TPR profile for the Cu_{Cr} catalyst (Figure 4.1.4) exhibited reduction between 488 K and 553K with a maximum reduction temperature at 533 K. Bulk chromium oxide (Cr_2O_3) showed no reduction below 773 K but copper (II) oxide reduced between 448 K and 553 K with maximum hydrogen consumption at 508 K.

The copper present in the Cu_{Cr} catalyst reduced at a higher temperature than bulk copper (II) oxide suggesting that the copper was stabilised by the presence of the chromium and that only the copper was reduced.

Figure 4.1.4. TPR profile for the Cu_{Cr} catalyst.



4.1.7 Nitrous Oxide Chemisorption and Copper Surface Area measurements

Nitrous oxide chemisorption studies gave a percentage copper present in the catalyst as 49.0 % (Table 4.1.3), which was in good agreement with the AAS metal ratio results and the theoretical copper:chromium 50:50 ratio.

Table 4.1.3. Nitrous oxide chemisorption results for the Cu_{Cr} catalyst.

% Cu in catalyst	49.0
% dispersion	4.75
Particle size (nm)	21.9
% calibrated dispersion	5.6
Calibrated particle size (nm)	18.6
Copper surface area ($\text{m}^2 \text{g}^{-1}$)	18.9

The average copper dispersion was 4.75 %, which quantified as an average particle size of 21.9 nm. The hydrogen consumption calibration resulted in a marginally larger dispersion of 5.6 % and therefore, a marginally smaller particle size (18.6 nm). The average copper surface area was found to have a value of $18.9 \text{ m}^2 \text{g}^{-1}$.

Bulk copper (II) oxide gave an average dispersion of 6 % with a particle size of 17.3 nm and the hydrogen consumption calibration gave an average dispersion of 6.5 % and particle size of 16.0 nm. The average copper area was $26.9 \text{ m}^2 \text{g}^{-1}$.

The Cu_{Cr} catalyst had a lower copper dispersion and a larger average particle size than bulk copper (II) oxide. This result was reflected in the copper surface area where the catalyst had a smaller value.

Table 4.1.4. Copper surface reduction temperatures for the Cu_{Cr} catalyst.

Temperature (K)	T_{initial}	T_{max}	T_{complete}
Cu_{Cr}	378	432	466

The Cu_Cr catalyst had a maximum copper surface reduction temperature of 432 K after starting to reduce at 378 K (Table 4.1.4). The surface reduction procedure was complete by 466 K. Bulk copper (II) oxide started to reduce at 403 K and was completed by 478 K with maximum hydrogen consumption at 433 K, suggesting no enhancement in surface copper stability during preparation of the Cu_Cr catalyst.

4.1.8 Elemental Analysis

Table 4.1.5.
Elemental Analysis results for the Cu_Cr precursor and calcined samples.

Element	C	H	N	S
Precursor	0.32	2.7	3.3	0.02
Calcined	0.05	1.8	nda	0.01

nda = non-detectable amount

Elemental analysis conducted on the precursor gave an average carbon content of 0.32 % and hydrogen content of 2.7 % (Table 4.1.5). An impurity, nitrogen was present in larger quantities with a content of 3.3 %, and sulfur, a further impurity, had a concentration of only 0.02 %. The nitrogen was either present from the metal nitrate salts or the ammonium base, both of which was used for the preparation. Sulfur was probably from a cumulation of the impurities of all the precursor solutes.

On calcination, the concentrations of these elements decreased with nitrogen declining the greatest quantity to a non-detectable amount. The hydrogen content decreased the least to 1.8 %. This decrease in concentrations of these detectable elements was due to the elevated temperature required for the calcination process, which results in the decomposition of the precursor.

A copper (II) oxide standard had carbon concentration of 0.20 % and non-detectable amounts of hydrogen, nitrogen and sulfur. Chromia contained a non-

detectable amount of carbon, hydrogen, nitrogen and sulfur.

4.1.9 BET Surface Area measurements

The catalyst gave a BET surface area measurement of $29.1 \text{ m}^2 \text{ g}^{-1}$ (Table 4.1.6) with a single point measurement of $28.3 \text{ m}^2 \text{ g}^{-1}$.

Table 4.1.6. BET surface area measurements for the Cu_{Cr} catalyst.

Catalyst Sample	Cu_{Cr}
Single Point ($\text{m}^2 \text{ g}^{-1}$)	28.3
BET surface area ($\text{m}^2 \text{ g}^{-1}$)	29.1

4.1.10 Summary

The method proposed by Wrobel *et al* [211] gave the correct Cu:Cr ratio but gave incomplete co-precipitation. The poorly crystalline precursor decomposed in several stages to give the calcined sample. The copper in the sample reduced at a higher temperature than bulk CuO but the Cu dispersion and surface areas were smaller. The BET surface area was also small. Impurities were observed in the precursor and calcined sample.

4.2 Cu/MgO/Al₂O₃ (50/10/40) (Cu_{Mg(10)Al})

4.2.1 Preparation

During an initial preparation, pH = 7 (⁷₃₀¹Cu_{Mg(10)Al})², it was observed that the filtrate contained a high concentration of copper, implying that a significant proportion had not co-precipitated. The precursor was pale blue and on calcination to temperatures of 973 K remained that colour. Exceeding this temperature, the catalyst exhibited a pale green colour, possibly indicative of malachite. On reduction above 623 K, samples rapidly altered in colour from blue to green to brown in quick succession.

However, repeating the procedure (⁷₃₀²Cu_{Mg(10)Al}) to overcome the high copper filtrate concentration gave a similar result. Also, the second preparation resulted in a darker blue sample than the first with a non-uniform coloration and a different consistency. The previous preparation resulted in very fine particle sizes but this precursor, gave larger sized particles.

In the light of this information, further preparations were conducted with increasing pH to attempt to overcome the problem of the high copper concentration in the filtrate. An experiment at pH = 7.5 (^{7.5}₃₀¹Cu_{Mg(10)Al}) was carried out and a decrease in the copper concentration in the filtrate observed. Filtration resulted in a similar coloured filtrate as the mother liquor, which was blue.

Increasing the pH to 8.25 (^{8.25}₃₀¹Cu_{Mg(10)Al}), further decreased the concentration of copper in the filtrate, but altered the texture of the crystallites. Particle sizes had increased with diameters measuring up to 6-7 μm. A preparation performed at pH = 9.5 (^{9.5}₃₀¹Cu_{Mg(10)Al}) increased the copper content in the precursor, but like the

²The pH used for preparation is denoted by the initial superscript, the subscript is the length aged in the mother liquor. The second superscript is required when duplicate preparations under the same preparatory conditions are conducted and value relates to the initial or subsequent preparation, for example ⁷₃₀¹Cu_{Mg(10)Al}. This catalyst was prepared at pH = 7, aged for 30 mins in the mother liquor and was the first preparation. This format is used throughout.

previous sample, the crystallite morphology was inconsistent with earlier preparations. The $^{8.25}_{30}\text{Cu}_{\text{Mg}(10)\text{Al}}$ and $^{8.25}_{30}\text{Cu}_{\text{Mg}(10)\text{Al}}$ samples had distinctive crystallite shape and the hard particles sheared along definitive planes. These two precursors were not fully characterised due to their inconsistency with prior preparations and were not used in microreactor experiments.

4.2.2 Differential Thermal Analysis

The DTA profile of the $^{7}_{30}{}^1\text{Cu}_{\text{Mg}(10)\text{Al}}$ showed an endothermic peak centred on 483 K (Figure 4.2.1) and was quickly followed by an exothermic peak at 503 K. Subsequent temperature increase resulted in, only deflections brought about from the heat capacitance of the sample.

The $^{7}_{30}{}^2\text{Cu}_{\text{Mg}(10)\text{Al}}$ resulted in a similar endothermic peak but increased in temperature to 498 K and endothermicity. A subsequent exothermic peak was also observed. An extra endothermic peak in this sample was present at 555 K.

Increasing the pH to 9.5 resulted in a small depression between 473-523 K before a definitive exothermic peak at 543 K. Little loss due to the heat capacitance is observed in this sample. The $^{7}_{30}{}^2\text{Cu}_{\text{Mg}(10)\text{Al}}$ and the $^{9.5}_{30}\text{Cu}_{\text{Mg}(10)\text{Al}}$ precursors were conducted at the University of Edinburgh.

4.2.3 X-ray Diffraction

The XRD pattern of the $^{7}_{30}{}^1\text{Cu}_{\text{Mg}(10)\text{Al}}$ precursor (Figure 4.2.2) closely corresponded to a hydrated aluminium ammonium hydroxycarbonate, $\text{NH}_4\text{Al}(\text{OH})_2\text{CO}_3 \cdot y\text{H}_2\text{O}$ [220]. The peaks were not very sharp, which could be interpreted as either a poorly crystalline sample or small particles. The $^{7}_{30}{}^2\text{Cu}_{\text{Mg}(10)\text{Al}}$ precursor gave an XRD pattern

Figure 4.2.1. DTA profiles for various $\text{Cu}_{\text{Mg}(10)\text{Al}}$ precursors.

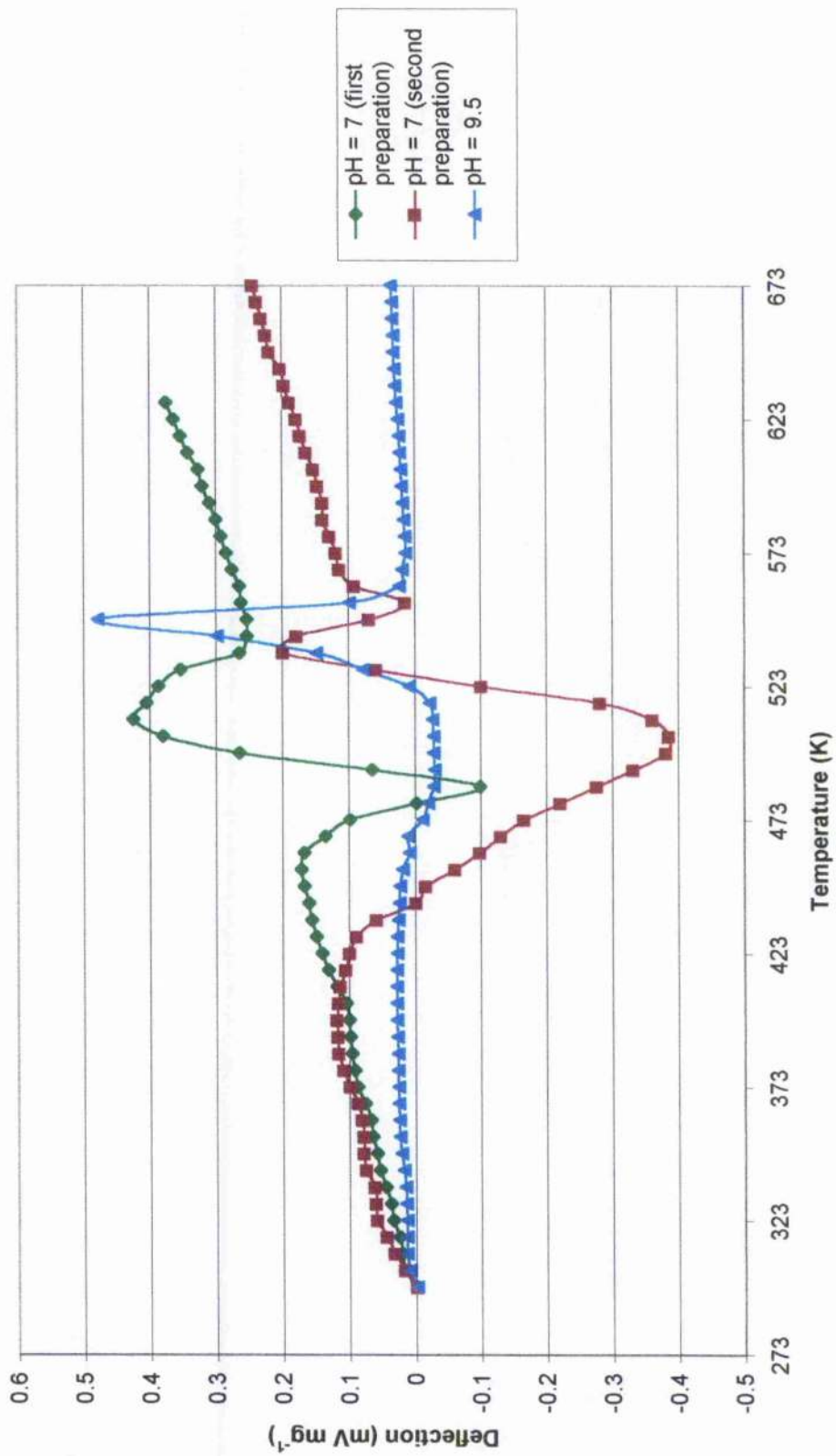
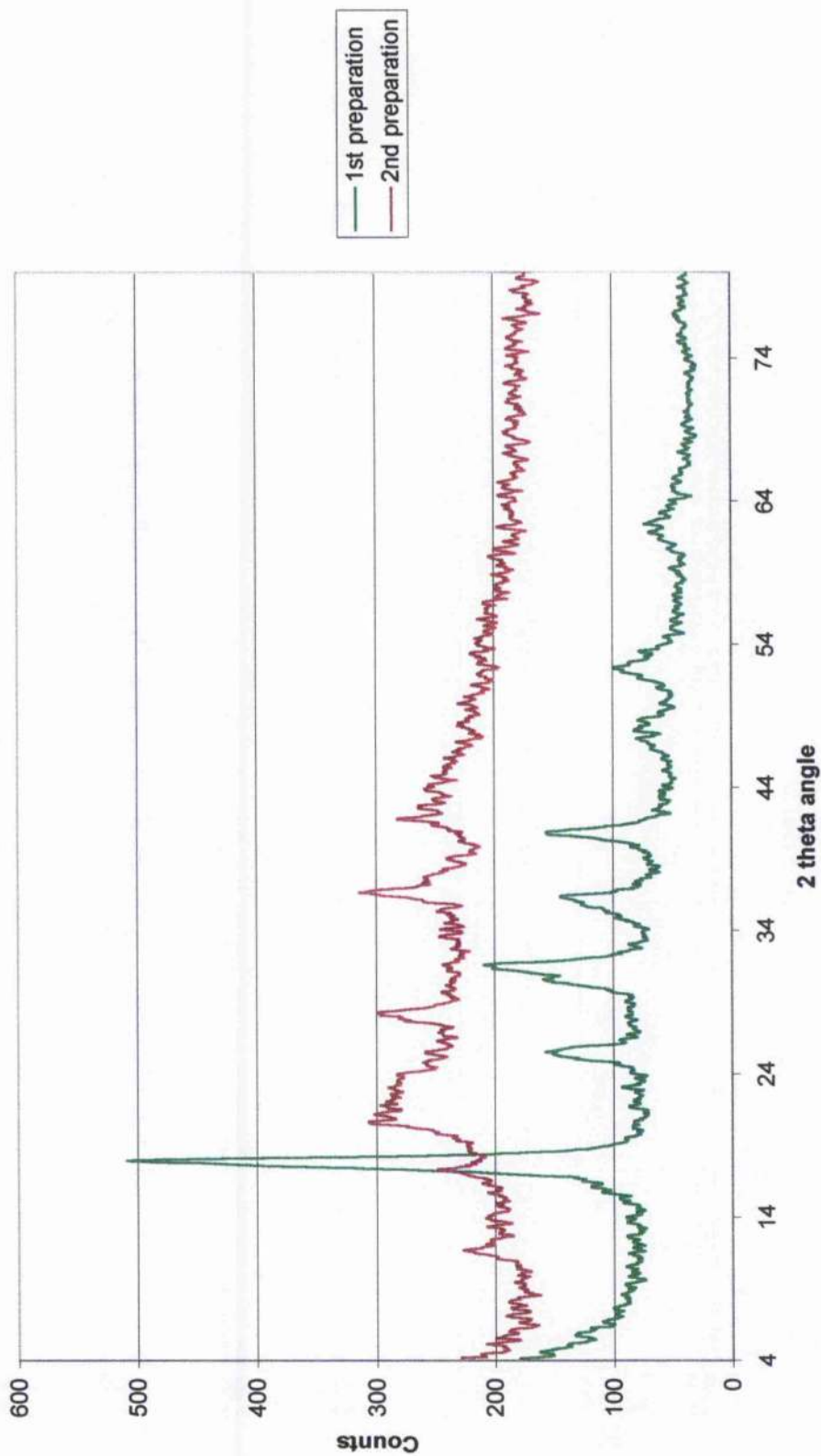


Figure 4.2.2. XRD patterns for the ${}^7\text{Cu}_{30}\text{Mg}_{10}\text{Al}$ precursors.



with peaks that can be observed as a mixture of gibbsite ($\text{Al}(\text{OH})_3$) [221], barringtonite ($\text{MgCO}_3 \cdot 2\text{H}_2\text{O}$) [222] and malachite ($\text{Cu}_2\text{CO}_3(\text{OH})_2$) [223] (Table 4.2.1).

Increasing to $\text{pH} = 7.5$, produced a poorly crystalline XRD pattern (Figure 4.2.3). The XRD patterns of $^{8.25}_{30}\text{Cu}_{\text{Mg}(10)\text{Al}}$ and $^{9.5}_{30}\text{Cu}_{\text{Mg}(10)\text{Al}}$ precursors showed peaks similar to that of $^7_{30}\text{Cu}_{\text{Mg}(10)\text{Al}}$ sample, barringtonite [222] and gibbsite [221] are both present but on this occasion little malachite [223] was observed.

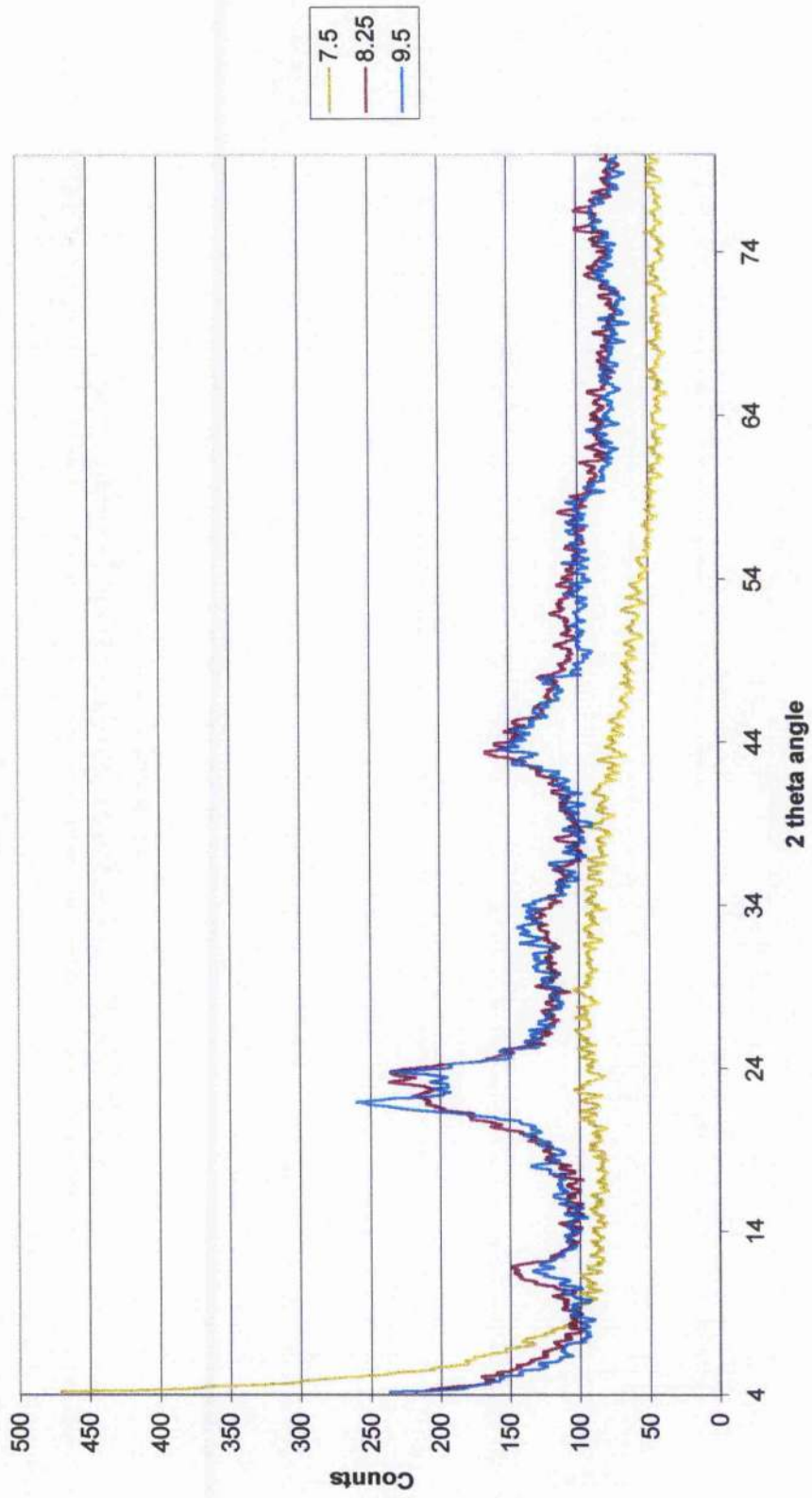
Table 4.2.1.
XRD d-spacing values (\AA) for the $^7_{30}\text{Cu}_{\text{Mg}(10)\text{Al}}$ precursor, with intensities presented in parentheses.

$^7_{30}\text{Cu}_{\text{Mg}(10)\text{Al}}$	$\text{Cu}_2\text{CO}_3(\text{OH})_2$ [223]	$\text{MgCO}_3 \cdot 2\text{H}_2\text{O}$ [222]	$\text{Al}(\text{OH})_3$ [221]
8.76(72)		8.68(100)	
5.93(79)	5.99(55)		
4.99(98)	5.05(75)		
4.86(96)			4.85(100)
4.30(90)			4.37(16)
3.67(95)	3.69(85)		
3.09(79)		3.09(100)	
2.94(79)		2.94(100)	
2.84(100)	2.85(100)		
2.50(90)		2.50(80)	

Table 4.2.2.
XRD d-spacing values (\AA) for the $^7_{30}\text{Cu}_{\text{Mg}(10)\text{Al}}$ catalyst, with intensities presented in parentheses.

$^7_{30}\text{Cu}_{\text{Mg}(10)\text{Al}}$	CuO [224]
2.74(53)	2.75(12)
2.51(100)	2.52(100)
2.31(91)	2.32(96)
1.87(46)	1.87(25)
1.77(38)	1.77(2)
1.59(37)	1.58(14)
1.50(41)	1.50(20)
1.41(43)	1.41(15)

Figure 4.2.3. XRD patterns for the $\text{Cu}_{\text{Mg}(10)\text{Al}}$ precursors with variation in pH.



Calcination at either 623 or 873 K of the ${}^{730}{}^{1}\text{Cu}_{\text{Mg}(10)\text{Al}}$ precursor resulted in a poorly crystalline sample (Figure 4.2.4), however, the second preparation at the same preparatory and calcination conditions gave crystallites of copper (II) oxide [224] (Table 4.2.2).

4.2.4 X-ray Fluorescence

The ${}^{730}{}^{1}\text{Cu}_{\text{Mg}(10)\text{Al}}$ precursor produced both copper K_{α} and K_{β} -lines, magnesium (K_{α} -line 1.254 keV) and aluminium K_{α} -line (K_{α} -line 1.487 keV) lines (Figure 4.2.5). Nickel (K_{α} -line 7.472 keV) was a substantial contaminant of this sample, present in concentrations far larger than iron K_{α} -line peak, which was small by comparison. Other contaminants included manganese (K_{α} -line 5.895 keV) and bromine ($K_{\alpha 1}$ -line (11.923 keV) and $K_{\beta 1}$ -line (13.290 keV)). Copper K_{α} -line sum peak at 16.082 keV was also observed. Both contaminants were from the ammonium base used on preparation.

When the preparation was repeated to try and rectify the copper co-precipitation problem, the second preparation precursor contained contaminants including iron (K_{α} -line), manganese (K_{α} -line), cobalt (K_{α} -line peak (6.925 keV)), nickel (K_{α} -line), sodium (K_{α} -line (1.041 keV)) and zinc (K_{α} -line peak (8.631 keV)). No relevant K_{β} -lines were observed, presumably due to the already small size of the K_{α} -line peaks. Magnesium (K_{α} -line), aluminium (K_{α} -line) and copper (K_{α} and K_{β} -lines) were all present in varying amounts with copper sum peaks (K_{α} -line and K_{β} -line (17.814 keV)) also visible.

Figure 4.2.4. XRD patterns for the $\text{Cu}_{\text{Mg(10)Al}}$ catalysts with variation in preparation conditions and calcination temperature (K).

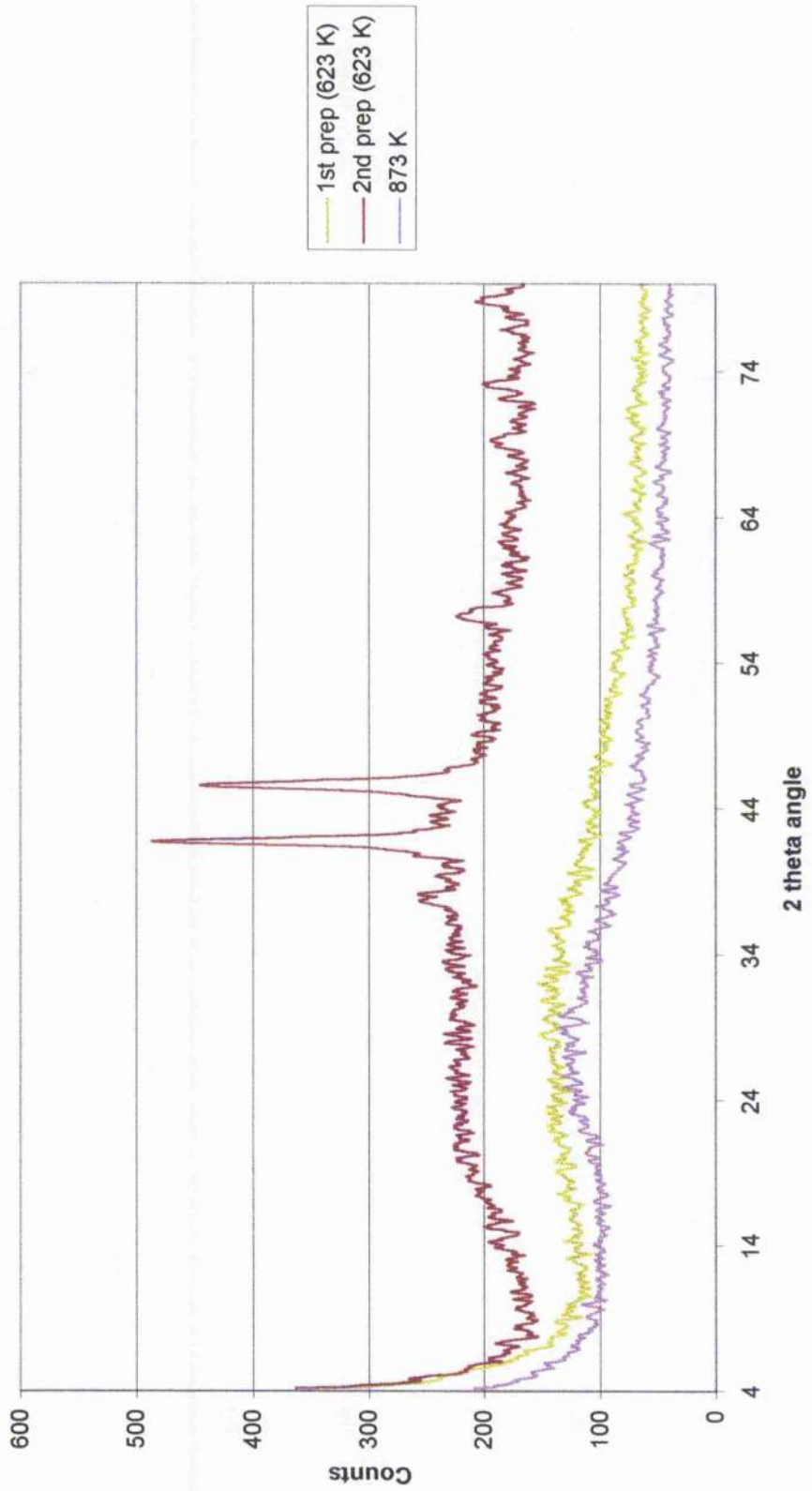


Figure 4.2.5. XRF spectrum for the $^{7}_{30}\text{Cu}_{\text{Mg}(10)\text{Al}}$ precursor.

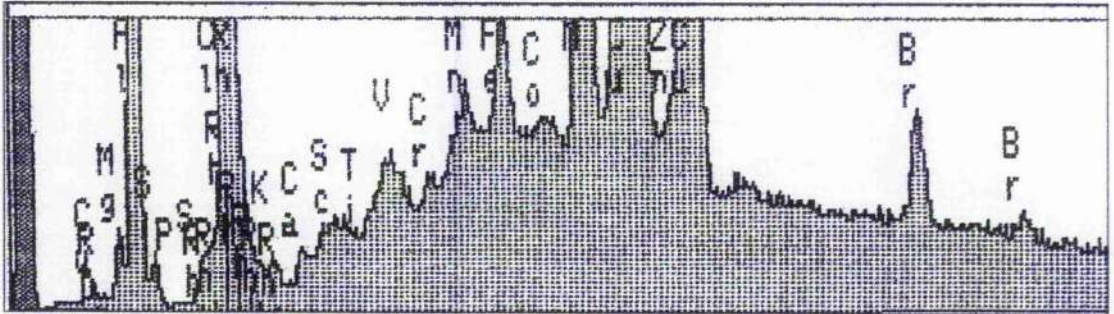


Figure 4.2.6. XRF spectrum for the $^{9.5}_{30}\text{Cu}_{\text{Mg}(10)\text{Al}}$ precursor.

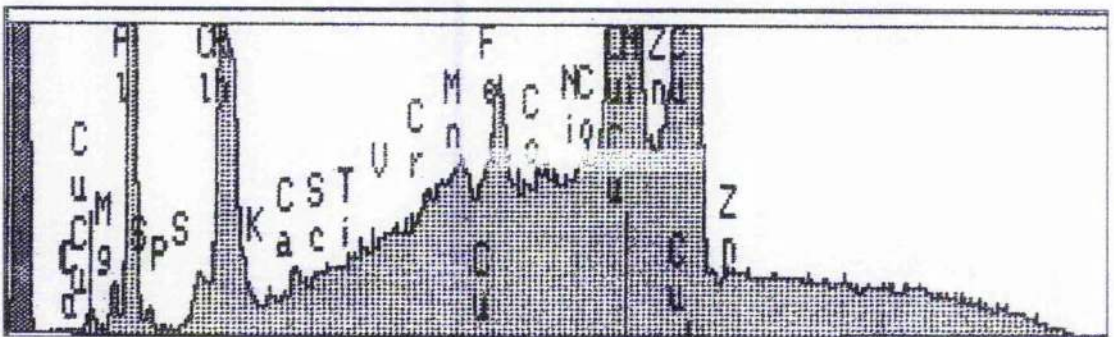


Figure 4.2.7. XRF spectrum for the calcined 623 K $^{7}_{30}\text{Cu}_{\text{Mg}(10)\text{Al}}$ catalyst.

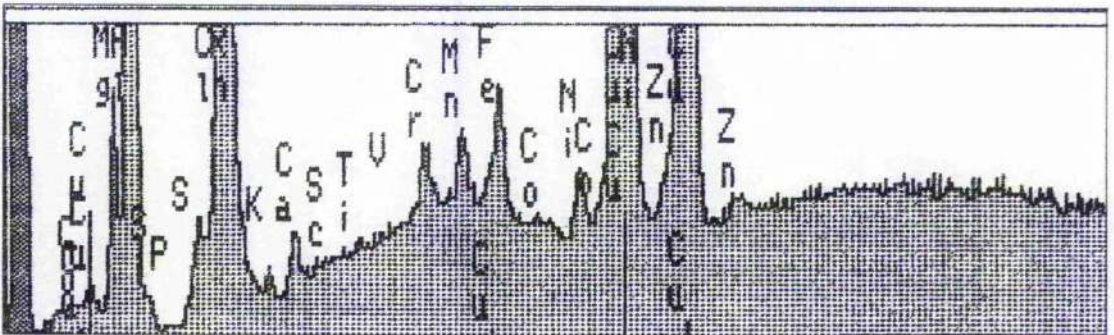
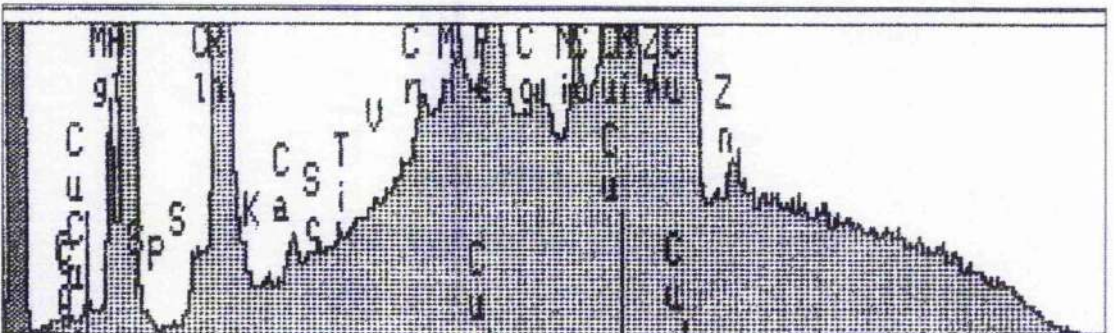


Figure 4.2.8. XRF spectrum for the calcined 873 K $^{7}_{30}\text{Cu}_{\text{Mg}(10)\text{Al}}$ catalyst.



Increasing the pH to 8.25 lowered the concentration of contaminants and increased the magnesium peak in the precursor. However, further increase to pH = 9.5 resulted in no change in concentration of the substituents (Figure 4.2.6).

The XRF spectrum (Figure 4.2.7) of the $^{7}_{30}\text{Cu}_{\text{Mg}(10)\text{Al}}$ catalyst calcined at 623 K, gave the presence of copper, magnesium and aluminium. Impurities that were also present were zinc, cobalt, iron, manganese, nickel and calcium. On increasing the calcination temperature, the peaks became more distinguishable against the background and were clearly observed in the spectrum for the precursor calcined at 873 K (Figure 4.2.8). This compares against the precursor where bromine was present. The decrease in the background had resulted in further peaks of zinc, cobalt, manganese and calcium being observed. All the impurities were from either the metal nitrate salts or the ammonium base.

With the inclusion of the chromium filter, no chlorine was observed in any sample.

4.2.5 Atomic Absorption Spectroscopy

Table 4.2.3. Percentage of copper co-precipitated (wt / wt) for the $\text{Cu}_{\text{Mg}(10)\text{Al}}$ catalysts with variation in preparation conditions.

pH	$^{7}_{30}\text{Cu}_{\text{Mg}(10)\text{Al}}$	$^{7}_{30}\text{Cu}_{\text{Mg}(10)\text{Al}}$	$^{7.5}_{30}\text{Cu}_{\text{Mg}(10)\text{Al}}$	$^{8.25}_{30}\text{Cu}_{\text{Mg}(10)\text{Al}}$	$^{9.5}_{30}\text{Cu}_{\text{Mg}(10)\text{Al}}$
Percentage co-precipitated (wt / wt)	16.6	20.6	27.4	31.2	37.6

The concentration of the copper content in the $^{7}_{30}\text{Cu}_{\text{Mg}(10)\text{Al}}$ catalyst proved to be only 16.6 % rather than the theoretical 50 % value (Table 4.2.3). The $^{7}_{30}\text{Cu}_{\text{Mg}(10)\text{Al}}$ catalyst contained only 20.6 % copper. At pH = 7.5 increased the copper concentration to

27.4 %. By pH = 8.25, the percentage of copper in the calcined catalyst had increased to 31.2 % and at pH = 9.5, 37.6 % of the catalyst was copper. Increasing the pH increased the quantity of copper co-precipitation. This was due to more favourable preparation conditions.

A complete AAS analysis was conducted on the $^{730}\text{Cu}_{\text{Mg}(10)\text{Al}}$ catalyst (Table 4.2.4), 88.2 % of the magnesium co-precipitated from the mother liquor and 28.0 % of the aluminium. This gave a final metal ratio of 28.6 % copper, 31.5 % magnesium and 40.0 % aluminium, which was considerably different from the theoretical ratio required.

Table 4.2.4. Metal composition for the $^{730}\text{Cu}_{\text{Mg}(10)\text{Al}}$ catalyst.

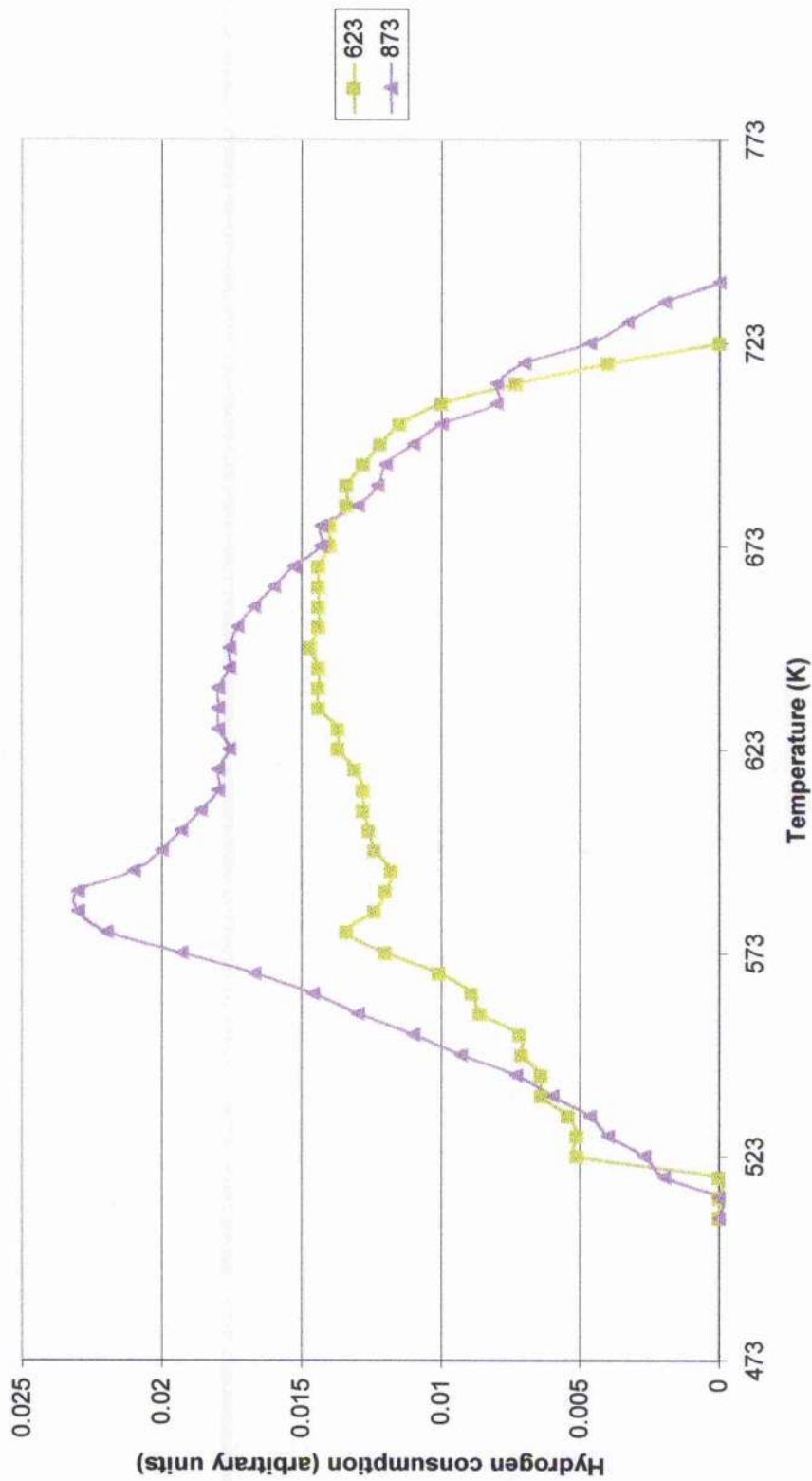
Element	Copper	Magnesium	Aluminium
Percentage co-precipitated (wt / wt)	16.6	88.2	28.0
Metal ratio	28.6	31.5	40.0

4.2.6 Temperature Programmed Reduction

The TPR profiles of the $^{730}\text{Cu}_{\text{Mg}(10)\text{Al}}$ catalysts (calcined at 623 K and 873 K) began reduction at 518 K and steadily increased to a peak at 593 K, which was more prominent in the higher calcined sample (Figure 4.2.9). A second noticeable reduction phase occurred from 623 K. The 623 K calcined sample showed this plateau until temperatures exceeding 673 K, while the other sample showed this feature up to 653 K.

The 623 K calcined sample completed reduction at a temperature of 728 K and the 873 K calcined sample at 738 K.

Figure 4.2.9. TPR profiles for the $\text{Cu}_{\text{Mg}(10)\text{Al}}$ catalysts with variation in calcination temperature (K).



4.2.7 Nitrous Oxide Chemisorption and Copper Surface Area measurements

Nitrous oxide chemisorption results gave a copper concentration of between 3 and 4 % (Table 4.2.5). This was considerably lower than the AAS results, presumable due to incomplete copper reduction. The dispersion of the 623 K calcined sample gave a copper dispersion of 55.2 %, which was considerable higher than the sample calcined at the more elevated temperature. The copper surface area values reflected the difference in dispersion with a larger result being observed for the 623 K calcined sample.

Table 4.2.5. Nitrous oxide chemisorption results for the $^{730}Cu_{Mg(10)Al}$ with variation in calcination temperature.

Calcination Temperature (K)	623	873
% Cu in catalyst	3.7	3.1
% dispersion	55.2	8.1
Particle size (nm)	1.9	12.8
% calibrated dispersion	58.4	8.4
Calibrated particle size (nm)	17.8	12.4
Copper surface area ($m^2 g^{-1}$)	13.5	5.3

However, the surface reduction temperatures for the $^{730}Cu_{Mg(10)Al}$ catalysts (Table 4.2.6) did not vary with calcination temperature, both samples start reducing at 378 K, a maximum reduction temperature of 441 K and completed by 506 K.

Table 4.2.6. Copper surface reduction for the $^{730}Cu_{Mg(10)Al}$ catalysts temperatures with variation in calcination temperature.

Temperature (K)	$T_{initial}$	T_{max}	$T_{complete}$
623	378	441	506
873	378	441	506

4.2.8 Elemental Analysis

The $^{7}_{30}\text{Cu}_{\text{Mg}(10)\text{Al}}$ precursors contained 1.9 % carbon, 2.8 % hydrogen, 2.5 % nitrogen and 0.02 % sulfur (Table 4.2.7). The $^{7}_{30}\text{Cu}_{\text{Mg}(10)\text{Al}}$ precursor resulted in a significant increase in all four detectable elements. The largest increase being observed with nitrogen.

Table 4.2.7. Elemental Analysis results for the $\text{Cu}_{\text{Mg}(10)\text{Al}}$ precursors with variation in pH.

Element	C	H	N	S
$^{7}_{30}\text{Cu}_{\text{Mg}(10)\text{Al}}$	1.9	2.8	2.5	0.02
$^{7}_{30}\text{Cu}_{\text{Mg}(10)\text{Al}}$	5.2	4.5	9.2	0.04
$^{8.25}_{30}\text{Cu}_{\text{Mg}(10)\text{Al}}$	0.14	3.8	9.9	0.03
$^{9.5}_{30}\text{Cu}_{\text{Mg}(10)\text{Al}}$	0.08	4.2	4.9	0.02

Increasing the pH to 8.25 dramatically reduced the carbon content and marginally the hydrogen and sulfur concentrations. Nitrogen showed an increase. By pH = 9.5, the carbon and sulfur content had decreased further. At this pH, the nitrogen content also decreased. Hydrogen however, increased in concentration.

Little difference in C, H or N concentrations was observed with variation in calcination temperature (Table 4.2.8) but sulfur increased.

Table 4.2.8. Elemental Analysis results for the $^{7}_{30}\text{Cu}_{\text{Mg}(10)\text{Al}}$ catalysts with variation in calcination temperature.

Element	C	H	N	S
623 K	1.5	3.6	nda	0.02
873 K	1.5	3.2	nda	0.03

nda = non-detectable amount

4.2.9 BET surface area measurements

The surface area for the $^{7}_{30}\text{Cu}_{\text{Mg}(10)\text{Al}}$ catalysts (Table 4.2.9) varied significantly with calcination temperature. The lower calcination temperature resulted in a BET surface

area of $641 \text{ m}^2 \text{ g}^{-1}$, while the other catalyst gave only a value of $49.7 \text{ m}^2 \text{ g}^{-1}$. The former was repeated to verify the very high surface area.

Table 4.2.9.
BET surface area measurements for the $^{73}\text{Cu}_{\text{Mg}(10)\text{Al}}$ catalysts with variation in calcination temperature.

Calcination temperature (K)	623	873
Single Point ($\text{m}^2 \text{ g}^{-1}$)	602	46.8
BET surface area ($\text{m}^2 \text{ g}^{-1}$)	641	49.7

4.2.10 Summary

Very low co-precipitation of all components was clearly observed. This resulted in a metal ratio different than the theoretical, non-homogeneous samples and various crystallite phases being formed. The relatively large magnesium concentration increased the stability by the decomposition temperatures. The increase in calcination temperature decreased the copper dispersion and surface areas and the BET surface areas. Impurities were observed in all samples regardless of calcination temperature.

4.3 Binary Catalysts

These catalysts were prepared as a basis for the subsequent ternary and tertiary catalysts and as a result were fully characterised. No microreactor experiments were on conducted on these catalysts.

4.3.1 Cu/MgO (60/40) (Cu_{Mg})

4.3.1.1 Preparation

During ageing, the mother liquor of most of the samples was pale blue in colour with two exceptions. The solution of the ¹⁰₃₀Cu_{Mg} sample converted to a black suspension, indicative of degradation signifying that the desired precursor was unstable and had decomposed. When ageing the ⁹₁₄₀Cu_{Mg} sample, the colour became a very dark blue, which indicated imminent decomposition into a suspension to that of the ¹⁰₃₀Cu_{Mg} sample, as a result, the preparatory conditions of pH = 10 was not pursued in the later ternary catalyst preparations.

The filtrate of the mother liquor in all preparations were clear, indicating that complete copper co-precipitation had occurred in all cases independent of pH.

All dried precursors except the ⁹₁₄₀Cu_{Mg} and the ¹⁰₃₀Cu_{Mg} were of similar pale turquoise colour, possibly indicative of malachite. The ⁹₁₄₀Cu_{Mg} and the ¹⁰₃₀Cu_{Mg} were dark turquoise and dark grey respectively, indicating that a different phase was formed during preparation under those conditions.

On calcination, all samples were various shades of brown, darkening with decreasing pH. The change in colour on calcination suggested that the precursors had decomposed.

4.3.1.2 Differential Thermal Analysis

The first peak was observed at 473 K and was evident for the $^8_{70}\text{Cu}_{\text{Mg}}$ and $^8_{140}\text{Cu}_{\text{Mg}}$ samples (Figure 4.3.1). This endothermic peak was indicative of the partial loss of water from the structure.

The major endothermic peak was present at 513 K and was present in all 3 samples. This was due to either further water loss or dehydroxylation. The $^8_{70}\text{Cu}_{\text{Mg}}$ sample showed the largest endothermic peak at this temperature, preceded by the $^8_{140}\text{Cu}_{\text{Mg}}$ precursor and finally the $^8_{30}\text{Cu}_{\text{Mg}}$ sample.

The last endothermic peak was observed between 693 and 698 K and was due to decarboxylation. The peak shifted to higher temperature on increasing the ageing time.

4.3.1.3 X-ray Diffraction

The XRD pattern (Figure 4.3.2) of the $^7_{30}\text{Cu}_{\text{Mg}}$ sample was very different from that of the pH = 8, 9 and 10 samples. The $^7_{30}\text{Cu}_{\text{Mg}}$ precursor consisted primarily of malachite ($\text{Cu}_2\text{CO}_3(\text{OH})_2$) [223] but the peaks 2θ values of 14.8° , 25.2° , 30.0° and 39.2° were chalconatronite ($\text{Na}_2\text{Cu}(\text{CO}_3)_2 \cdot 3\text{H}_2\text{O}$) [225]. The remaining precursors in this figure all showed a small peak at 14.8° , which decreased with increasing pH.

Comparison with variation in ageing time for the pH = 8 precursors was shown in Figure 4.3.3. The $^8_{70}\text{Cu}_{\text{Mg}}$ precursor contained a mixture of phases, these are $\text{Na}_2\text{Cu}(\text{CO}_3)_2 \cdot 3\text{H}_2\text{O}$ [225], $\text{CuO} \cdot 3\text{H}_2\text{O}$ [226] and $\text{MgCO}_3 \cdot 2\text{H}_2\text{O}$ [222] (Table 4.3.1). The sample prepared for $^8_{140}\text{Cu}_{\text{Mg}}$ also showed these peaks but with lower crystallinity.

Calcination resulted in large CuO [224] crystallites being formed, which were clearly evident in the $^7_{30}\text{Cu}_{\text{Mg}}$ sample (Figure 4.3.4). These peaks decreased with

Figure 4.3.1. DTA profiles for the ${}^8\text{Cu}_{\text{Mg}}$ precursors with variation in ageing time.

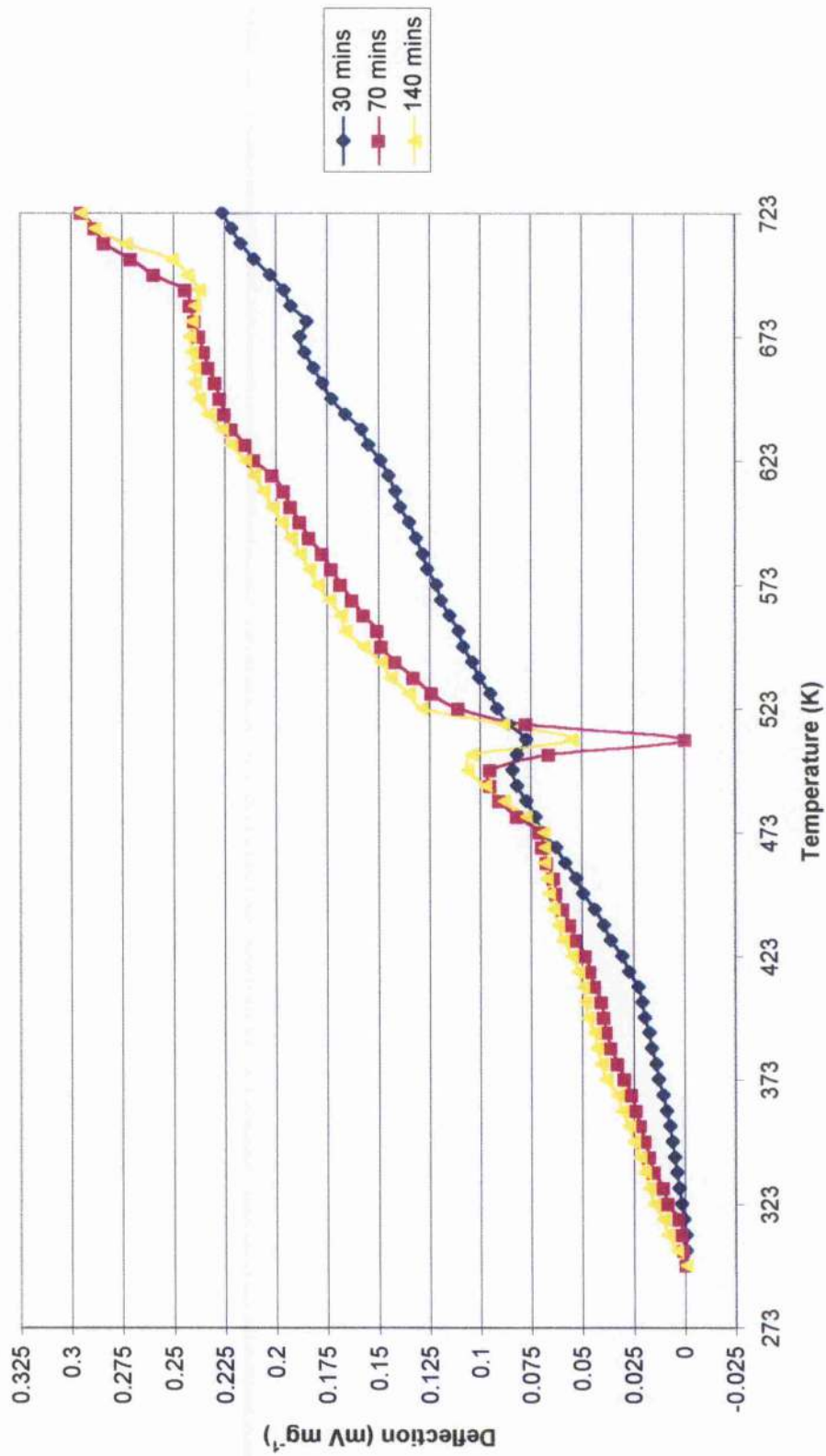


Figure 4.3.2. XRD patterns for the Cu_{Mg} precursors with variation in pH (30 mins ageing time).

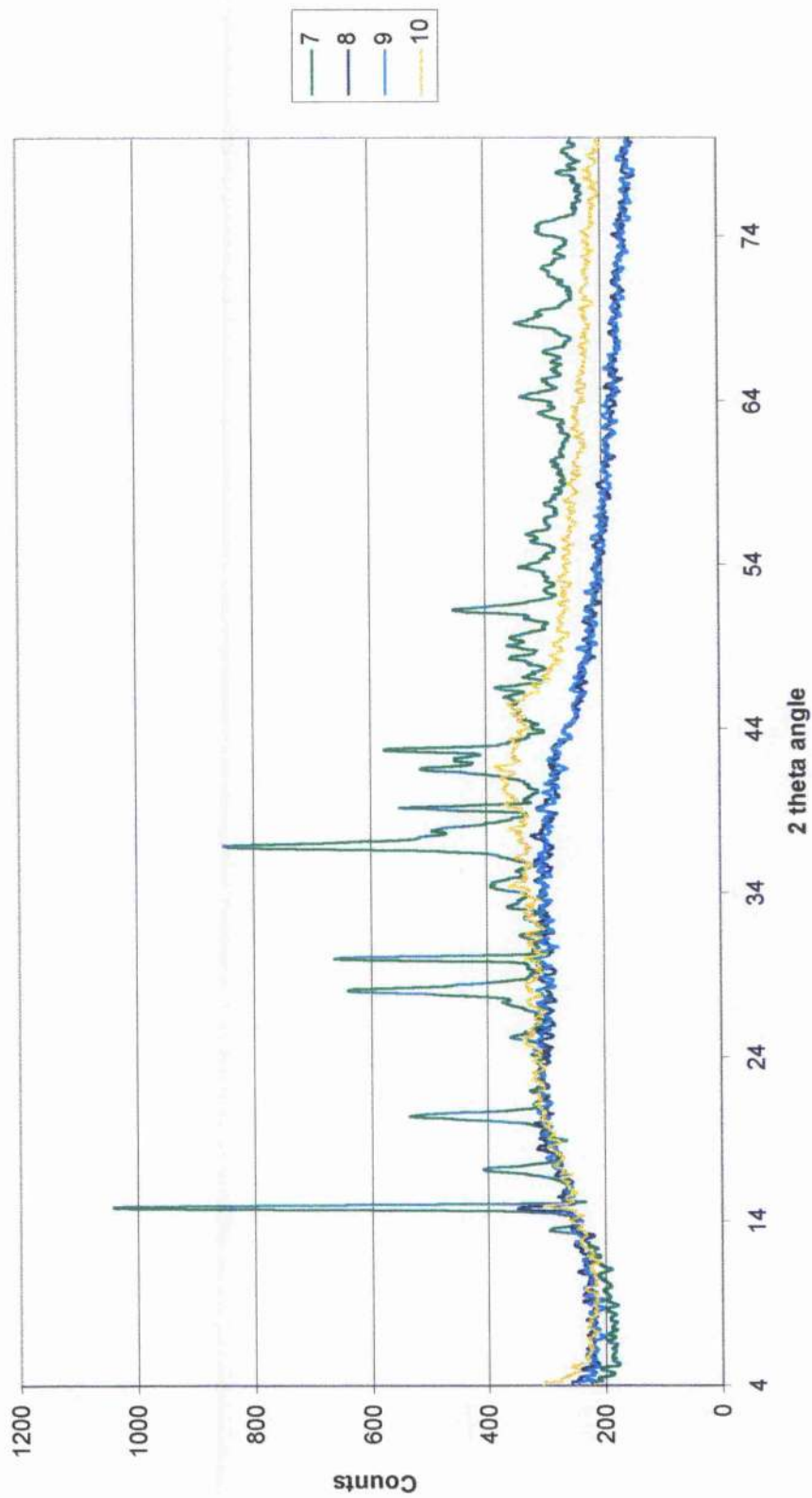


Figure 4.3.3.
XRD patterns for the $^8\text{Cu}_{\text{Mg}}$ precursors with variation in ageing time.

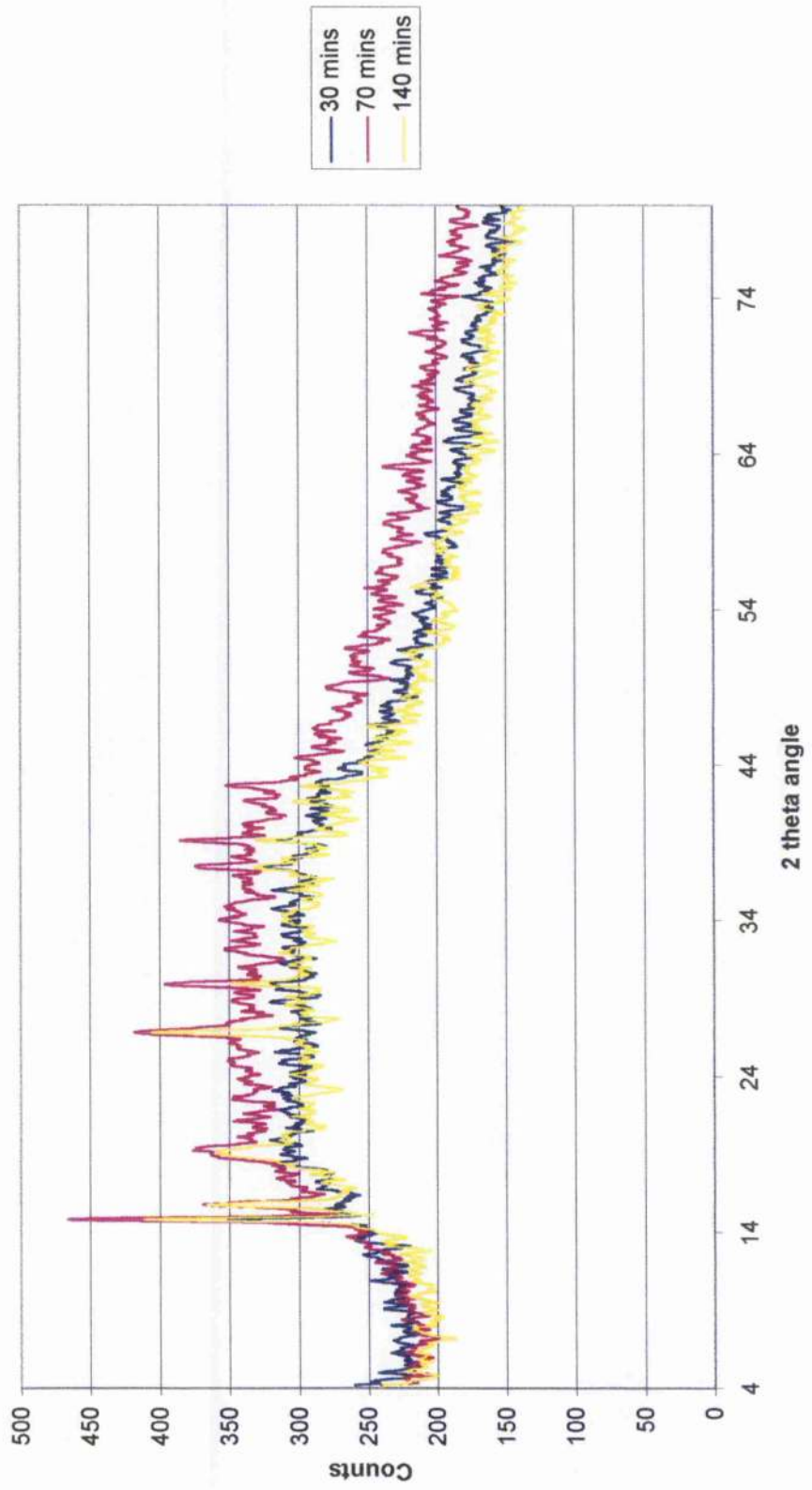
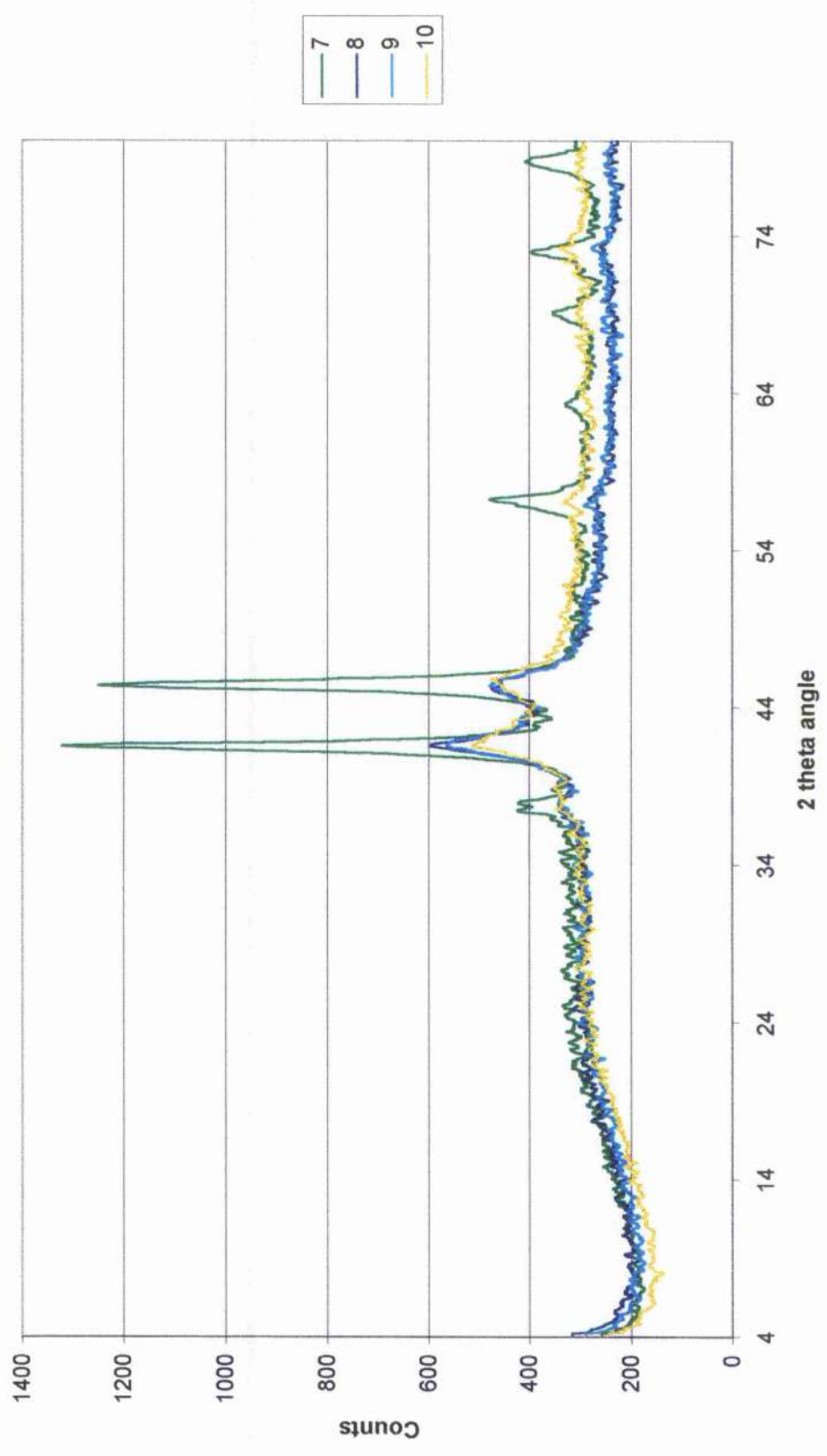


Figure 4.3.4. XRD patterns for the Cu_{Mg} catalysts with variation in pH (30 mins ageing time).



increasing pH. The XRD patterns for the pH = 8 catalysts show Cu(II)O [224] peaks (Figure 4.3.5), which decreased with lower ageing time.

Table 4.3.1. XRD d-spacing values (Å) for the ${}^8{}_{70}\text{Cu}_{\text{Mg}}$ precursor, with intensities presented in parentheses.

${}^8{}_{70}\text{Cu}_{\text{Mg}}$	$\text{Na}_2\text{Cu}(\text{CO}_3)_2 \cdot 3\text{H}_2\text{O}$ [225]	$\text{CuO} \cdot 3\text{H}_2\text{O}$ [226]	$\text{MgCO}_3 \cdot 2\text{H}_2\text{O}$ [222]
6.94(100)	6.90(100)		
6.52(79)		6.52(20)	
5.29(80)			5.25(20)
3.86(90)			3.87(20)
3.47(85)	3.45(40)		
2.78(80)	2.78(30)	2.77(20)	
2.67(83)	2.67(50)	2.63(100)	
2.46(76)	2.46(40)		

The ${}^9{}_{140}\text{Cu}_{\text{Mg}}$ precursor XRD profile (Figure 4.3.6) was a poorly crystalline sample and on calcination, bulk CuO [224] was formed.

4.3.1.4 X-ray Fluorescence

At pH = 7, the magnesium $\text{K}\alpha$ -line (1.254keV) peak was barely visible unlike the copper $\text{K}\alpha$ and $\text{K}\beta$ -line peaks, which were significantly larger. Copper sum peaks were also present at higher keV. Iron ($\text{K}\alpha$ -line peak), calcium ($\text{K}\alpha$ -line peak) and potassium ($\text{K}\alpha$ -line peak) were also present in these precursors with the iron peak being observed in the largest concentration. The spectrum of the ${}^8{}_{70}\text{Cu}_{\text{Mg}}$ precursor was shown in Figure 4.3.7.

Upon calcination, the background noise decreased, which consequently attenuated the calcium, iron and potassium peaks enabling them to become more discernible. The ${}^8{}_{30}\text{Cu}_{\text{Mg}}$ and ${}^8{}_{140}\text{Cu}_{\text{Mg}}$ catalysts were shown in Figure 4.3.8 and 4.3.9

Figure 4.3.5. XRD patterns for the $^{\circ}\text{Cu}_{\text{Mg}}$ catalysts with variation in ageing time.

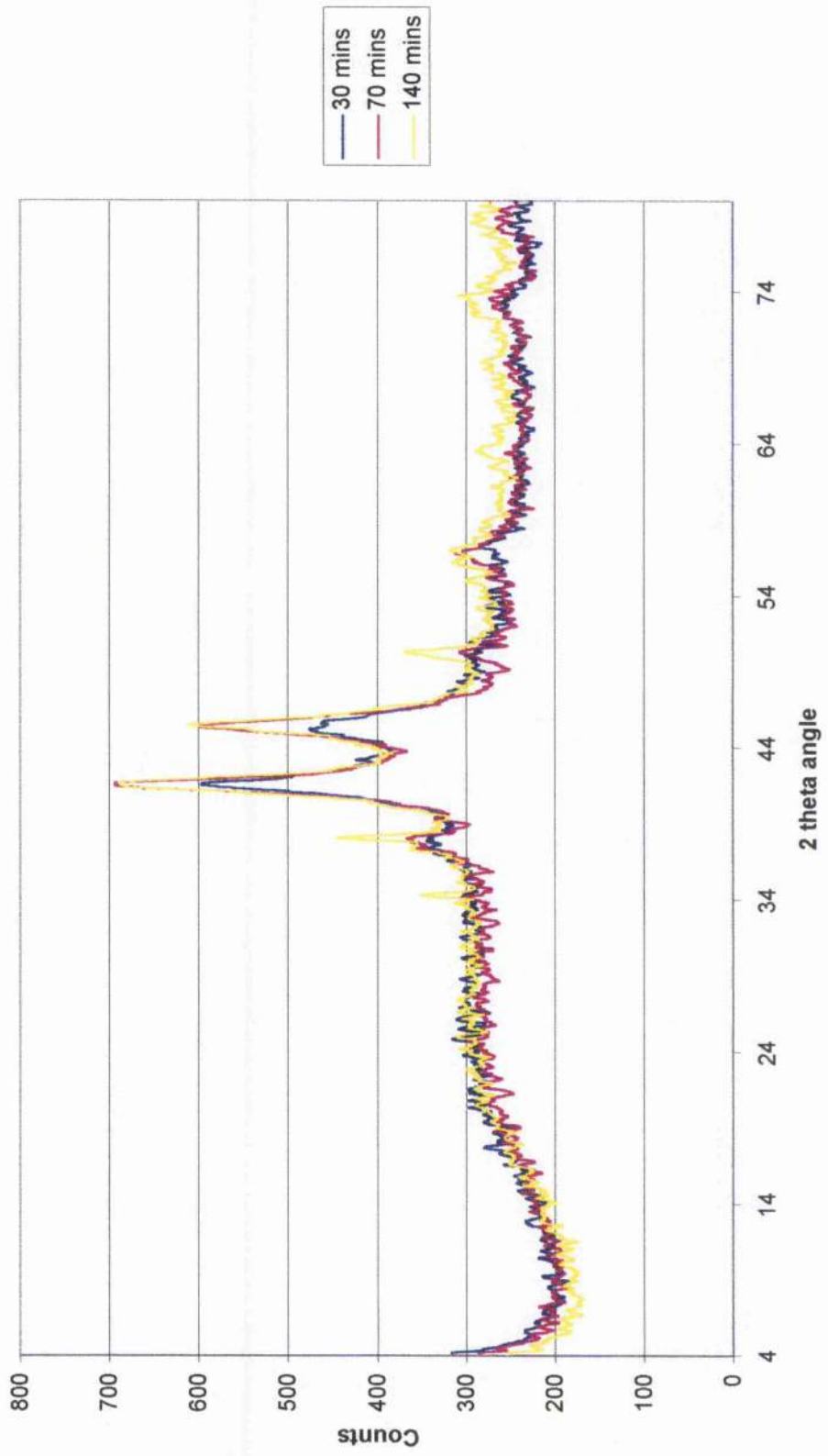


Figure 4.3.6. XRD patterns for the $^{99}\text{Tm}^{3+}$ precursor and catalyst.

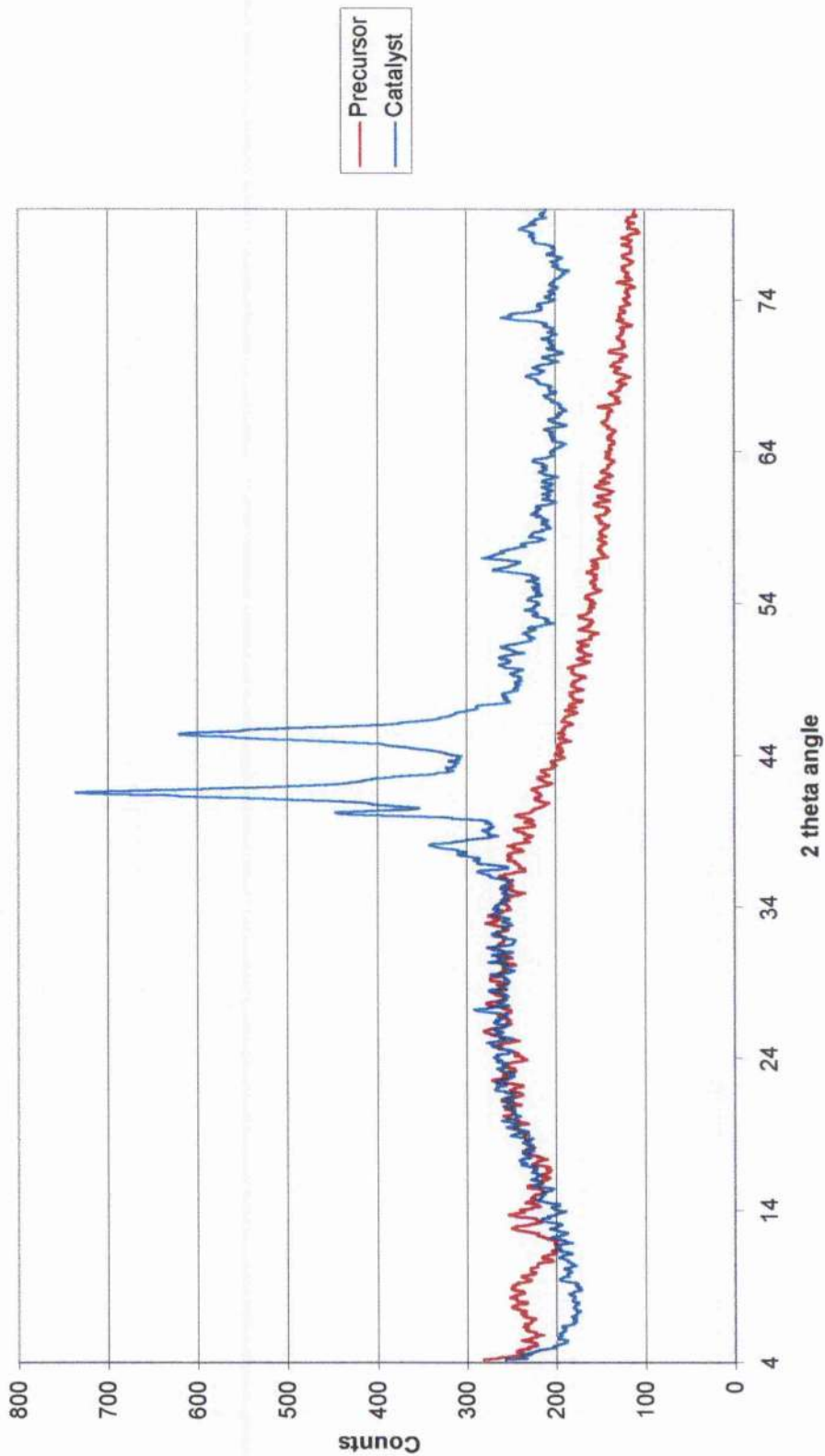


Figure 4.3.7. XRF spectrum for the $^{87}\text{Cu}_{\text{Mg}}$ precursor.

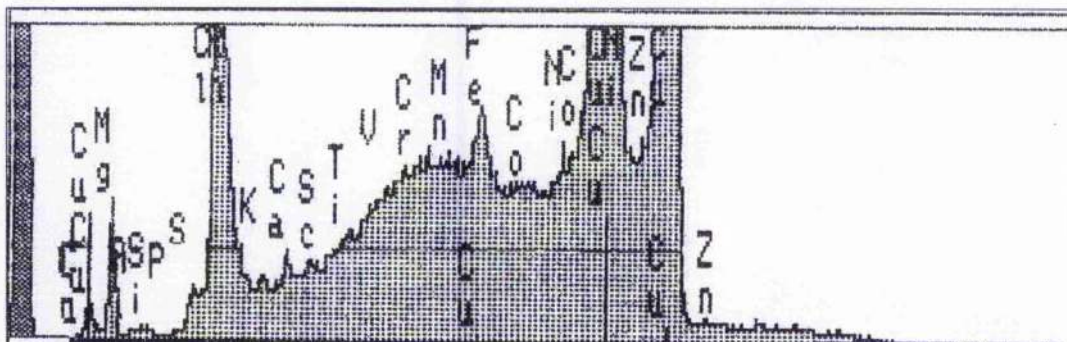


Figure 4.3.8. XRF spectrum for the $^{83}\text{Cu}_{\text{Mg}}$ catalyst.

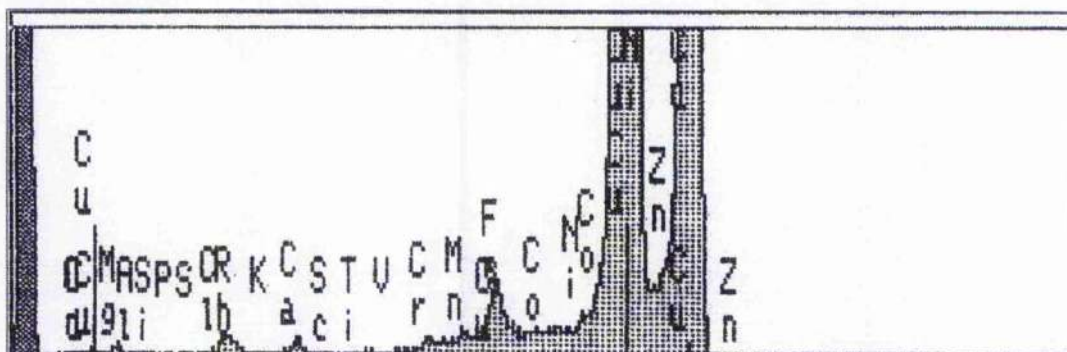
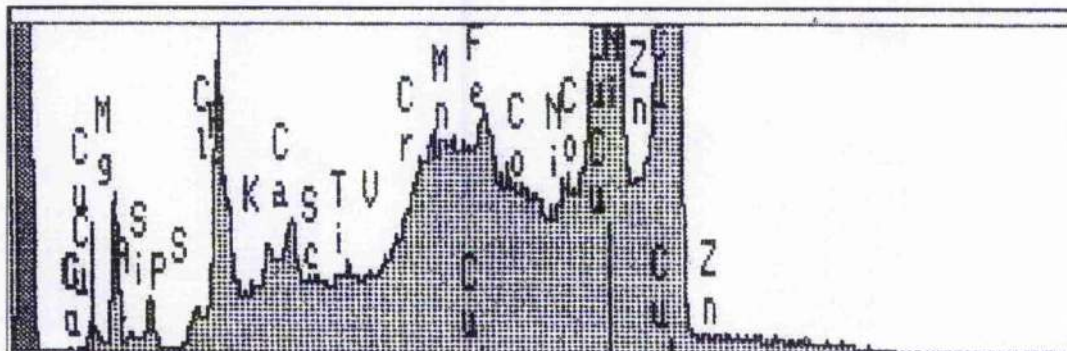


Figure 4.3.9. XRF spectrum for the $^{140}\text{Cu}_{\text{Mg}}$ catalyst.



respectively. The peak height of iron increased with pH and ageing time. No change was observed with potassium or calcium.

Addition of the chromium filter, confirmed that no chlorine was present in any of these precursors or catalysts.

4.3.1.5 Atomic Absorption Spectroscopy

No copper AAS analysis was conducted on any of the calcined samples as it was deemed unnecessary, as all the filtrate solutions were clear. However, magnesium AAS (Table 4.3.2) on the dark brown catalysts were performed.

When varying the pH (30 mins ageing), it was evident that a maximum magnesium co-precipitation occurred between pH = 8 and 9. Increasing the ageing time above 30 mins, the magnesium concentration decreased to approximately a third of the desired concentration. At lower pH, magnesium did not co-precipitate and at high pH and lengthening ageing time, the magnesium redissolved into liquid form.

Table 4.3.2. Percentage of magnesium co-precipitated (wt / wt) for the Cu_{Mg} catalysts with variation in preparation conditions.

Preparation pH	7	8	9	10
30 mins	10.7	72.5	55.9	33.0
70 mins	-	67.2	52.5	-
140 mins	-	32.3	33.0	-

Table 4.3.3. Copper metal ratio for the Cu_{Mg} catalysts with variation in preparation conditions.

Preparation pH	7	8	9	10
30 mins	93.3	67.4	72.9	82.0
70 mins	-	69.1	74.1	-
140 mins	-	82.3	82.0	-

Tables 4.3.3 and 4.3.4 showed the final metal ratio for the Cu_{Mg} catalysts. The catalyst

that was closest to the required ratio was the $^8_{30}\text{Cu}_{\text{Mg}}$ catalyst with the $^7_{30}\text{Cu}_{\text{Mg}}$ being the worst. As a result of the low magnesium concentration in the $^7_{30}\text{Cu}_{\text{Mg}}$ catalyst, preparation conditions at this pH were discounted.

Table 4.3.4. Magnesium metal ratio for the Cu_{Mg} catalysts with variation in preparation conditions.

Preparation pH	7	8	9	10
30 mins	6.7	32.6	27.2	18.0
70 mins	-	30.9	25.9	-
140 mins	-	17.7	18.0	-

4.3.1.6 Temperature Programmed Reduction

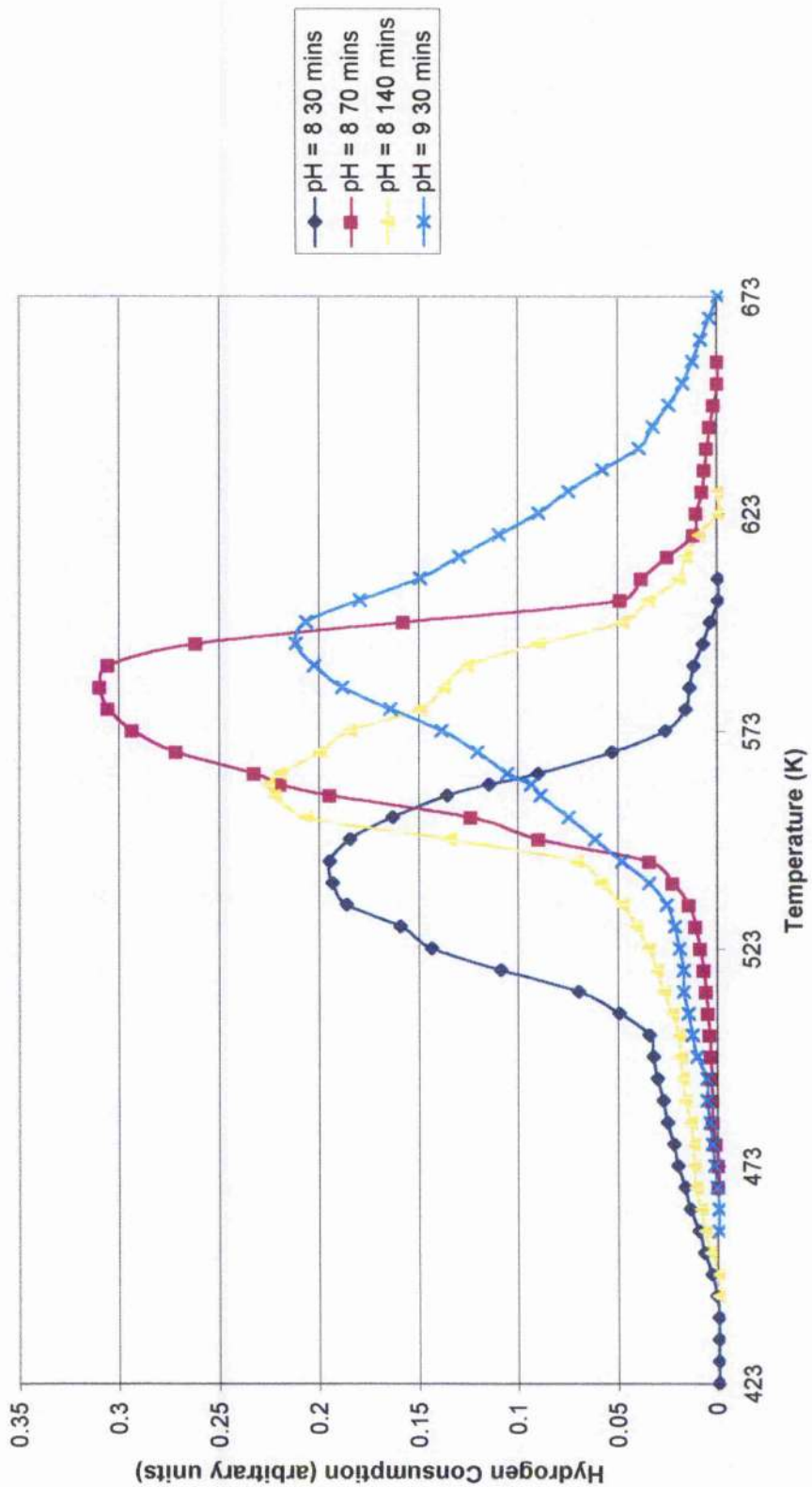
The profile of the $^8_{30}\text{Cu}_{\text{Mg}}$ catalyst gradually consumed hydrogen until 503 K whereupon a sharp increase occurred until a T_{max} of 543 K (Figure 4.3.10). Hydrogen consumption decreased sharply to 573 K and by 603 K reduction was complete.

The $^8_{70}\text{Cu}_{\text{Mg}}$ sample had a T_{max} of 573 K with no obvious sign of reduction around 493-513 K. The sample reduced to a greater extent than the other two preparations as more hydrogen was consumed. After the maximum reduction temperature, the quantity of reduction decreased drastically before completion at 653 K.

The main reduction process for the $^8_{140}\text{Cu}_{\text{Mg}}$ sample occurred at ca. 560 K, with a small amount being reduced around 493-513 K.

The $^9_{30}\text{Cu}_{\text{Mg}}$ catalyst gave the broadest range of reduction temperatures of these four profiles. The quantity of reduction increased slowly until 538 K where hydrogen consumption increased rapidly until a maximum reduction temperature of 593 K. The reduction process was complete by 673 K.

Figure 4.3.10. TPR profiles for the Cu_{10}g catalysts with variation in preparation conditions.



4.3.1.7 Nitrous Oxide Chemisorption and Copper Surface Area measurements

The ${}^8_{70}\text{Cu}_{\text{Mg}}$ samples had the largest dispersion of the four samples at 12.4 %, and therefore the smallest copper particle size (Table 4.3.5). No trend was observed with variation in ageing time or pH. Considering the quantity of copper present in the catalyst, the copper surface areas reflected the dispersion, the larger the dispersion, the larger the copper surface area. These catalysts all had a copper content percentage above the 60 % empirical value. This was due to AAS results proposing incomplete magnesium co-precipitation.

Table 4.3.5. Nitrous oxide chemisorption results for the Cu_{Mg} catalysts with variation in preparation conditions.

Catalyst	${}^8_{30}\text{Cu}_{\text{Mg}}$	${}^8_{70}\text{Cu}_{\text{Mg}}$	${}^8_{140}\text{Cu}_{\text{Mg}}$	${}^9_{30}\text{Cu}_{\text{Mg}}$
% Cu in catalyst	70.4	71.1	69.3	61.1
% dispersion	9.0	12.4	6.4	10.3
Particle size (nm)	11.6	8.4	16.3	10.3
% calibrated dispersion	9.8	13.0	7.3	10.6
Calibrated particle size (nm)	10.6	8.0	14.2	10.0
Copper surface area ($\text{m}^2 \text{g}^{-1}$)	41.8	65.2	31.6	40.6

Table 4.3.6. Copper surface reduction temperatures for the Cu_{Mg} catalysts with variation in preparation conditions.

Temperature (K)	T_{initial}	T_{max}	T_{complete}
${}^8_{30}\text{Cu}_{\text{Mg}}$	403	436	463
${}^8_{70}\text{Cu}_{\text{Mg}}$	421	463	498
${}^8_{140}\text{Cu}_{\text{Mg}}$	423	453	483
${}^9_{30}\text{Cu}_{\text{Mg}}$	418	467	506

Surface reduction temperatures differ with preparation conditions (Table 4.3.6). The highest copper surface reduction temperature was observed with the ${}^9{}_{30}\text{Cu}_{\text{Mg}}$ catalyst of 467 K. This temperature was over 30 K greater than the ${}^8{}_{30}\text{Cu}_{\text{Mg}}$ sample. At pH = 8, the ${}^8{}_{70}\text{Cu}_{\text{Mg}}$ sample had the highest copper surface reduction temperature of 453 K.

4.3.1.8 Elemental Analysis

Table 4.3.7. Elemental Analysis results for the ${}^{\text{pH}}{}_{\text{Cu}}\text{Cu}_{\text{Mg}}$ precursors with variation in preparation conditions.

Element	C	H	N	S
${}^7{}_{30}\text{Cu}_{\text{Mg}}$	4.1	1.4	0.64	0.01
${}^8{}_{30}\text{Cu}_{\text{Mg}}$	6.3	2.3	nda	0.01
${}^8{}_{70}\text{Cu}_{\text{Mg}}$	5.8	2.3	0.03	0.01
${}^8{}_{140}\text{Cu}_{\text{Mg}}$	6.7	2.6	0.15	0.02
${}^9{}_{30}\text{Cu}_{\text{Mg}}$	6.4	2.5	nda	0.01
${}^9{}_{30}\text{Cu}_{\text{Mg}}$	6.0	2.3	nda	0.01
${}^9{}_{140}\text{Cu}_{\text{Mg}}$	5.6	2.2	0.02	0.01
${}^{10}{}_{30}\text{Cu}_{\text{Mg}}$	5.3	2.3	0.07	nda

nda = non-detectable amount

The elemental analysis results showed an increase in carbon, hydrogen and sulfur concentrations with increasing pH from 7 to 8 (Table 4.3.7), while nitrogen decreased considerably.

At pH = 8, no correlation in carbon, hydrogen and sulfur content was observed with increase in ageing time yet the nitrogen concentration increased. Little difference was observed for carbon, hydrogen and sulfur from pH = 8 to 9 but the nitrogen decreased.

Increasing in pH from 9 to 10, the carbon and sulfur concentrations decreased with hydrogen remaining at a similar value and nitrogen increasing to 0.07 %.

Calcination resulted in a general decrease in the concentration of all four detectable elements (Table 4.3.8). The carbon, hydrogen and nitrogen content increased from pH = 7 to 8, carbon by a factor of nine. No trend was observed with variation in ageing time at pH = 8 for carbon, hydrogen and sulfur but the nitrogen content increased.

An increase in carbon content was observed when increasing the pH = 8 to 9. No variation was observed for hydrogen or sulfur but again, nitrogen decreased in concentration.

From pH = 9 to 10 resulted in no change in carbon, nitrogen or sulfur but nitrogen increased slightly.

The last three tabulated catalysts were only conducted once.

Table 4.3.8. Elemental Analysis results for the Cu_{Mg} catalysts with variation in preparation conditions.

Element	C	H	N	S
⁷ ₃₀ Cu _{Mg}	0.29	0.26	nda	0.01
⁸ ₃₀ Cu _{Mg}	2.3	0.99	0.01	nda
⁸ ₇₀ Cu _{Mg}	2.1	0.65	0.14	0.01
⁸ ₁₄₀ Cu _{Mg}	3.3	1.3	0.15	0.01
⁹ ₃₀ Cu _{Mg}	2.6	1.3	nda	0.01
⁹ ₃₀ Cu _{Mg}	2.9	1.2	nda	0.01
⁹ ₁₄₀ Cu _{Mg}	3.5	0.79	nda	0.01
¹⁰ ₃₀ Cu _{Mg}	3.1	1.3	0.04	0.01

nda = non-detectable amount

4.3.1.9 BET Surface Area measurements

Table 4.3.9. BET surface area measurements for various Cu_{Mg} catalysts with variation in preparation conditions.

Catalyst	⁷ ₃₀ Cu _{Mg}	⁸ ₃₀ Cu _{Mg}	⁸ ₇₀ Cu _{Mg}	⁸ ₁₄₀ Cu _{Mg}	⁹ ₃₀ Cu _{Mg}
Single Point (m ² g ⁻¹)	35.1	25.9	23.5	19.4	15.4
BET surface area (m ² g ⁻¹)	36.0	27.7	24.2	20.3	15.9

The BET surface area measurements decreased with increasing pH and ageing time from a maximum of $36.0 \text{ m}^2 \text{ g}^{-1}$ for the ${}^7_{30}\text{Cu}_{\text{Mg}}$ catalyst to $15.9 \text{ m}^2 \text{ g}^{-1}$ for the ${}^9_{30}\text{Cu}_{\text{Mg}}$ (Table 4.3.9).

4.3.2 Cu/Al₂O₃ (60/40) (Cu_{Al})

4.3.2.1 Preparation

Filtration of the mother liquor that was prepared at ${}^7_{30}\text{Cu}_{\text{Al}}$, produced a filtrate that was completely clear with no visible sign of residual copper.

For the three pH = 8 precursors, there was an approximate copper concentration of 2000-3000 ppm and a very small quantity of precipitate, with the amount decreasing with ageing time. The increase in pH to 9 considerably increased the copper filtrate concentration. The copper blue colouring significantly decreased with ageing time to ca. 2000 ppm with quantity of precipitate reducing proportionally. By pH = 10, the precipitate was held as a suspension in the filtrate.

After drying, the appearance of the precursors had altered. The ${}^7_{30}\text{Cu}_{\text{Al}}$ sample was sky blue in colour becoming darker with increasing to pH = 8 and lengthening ageing time. At pH = 9, the blue colour started to be replaced by a green colour, presumably that of malachite, again darkening on ageing to 140 mins. By pH = 10, the precipitate was almost entirely green.

On calcination, the samples went brown and darkened with increasing ageing time and decreasing pH when only aged for 30 mins. The darkest sample, the ${}^9_{140}\text{Cu}_{\text{Al}}$ precursor was almost black. The change in colour on calcination suggested decomposition of the precursor.

After 10 days, the washings were re-examined, with a general increase in green malachite based precipitate being observed for the pH = 8 and 9 samples. No change was observed for the pH = 7 and 10 samples.

4.3.2.2 Differential Thermal Analysis

The ${}^8_{30}\text{Cu}_{\text{Al}}$ precursor showed two peaks (Figure 4.3.11), both of which are endothermic. The initial peak was centred on 398 K and the second at 508 K. Increasing the ageing time to 70 mins shifted the first endothermic peak to 413 K and decreased the second peak to 503 K. The ${}^8_{140}\text{Cu}_{\text{Al}}$ sample had similar temperature values to the 30 mins sample but the first peak was smaller.

The ${}^9_{30}\text{Cu}_{\text{Al}}$ sample had a similar endothermic peak at 398-403 K but was larger in size. The second endothermic peak was present at 548 K, which was considerably higher in temperature when compared to the pH precursors.

The general upward trend was due to the heat capacitance of the samples. These precursors were conducted at the University of Edinburgh.

4.3.2.3 X-ray Diffraction

Increasing the pH of the 30 mins precursors resulted in a change of structure and subsequent enhancement of crystallinity (Figure 4.3.12). The ${}^7_{30}\text{Cu}_{\text{Al}}$ sample showed peaks consistent with malachite ($\text{Cu}_2\text{CO}_3(\text{OH})_2$) [223] and at pH = 9 and 10, these were present as $\text{Cu}_6\text{Al}_2(\text{OH})_{16}\text{CO}_3 \cdot 4\text{H}_2\text{O}$ [227], which was analogous to hydrotalcite. The pH = 8 precursors only showed the main $\text{Cu}_6\text{Al}_2(\text{OH})_{16}\text{CO}_3 \cdot 4\text{H}_2\text{O}$ [227] peaks at a d-spacing values of 7.49 and 3.74 Å.

Figure 4.3.11. DTA profiles for the Cu_{Al} precursors with variation in preparation conditions.

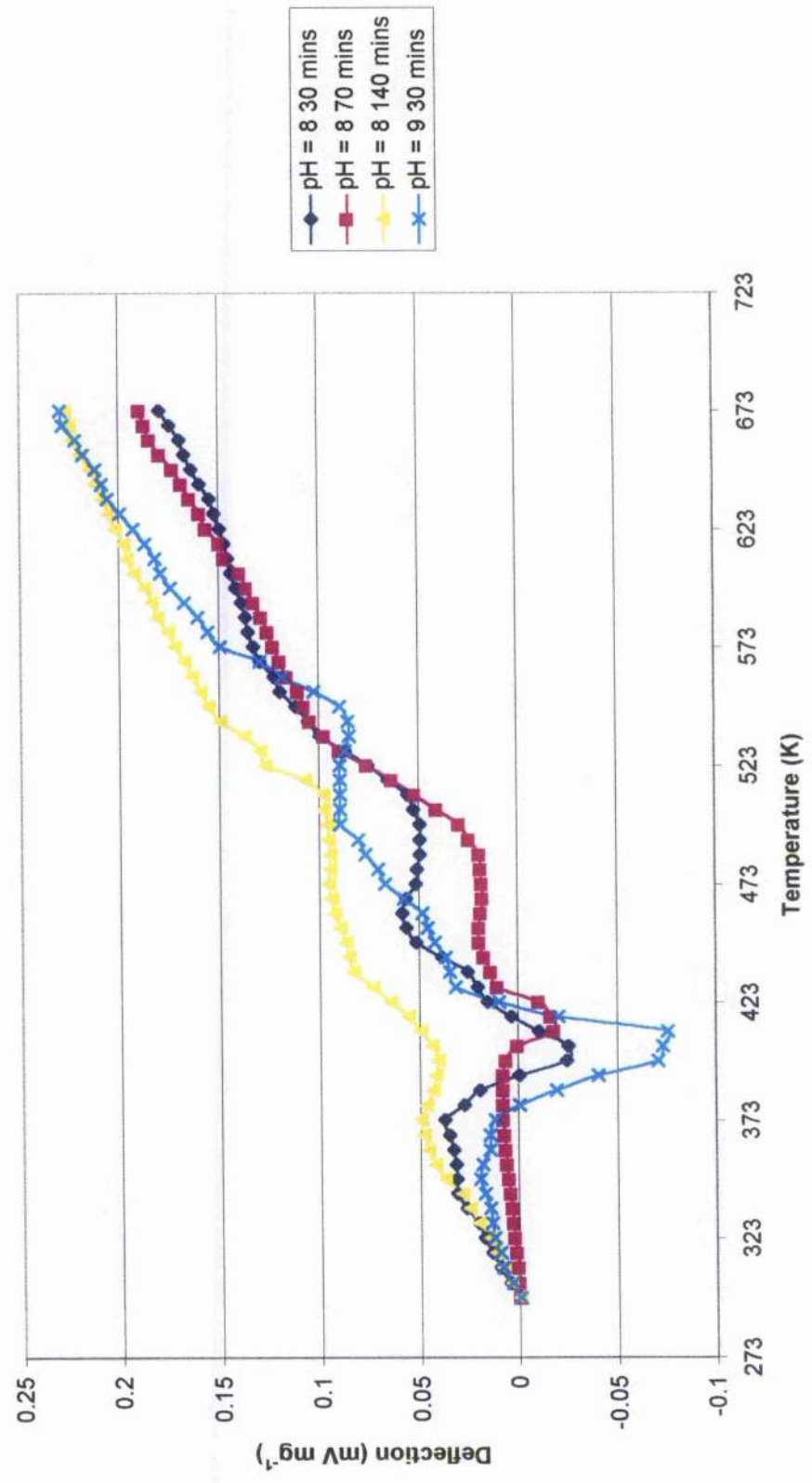
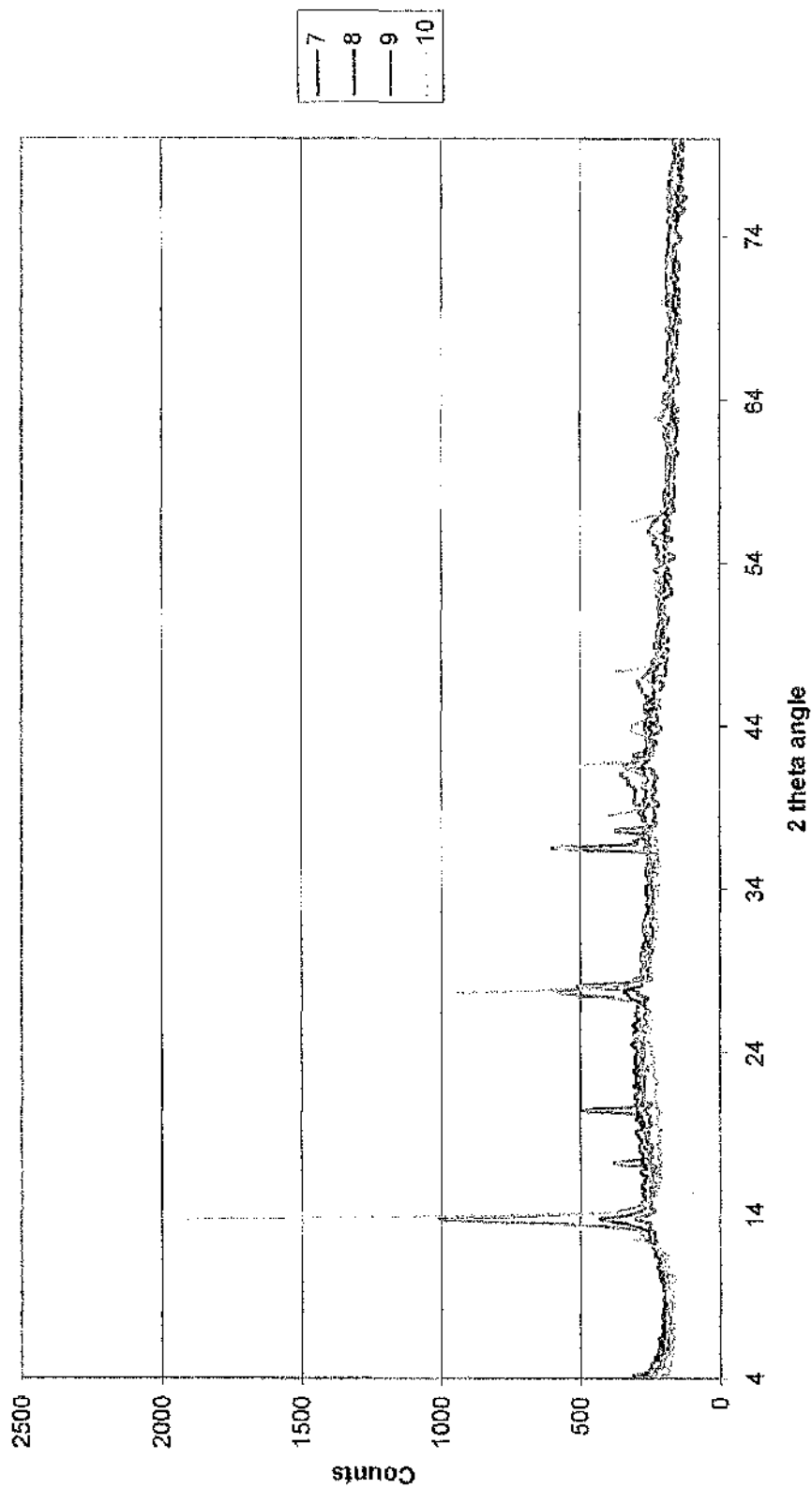


Figure 4.3.12. XRD patterns for the Cu_{Al} precursors with variation in pH (30 mins ageing time).



Little variation in crystallinity with ageing time was observed for the pH = 8 precursors (Figure 4.3.13), with only two peaks visible for all three precursors. These peaks had been assigned as $\text{Cu}_6\text{Al}_2(\text{OH})_{16}\text{CO}_3 \cdot 4\text{H}_2\text{O}$ [227].

Calcination resulted in large peaks of CuO [224] being formed for the $^7_{30}\text{Cu}_{\text{Al}}$ catalyst (Figure 4.3.14). These peaks decreased with pH and were indistinguishable from the background by pH = 9.

Increasing the ageing time from $^6_{30}\text{Cu}_{\text{Al}}$ to $^8_{140}\text{Cu}_{\text{Al}}$ catalysts, resulted in an increase in bulk CuO formation with ageing time (Figure 4.3.15).

The precursor prepared at $^9_{140}\text{Cu}_{\text{Al}}$, showed an XRD pattern (Figure 4.3.16) with peaks of malachite [223] being present, except the peak at 2θ value of 18.2° , which was a mixture of either chalconatronite ($\text{Na}_2\text{Cu}(\text{CO}_3)_2 \cdot 3\text{H}_2\text{O}$) [226], dawsonite ($\text{NaAlCO}_3(\text{OH})_2$) [228] or CuAlO_2 [229]. Due to the width of the peak, it was impossible to discern which preferential structure the precursor was likely to be. Calcination resulted in peaks of CuO [224] being visible.

4.3.2.4 X-ray Fluorescence

Copper (K_α -line and K_β -line peaks) and aluminium (K_α -line peak 1.487 keV) were present in the precursors. Increasing the pH from 7 (Figure 4.3.17) to 10 (Figure 4.3.18), increased the concentration of iron and potassium from minute. Calcium was also present in minute amounts but varied little with pH. No difference in concentration was noted with lengthening ageing time with either of these elements.

At pH = 8, cobalt K_α -line (6.925 keV) emerged with lengthening ageing time but still with a concentration lower than that of iron, calcium or potassium. Lower pH co-precipitation (pH = 7 and 8) produced a small quantity of chromium (K_α -line 5.411 keV) and a tiny amount of manganese (K_α -line 5.895 keV). By pH = 10, the

Figure 4.3.13. XRD patterns for the ${}^8\text{Cu}_{\text{Al}}$ precursors with variation in ageing time.

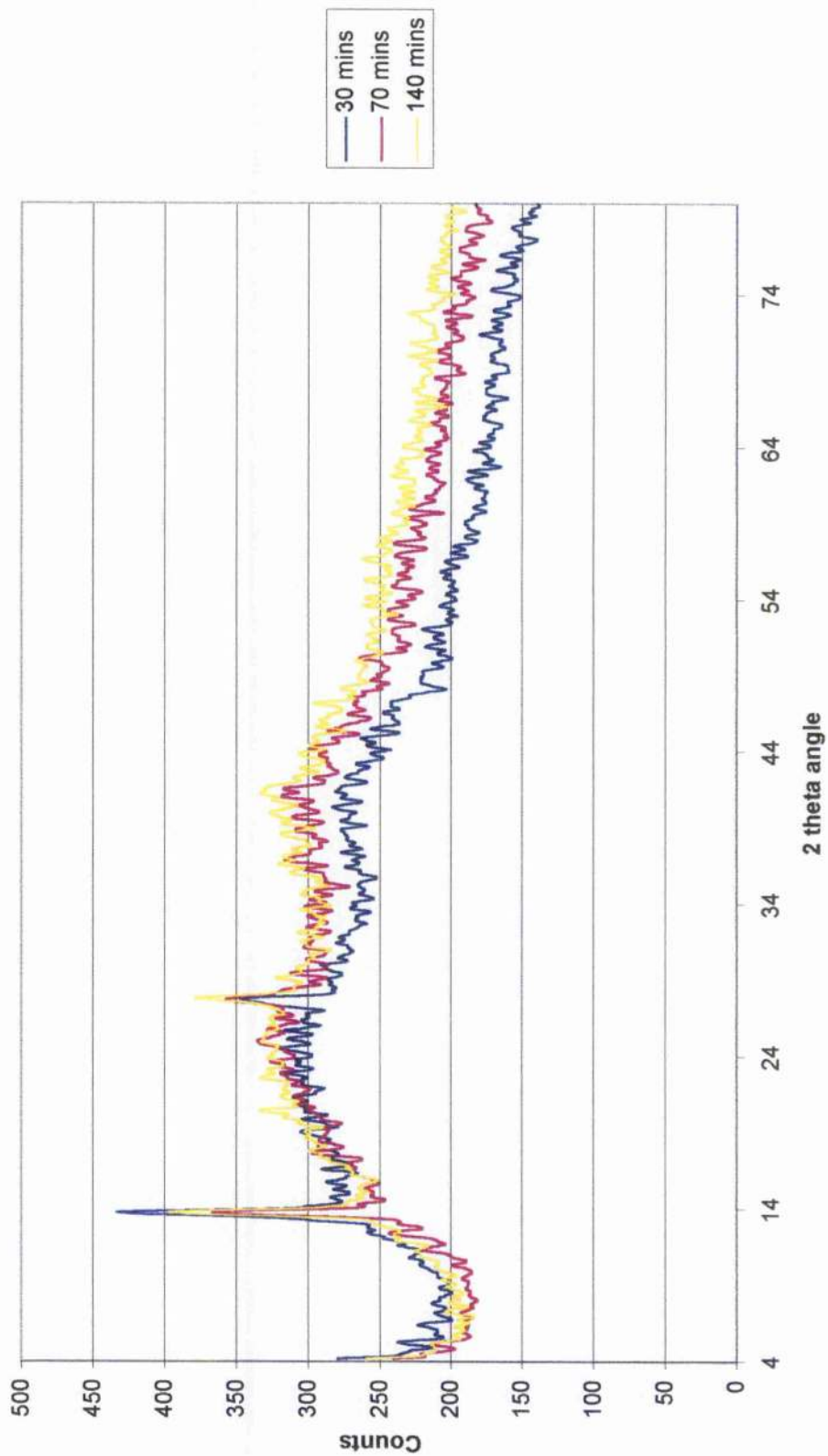


Figure 4.3.14. XRD patterns for the Cu_{Al} catalysts with variation in pH (30 mins ageing time).

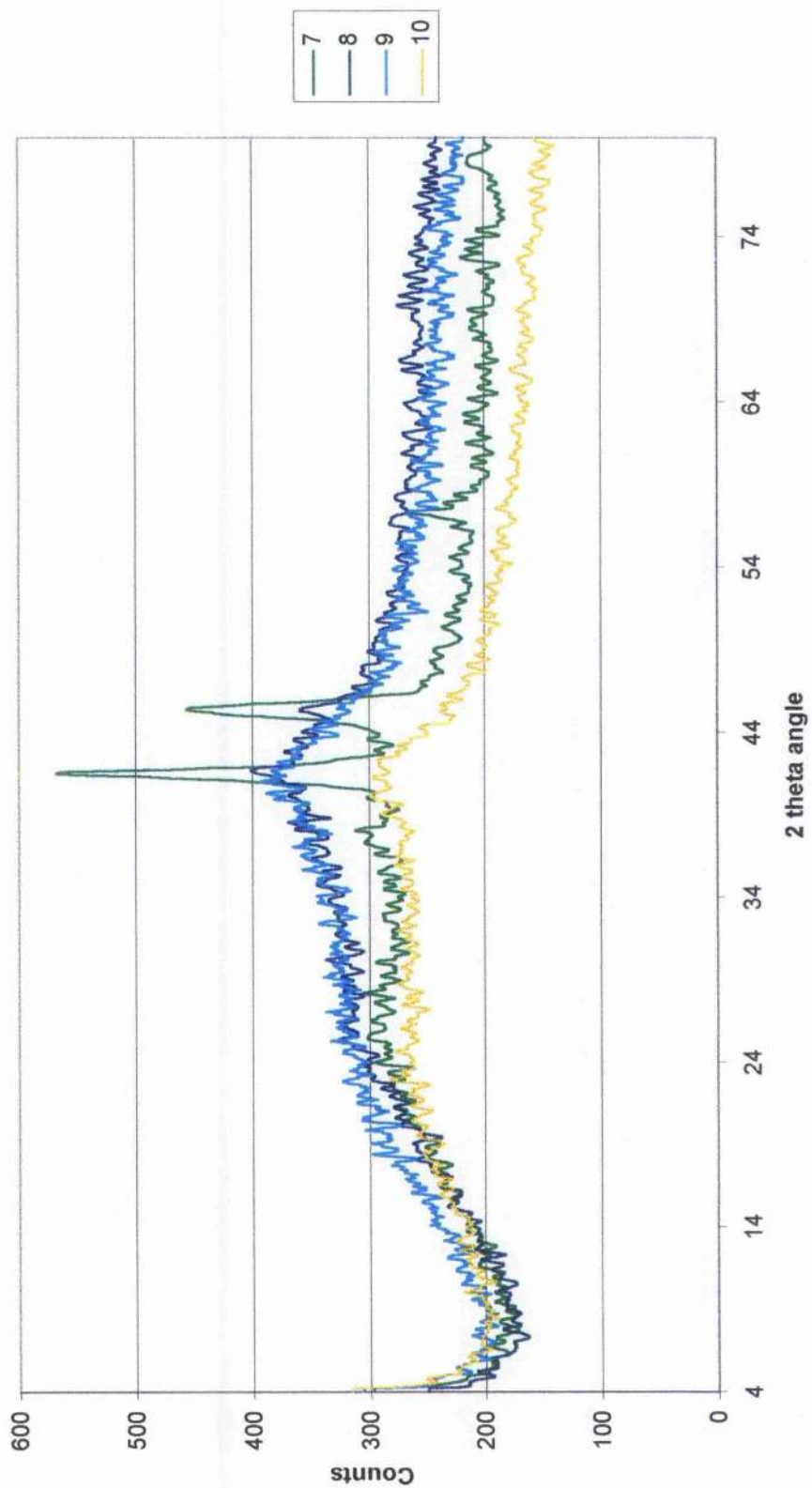


Figure 4.3.15.
XRD patterns for the $^8\text{Cu}_{\text{Al}}$ catalysts with variation in ageing time.

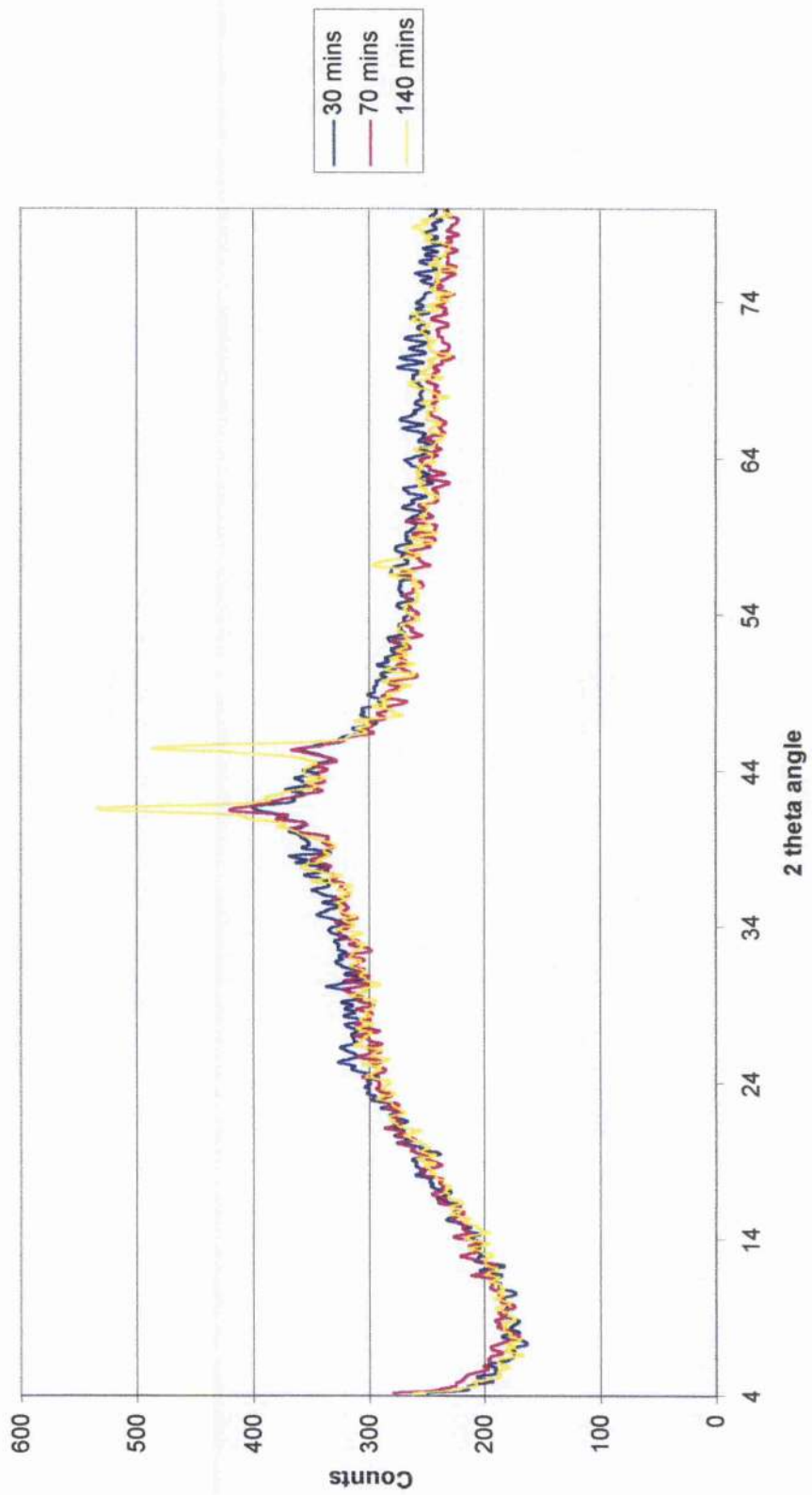


Figure 4.3.16. XRD patterns for the ${}^9\text{Cu}_{\text{Al}}$ precursor and catalyst.

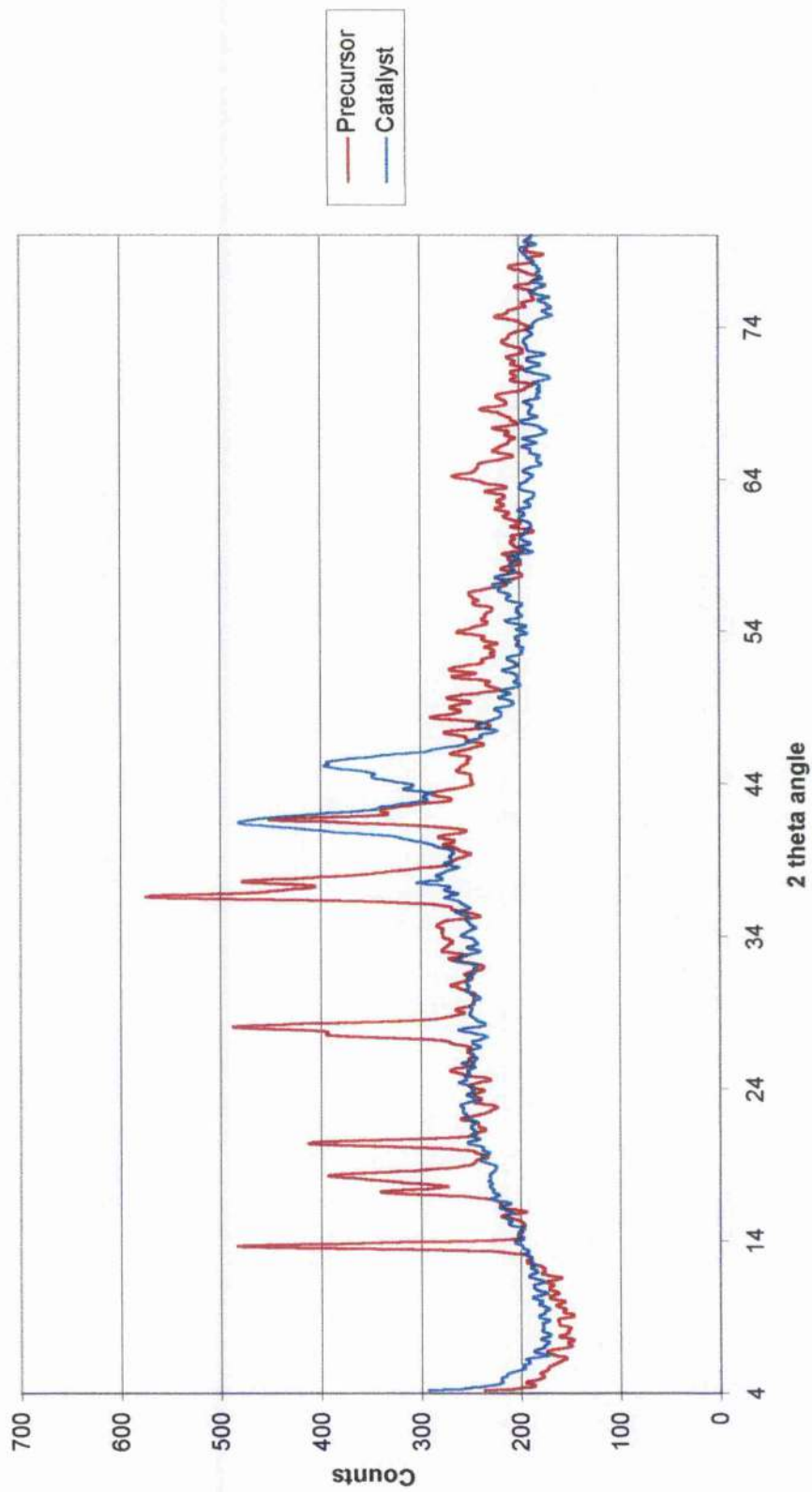


Figure 4.3.17. XRF spectrum for the $^{70}\text{Cu}_{\text{Al}}$ precursor.

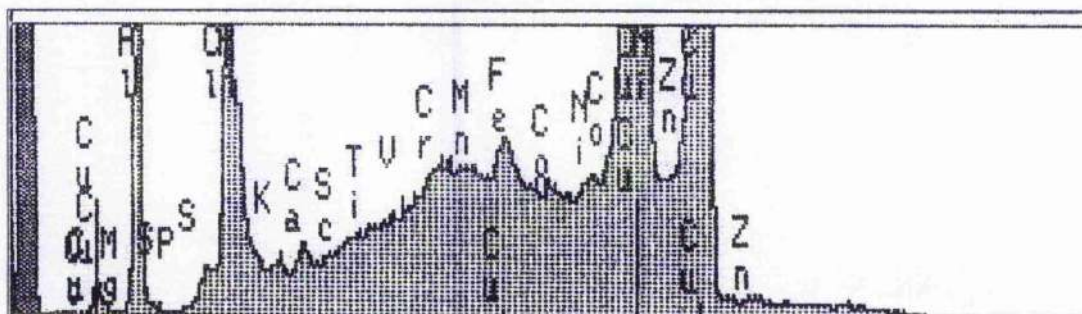


Figure 4.3.18. XRF spectrum for the $^{100}\text{Cu}_{\text{Al}}$ precursor.

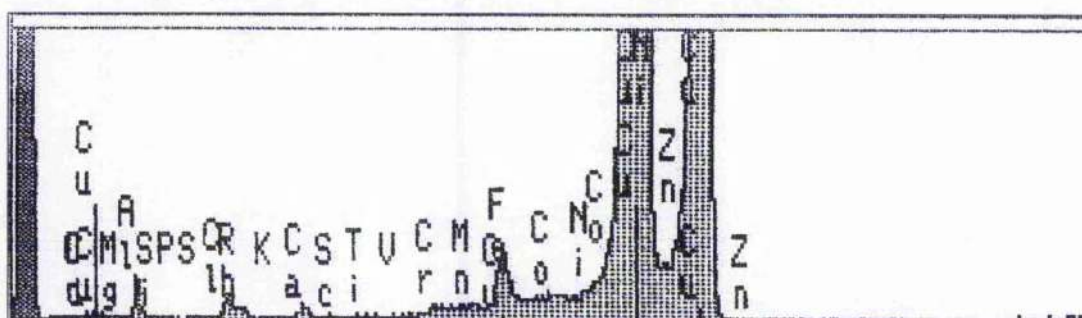


Figure 4.3.19. XRF spectrum for the $^{80}\text{Cu}_{\text{Al}}$ catalyst.

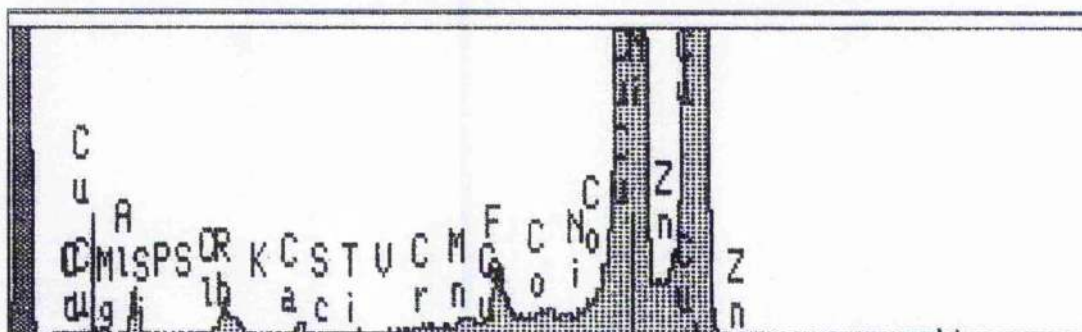
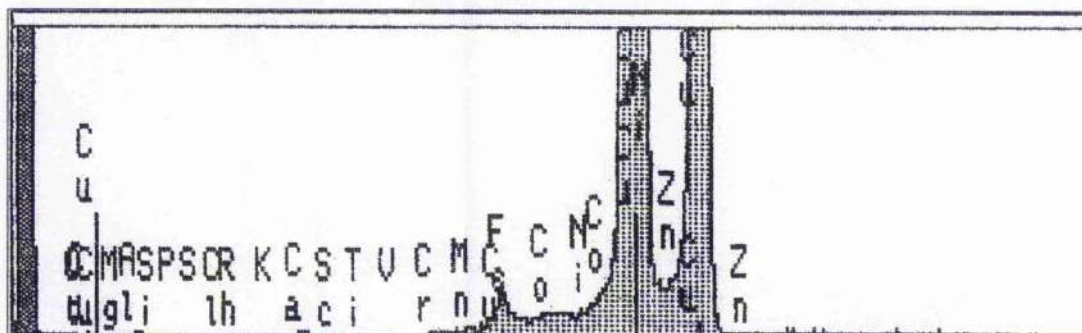


Figure 4.3.20. XRF spectrum for the filtered $^{80}\text{Cu}_{\text{Al}}$ catalyst.



background noise and aluminium ($K\alpha$ -line) peak had both decreased in size, the latter due to less favourable co-precipitation conditions.

Calcination resulted in little change in peak heights and therefore, concentrations (Figure 4.3.19).

Addition of the chromium filter, resulted in no chlorine being detected. The filtered version of the previous figure was shown in Figure 4.3.20.

4.3.2.5 Atomic Absorption Spectroscopy

Table 4.3.10. Percentage of copper co-precipitated (wt / wt) for the Cu_{Al} catalysts with variation in preparation conditions.

Preparation pH	7	8	9	10
30 mins	97.6	95.7	87.9	87.7
70 mins	-	88.6	84.9	-
140 mins	-	87.0	68.9	-

Table 4.3.11. Percentage of aluminium precipitated (wt / wt) for the Cu_{Al} catalysts with variation in preparation conditions.

Preparation pH	7	8	9	10
30 mins	69.4	66.5	55.9	54.1
70 mins	-	62.4	53.8	-
140 mins	-	60.6	51.9	-

The percentage of co-precipitated copper decreased with increasing pH and ageing time (Table 4.3.10). Aluminium showed a similar trend (Table 4.3.11). From these tables, it can be observed a maximum of both elements occurs at lower pH and shorter ageing times.

The final copper concentrations in the catalysts were presented in Table 4.3.12 and aluminium in Table 4.3.13. The catalyst closest to the theoretical ratio of copper:aluminium 60:40 was prepared at pH = 7 and the worst occurred at a pH of 10.

Table 4.3.12. Copper metal ratio for the Cu_{Al} catalysts with variation in preparation conditions.

Preparation pH	7	8	9	10
30 mins	67.5	70.3	70.2	70.7
70 mins	-	68.0	70.3	-
140 mins	-	68.3	68.7	-

Table 4.3.13. Aluminium metal ratio for the Cu_{Al} catalysts with variation in preparation conditions.

Preparation pH	7	8	9	10
30 mins	32.4	29.7	29.8	29.2
70 mins	-	32.0	29.7	-
140 mins	-	31.7	21.3	-

4.3.2.6 Temperature Programmed Reduction

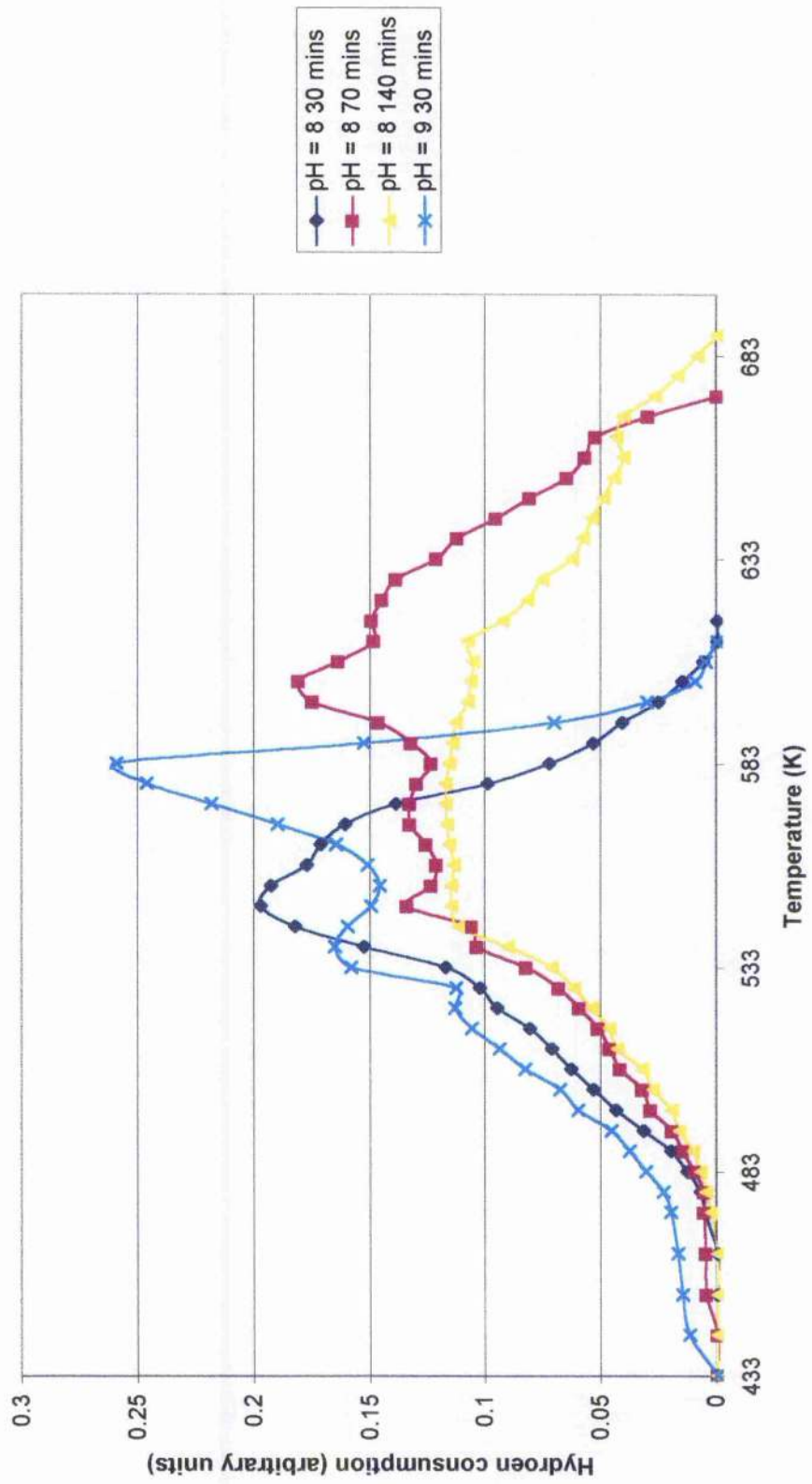
The ⁸₃₀Cu_{Al} sample started reducing around 473 K (Figure 4.3.21), steadily increasing to a T_{max} at 548 K via a slight mound at 513 K. A second phase was observed at 563 K, before culmination at 623 K.

The ⁸₇₀Cu_{Al} reduction profile increased to an initial T_{max} at 548 K. A second T_{max} occurred at 573 K. The largest and final T_{max} transpired at 608 K. The hydrogen consumption gradually decreased until termination at 673 K.

A similar initial increase was observed between the ⁸₇₀Cu_{Al} and ⁸₁₄₀Cu_{Al} samples to a temperature of 548 K. However, the ⁸₁₄₀Cu_{Al} catalyst continued to consume hydrogen at this quantity until ca. 593 K. The reduction process was complete at 688 K. No definitive peak was detected with the ⁸₁₄₀Cu_{Al} catalyst, only a plateau was observed.

The ⁹₃₀Cu_{Al} catalyst had the lowest initial reduction temperature of 433 K when compared to the other three profiles. The profile showed two distinct maximum

Figure 4.3.21.
TPR profiles for the Cu_{Al} catalysts with variation in preparation conditions.



reduction peaks, the former at 538 K and the latter, the larger at 583 K. A rapid decrease in the quantity of reduction was observed until culmination at 608 K.

4.3.2.7 Nitrous Oxide Chemisorption and Copper Surface Area measurements

Copper concentration in the catalyst fluctuated with ageing time, a larger quantity of copper was observed at longer ageing time (Table 4.3.14). A decrease in dispersion and copper surface area was observed with increasing ageing time and pH. The ${}^8_{30}\text{Cu}_{\text{Al}}$ catalyst had the largest dispersion at 10.9 % with the calibrated dispersion being marginally larger at 11.6 %. The copper surface area of this catalyst was considerably larger than the other samples.

Table 4.3.14. Nitrous oxide chemisorption results for the Cu_{Al} catalysts with variation in preparation conditions.

Catalyst	${}^8_{30}\text{Cu}_{\text{Al}}$	${}^8_{70}\text{Cu}_{\text{Al}}$	${}^8_{140}\text{Cu}_{\text{Al}}$	${}^9_{30}\text{Cu}_{\text{Al}}$
% Cu in catalyst	66.6	65.7	66.0	63.5
% dispersion	10.9	5.6	5.0	3.0
Particle size (nm)	9.5	18.6	20.8	34.7
% calibrated dispersion	11.6	6.6	5.7	3.6
Calibrated particle size (nm)	9.0	15.8	18.2	28.9
Copper surface area ($\text{m}^2 \text{g}^{-1}$)	45.3	26.4	17.5	15.5

Table 4.3.15. Copper surface reduction temperatures for the Cu_{Al} catalysts with variation in preparation conditions.

Temperature (K)	T_{initial}	T_{max}	T_{complete}
${}^8_{30}\text{Cu}_{\text{Al}}$	421	461	510
${}^8_{70}\text{Cu}_{\text{Al}}$	399	440	498
${}^8_{140}\text{Cu}_{\text{Al}}$	393	433	478
${}^9_{30}\text{Cu}_{\text{Al}}$	378	413	478

The $^8_{30}\text{CuAl}$ catalyst had the highest copper surface reduction maximum at 461 K (Table 4.3.15). The copper surface reduction temperatures decreased in temperatures with increasing ageing time and pH.

4.3.2.8 Elemental Analysis

The carbon concentration in the precursors increased with lengthening ageing time with the maximum concentration being present in the $^9_{140}\text{CuAl}$ sample (Table 4.3.16). Hydrogen content values decreased with lengthening ageing time. The same correlation cannot be drawn with the nitrogen concentrations, as the values varied widely. The sulfur concentrations were very low with six of the eight samples having amounts that were non-detectable.

Table 4.3.16. Elemental Analysis results for the CuAl precursors with variation in preparation conditions.

Element	C	H	N	S
$^7_{30}\text{CuAl}$	3.4	2.6	0.11	nda
$^8_{30}\text{CuAl}$	3.8	3.1	0.16	0.01
$^8_{70}\text{CuAl}$	4.0	2.7	0.28	0.01
$^8_{140}\text{CuAl}$	4.3	2.5	0.15	nda
$^9_{30}\text{CuAl}$	3.0	2.7	0.10	nda
$^9_{70}\text{CuAl}$	3.8	2.4	0.39	nda
$^9_{140}\text{CuAl}$	5.8	1.8	0.30	nda
$^{10}_{140}\text{CuAl}$	2.1	2.9	0.13	nda

nda = non-detectable amount

The carbon and hydrogen concentrations decreased on calcination, nitrogen and sulfur are unaffected (Table 4.3.17). Increasing the pH from 7 to 8 increased the carbon, hydrogen, nitrogen and sulfur content. The $^8_{30}\text{CuAl}$ catalyst showed a larger carbon concentration than the other samples prepared at that pH. However, the nitrogen content was significantly lower. Carbon and hydrogen had their lowest concentration

after 70 mins preparation but the sulfur and nitrogen values were higher than the remaining pH = 8 catalysts.

Table 4.3.17. Elemental Analysis results for the Cu_{Al} catalysts with variation in preparation conditions.

Element	C	H	N	S
⁷ ₃₀ Cu _{Al}	0.82	0.38	nda	nda
⁸ ₃₀ Cu _{Al}	2.4	0.50	nda	0.01
⁸ ₇₀ Cu _{Al}	1.8	0.36	0.64	0.02
⁸ ₁₄₀ Cu _{Al}	1.9	0.63	0.56	0.01
⁹ ₃₀ Cu _{Al}	2.0	0.51	nda	nda
⁹ ₇₀ Cu _{Al}	1.7	0.55	0.07	nda
⁹ ₁₄₀ Cu _{Al}	2.0	0.53	0.09	0.01
¹⁰ ₁₄₀ Cu _{Al}	2.0	0.52	nda	0.01

nda = non-detectable amount

At pH = 9, again nitrogen was not detectable in the 30 mins catalyst. Carbon concentrations were overall lower than the ⁸Cu_{Al} catalysts. Hydrogen and sulfur had similar values, the concentration of nitrogen was significantly lower with the ⁸₇₀Cu_{Al} and ⁸₁₄₀Cu_{Al} catalysts.

From ⁹₃₀Cu_{Al} to ¹⁰₃₀Cu_{Al} preparation conditions, carbon, hydrogen and nitrogen remained very similar in content but sulfur increased slightly.

All elemental analysis samples were conducted once.

4.3.2.9 BET Surface Area measurements

Table 4.3.18.

BET surface area measurements for the Cu_{Al} catalysts with variation in preparation conditions.

Catalyst	⁷ ₃₀ Cu _{Al}	⁸ ₃₀ Cu _{Al}	⁸ ₇₀ Cu _{Al}	⁸ ₁₄₀ Cu _{Al}	⁹ ₃₀ Cu _{Al}
Single Point (m ² g ⁻¹)	148.8	71.0	57.8	68.4	84.7
BET surface area (m ² g ⁻¹)	151.8	72.9	59.2	70.1	86.8

The BET surface areas of the Cu_{Al} catalysts (Table 4.3.18) decreased significantly with increasing in pH above 7 preparatory conditions. Little variation in surface area was observed between the ⁸₃₀Cu_{Al} and the ⁸₁₄₀Cu_{Al} catalyst, however, the ⁸₇₀Cu_{Al} sample was over 10 m² g⁻¹ lower.

4.3.3 Summary

At low and high pH, either the undesired phase was formed or decomposed on preparation. This gave an optimum pH of 8 and 9. At longer ageing times, more dissolution occurred. The copper dispersion and surface areas were independent of ageing time and BET surface area.

4.4 Cu/MgO/Al₂O₃ (60/2/38) (Cu_{Mg(2)Al})

4.4.1 Preparation

Filtering the mother liquor resulted in a sky blue filtrate, indicating incomplete copper co-precipitation. This occurred regardless of pH (8 or 9) or ageing time (30, 70 or 140 mins). The ⁹₁₄₀Cu_{Mg(2)Al} filtrate had the largest copper concentration with an approximately value of 10,000 ppm.

After drying, the pH = 8 sky blue precursors darkened with increasing ageing time in shades of pale blue. The pH = 9 precursors showed partial degradation, which increased with lengthening ageing time to 60 % total coverage by the ⁹₁₄₀Cu_{Mg(2)Al} precursor.

On calcination, all pH = 8 samples went dark green, lightening on increasing ageing time. The change in colour indicated precursor decomposition.

The pH = 9 precursors and catalysts were omitted from microreactor experiments and complete characterisation.

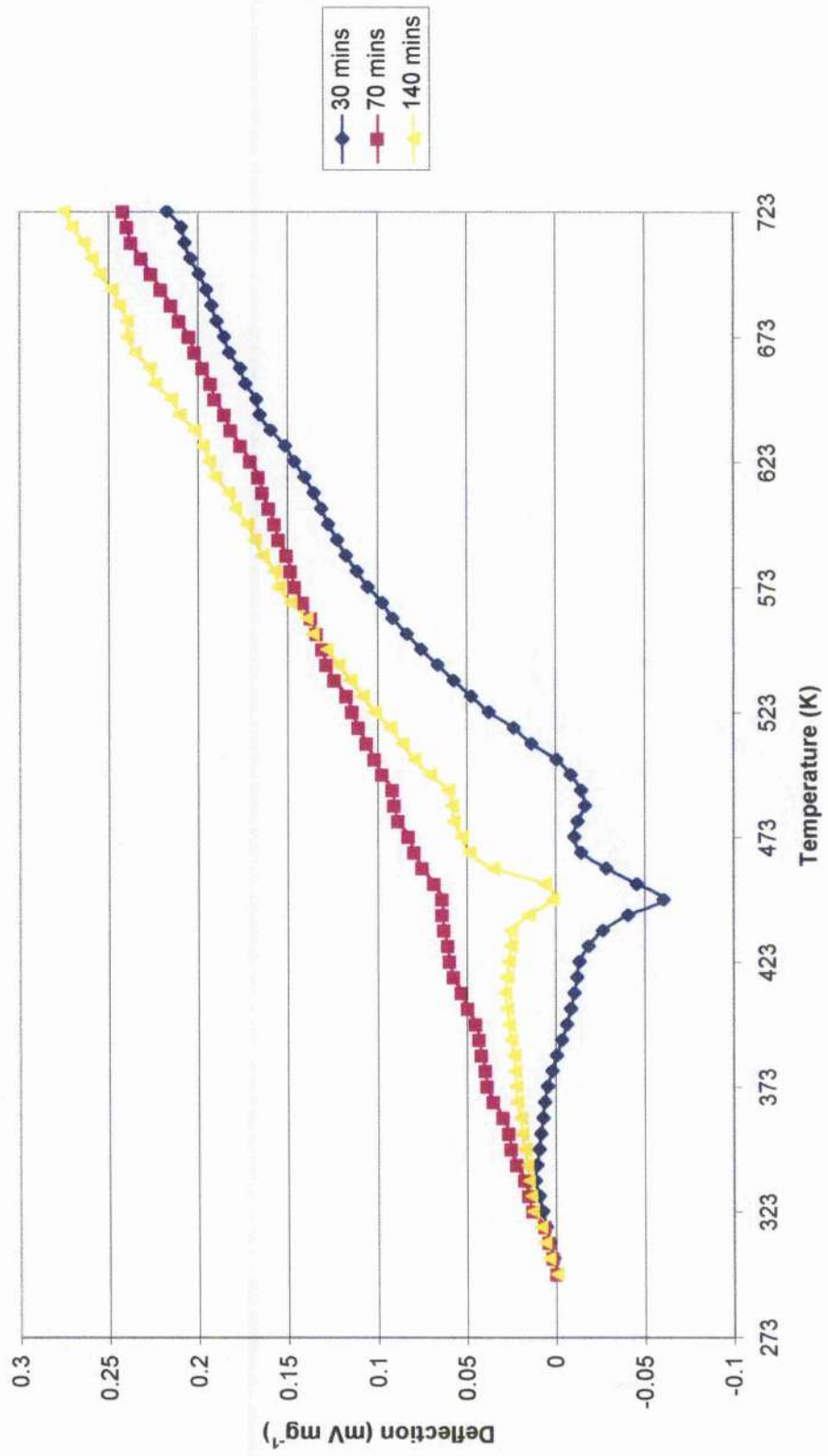
4.4.2 Differential Thermal Analysis

The DTA profile of the ⁸₃₀Cu_{Mg(2)Al} precursor exhibited a downward endothermic gradient from 348 to 423 K, whereupon an endothermic peak occurred at 448 K (Figure 4.4.1). The downward gradient was indicative of water loss due to a damp sample, while the peak was H-bonded water and possibly partially dehydroxylation.

A second endothermic peak was present at 488 K, which was either dehydroxylation and/or decarboxylation. Above this temperature to 823 K, a gradual increase ensued due to the heat capacitance of these samples.

The ⁸₁₄₀Cu_{Mg(2)Al} precursor showed a profile similar as the ⁸₃₀Cu_{Mg(2)Al} sample with no change in endothermic peak temperatures being observed. However, the

Figure 4.4.1. DTA profiles for the ${}^8\text{Cu}_{\text{Mg(2)Al}}$ precursors with variation in ageing time.



$^8_{70}\text{Cu}_{\text{Mg}(2)\text{Al}}$ sample showed little sign of decomposition, as the endothermic peak at 448 and 488 K were small by comparison to the $^8_{30}\text{Cu}_{\text{Mg}(2)\text{Al}}$ and $^8_{140}\text{Cu}_{\text{Mg}(2)\text{Al}}$ precursors.

The $^9_{30}\text{Cu}_{\text{Mg}(2)\text{Al}}$ precursor profile (Figure 4.4.2) showed a similar endothermic peak present at 448 K that was apparent in the pH = 8 precursors profiles but the second endothermic peak occurring at a higher temperature of 498 K did not. The partially degraded $^9_{140}\text{Cu}_{\text{Mg}(2)\text{Al}}$ showed further decomposition steps to the $^9_{30}\text{Cu}_{\text{Mg}(2)\text{Al}}$ precursor. The endothermic peak centred on 448 K was small in comparison to the peak at 513 K. This peak transpired at a higher temperature than the previous precursors. An additional endothermic peak occurred with this sample at 561 K.

4.4.3 X-ray Diffraction

The XRD patterns of the three pH = 8 samples (Figure 4.4.3) were analogous to the crystallite phase, hydrotalcite ($\text{Mg}_6\text{Al}_2\text{CO}_3(\text{OH})_{16}\cdot 4\text{H}_2\text{O}$) [230] (Table 4.4.1). Lengthening ageing time resulted in increased crystallinity. The peaks differ slightly from the definitive 2θ angles as the mineral hydrotalcite has no copper content, which will alter the unit cell dimensions.

Table 4.4.1. XRD d-spacing values (Å) for the $^8_{140}\text{Cu}_{\text{Mg}(2)\text{Al}}$ precursor, with intensities presented in parentheses.

$^8_{140}\text{Cu}_{\text{Mg}(2)\text{Al}}$	$\text{Mg}_6\text{Al}_2\text{CO}_3(\text{OH})_{16}\cdot 4\text{H}_2\text{O}$ [230]
7.39(100)	7.69(100)
3.72(59)	3.88(70)
2.43(42)	2.58(20)
2.16(40)	2.30(20)
1.81(35)	1.96(20)
1.64(32)	1.75(10)

The $^9_{140}\text{Cu}_{\text{Mg}(2)\text{Al}}$ showed a different structure to that of the pH = 8 and $^9_{70}\text{Cu}_{\text{Mg}(2)\text{Al}}$ precursors (Figure 4.4.4). At these preparatory conditions, the hydrotalcite-like

Figure 4.4.2. DTA profiles for the ${}^9\text{Cu}_{\text{Mg}2\text{Al}}$ precursors with variation in ageing time.

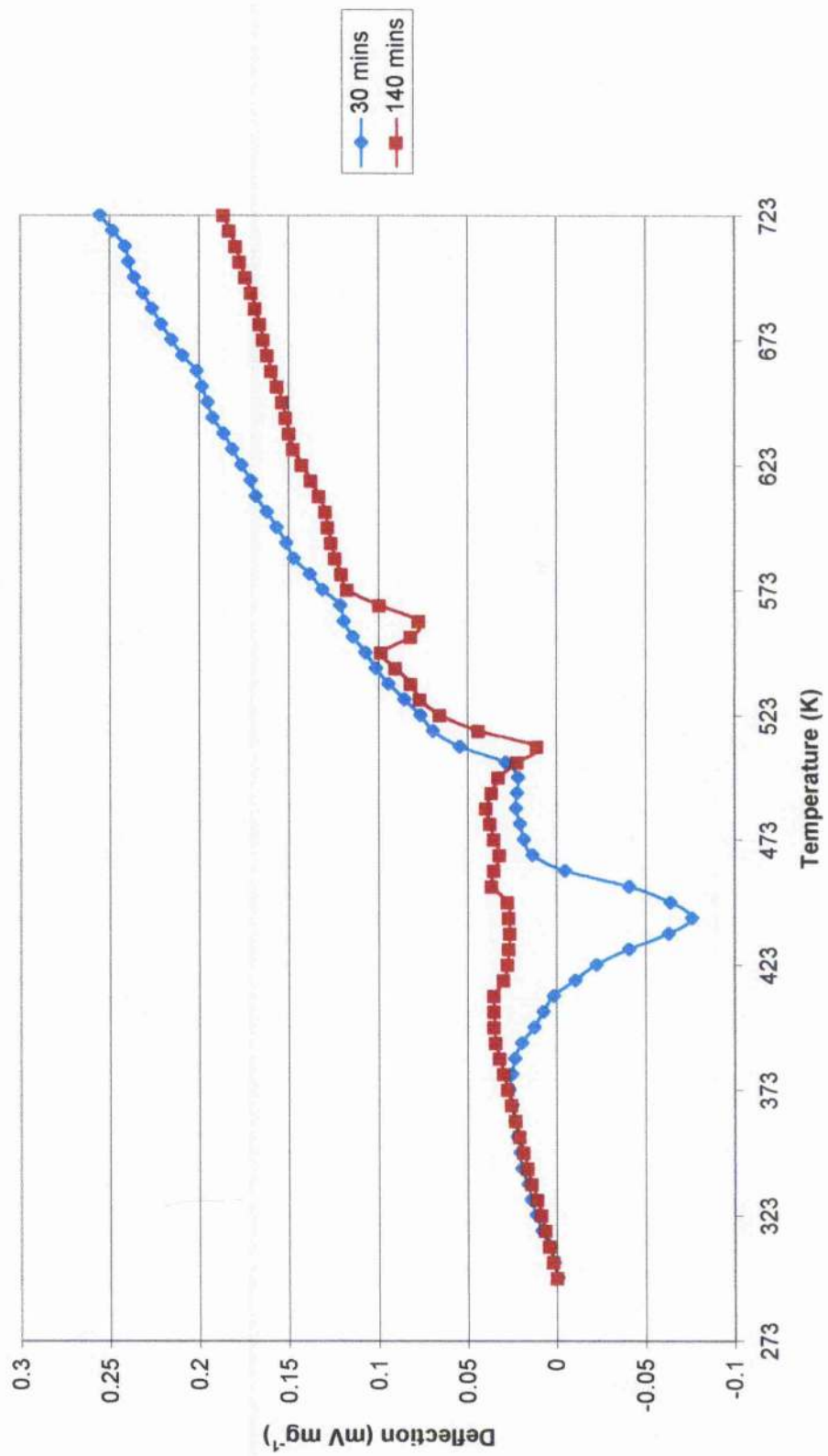


Figure 4.4.3. XRD patterns for the ${}^8\text{Cu}_{\text{Mg}(2)\text{Al}}$ precursors with variation in ageing time.

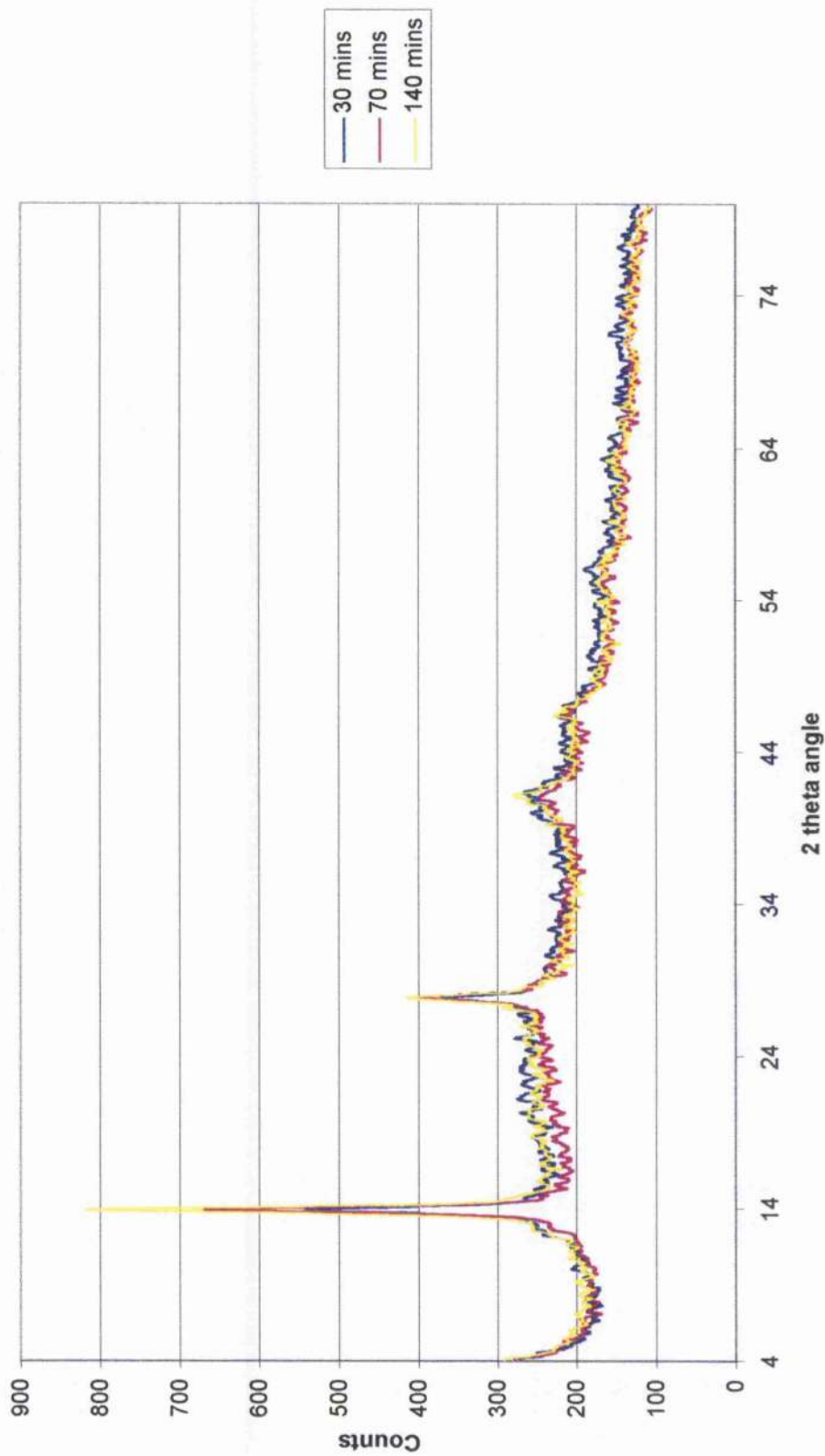
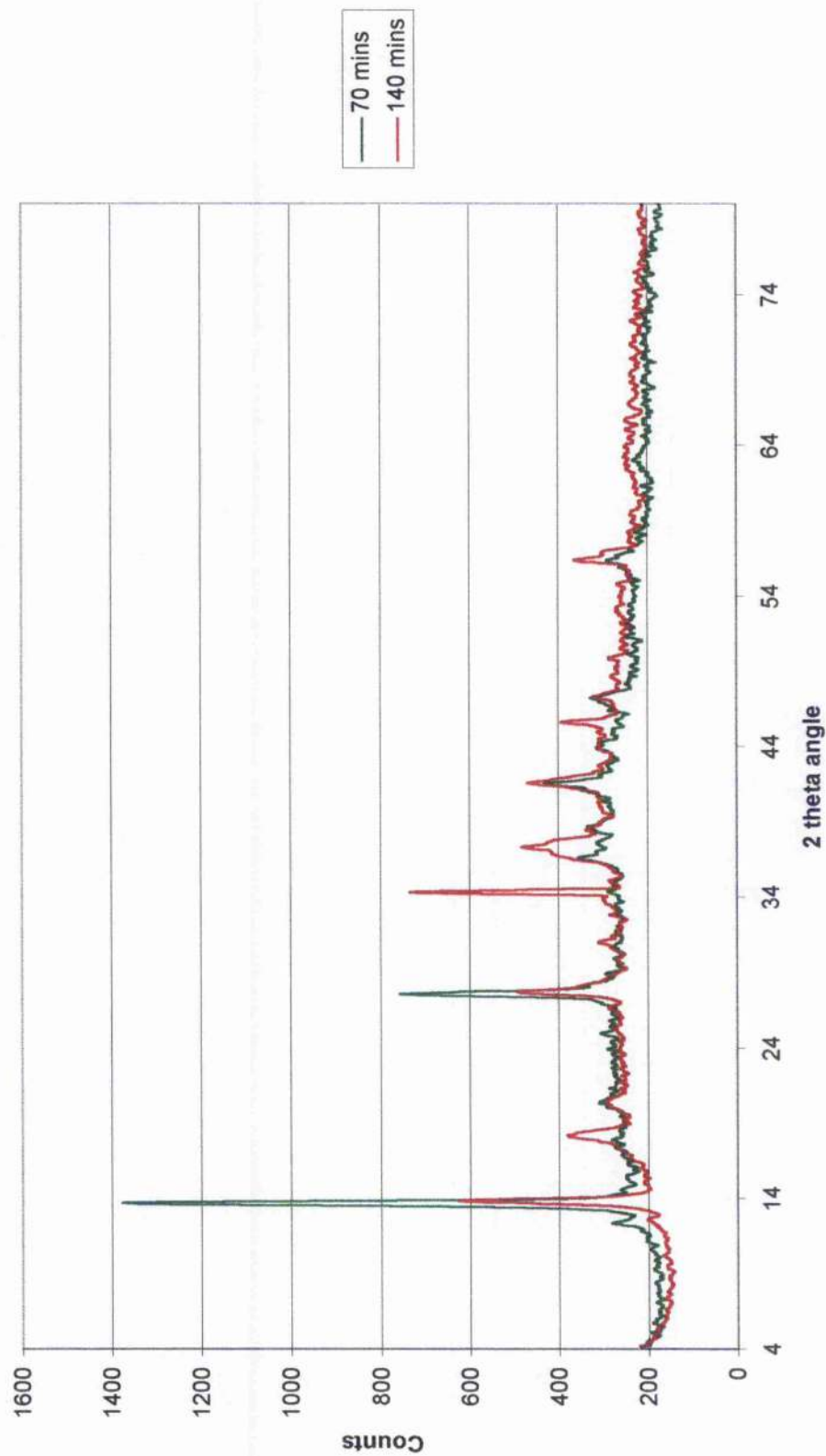


Figure 4.4.4. XRD patterns for the ${}^9\text{Cu}_{\text{Mg}(2)\text{Al}}$ precursors with variation in ageing time.



structure had decomposed to form primarily malachite [223]. The peak with a 2θ angle of 18.3° was either the presence of CuAlO_2 [229], $\text{Na}_2\text{Cu}(\text{CO}_3)_2 \cdot 3\text{H}_2\text{O}$ [225] or $\text{NaAlCO}_3 \cdot (\text{OH})_2$ [228].

Calcination of the $\text{pH} = 8$ samples gave XRD patterns (Figure 4.4.5) present with two peaks indicative of copper (II) oxide [224], all with similar sized peaks.

4.4.4 X-ray Fluorescence

The ${}^8_{30}\text{Cu}_{\text{Mg}(2)\text{Al}}$ precursor showed the presence of both copper (K_α and K_β -lines) and aluminium (K_α -line) but little magnesium (Figure 4.4.6). Iron (K_α -line) was the largest impurity, followed by cobalt (K_α -line), calcium (K_α -line) and possibly zinc (K_β -line) but it was difficult to distinguish the zinc K_α -line peak from the large presence of the copper. The calcium K_α -line was barely observable from the background. This sample was performed on the EDX machine connected to the Electron Microscope at the University of Glasgow.

The ${}^9_{30}\text{Cu}_{\text{Mg}(2)\text{Al}}$ precursor (Figure 4.4.7) showed less impurities than the previous sample, especially iron. No calcium, zinc or cobalt were seen either, however, the calcium (K_α -line) concentration had increased. Potassium (K_α -line) was present at this increased pH .

Post calcination, the background of the ${}^8_{30}\text{Cu}_{\text{Mg}(2)\text{Al}}$ catalyst (Figure 4.4.8) was more defined than the preceding precursors. Copper (K_α and K_β -lines) and aluminium (K_α -line) peaks were still present. However, a magnesium (K_α -line) peak cannot be observed in the XRF spectrum. Iron (K_α -line) and calcium (K_α -line) were still present from the precursor. Potassium (K_α -line) was now observed due to the decrease in the background noise. Calcination had also declined the cobalt (K_α -line) peak height.

Figure 4.4.5. XRD patterns for the ${}^8\text{Cu}_{\text{Mg}(2)\text{Al}}$ catalysts with variation in ageing time.

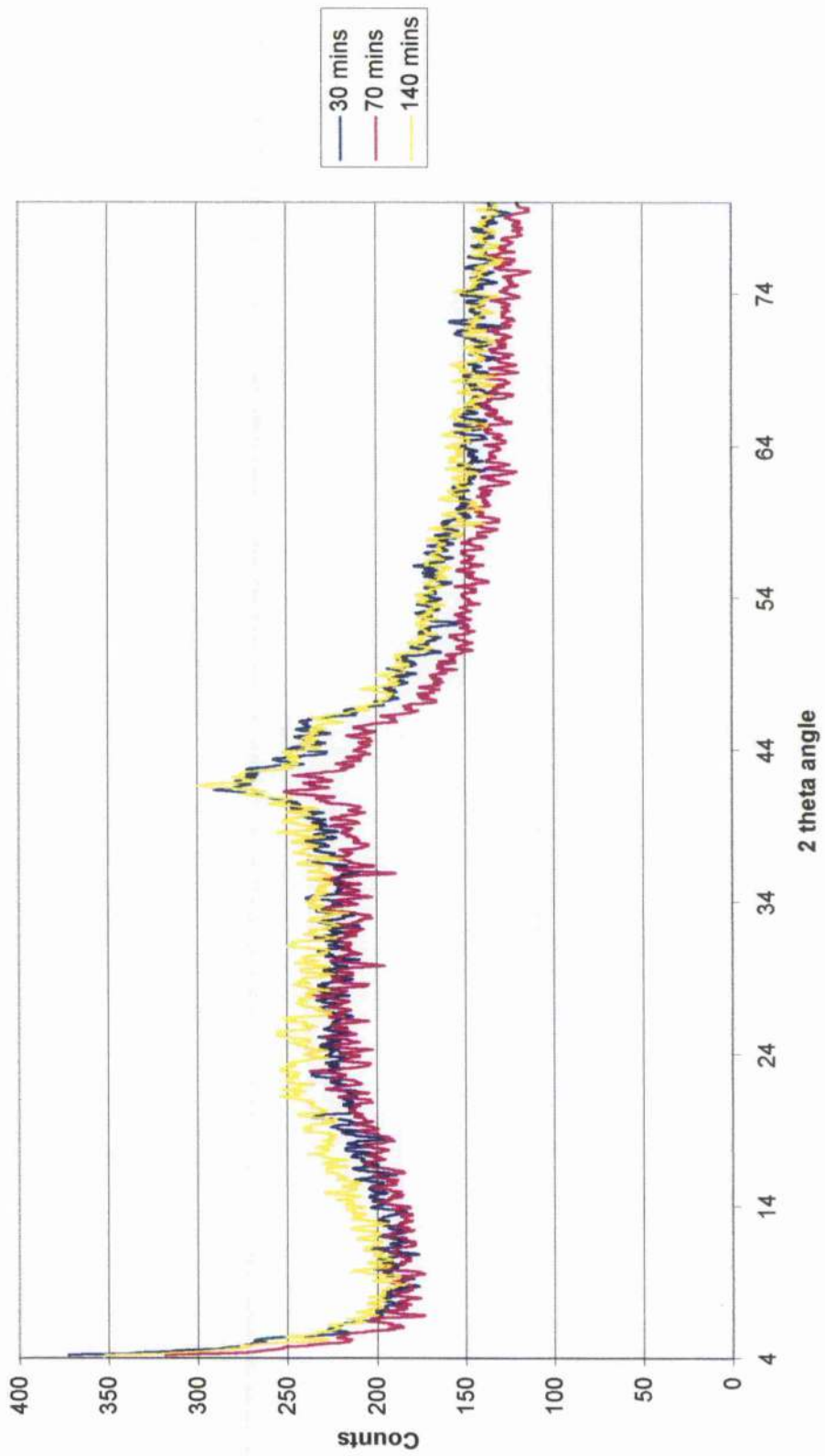


Figure 4.4.6. XRF spectrum for the $^{83}\text{Cu}_{\text{Mg}(2)\text{Al}}$ precursor.

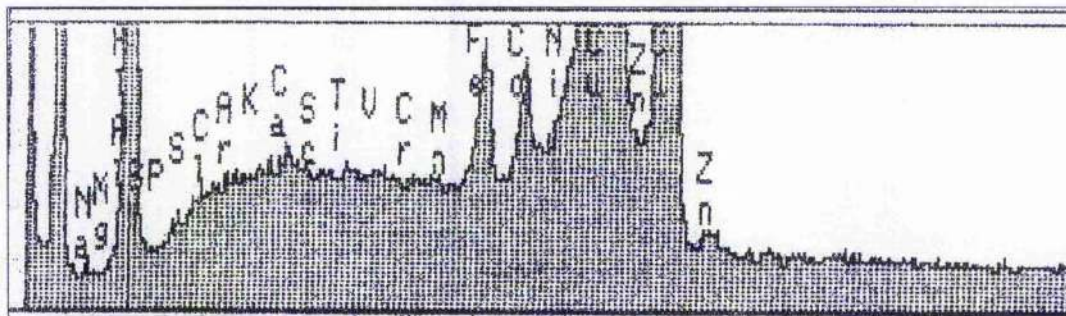


Figure 4.4.7. XRF spectrum for the $^{93}\text{Cu}_{\text{Mg}(2)\text{Al}}$ precursor.

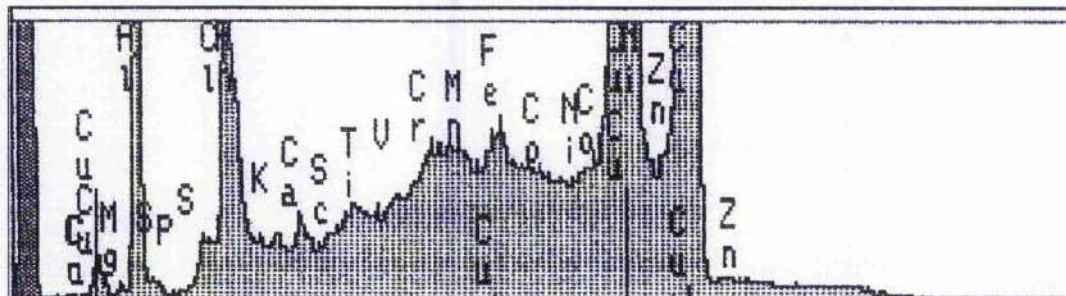


Figure 4.4.8. XRF spectrum for the $^{83}\text{Cu}_{\text{Mg}(2)\text{Al}}$ catalyst.

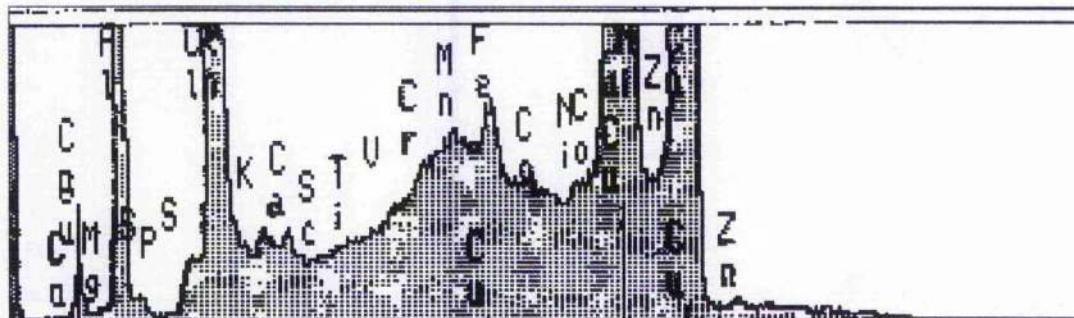
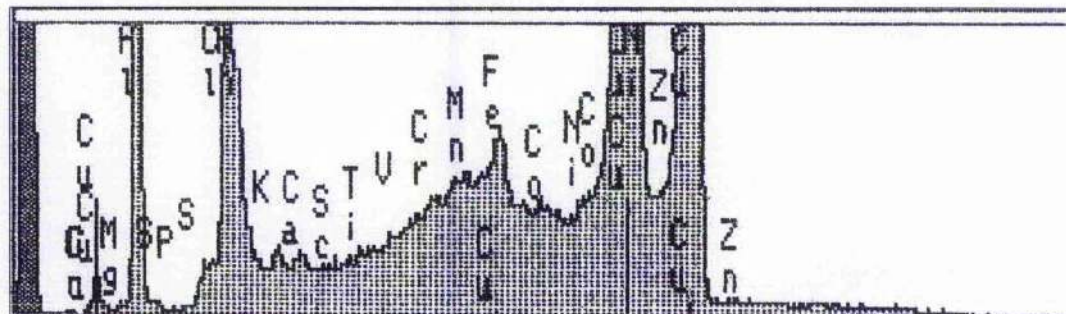


Figure 4.4.9. XRF spectrum for the $^{87}\text{Cu}_{\text{Mg}(2)\text{Al}}$ catalyst.



A representative sample, the ${}^8{}_{70}\text{Cu}_{\text{Mg}(2)\text{Al}}$ catalyst spectrum was presented in Figure 4.4.9, as lengthening the ageing time resulted in little change in concentrations of the contaminants.

On addition of the chromium filter, the spectra showed no signs of chlorine present in either the precursors or calcined samples.

4.4.5 Atomic Absorption Spectroscopy

All three components of the pH = 8 catalysts were tested with AAS (Table 4.4.2). The percentage of both co-precipitated copper and aluminium decreased with increasing ageing time. Copper reduced from 98.1 % to 76.2 % and aluminium from 93.0 % to 86.7 %. No trend was apparent for magnesium, as the ${}^8{}_{30}\text{Cu}_{\text{Mg}(2)\text{Al}}$ and the ${}^8{}_{140}\text{Cu}_{\text{Mg}(2)\text{Al}}$ catalyst had similar concentrations with the ${}^8{}_{70}\text{Cu}_{\text{Mg}(2)\text{Al}}$ sample having a value of over 20 % greater. These results suggested that the shorter ageing times were beneficial for copper and aluminium co-precipitation but a slightly longer ageing time was required for magnesium.

Table 4.4.2. Percentage of copper, magnesium and aluminium co-precipitated (wt / wt) for the $\text{Cu}_{\text{Mg}(2)\text{Al}}$ catalysts with variation in ageing time.

Element	Copper	Magnesium	Aluminium
${}^8{}_{30}\text{Cu}_{\text{Mg}(2)\text{Al}}$	98.1	35.2	93.0
${}^8{}_{70}\text{Cu}_{\text{Mg}(2)\text{Al}}$	81.4	55.8	89.7
${}^8{}_{140}\text{Cu}_{\text{Mg}(2)\text{Al}}$	76.2	33.4	86.7

A final catalyst composition was calculated (Table 4.4.3), with the copper ratio present in the ${}^8{}_{30}\text{Cu}_{\text{Mg}(2)\text{Al}}$ catalyst being greater than the theoretical 60 %. The aluminium in the ${}^8{}_{70}\text{Cu}_{\text{Mg}(2)\text{Al}}$ and ${}^8{}_{140}\text{Cu}_{\text{Mg}(2)\text{Al}}$ catalysts had a higher metal ratio than the theoretical figure. This was due to incomplete co-precipitation of the other two components of the catalyst.

Table 4.4.3. Metal ratios of copper, magnesium and aluminium for the $\text{Cu}_{\text{Mg}(2)\text{Al}}$ catalysts with variation in ageing time.

Element	Copper	Magnesium	Aluminium
$^8_{30}\text{Cu}_{\text{Mg}(2)\text{Al}}$	62.0	0.8	37.2
$^8_{70}\text{Cu}_{\text{Mg}(2)\text{Al}}$	58.1	1.3	40.6
$^8_{140}\text{Cu}_{\text{Mg}(2)\text{Al}}$	57.6	0.9	41.5

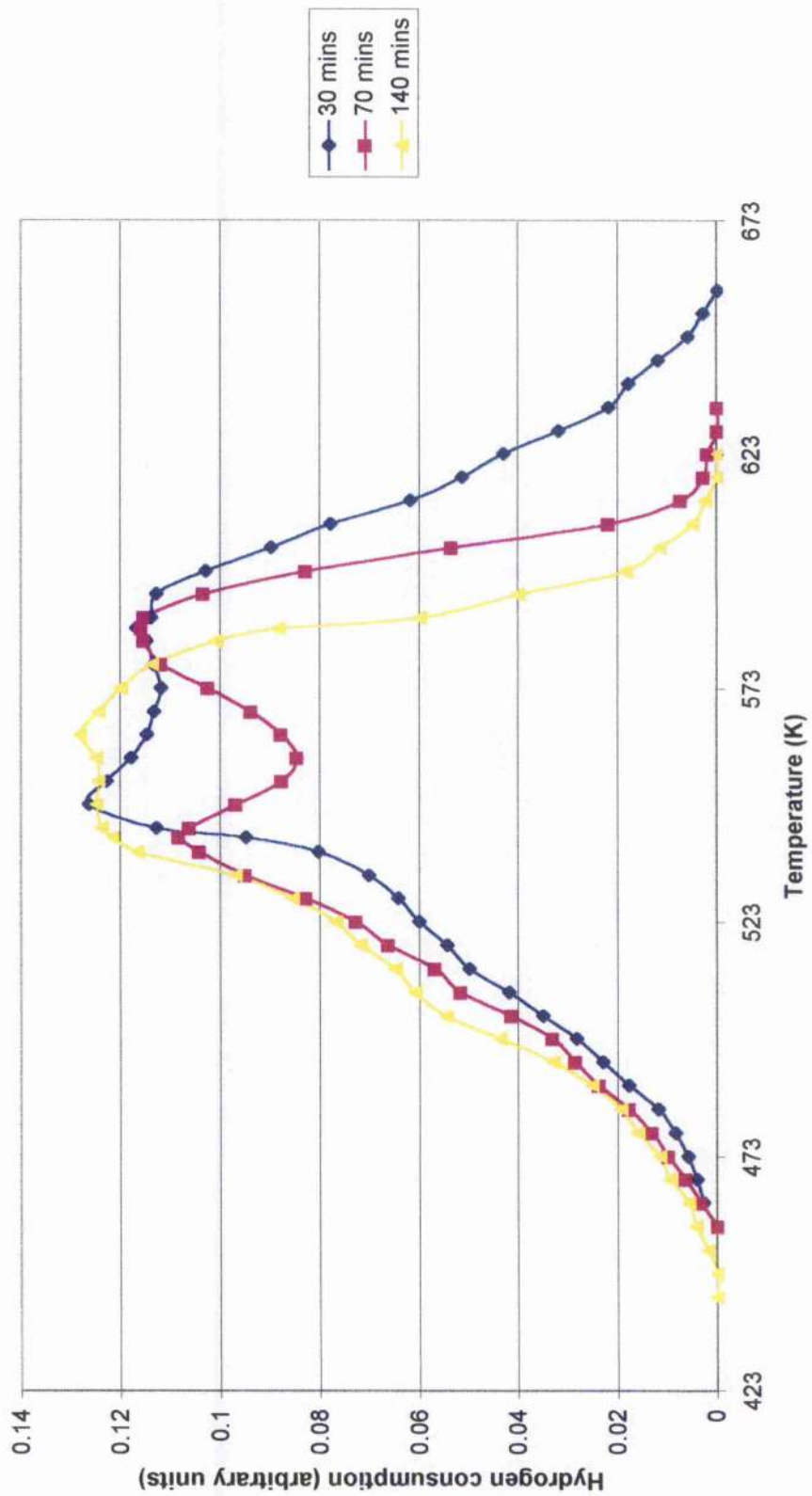
4.4.6 Temperature Programmed Reduction

The $^8_{30}\text{Cu}_{\text{Mg}(2)\text{Al}}$ catalyst profile showed three different peaks were present in the sample (Figure 4.4.10). The first peak was observed at around 508 K, which occurred at the same temperature as bulk Cu(II)O . The profile then increased to give a maximum reduction temperature of 543 K. The quantity of reduction decreased marginally to give a 3rd peak at ca. 588 K with the reduction process being completed by 653 K.

The $^8_{70}\text{Cu}_{\text{Mg}(2)\text{Al}}$ sample gave a marginal peak at 508 K before continuing to increase in hydrogen consumption to a maximum reduction temperature of 543 K. This temperature was equivalent to the previous sample. The profile then decreased in reduction quantity by approximately 15-20 %, increasing in reduction again at 553 K reaching the second maximum reduction temperature at 585 K and completing reduction by 623 K. The second maximum reduction peak at 585 K occurred in larger quantities than the first peak at 543 K. It also occurred at a similar temperature to the $^8_{30}\text{Cu}_{\text{Mg}(2)\text{Al}}$ catalyst.

The $^8_{140}\text{Cu}_{\text{Mg}(2)\text{Al}}$ catalyst profile gradually increased to the peak maximum at 543 K with a slight peak around 493-513 K. This maximum reduction temperature was similar to the other previous two samples but the sample continued to reduce at this amount and a different peak emerged forming a plateau to a temperature of 563 K. Reduction was complete by 623 K.

Figure 4.4.10.
TPR profiles for the ${}^8\text{Cu}_{\text{Mg(2)Al}}$ catalysts with variation in ageing time.



4.4.7 Nitrous Oxide Chemisorption and Copper Surface Area measurements

Nitrous oxide chemisorption studies were conducted on the pH = 8 catalysts with the results presented in Table 4.4.4. The $^8_{30}\text{Cu}_{\text{Mg}(2)\text{Al}}$ catalyst showed the largest dispersion of this series of catalyst at 7.9 %. This catalyst had a maximum copper surface area of $34.8 \text{ m}^2 \text{ g}^{-1}$ and particle size of 13.2 nm. A decrease in dispersion values and copper surface areas were observed with increase in ageing time, which suggested that the particles conglomerate during preparation.

The percentage of copper present in the $^8_{30}\text{Cu}_{\text{Mg}(2)\text{Al}}$ catalyst was larger than the theoretical value. A similar correlation cannot be observed with lengthening ageing time.

Table 4.4.4. Nitrous oxide chemisorption results for the $\text{Cu}_{\text{Mg}(2)\text{Al}}$ catalysts with variation in ageing time.

Ageing Time	$^8_{30}\text{Cu}_{\text{Mg}(2)\text{Al}}$	$^8_{70}\text{Cu}_{\text{Mg}(2)\text{Al}}$	$^8_{140}\text{Cu}_{\text{Mg}(2)\text{Al}}$
% Cu in catalyst	60.4	55.0	58.7
% dispersion	7.9	6.2	5.9
Particle size (nm)	13.2	16.8	17.6
% calibrated dispersion	8.0	6.5	6.3
Calibrated particle size (nm)	13.0	16.0	16.5
Copper surface area ($\text{m}^2 \text{ g}^{-1}$)	34.8	34.0	23.1

The $^8_{70}\text{Cu}_{\text{Mg}(2)\text{Al}}$ sample showed the highest maximum reduction temperature of the copper surface for this series of catalysts (Table 4.4.5). The temperature of 433 K was marginally higher than the $^8_{30}\text{Cu}_{\text{Mg}(2)\text{Al}}$ catalyst temperature of 431 K and significantly higher than the $^8_{140}\text{Cu}_{\text{Mg}(2)\text{Al}}$ sample. The $^8_{30}\text{Cu}_{\text{Mg}(2)\text{Al}}$ catalyst had a more elevated completed surface reduction temperature than the $^8_{70}\text{Cu}_{\text{Mg}(2)\text{Al}}$ sample.

Table 4.4.5. Copper surface reduction temperatures for the $\text{Cu}_{\text{Mg}(2)\text{Al}}$ catalysts with variation in ageing time.

Temperature (K)	T_{initial}	T_{max}	T_{complete}
${}^8_{30}\text{Cu}_{\text{Mg}(2)\text{Al}}$	383	431	483
${}^8_{70}\text{Cu}_{\text{Mg}(2)\text{Al}}$	389	433	470
${}^8_{140}\text{Cu}_{\text{Mg}(2)\text{Al}}$	378	403	458

4.4.8 Elemental Analysis

The carbon content for the pH = 8 precursors were all of a similar value (Table 4.4.6). Hydrogen showed little variation with ageing time. The concentration of nitrogen was not detected in the ${}^8_{70}\text{Cu}_{\text{Mg}(2)\text{Al}}$ and ${}^8_{140}\text{Cu}_{\text{Mg}(2)\text{Al}}$ samples but the ${}^8_{30}\text{Cu}_{\text{Mg}(2)\text{Al}}$ catalyst had a nitrogen content of 0.10 %. Sulfur did not vary with lengthening ageing time at pH = 8 as a maximum of 0.01 %. At pH = 9, the ${}^9_{30}\text{Cu}_{\text{Mg}(2)\text{Al}}$ precursor had a non-detectable amount while the ${}^8_{70}\text{Cu}_{\text{Mg}(2)\text{Al}}$ sample had a value of 0.01 %.

Table 4.4.6. Elemental Analysis results for the $\text{Cu}_{\text{Mg}(2)\text{Al}}$ precursors with variation in preparation conditions.

Element	C	H	N	S
${}^8_{30}\text{Cu}_{\text{Mg}(2)\text{Al}}$	2.5	3.0	0.10	0.01
${}^8_{70}\text{Cu}_{\text{Mg}(2)\text{Al}}$	2.6	3.0	nda	0.01
${}^8_{140}\text{Cu}_{\text{Mg}(2)\text{Al}}$	2.4	3.1	nda	0.01
${}^9_{30}\text{Cu}_{\text{Mg}(2)\text{Al}}$	3.2	2.2	0.92	nda
${}^9_{70}\text{Cu}_{\text{Mg}(2)\text{Al}}$	2.9	2.4	0.79	0.01

nda = non-detectable amount

Incrementing the pH from 8 to 9 resulted in an increase in carbon content with the ${}^9_{30}\text{Cu}_{\text{Mg}(2)\text{Al}}$ precursor containing more than the ${}^9_{70}\text{Cu}_{\text{Mg}(2)\text{Al}}$ sample. The change in pH increased the nitrogen concentration considerably. Hydrogen and sulfur both decreased.

Calcination decreased the concentrations of carbon, hydrogen and sulfur (Table 4.4.7). The ${}^8_{30}\text{Cu}_{\text{Mg}(2)\text{Al}}$ sample showed the largest decrease in carbon concentration. The ${}^8_{70}\text{Cu}_{\text{Mg}(2)\text{Al}}$ catalyst decreased the carbon and hydrogen concentrations by the least amount. The nitrogen concentration values appeared to be erroneous, as these values increased after calcination.

Table 4.4.7. Elemental Analysis results for the $\text{Cu}_{\text{Mg}(2)\text{Al}}$ catalysts with variation in ageing time.

Element	C	H	N	S
${}^8_{30}\text{Cu}_{\text{Mg}(2)\text{Al}}$	1.5	0.95	0.69	nda
${}^8_{70}\text{Cu}_{\text{Mg}(2)\text{Al}}$	2.0	0.99	0.06	nda
${}^8_{140}\text{Cu}_{\text{Mg}(2)\text{Al}}$	1.9	0.86	0.08	0.01

nda = non-detectable amount

4.4.9 BET Surface Area measurements

BET surface area measurements were conducted on the pH = 8 catalysts (Table 4.4.8) with no correlation in lengthening ageing time being observed. The ${}^8_{30}\text{Cu}_{\text{Mg}(2)\text{Al}}$ sample had the largest surface area and the ${}^8_{70}\text{Cu}_{\text{Mg}(2)\text{Al}}$ catalyst, the smallest.

Table 4.4.8. BET surface area measurements for the $\text{Cu}_{\text{Mg}(2)\text{Al}}$ catalysts with variation in ageing time.

Ageing Time	${}^8_{30}\text{Cu}_{\text{Mg}(2)\text{Al}}$	${}^8_{70}\text{Cu}_{\text{Mg}(2)\text{Al}}$	${}^8_{140}\text{Cu}_{\text{Mg}(2)\text{Al}}$
Single Point ($\text{m}^2 \text{g}^{-1}$)	97.5	77.4	88.8
BET surface area ($\text{m}^2 \text{g}^{-1}$)	100.0	79.2	91.0

4.4.10 Summary

At increased pH and ageing time, increased incomplete co-precipitation and degraded precursors. The required hydrotalcite-like phase was formed, which decreased in crystallinity with shorter ageing times and decomposed on calcination. Shorter ageing

times increased the copper dispersion, surface area and maximum surface reduction temperature but the BET surface area was independent. The TPR profile of the ${}^8_{70}\text{Cu}_{\text{Mg}(2)\text{Al}}$ catalyst was different than the ${}^8_{30}\text{Cu}_{\text{Mg}(2)\text{Al}}$ and ${}^8_{140}\text{Cu}_{\text{Mg}(2)\text{Al}}$ catalysts and the BET surface area was noticeably lower.

4.5 Cu/MgO/Al₂O₃ (60/5/35) (Cu_{Mg(5)Al})

4.5.1 Preparation

The mother liquor of the pH = 8 samples was deep blue in colour and filtration resulted in a sky blue filtrate. This was indicative of incomplete copper co-precipitation. The filtrate had a maximum copper concentration of only 2000 ppm, the value was less for shorter ageing times, reducing to approximately 1000 ppm for the ⁸₃₀Cu_{Mg(5)Al} precursor. The precursors were pale blue in colour.

Increasing the pH from 8 to 9, the filtrate of the ⁹₃₀Cu_{Mg(5)Al} precursor increased the copper concentration to 6000-7000 ppm. The damp precursor appeared darker than the pH = 8 precursor. It also had a different texture, which was indicative of peptisation. Peptisation resulted in a flaky consistency.

Drying resulted in the ⁸₃₀Cu_{Mg(5)Al} and ⁸₇₀Cu_{Mg(5)Al} samples showing no signs of degradation but the ⁸₁₄₀Cu_{Mg(5)Al} precursor displayed black tinges at the edges of the crystallites. The ⁹₃₀Cu_{Mg(5)Al} precursor had degraded more and was consequently not fully characterised and omitted from microreactor experiments.

On calcination, all samples went green, which darkened in shades on increasing ageing time. The partial decomposition of the ⁸₁₄₀Cu_{Mg(5)Al} resulted in an increase in density of the oxide catalyst of almost 175 % upon comparison to the other samples.

After leaving the washings for a week, the ⁹₃₀Cu_{Mg(5)Al} sample resulted in a green malachite-like precipitate and also a green solution being present. The ⁸₁₄₀Cu_{Mg(5)Al} sample also resulted in a green precipitate and a partial green solution but in lower amounts and concentrations respectively. Reducing the ageing time decreased the precipitate concentration and retained the initial blue filtrate colour.

4.5.2 Differential Thermal Analysis

The ${}^8{}_{30}\text{Cu}_{\text{Mg}(5)\text{Al}}$ precursor showed 2 endothermic peaks, the initial peak is present at 413 K and the latter at 523 K (Figure 4.5.1). The former peak can be ascribed as H-bonded water loss from the intercalating hydrotalcite-like layers and the latter as dehydroxylation. No further change was observed between 623 and 823 K, the deflection just being due to the heat capacitance of the sample.

The DTA profile of the ${}^8{}_{70}\text{Cu}_{\text{Mg}(5)\text{Al}}$ sample showed a large endothermic peak at ca. 443 K. A second endothermic peak was present at 508 K with further minute endothermic peaks at 598 and 648 K being tangibly observed.

The ${}^8{}_{140}\text{Cu}_{\text{Mg}(5)\text{Al}}$ sample showed several endothermic peaks. They were observed at 393-403, 443, 508 and 598 K. The ${}^9{}_{30}\text{Cu}_{\text{Mg}(5)\text{Al}}$ precursor showed similar peaks as the ${}^8{}_{30}\text{Cu}_{\text{Mg}(5)\text{Al}}$ sample. The endothermic peak was present at 413 K and the second at 523 K. However, this latter peak was significantly smaller than the ${}^8{}_{30}\text{Cu}_{\text{Mg}(5)\text{Al}}$ precursor. A third endothermic peak was also present at 613 K, which was not seen in the previous precursors. The ${}^8{}_{30}\text{Cu}_{\text{Mg}(5)\text{Al}}$ and ${}^9{}_{30}\text{Cu}_{\text{Mg}(5)\text{Al}}$ precursors were conducted at the University of Edinburgh.

4.5.3 X-ray Diffraction

The ${}^8{}_{30}\text{Cu}_{\text{Mg}(5)\text{Al}}$, ${}^8{}_{70}\text{Cu}_{\text{Mg}(5)\text{Al}}$ and ${}^9{}_{30}\text{Cu}_{\text{Mg}(5)\text{Al}}$ precursors showed high crystallinity resulting in a hydrotalcite-like structure [230] (Figure 4.5.2).

The ${}^8{}_{140}\text{Cu}_{\text{Mg}(5)\text{Al}}$ precursor appeared completely different to that of the previous precursors. Comparatively, the precursor was very poorly crystalline resulting from the decomposition of the hydrotalcite-like structure (13.85 °, 27.8 ° and 41.3 °) and the introduction of barringtonite ($\text{MgCO}_3 \cdot 2\text{H}_2\text{O}$) [222] (33.7 ° and 34.3 °). The 2θ angle of 34.3 ° peak was more prominent in the calcined sample (Figure 4.5.3) with the two

Figure 4.5.1. DTA profiles for the $\text{Cu}_{\text{Mg}(\text{Al})}$ precursors with variation in preparation conditions.

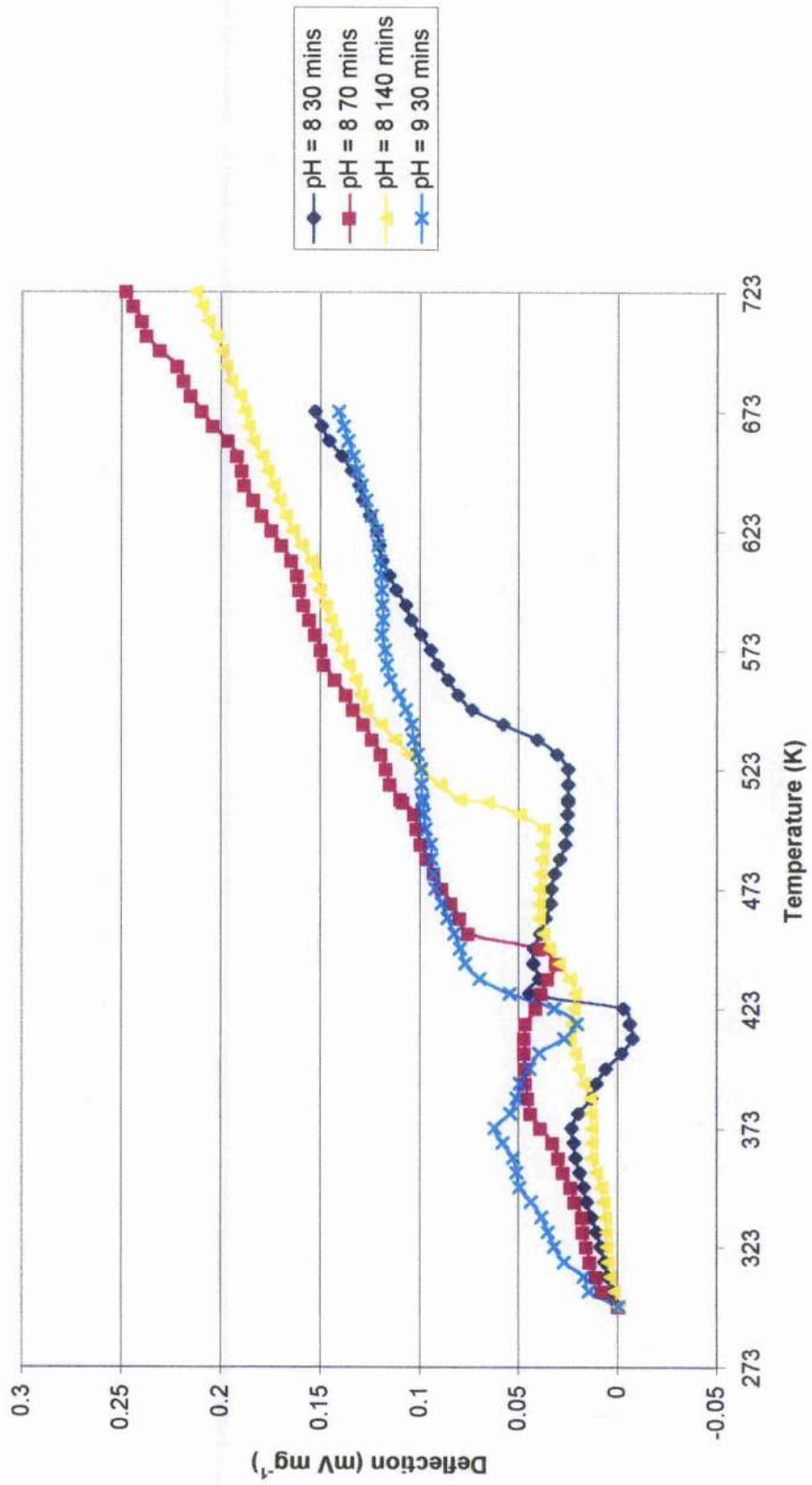


Figure 4.5.2. XRD patterns for the $\text{Cu}_{\text{Mg(6)Al}}$ precursors with variation in preparation conditions.

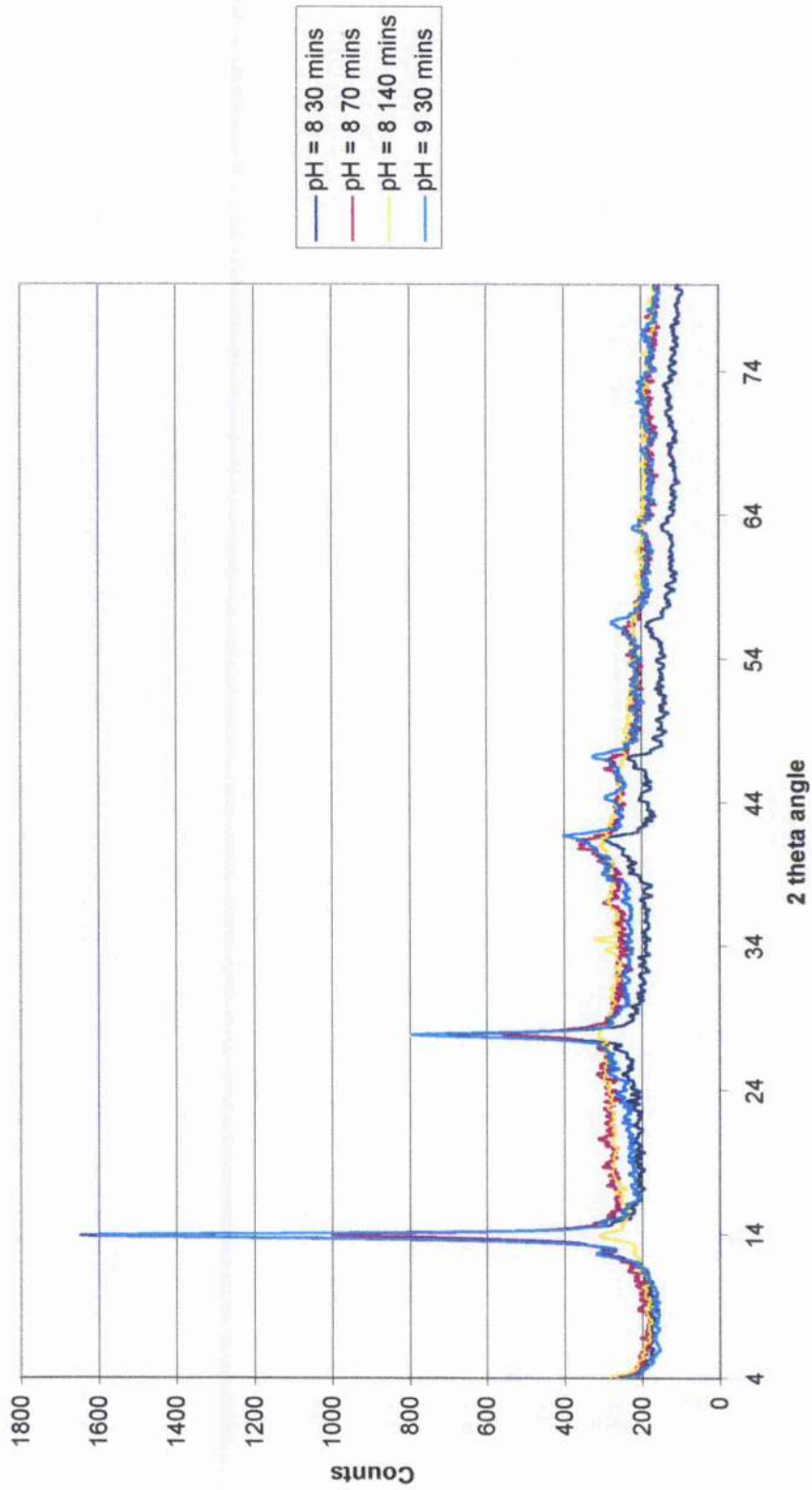
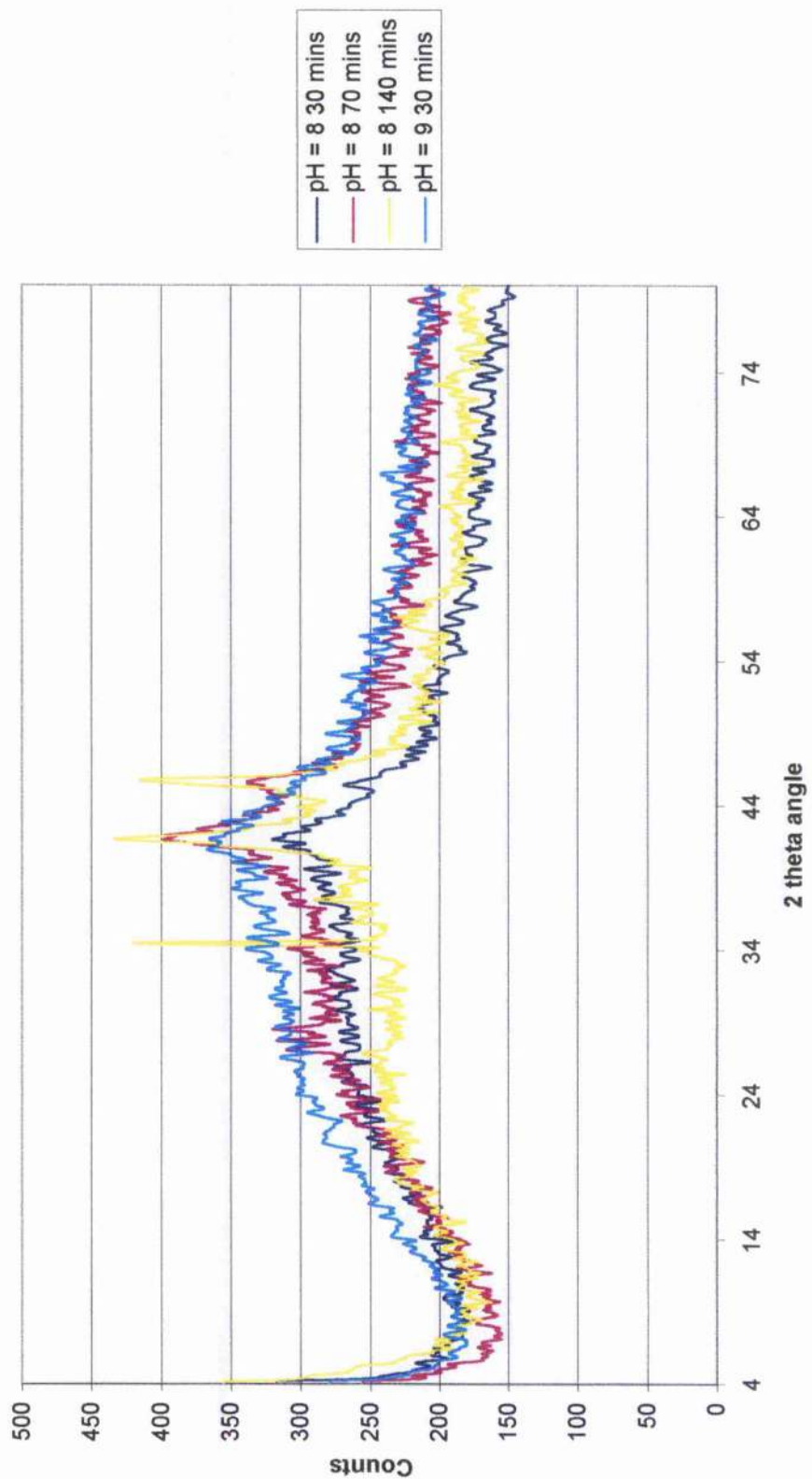


Figure 4.5.3. XRD patterns for the $\text{Cu}_{\text{Mg(5)Al}}$ catalysts with variation in preparation conditions.



other significant peaks (41.7° and 46.3°) and side peaks at 37.2° and 56.7° present as copper (II) oxide [224].

Calcination of the remaining precursors resulted in decomposition of the hydrotaalcite-like structure (Figure 4.5.3) into copper (II) oxide [224] with 2θ angle values of 41.4° and 45.4° . The ${}^8_{30}\text{Cu}_{\text{Mg}(5)\text{Al}}$ and the ${}^9_{30}\text{Cu}_{\text{Mg}(5)\text{Al}}$ catalysts showed the smallest peaks.

4.5.4 X-ray Fluorescence

The main peaks observed in the precursors were both the copper K_α and K_β -line peaks and the aluminium K_α -line peak. The magnesium K_α -line was very small and just distinguishable from the background. Iron (K_α -line peak) was the main contaminant with a small amount of sodium (K_α -line), potassium (K_α -line) and calcium (K_α -line) being present. Little variation was observed with ageing time. The XRF spectrum of the ${}^8_{140}\text{Cu}_{\text{Mg}(5)\text{Al}}$ precursor was shown in Figure 4.5.4.

Increasing the pH from 8 to 9 resulted in the appearance of a small cobalt (K_α -line) peak. The filtered spectrum was shown in Figure 4.5.5. No chlorine was present in any precursor.

Calcination resulted in little variance in concentration of elements being observed when compared to the precursors, as the same elements were present in similar quantities. Figure 4.5.6 showed the ${}^8_{70}\text{Cu}_{\text{Mg}(5)\text{Al}}$ catalyst.

Addition of the filter resulted in no chlorine being found in the calcined samples. The ${}^8_{140}\text{Cu}_{\text{Mg}(5)\text{Al}}$ catalyst is shown in Figure 4.5.7.

Figure 4.5.4. XRF spectrum for the $^{8140}\text{Cu}_{\text{Mg}(5)\text{Al}}$ precursor.

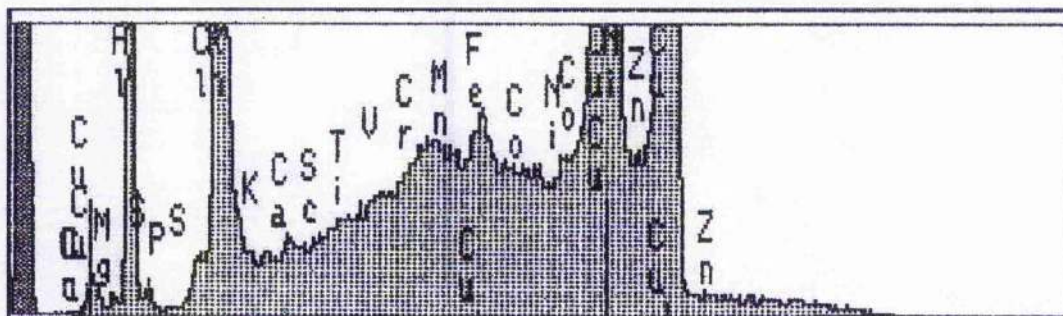


Figure 4.5.5. XRF spectrum for the filtered $^{930}\text{Cu}_{\text{Mg}(5)\text{Al}}$ precursor.

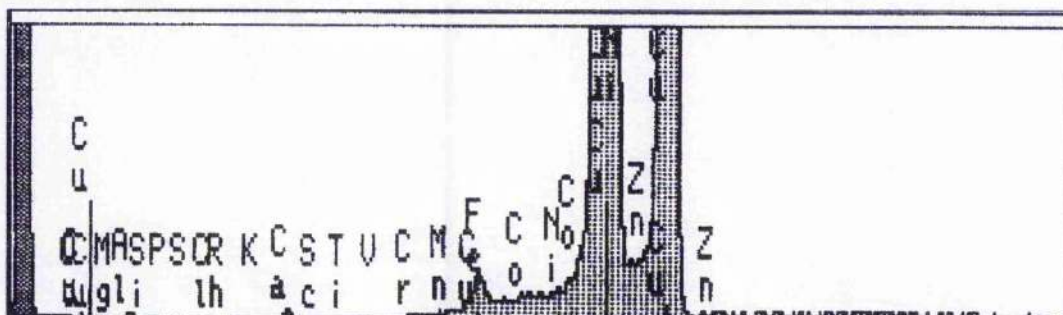


Figure 4.5.6. XRF spectrum for the $^{870}\text{Cu}_{\text{Mg}(5)\text{Al}}$ catalyst.

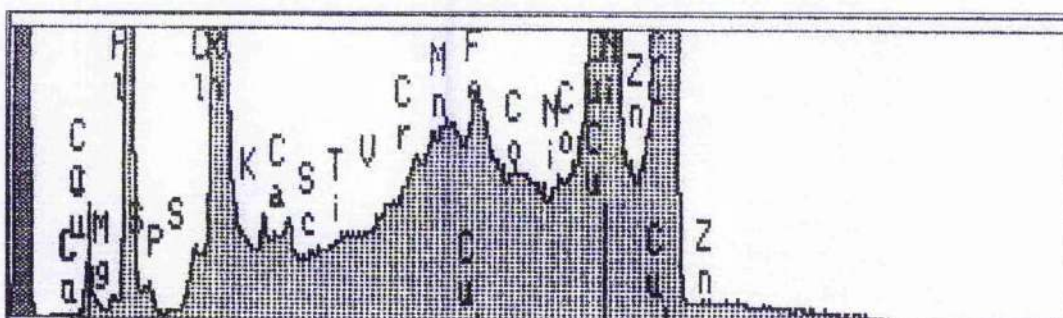
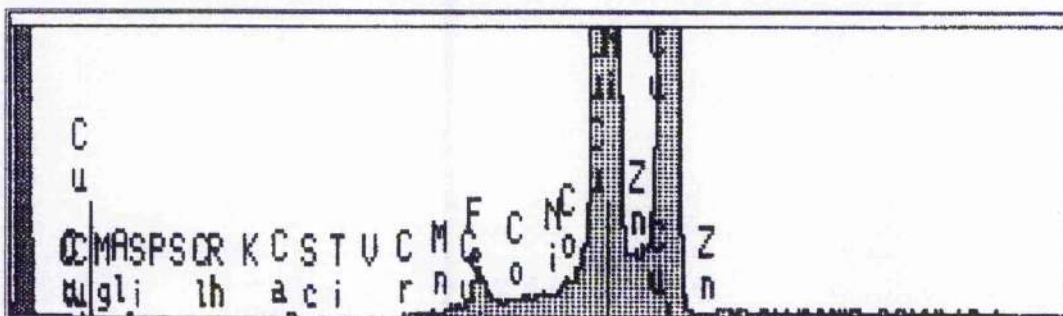


Figure 4.5.7. XRF spectrum for the filtered $^{8140}\text{Cu}_{\text{Mg}(5)\text{Al}}$ catalyst.



4.5.5 Atomic Absorption Spectroscopy

The percentage of pH = 8 metal co-precipitation of copper and magnesium decreased with increasing ageing time (Table 4.5.1). Magnesium showed a larger affect. However, aluminium did not follow a similar trend. The decrease in percentage of aluminium co-precipitation reduced dramatically from the ${}^8_{30}\text{Cu}_{\text{Mg}(5)\text{Al}}$ to the ${}^8_{70}\text{Cu}_{\text{Mg}(5)\text{Al}}$ catalyst before increasing slightly to the ${}^8_{140}\text{Cu}_{\text{Mg}(5)\text{Al}}$ sample.

The metal ratio of this series of catalysts was presented in Table 4.5.2 with all copper values greater than the theoretical figure of 60. This was due to the incomplete co-precipitation of the two other components. Both the aluminium and magnesium ratio values were all lower than the theoretical values. The ${}^8_{30}\text{Cu}_{\text{Mg}(5)\text{Al}}$ catalyst had the closest ratios to the theoretical requirement.

Table 4.5.1. Percentage of copper, magnesium and aluminium co-precipitated (wt / wt) for the $\text{Cu}_{\text{Mg}(5)\text{Al}}$ catalysts with variation in ageing time.

Element	Copper	Magnesium	Aluminium
${}^8_{30}\text{Cu}_{\text{Mg}(5)\text{Al}}$	98.5	70.8	96.0
${}^8_{70}\text{Cu}_{\text{Mg}(5)\text{Al}}$	98.3	65.9	69.0
${}^8_{140}\text{Cu}_{\text{Mg}(5)\text{Al}}$	96.0	57.4	76.3

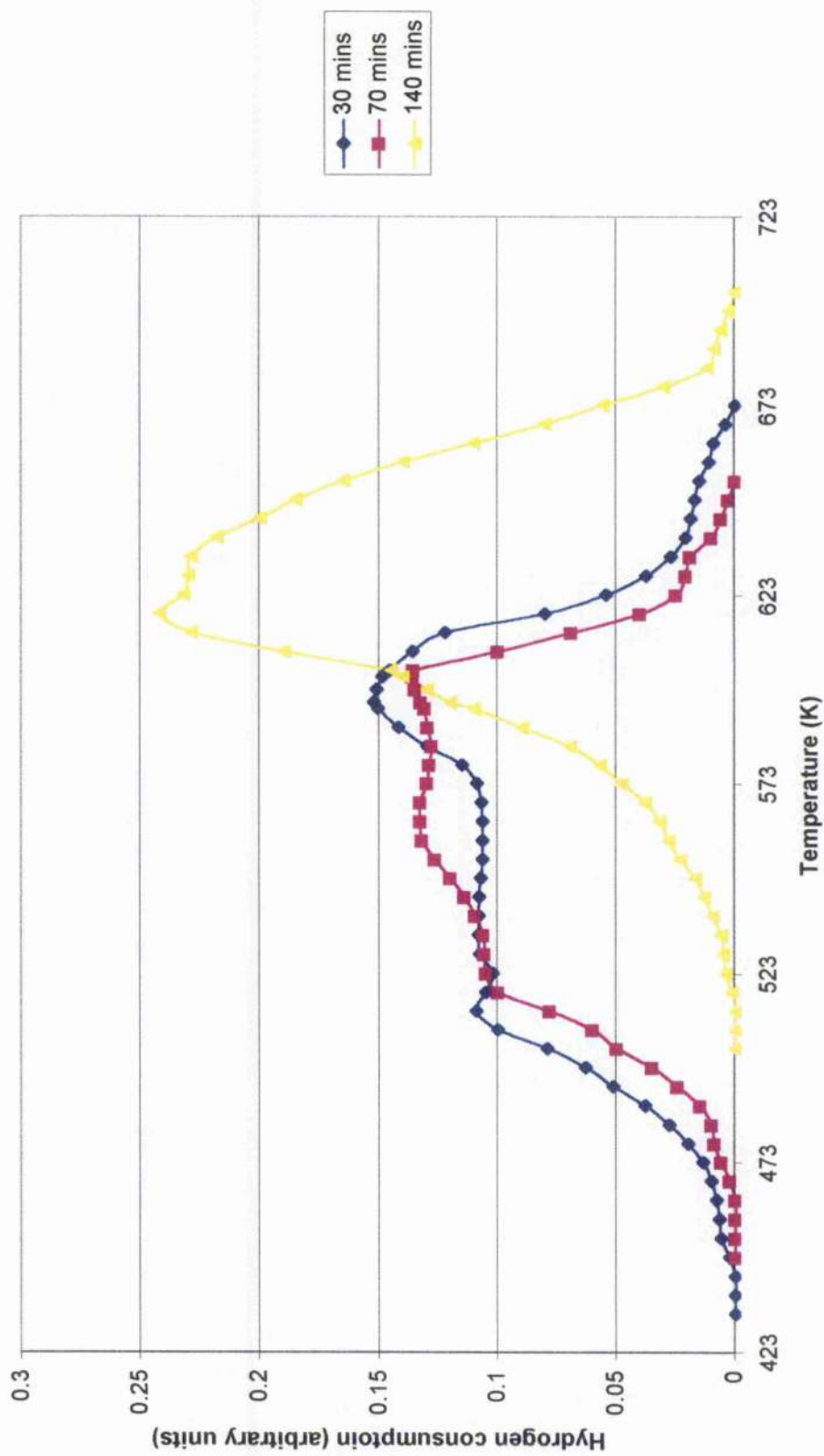
Table 4.5.2. Metal ratios of copper, magnesium and aluminium for the $\text{Cu}_{\text{Mg}(5)\text{Al}}$ catalysts with variation in ageing time.

Element	Copper	Magnesium	Aluminium
${}^8_{30}\text{Cu}_{\text{Mg}(5)\text{Al}}$	61.4	3.7	34.9
${}^8_{70}\text{Cu}_{\text{Mg}(5)\text{Al}}$	68.2	3.8	28.0
${}^8_{140}\text{Cu}_{\text{Mg}(5)\text{Al}}$	66.1	3.3	30.6

4.5.6 Temperature Programmed Reduction

The ${}^8_{30}\text{Cu}_{\text{Mg}(5)\text{Al}}$ catalyst began reducing at a temperature of 443 K increasing to a local maximum reduction temperature of 513 K (Figure 4.5.8). The quantity of reduction decreased slightly to 523 K and maintained to reduce at this quantity until 573 K. The

Figure 4.5.8. TPR profiles for the ${}^8\text{Cu}_{\text{Mg}(\text{S})\text{Al}}$ catalysts with variation in ageing time.



profile increased to the global maximum reduction temperature at 595 K. The reduction was complete by 673 K.

The ${}^8{}_{70}\text{Cu}_{\text{Mg}(\text{S})\text{Al}}$ sample had a similar profile to the previous catalyst, a gradual increase in reduction from 463 to 523 K. Hydrogen consumption increased slightly to the maximum reduction temperature of 563 K. The third reduction peak was observed at 603 K before the profile rapidly decreased in hydrogen consumption to 623 K whereupon the catalyst completes reduction at 653 K.

The ${}^8{}_{140}\text{Cu}_{\text{Mg}(\text{S})\text{Al}}$ catalyst was different to that of the previous two preparations. Reduction started at a higher temperature of 523-533 K increasing to a maximum reduction temperature of 618 K. The quantity of reduction decreased only marginally to a plateau between 623 and 633 K before completing reduction by 703 K. This catalyst reduced over a narrower temperature range.

4.5.7 Nitrous Oxide Chemisorption and Copper Surface Area measurements

Table 4.5.3. Nitrous oxide chemisorption results for the $\text{Cu}_{\text{Mg}(\text{S})\text{Al}}$ catalysts with variation in ageing time.

Ageing Time	${}^8{}_{30}\text{Cu}_{\text{Mg}(\text{S})\text{Al}}$	${}^8{}_{70}\text{Cu}_{\text{Mg}(\text{S})\text{Al}}$	${}^8{}_{140}\text{Cu}_{\text{Mg}(\text{S})\text{Al}}$
% Cu in catalyst	62.9	62.1	66.0
% dispersion	10.5	10.7	7.7
Particle size (nm)	9.9	9.7	13.5
% calibrated dispersion	11.1	11.6	8.1
Calibrated particle size (nm)	9.4	9.0	12.8
Copper surface area ($\text{m}^2 \text{g}^{-1}$)	36.9	39.0	34.5

The ${}^8{}_{140}\text{Cu}_{\text{Mg}(\text{S})\text{Al}}$ sample had the lowest copper dispersion value (Table 4.5.3), the highest percentage of copper present in the catalyst and the smallest copper surface

area. Little difference was observed with the remaining two samples in dispersion, particle size and the copper surface area.

The ${}^8_{140}\text{Cu}_{\text{Mg}(5)\text{Al}}$ catalyst had a copper surface area, which was only slightly smaller than the ${}^8_{30}\text{Cu}_{\text{Mg}(5)\text{Al}}$ and ${}^8_{70}\text{Cu}_{\text{Mg}(5)\text{Al}}$ catalysts, even though the dispersion was significantly lower.

Table 4.5.4. Copper surface reduction temperatures for the $\text{Cu}_{\text{Mg}(5)\text{Al}}$ catalysts with variation in ageing time.

Temperature (K)	T_{initial}	T_{max}	T_{complete}
${}^8_{30}\text{Cu}_{\text{Mg}(5)\text{Al}}$	393	453	513
${}^8_{70}\text{Cu}_{\text{Mg}(5)\text{Al}}$	391	448	509
${}^8_{140}\text{Cu}_{\text{Mg}(5)\text{Al}}$	398	493	543

The copper surface reduction temperature for both the ${}^8_{30}\text{Cu}_{\text{Mg}(5)\text{Al}}$ and the ${}^8_{70}\text{Cu}_{\text{Mg}(5)\text{Al}}$ catalysts displayed a maximum of similar value (Table 4.5.4). However, the ${}^8_{140}\text{Cu}_{\text{Mg}(5)\text{Al}}$ sample had a maximum reduction temperature a further 40 K higher, even though the initial reduction temperature was close in value to the two other samples. The ${}^8_{140}\text{Cu}_{\text{Mg}(5)\text{Al}}$ catalyst completed reduction at a proportionately higher temperature and thus had a wider range of surface reduction temperatures, this occurred regardless of the small dispersion.

4.5.8 Elemental Analysis

There was a marginal increase in carbon concentration with increasing ageing time and pH (Table 4.5.5). Nitrogen and sulfur showed a similar trend with the former increasing more dramatically. Hydrogen opposed the trend and decreased. The ${}^8_{30}\text{Cu}_{\text{Mg}(5)\text{Al}}$ and ${}^8_{70}\text{Cu}_{\text{Mg}(5)\text{Al}}$ precursors showed little difference in concentrations of the detectable elements.

Table 4.5.5. Elemental Analysis results for the $\text{Cu}_{\text{Mg}(5)\text{Al}}$ precursors with variation in preparation conditions.

Element	C	H	N	S
$^8_{30}\text{Cu}_{\text{Mg}(5)\text{Al}}$	2.6	3.0	nda	nda
$^8_{70}\text{Cu}_{\text{Mg}(5)\text{Al}}$	2.5	2.9	nda	nda
$^8_{140}\text{Cu}_{\text{Mg}(5)\text{Al}}$	2.7	2.4	1.3	0.01
$^9_{30}\text{Cu}_{\text{Mg}(5)\text{Al}}$	2.9	2.6	1.1	0.01

nda = non-detectable amount

The carbon content in these catalysts (Table 4.5.6) decreased with increasing ageing time. The $^9_{30}\text{Cu}_{\text{Mg}(5)\text{Al}}$ catalyst did not decrease proportionately as the $^8_{140}\text{Cu}_{\text{Mg}(5)\text{Al}}$ sample. At pH = 8, the hydrogen concentration increased with lengthening ageing time with the $^9_{30}\text{Cu}_{\text{Mg}(5)\text{Al}}$ catalyst decreasing by the largest quantity from the precursor. The nitrogen concentrations must have been incorrect, as the pH = 8 precursor values were lower than the calcined catalysts. This statement also applied to the sulfur content of the $^8_{70}\text{Cu}_{\text{Mg}(5)\text{Al}}$ catalyst. The remaining values decreased on calcination. The $^9_{30}\text{Cu}_{\text{Mg}(5)\text{Al}}$ sample was conducted only once.

Table 4.5.6. Elemental Analysis results for the $\text{Cu}_{\text{Mg}(5)\text{Al}}$ catalysts with variation in preparation conditions.

Element	C	H	N	S
$^8_{30}\text{Cu}_{\text{Mg}(5)\text{Al}}$	2.2	0.55	0.14	nda
$^8_{70}\text{Cu}_{\text{Mg}(5)\text{Al}}$	2.0	0.90	0.18	0.01
$^8_{140}\text{Cu}_{\text{Mg}(5)\text{Al}}$	1.0	1.5	1.7	nda
$^9_{30}\text{Cu}_{\text{Mg}(5)\text{Al}}$	1.8	0.31	0.02	nda

nda = non-detectable amount

4.5.9 BET Surface Area measurements

Surface area measurements of the pH = 8 catalysts varied by $22 \text{ m}^2 \text{ g}^{-1}$ (Table 4.5.7). The $^8_{70}\text{Cu}_{\text{Mg}(5)\text{Al}}$ sample had the largest BET surface area of this series of catalyst at $66.7 \text{ m}^2 \text{ g}^{-1}$ with the other two samples having similar values.

Table 4.5.7. BET surface area measurements for the $\text{Cu}_{\text{Mg}(5)\text{Al}}$ catalysts with variation in ageing time.

Ageing Time	$^8_{30}\text{Cu}_{\text{Mg}(5)\text{Al}}$	$^8_{70}\text{Cu}_{\text{Mg}(5)\text{Al}}$	$^8_{140}\text{Cu}_{\text{Mg}(5)\text{Al}}$
Single Point ($\text{m}^2 \text{g}^{-1}$)	48.6	66.4	44.8
BET surface area ($\text{m}^2 \text{g}^{-1}$)	49.4	66.7	45.1

4.5.10 Summary

At increased pH, the precursor was partially degraded. Longer ageing times increased dissolution but the hydrotalcite-like phase was still present. A different XRD pattern, DTA and TPR profiles were observed with the $^8_{140}\text{Cu}_{\text{Mg}(5)\text{Al}}$ catalyst when compared to the $^8_{30}\text{Cu}_{\text{Mg}(5)\text{Al}}$ and $^8_{70}\text{Cu}_{\text{Mg}(5)\text{Al}}$ catalysts. The copper dispersion, copper and BET surface areas were independent of ageing time.

4.6 Cu/MgO/Al₂O₃ (60/7/35) (Cu_{Mg(7)Al})

4.6.1 Preparation

Due to the problem of incomplete magnesium co-precipitation, the initial concentration of the magnesium was increased with respect to the other components.

Filtration of the mother liquor resulted in a pale blue filtrate, indicating the presence of copper in the filtrate. The concentration did not vary greatly among the pH = 8 filtrates, all values were between 3000 and 5000 ppm. The ⁹₃₀Cu_{Mg(7)Al} precursor gave a higher concentration of copper in the filtrate with an approximate value of 6000-7000 ppm.

The pH = 8 precursors were pale blue in colour but the ⁹₃₀Cu_{Mg(7)Al} precursor was peptised, which was different in consistency to the pH = 8 samples. After drying, the ⁸₁₄₀Cu_{Mg(7)Al} precursor had partially degraded, as it showed the black colouring around the edges of the crystallites.

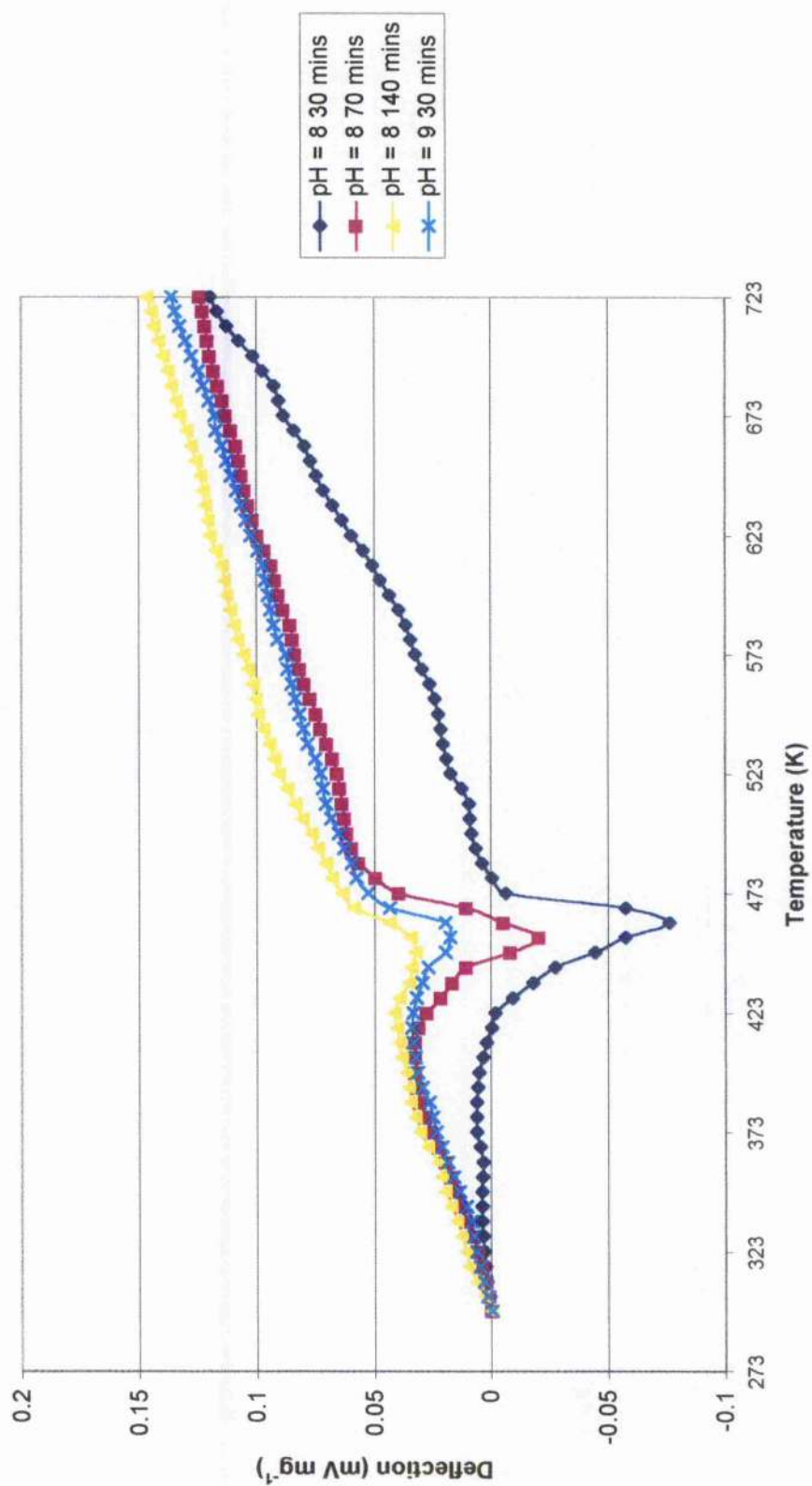
During calcination, the samples became green, with the ⁹₃₀Cu_{Mg(7)Al} catalyst considerably darker than the pH = 8 samples. The ⁸₃₀Cu_{Mg(7)Al} and ⁸₁₄₀Cu_{Mg(7)Al} samples were of similar colour while the ⁸₇₀Cu_{Mg(7)Al} catalyst was darker.

Two weeks after the preparation, the filtrate washings were re-examined with a larger amount of copper based precipitate being present with lengthening ageing time and increase in pH.

4.6.2 Differential Thermal Analysis

The DTA profiles of the ⁸₃₀Cu_{Mg(7)Al} precursor showed a large endothermic peak present at a temperature of ca. 460 K (Figure 4.6.1). The magnitude and temperature of this peak decreased with increasing ageing time and pH. The profile of the ⁸₁₄₀Cu_{Mg(7)Al} precursor had the smallest peak height and the lowest temperature for the

Figure 4.6.1. DTA profiles for the $\text{Cu}_{\text{Mg(7)Al}}$ precursors with variation in preparation conditions.



endothermic peak to occur. No further peaks in any profile were observed above the temperature of 473 K until culmination at 823 K.

4.6.3 X-ray Diffraction

All the XRD patterns of the precursors showed the hydrotalcite-like [230] structure (Figure 4.6.2). The peak heights increased with decreasing ageing time and pH. Side peaks present at 12.6° and 25.1° were the emergence of hydrotalcite [230].

Calcination resulted in decomposition of the hydrotalcite-like structure (Figure 4.6.3) into small and broad copper (II) oxide peaks [224] centred on 41.8° and 45.4° . The ${}^8_{70}\text{Cu}_{\text{Mg}(7)\text{Al}}$ catalyst showed the largest CuO peaks.

4.6.4 X-ray Fluorescence

The spectrum of the ${}^8_{30}\text{Cu}_{\text{Mg}(7)\text{Al}}$ precursor (Figure 4.6.4) was a representative spectrum of the 3 pH = 8 and pH = 9 precursors, as all showed the same peaks with equal intensity. The precursor XRF spectrum showed copper K_α and K_β -line peaks, the aluminium K_α -line peak and again a negligible magnesium K_α -line peak. An iron (K_α -line) peak was also present but so are calcium (K_α -line), sodium (K_α -line), titanium (K_α -line) and potassium (K_α -line) peaks. Other contaminants included chromium (K_α -line) and manganese (K_α -line). The addition of the chromium filter resulted in the spectrum shown in Figure 4.6.5, with no chlorine being observed.

Calcination resulted in the decrease of the iron (K_α -line) peak, titanium (K_α -line) and calcium (K_α -line) peak. However, a cobalt (K_α -line) peak emerged. The spectra of the unfiltered and filtered ${}^8_{30}\text{Cu}_{\text{Mg}(7)\text{Al}}$ catalyst were shown in Figures 4.6.6 and 4.6.7 respectively.

Figure 4.6.2. XRD patterns for the $\text{Cu}_{\text{Mg(7)Al}}$ precursors with variation in preparation conditions.

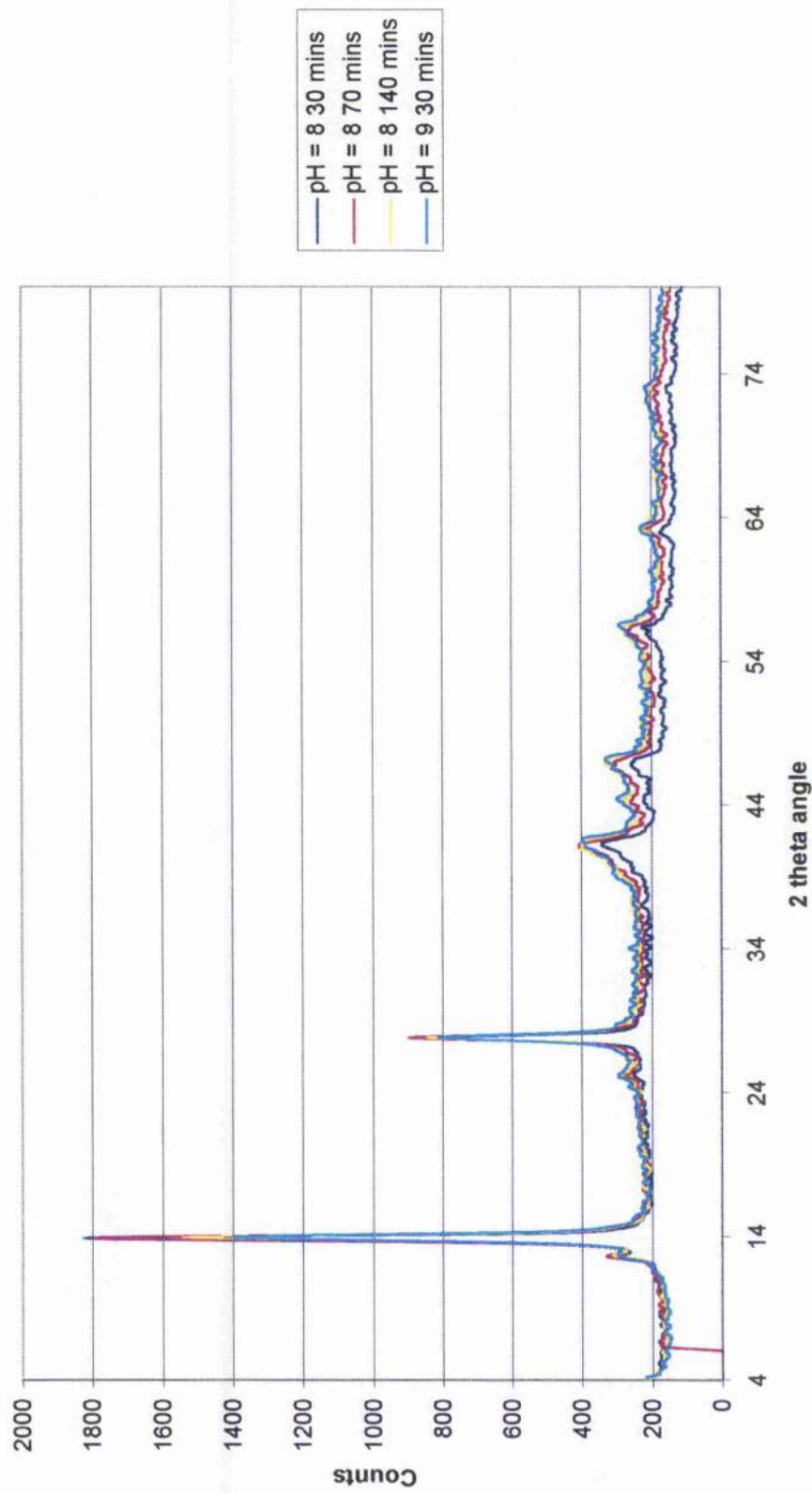


Figure 4.6.3. XRD patterns for the $\text{Cu}_{\text{Mg}(7)\text{Al}}$ catalysts with variation in preparation conditions.

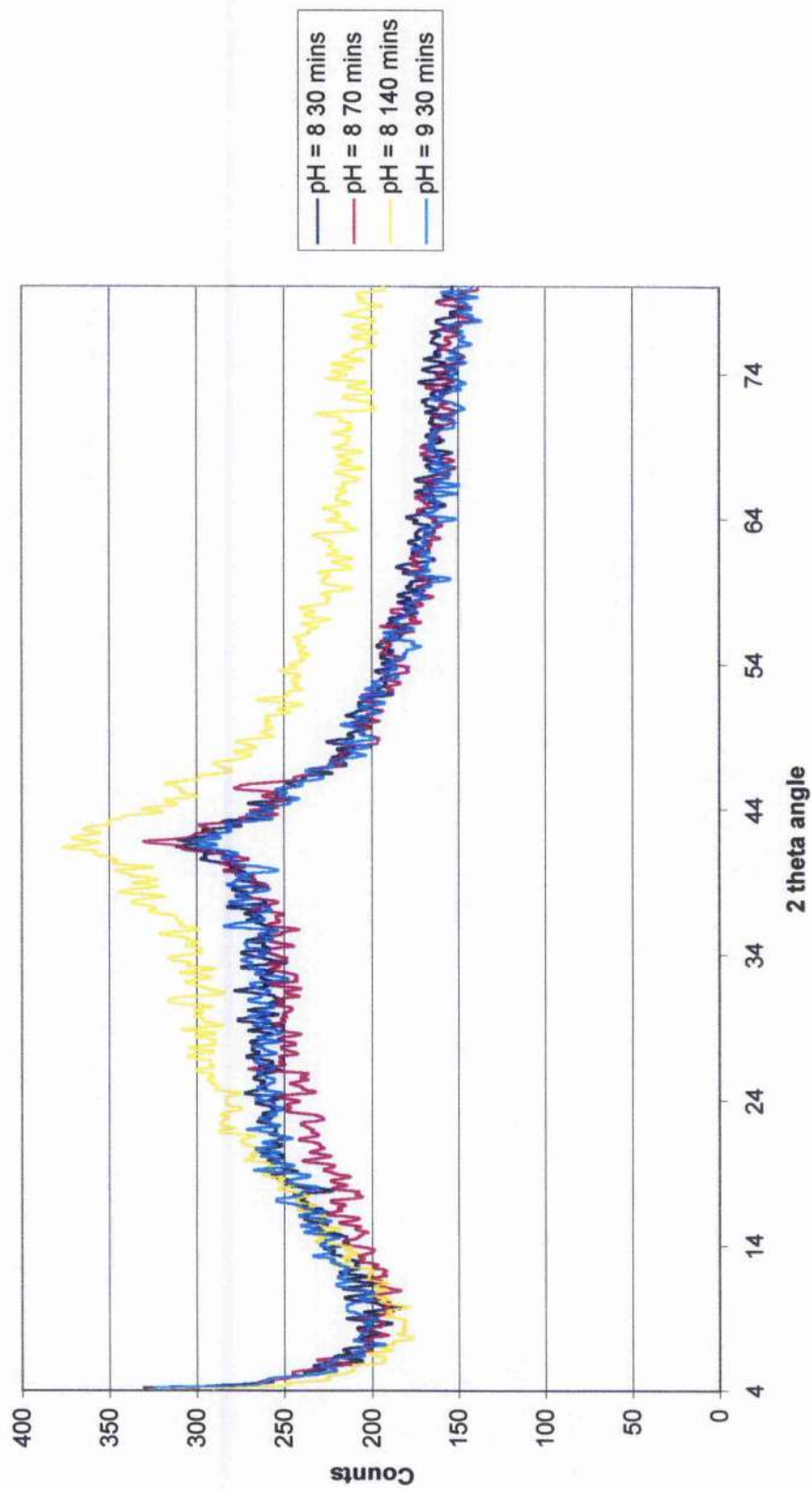


Figure 4.6.4. XRF spectrum for the $^{83}\text{Cu}_{\text{Mg}(7)\text{Al}}$ precursor.

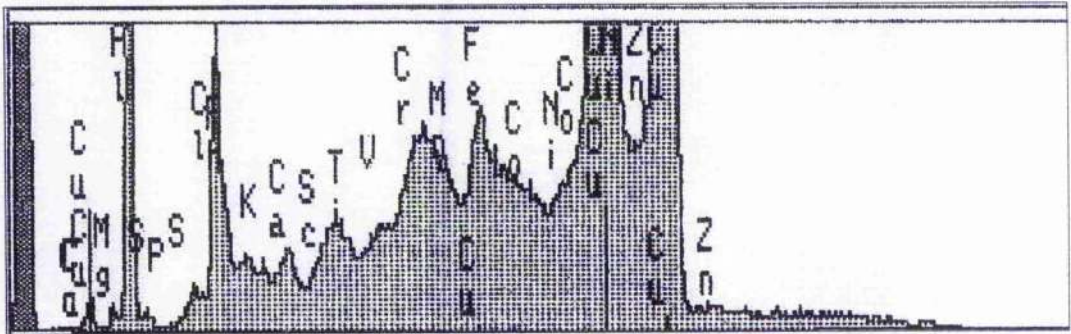


Figure 4.6.5. XRF spectrum for the filtered $^{83}\text{Cu}_{\text{Mg}(7)\text{Al}}$ precursor.

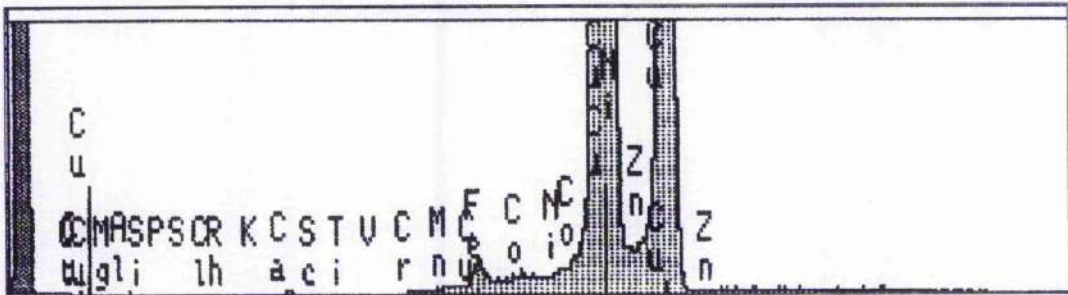


Figure 4.6.6. XRF spectrum for the $^{83}\text{Cu}_{\text{Mg}(7)\text{Al}}$ catalyst.

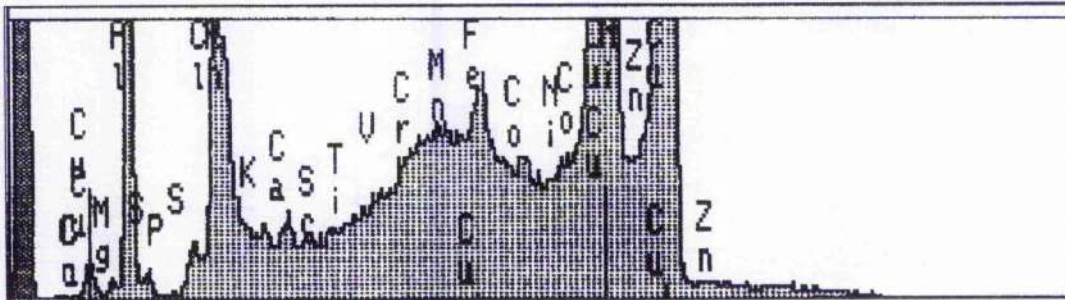
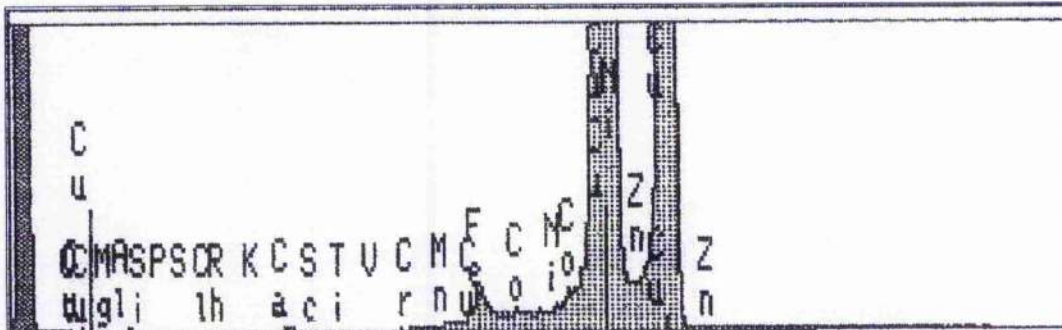


Figure 4.6.7. XRF spectrum for the filtered $^{83}\text{Cu}_{\text{Mg}(7)\text{Al}}$ catalyst.



4.6.5 Atomic Absorption Spectroscopy

The percentage of co-precipitated copper varied little between the ${}^8_{30}\text{Cu}_{\text{Mg}(7)\text{Al}}$ and ${}^8_{70}\text{Cu}_{\text{Mg}(7)\text{Al}}$ samples (Table 4.6.1). However, increasing in ageing time to ${}^8_{140}\text{Cu}_{\text{Mg}(7)\text{Al}}$, increased the copper concentration. At pH = 9, this value was increased further.

No correlation in co-precipitated magnesium was observed with ageing time or pH, the values only varied by 15 %. The highest magnesium co-precipitation percentage occurred with the ${}^8_{70}\text{Cu}_{\text{Mg}(7)\text{Al}}$ sample.

The percentage of co-precipitated aluminium increased with pH from 8 to 9. The low percentage of co-precipitated aluminium at ${}^8_{70}\text{Cu}_{\text{Mg}(7)\text{Al}}$ was counteracted by a higher magnesium value.

Table 4.6.1. Percentage of copper, magnesium and aluminium co-precipitated (wt / wt) for the $\text{Cu}_{\text{Mg}(7)\text{Al}}$ catalysts with variation preparation conditions.

Element	Copper	Magnesium	Aluminium
${}^8_{30}\text{Cu}_{\text{Mg}(7)\text{Al}}$	78.1	55.6	85.3
${}^8_{70}\text{Cu}_{\text{Mg}(7)\text{Al}}$	78.0	64.0	84.3
${}^8_{140}\text{Cu}_{\text{Mg}(7)\text{Al}}$	82.6	49.5	85.7
${}^9_{30}\text{Cu}_{\text{Mg}(7)\text{Al}}$	86.0	62.2	87.4

Table 4.6.2. Metal ratios of copper, magnesium and aluminium for the $\text{Cu}_{\text{Mg}(7)\text{Al}}$ catalysts with variation in preparation conditions.

Element	Copper	Magnesium	Aluminium
${}^8_{30}\text{Cu}_{\text{Mg}(7)\text{Al}}$	58.0	4.8	37.1
${}^8_{70}\text{Cu}_{\text{Mg}(7)\text{Al}}$	57.9	5.5	36.5
${}^8_{140}\text{Cu}_{\text{Mg}(7)\text{Al}}$	59.6	4.2	36.1
${}^9_{30}\text{Cu}_{\text{Mg}(7)\text{Al}}$	59.6	5.0	35.3

The catalyst closest to the theoretical metal ratio was the ${}^9_{30}\text{Cu}_{\text{Mg}(7)\text{Al}}$ sample (Table 4.6.2), which was then followed by the ${}^8_{30}\text{Cu}_{\text{Mg}(7)\text{Al}}$ catalyst. This suggested that shorter ageing times gave a metal ratio closer to the theoretical value than with longer

Figure 4.6.8. TPR profiles for the $\text{Cu}_{\text{Mg(7)Al}}$ catalysts with variation in preparation conditions.

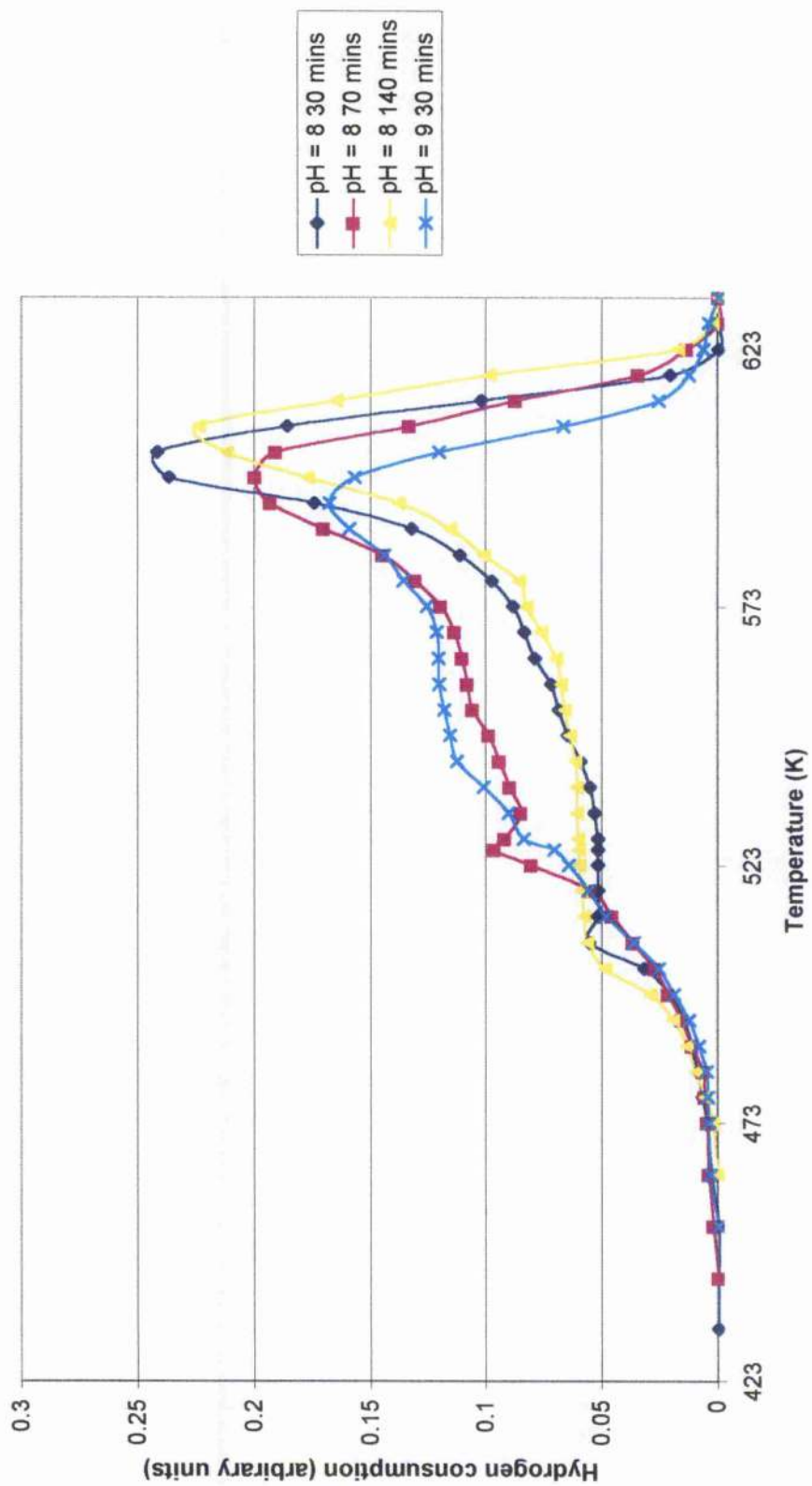


Table 4.6.3. Nitrous oxide chemisorption results for the $\text{Cu}_{\text{Mg}(7)\text{Al}}$ catalysts with variation in preparation conditions.

Catalyst	$^8_{30}\text{Cu}_{\text{Mg}(7)\text{Al}}$	$^8_{70}\text{Cu}_{\text{Mg}(7)\text{Al}}$	$^8_{140}\text{Cu}_{\text{Mg}(7)\text{Al}}$	$^9_{30}\text{Cu}_{\text{Mg}(7)\text{Al}}$
% Cu in catalyst	58.1	56.7	58.6	58.7
% dispersion	11.3	5.5	3.7	3.1
Particle size (nm)	9.2	18.9	28.1	33.5
% calibrated dispersion	11.8	6.2	4.3	3.7
Calibrated particle size (nm)	8.9	16.8	24.2	28.1
Copper surface area ($\text{m}^2 \text{g}^{-1}$)	38.6	20.5	15.5	14.4

Table 4.6.4. Copper surface reduction temperatures for the $\text{Cu}_{\text{Mg}(7)\text{Al}}$ catalysts with variation in preparation conditions.

Temperature (K)	T_{initial}	T_{max}	T_{complete}
$^8_{30}\text{Cu}_{\text{Mg}(7)\text{Al}}$	397	445	510
$^8_{70}\text{Cu}_{\text{Mg}(7)\text{Al}}$	381	431	493
$^8_{140}\text{Cu}_{\text{Mg}(7)\text{Al}}$	388	421	481
$^9_{30}\text{Cu}_{\text{Mg}(7)\text{Al}}$	391	433	461

The initial copper surface reduction temperature of this series of catalyst followed a similar trend with the $^8_{30}\text{Cu}_{\text{Mg}(7)\text{Al}}$ catalyst having the highest temperature, which was then followed by the $^9_{30}\text{Cu}_{\text{Mg}(7)\text{Al}}$ sample. However, the remaining samples did not decrease in the same manner as the maximum copper surface reduction temperatures.

The completion temperatures decreased with increasing ageing time and pH.

4.6.8 Elemental Analysis

The carbon content of the $^8_{70}\text{Cu}_{\text{Mg}(7)\text{Al}}$ precursor was marginally higher than the other samples, with the remaining samples having a similar value (Table 4.6.5). Hydrogen

concentrations varied less than the carbon content values with the ${}^8_{30}\text{Cu}_{\text{Mg}(7)\text{Al}}$ precursor having the small carbon and hydrogen concentrations. The nitrogen percentages were non-detectable. The sulfur content of all the precursors had similar values of the same order of magnitude with the ${}^8_{140}\text{Cu}_{\text{Mg}(7)\text{Al}}$ precursor being exceptional as it has a value, which was slightly higher. The elemental analysis on the precursors was conducted only once.

Table 4.6.5. Elemental Analysis results for the $\text{Cu}_{\text{Mg}(7)\text{Al}}$ precursors with variation in preparation conditions.

Element	C	H	N	S
${}^8_{30}\text{Cu}_{\text{Mg}(7)\text{Al}}$	2.0	2.9	nda	nda
${}^8_{70}\text{Cu}_{\text{Mg}(7)\text{Al}}$	2.3	2.8	nda	nda
${}^8_{140}\text{Cu}_{\text{Mg}(7)\text{Al}}$	2.1	2.9	nda	0.01
${}^9_{30}\text{Cu}_{\text{Mg}(7)\text{Al}}$	2.0	2.9	nda	nda

nda = non-detectable amount

Table 4.6.6. Elemental Analysis results for the $\text{Cu}_{\text{Mg}(7)\text{Al}}$ catalysts with variation in preparation conditions.

Element	C	H	N	S
${}^8_{30}\text{Cu}_{\text{Mg}(7)\text{Al}}$	2.2	0.39	0.11	0.01
${}^8_{70}\text{Cu}_{\text{Mg}(7)\text{Al}}$	2.1	0.63	0.34	0.02
${}^8_{140}\text{Cu}_{\text{Mg}(7)\text{Al}}$	2.2	0.57	0.07	0.01
${}^9_{30}\text{Cu}_{\text{Mg}(7)\text{Al}}$	2.1	0.79	0.11	nda

nda = non-detectable amount

The carbon content of the calcined catalysts, again were all of similar value (Table 4.6.6). The hydrogen concentration of the ${}^8_{30}\text{Cu}_{\text{Mg}(7)\text{Al}}$ catalyst was considerably lower than the remaining samples, which increased in value with pH. The nitrogen content increased from the ${}^8_{30}\text{Cu}_{\text{Mg}(7)\text{Al}}$ to the ${}^8_{70}\text{Cu}_{\text{Mg}(7)\text{Al}}$ catalysts and then decreased to the ${}^8_{140}\text{Cu}_{\text{Mg}(7)\text{Al}}$ sample. The pH = 8 and ${}^9_{30}\text{Cu}_{\text{Mg}(7)\text{Al}}$ catalysts both contained an almost identical quantity of nitrogen. The sulfur content of the ${}^8_{70}\text{Cu}_{\text{Mg}(7)\text{Al}}$ was slightly higher than the other samples. The remaining samples decreased with increasing pH.

4.6.9 BET Surface Area measurements

The surface area increases with pH but no trend was observed (Table 4.6.7) with increasing ageing time. The ${}^8_{70}\text{Cu}_{\text{Mg}(7)\text{Al}}$ sample had the largest surface area for the pH = 8 catalysts, followed by the ${}^8_{140}\text{Cu}_{\text{Mg}(7)\text{Al}}$ catalyst. Surprisingly, the ${}^8_{30}\text{Cu}_{\text{Mg}(7)\text{Al}}$ catalyst had the smallest surface area of the four samples at $30.4 \text{ m}^2 \text{ g}^{-1}$.

Table 4.6.7. BET surface area measurements for the $\text{Cu}_{\text{Mg}(7)\text{Al}}$ catalysts with variation in preparation conditions.

Catalyst	${}^8_{30}\text{Cu}_{\text{Mg}(7)\text{Al}}$	${}^8_{70}\text{Cu}_{\text{Mg}(7)\text{Al}}$	${}^8_{140}\text{Cu}_{\text{Mg}(7)\text{Al}}$	${}^9_{30}\text{Cu}_{\text{Mg}(7)\text{Al}}$
Single Point ($\text{m}^2 \text{ g}^{-1}$)	29.3	39.6	32.7	50.6
BET surface area ($\text{m}^2 \text{ g}^{-1}$)	30.4	42.7	32.6	51.8

4.6.10 Summary

Incomplete co-precipitation increased with lengthening ageing time and pH. Similar TPR and DTA profiles were observed with the different metal ratio compositions. Increasing ageing time decreased the copper dispersion, copper surface areas and copper maximum reduction temperature. The BET surface area increased with pH.

4.7 K/Cu/MgO/Al₂O₃ (K60/7/35) (Cu_{MgAlK})

4.7.1 Preparation

The dried precursors were light grey in colour, darkening with increasing ageing time and pH. Calcination resulted in the samples becoming dark green catalysts with the darkest sample being the catalyst prepared at ⁸₇₀Cu_{MgAlK}.

4.7.2 Differential Thermal Analysis

The University of Edinburgh conducted samples all displayed an endothermic peak centring on 413 K (Figure 4.7.1). The smallest peak at this temperature was the ⁸₁₄₀Cu_{MgAlK} sample, the remaining precursors showed a peak of similar magnitude. After this temperature, the gradual increase in deflection was due to heat capacitance of each precursor.

4.7.3 X-ray Diffraction

All precursors showed the hydrotalcite-like [230] phase (Figure 4.7.2), with the ⁸₃₀Cu_{MgAlK} sample having the greatest crystallinity. The crystallinity decreased with increasing ageing time and pH. The peak at 12.6 ° was indicative of hydrotalcite [230] with little variation in peak height being observed with lengthening ageing time and pH.

Calcination resulted in the decomposition of the hydrotalcite-like phase and the appearance of CuO [224] (Figure 4.7.3). The pH = 8 catalysts all had similar sized peaks, with crystallinity decreasing to pH = 9.

4.7.4 X-ray Fluorescence

The ⁸₃₀Cu_{MgAlK} precursor showed the presence of both copper K_α and K_β-line peaks

Figure 4.7.1. DTA profiles for the Cu_{MgAlK} precursors with variation in preparation conditions.

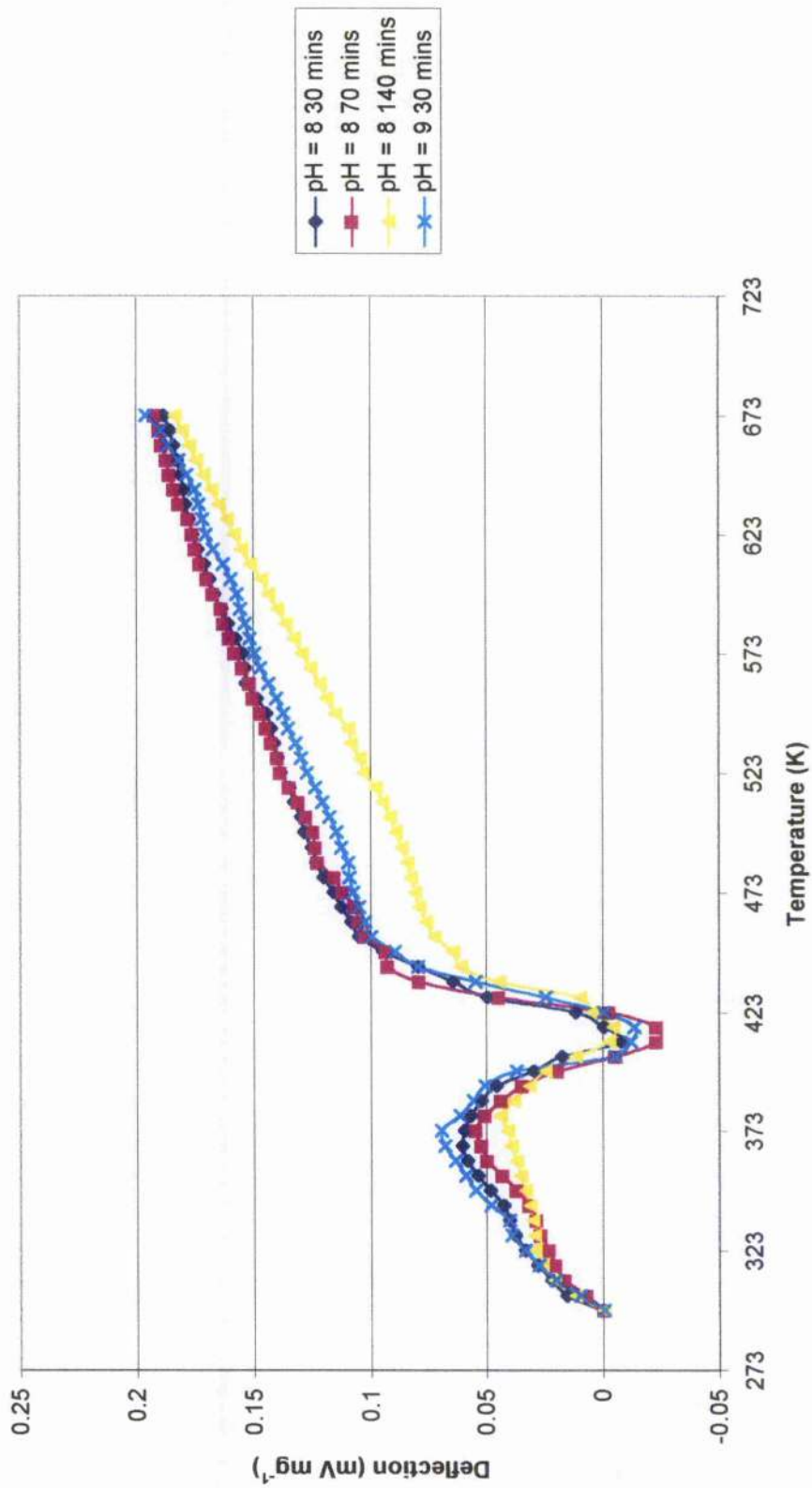


Figure 4.7.2. XRD patterns for the Cu_{MgAlK} precursors with variation in preparation conditions.

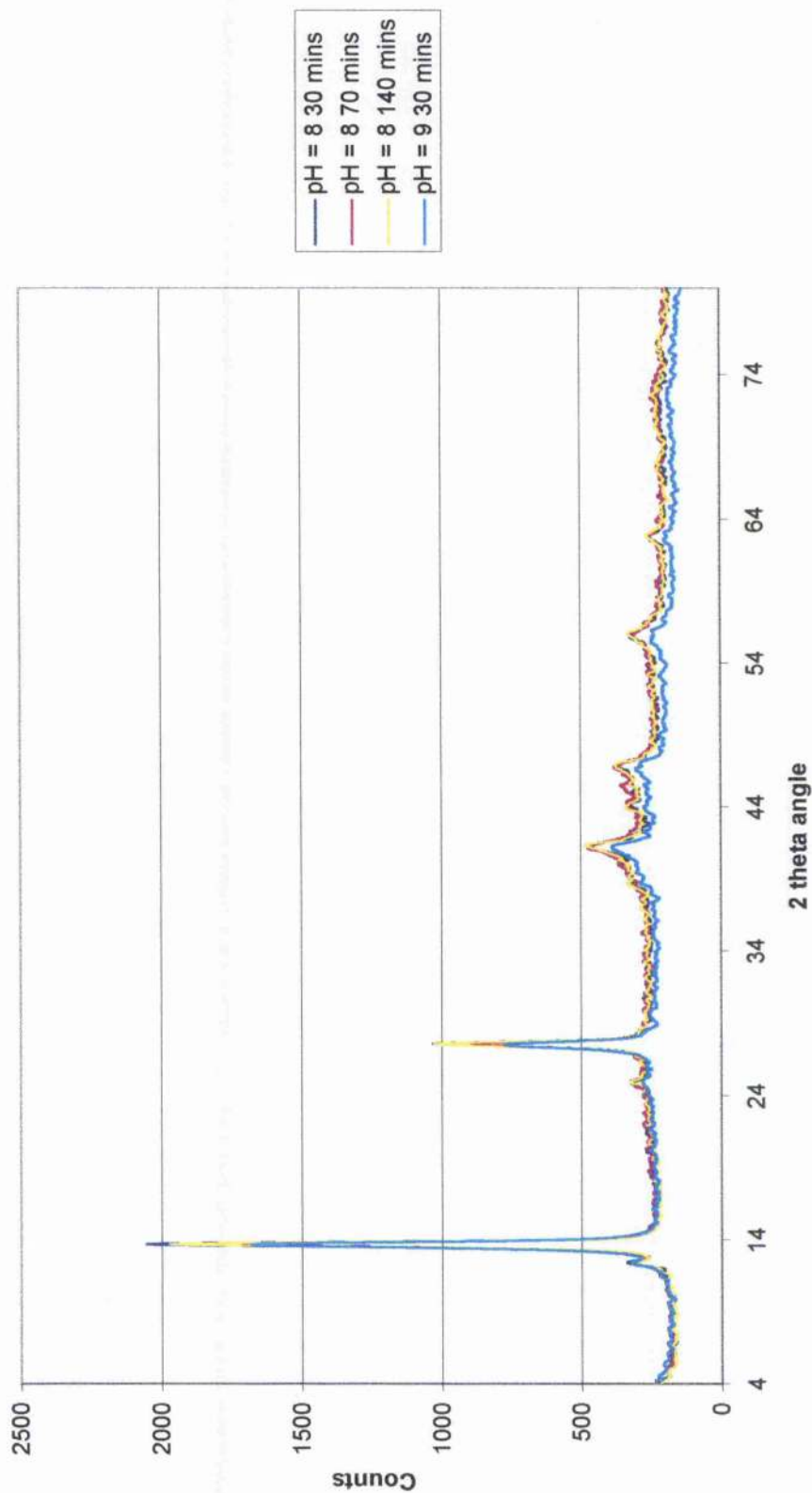


Figure 4.7.3. XRD patterns for the Cu_{MgAlK} catalysts with variation in preparation conditions.

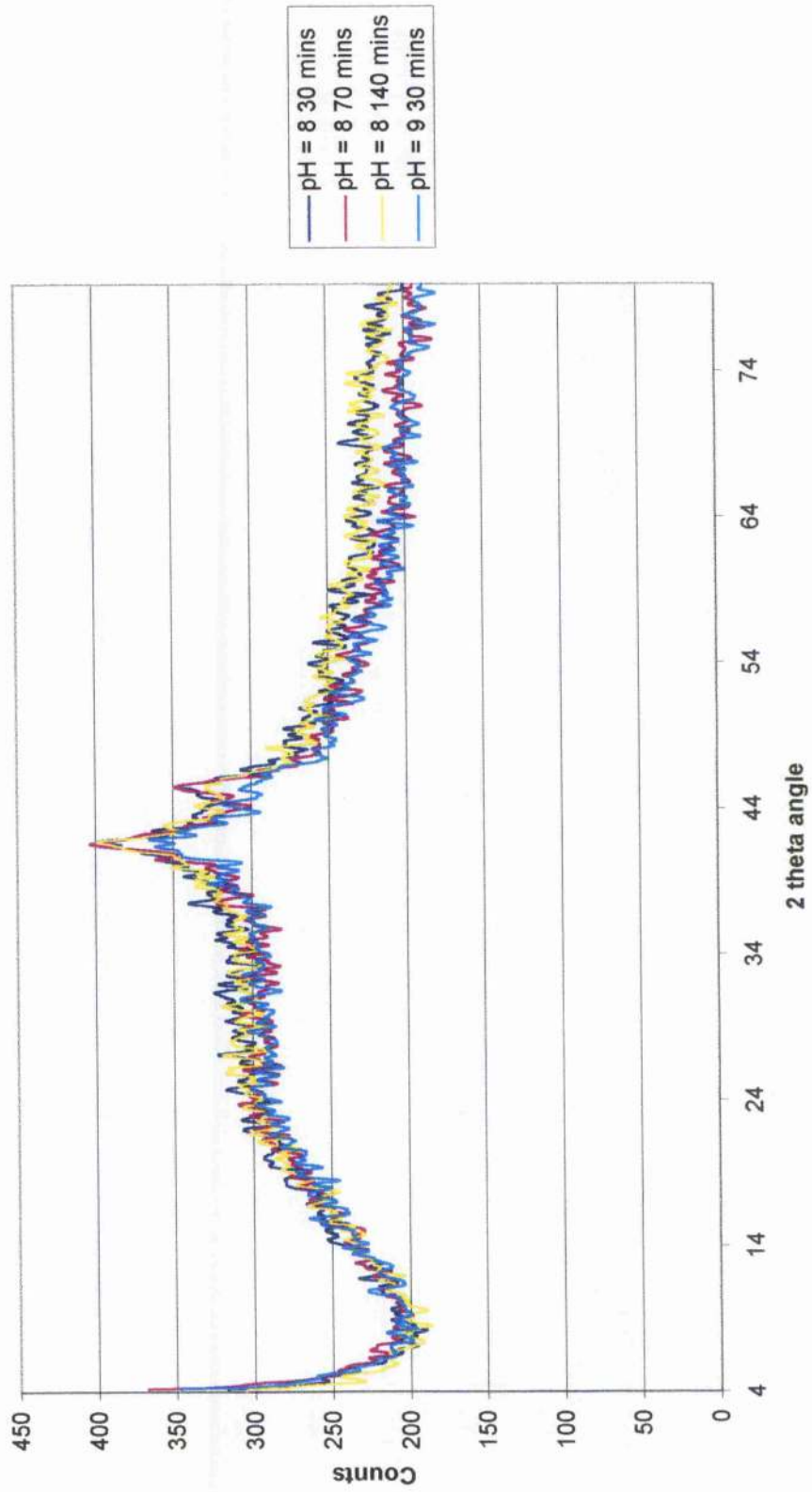


Figure 4.7.4. XRF spectrum for the $^{83}\text{Cu}_{\text{MgAlK}}$ precursor.

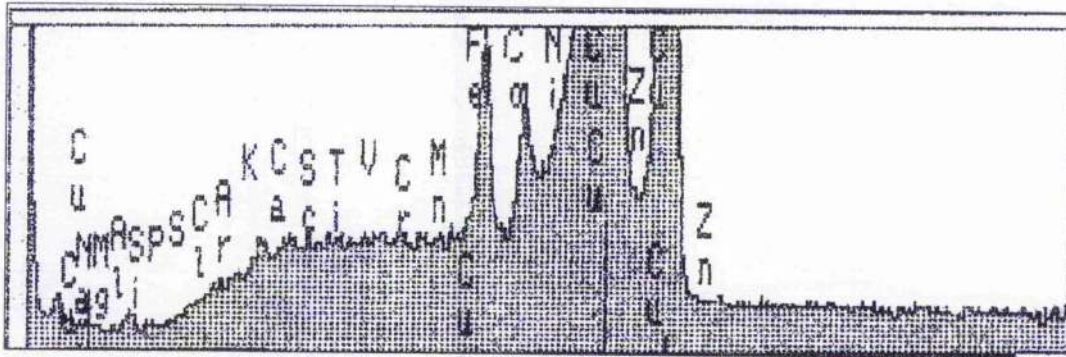
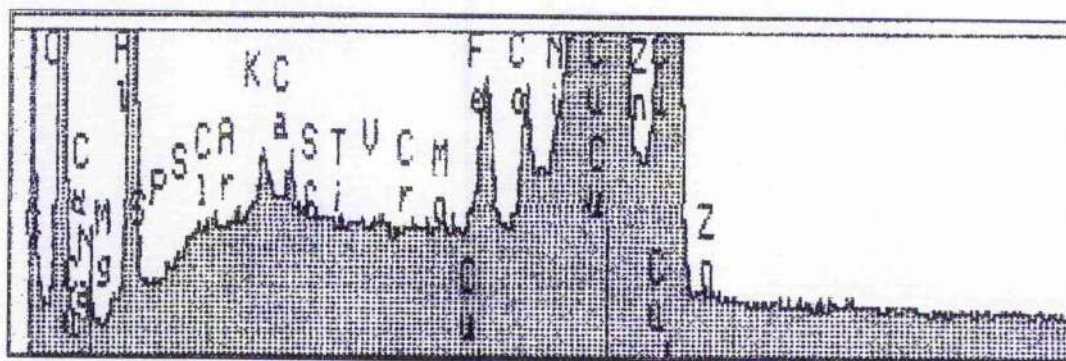


Figure 4.7.5. XRF spectrum for the $^{87}\text{Cu}_{\text{MgAlK}}$ catalyst.



(Figure 4.7.4). Little aluminium (K_{α} -line) and magnesium (K_{α} -line) were visible in this sample. However, the impurities of iron (K_{α} -line) and cobalt (K_{α} -line) were present in larger quantities. A small potassium (K_{α} -line) peak was also observed.

Calcination of the ${}^8_{70}\text{Cu}_{\text{MgAlK}}$ sample showed visible copper K_{α} and K_{β} -line peaks (Figure 4.7.5). The aluminium (K_{α} -line) peak was also clearly observed, however, no magnesium (K_{α} -line) peak was seen. Large iron (K_{α} -line) and cobalt (K_{α} -line) peaks were still distinctive in the calcined catalyst. Calcination also resulted in the presence of a larger potassium (K_{α} -line) peak and the emergence of a calcium (K_{α} -line) peak. Carbon (K_{α} -line) was also visible. These samples were conducted on the EDX machine at the University of Glasgow so the interfering Rh L-lines were not observed.

4.7.5 Atomic Absorption Spectroscopy

Table 4.7.1. Percentage of wet-impregnated potassium (wt / wt) for the Cu_{MgAlK} catalysts with variation in preparation conditions.

Element	Potassium
${}^8_{30}\text{Cu}_{\text{MgAlK}}$	270
${}^8_{70}\text{Cu}_{\text{MgAlK}}$	155
${}^8_{140}\text{Cu}_{\text{MgAlK}}$	289
${}^9_{30}\text{Cu}_{\text{MgAlK}}$	311

The quantity of potassium in each catalyst was well above the anticipated value (Table 4.7.1). The ${}^9_{30}\text{Cu}_{\text{MgAlK}}$ catalyst contained the most amount of potassium. No correlation was observed at $\text{pH} = 8$ with variation in ageing time as the ${}^8_{70}\text{Cu}_{\text{MgAlK}}$ sample had a value considerably lower than the two other samples.

The percentage of copper, magnesium and aluminium were repeated for these catalysts. A good agreement was found with the results shown in Table 4.6.1.

The metal ratio of copper (Table 4.7.2) for the ${}^8_{30}\text{Cu}_{\text{MgAlK}}$ catalyst had the same value as the ${}^8_{70}\text{Cu}_{\text{MgAlK}}$ catalyst. Likewise, the same can be said for the ${}^8_{140}\text{Cu}_{\text{MgAlK}}$ and ${}^9_{30}\text{Cu}_{\text{MgAlK}}$ catalysts. No correlation was observed with magnesium concentration among variation in pH or preparatory ageing time. The aluminium ratio decreased with lengthening ageing time and increasing pH from 8 to 9.

The potassium ratio was greater at the longest ageing time and the increased pH. The low potassium concentration of the ${}^8_{70}\text{Cu}_{\text{MgAlK}}$ catalyst was counteracted by a large magnesium ratio.

Table 4.7.2. Metal ratios of copper, magnesium, aluminium and potassium for the Cu_{MgAlK} catalysts with variation in preparation conditions.

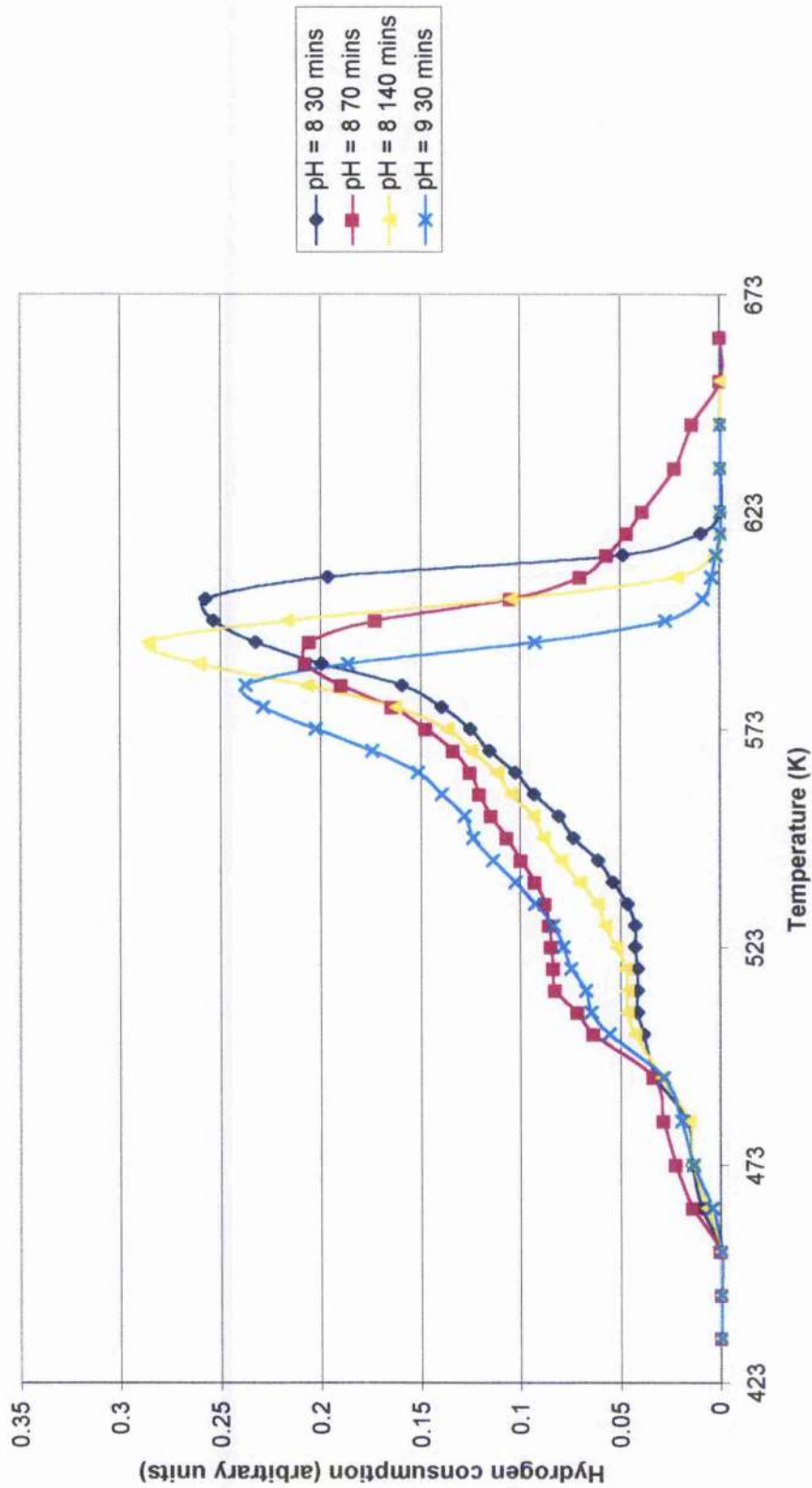
Element	Copper	Magnesium	Aluminium	Potassium
${}^8_{30}\text{Cu}_{\text{MgAlK}}$	57.8	4.8	37.0	0.3
${}^8_{70}\text{Cu}_{\text{MgAlK}}$	57.8	5.5	36.4	0.2
${}^8_{140}\text{Cu}_{\text{MgAlK}}$	59.4	4.2	36.0	0.4
${}^9_{30}\text{Cu}_{\text{MgAlK}}$	59.4	5.0	35.2	0.4

4.7.6 Temperature Programmed Reduction

The TPR profiles of the ${}^8_{30}\text{Cu}_{\text{MgAlK}}$ and ${}^8_{140}\text{Cu}_{\text{MgAlK}}$ catalysts were similar in shape (Figure 4.7.6). Both started reduction at 453 K and increased to a plateau between 503 and 523 K. They both increased in quantity of reduction at an almost identical rate to their respective maximum reduction temperatures. The ${}^8_{30}\text{Cu}_{\text{MgAlK}}$ catalyst had a maximum reduction temperature of 603 K and the ${}^8_{140}\text{Cu}_{\text{MgAlK}}$ sample, 593 K. After this temperature, they both decreased rapidly in reduction until completion to 623 K.

The ${}^8_{70}\text{Cu}_{\text{MgAlK}}$ catalyst's reduction profile started reduction at 453 K and increased steadily to a plateau by 503 K where it remained until 523 K. The quantity of hydrogen consumed was substantially more than the ${}^8_{30}\text{Cu}_{\text{MgAlK}}$ and ${}^8_{140}\text{Cu}_{\text{MgAlK}}$ catalysts. The hydrogen consumption increased after 523 K to the maximum reduction

Figure 4.7.6. TPR profiles for the Cu_{MgAlK} catalysts with variation in preparation conditions.



temperature at 593 K. Above 593 K, the quantity of reduction decreased more slowly than the other 3 profiles, as it finally completes reduction by 653 K, 30 K greater than the other samples.

The final catalyst profile, the $^9_{30}\text{Cu}_{\text{MgAlK}}$ sample increased similarly to the $^8_{70}\text{Cu}_{\text{MgAlK}}$ profile, however, in this instance, no plateau was observed between 503 and 523 K only a gradual increase in reduction quantity. The maximum reduction temperature occurred at 583 K and was concluded by 613 K.

The $^8_{30}\text{Cu}_{\text{MgAlK}}$ catalyst had the highest maximum reduction temperature at 603 K and the $^9_{30}\text{Cu}_{\text{MgAlK}}$ sample had the lowest at 583 K.

4.7.7 Nitrous Oxide Chemisorption and Copper Surface Area measurements

Table 4.7.3. Nitrous oxide chemisorption results for the Cu_{MgAlK} catalysts with variation in preparation conditions.

Catalyst	$^8_{30}\text{Cu}_{\text{MgAlK}}$	$^8_{70}\text{Cu}_{\text{MgAlK}}$	$^8_{140}\text{Cu}_{\text{MgAlK}}$	$^9_{30}\text{Cu}_{\text{MgAlK}}$
% Cu in catalyst	56.0	55.6	56.0	57.9
% dispersion	13.7	6.0	5.7	4.6
Particle size (nm)	7.66	17.3	18.2	22.6
% calibrated dispersion	14.3	6.5	6.1	5.3
Calibrated particle size (nm)	7.3	16.0	17.0	19.6
Copper surface area ($\text{m}^2 \text{g}^{-1}$)	32.9	29.1	20.7	20.5

The percentage of copper present in the catalyst was lower for the pH = 8 catalysts than the $^9_{30}\text{Cu}_{\text{MgAlK}}$ catalyst (Table 4.7.3). The copper dispersion values for the $^8_{30}\text{Cu}_{\text{MgAlK}}$ sample was the largest in this series of catalyst, the values decreased with increasing ageing time and pH. Copper surface area displayed a similar trend with the

$^8_{30}\text{Cu}_{\text{MgAlK}}$ catalyst having the largest surface area of $32.9 \text{ m}^2 \text{ g}^{-1}$, decreasing to $20.5 \text{ m}^2 \text{ g}^{-1}$ for the $^9_{30}\text{Cu}_{\text{MgAlK}}$ sample.

The maximum copper surface reduction temperature was the highest for the $^8_{30}\text{Cu}_{\text{MgAlK}}$, again decreasing with increasing ageing time and pH (Table 4.7.4). The copper surface reduction temperatures started at 383 K apart from the $^8_{140}\text{Cu}_{\text{MgAlK}}$, which started 10 K lower. The completion temperatures decreased from 493 to 453 K with lengthening ageing time. The $^9_{30}\text{Cu}_{\text{MgAlK}}$ catalyst had a value of 461K.

Table 4.7.4. Copper surface reduction temperatures for the Cu_{MgAlK} catalysts with variation in preparation conditions.

Temperature (K)	T_{initial}	T_{max}	T_{complete}
$^8_{30}\text{Cu}_{\text{MgAlK}}$	383	440	493
$^8_{70}\text{Cu}_{\text{MgAlK}}$	383	424	463
$^8_{140}\text{Cu}_{\text{MgAlK}}$	373	423	453
$^9_{30}\text{Cu}_{\text{MgAlK}}$	383	411	458

4.7.8 Elemental Analysis

There was no variation in carbon concentration at $\text{pH} = 8$ with variation in ageing time (Table 4.7.5), however at $\text{pH} = 9$, the content decreased. Hydrogen values decreased from the $^8_{70}\text{Cu}_{\text{MgAlK}}$ to $^8_{30}\text{Cu}_{\text{MgAlK}}$ and finally $^8_{140}\text{Cu}_{\text{MgAlK}}$. The $^9_{30}\text{Cu}_{\text{MgAlK}}$ precursor had the same concentration as the $^8_{140}\text{Cu}_{\text{MgAlK}}$ sample. The sulfur content of the $^8_{30}\text{Cu}_{\text{MgAlK}}$ sample was slightly larger than the remaining samples, which all had a non-detectable amount.

The carbon content of the $^8_{30}\text{Cu}_{\text{MgAlK}}$, $^8_{140}\text{Cu}_{\text{MgAlK}}$ and $^9_{30}\text{Cu}_{\text{MgAlK}}$ had all increased, but were within experimental error (Table 4.7.5). Again the $^8_{30}\text{Cu}_{\text{MgAlK}}$ had the largest carbon concentration. The $^8_{70}\text{Cu}_{\text{MgAlK}}$ sample was the only sample whose carbon content had decreased.

Table 4.7.5. Elemental Analysis results for the Cu_{MgAlK} precursors with variation in preparation conditions.

Element	C	H	N	S
$^8_{30}\text{Cu}_{\text{MgAlK}}$	1.8	2.8	nda	0.01
$^8_{70}\text{Cu}_{\text{MgAlK}}$	1.8	2.9	nda	nda
$^8_{140}\text{Cu}_{\text{MgAlK}}$	1.8	2.7	nda	nda
$^9_{30}\text{Cu}_{\text{MgAlK}}$	1.5	2.7	nda	nda

nda = non-detectable amount

The hydrogen concentration of the $^9_{30}\text{Cu}_{\text{MgAlK}}$ catalyst was greater than the $\text{pH} = 8$ samples, which varied little with ageing time but all samples showed a decrease with calcination. Most of the nitrogen in these samples was undetectable, however, the erroneous $^8_{70}\text{Cu}_{\text{MgAlK}}$ sample surprisingly contained 0.15 %. The sulfur content of these catalysts was still very low. All precursors and calcined samples were conducted once.

Table 4.7.6. Elemental Analysis results for the Cu_{MgAlK} catalysts with variation in preparation conditions.

Element	C	H	N	S
$^8_{30}\text{Cu}_{\text{MgAlK}}$	2.1	0.40	nda	nda
$^8_{70}\text{Cu}_{\text{MgAlK}}$	1.5	0.65	0.15	0.01
$^8_{140}\text{Cu}_{\text{MgAlK}}$	1.9	0.58	nda	nda
$^9_{30}\text{Cu}_{\text{MgAlK}}$	1.6	0.94	nda	nda

nda = non-detectable amount

4.7.9 BET Surface Area measurements

Table 4.7.7. BET surface area measurements for the Cu_{MgAlK} catalysts with variation in preparation conditions and the $^8_{30}\text{Cu}_{\text{MgAlK}}$ precursor.

Catalyst	$^8_{30}\text{Cu}_{\text{MgAlK}}$ (precursor)	$^8_{30}\text{Cu}_{\text{MgAlK}}$	$^8_{70}\text{Cu}_{\text{MgAlK}}$	$^8_{140}\text{Cu}_{\text{MgAlK}}$	$^9_{30}\text{Cu}_{\text{MgAlK}}$
Single Point ($\text{m}^2 \text{g}^{-1}$)	35.5	46.2	55.0	41.6	48.7
BET surface area ($\text{m}^2 \text{g}^{-1}$)	36.2	48.0	56.9	42.8	50.3

The BET surface area measurement showed an increase of the ${}^8{}_{30}\text{Cu}_{\text{MgAlK}}$ sample from precursor to catalyst (Table 4.7.7). The pH = 8 catalyst with the largest surface was the sample prepared after ${}^8{}_{70}\text{Cu}_{\text{MgAlK}}$ with the ${}^8{}_{140}\text{Cu}_{\text{MgAlK}}$ catalyst having the lowest.

From ${}^8{}_{30}\text{Cu}_{\text{MgAlK}}$ to ${}^9{}_{30}\text{Cu}_{\text{MgAlK}}$ slightly increased the BET surface area from 48.0 to 50.3 $\text{m}^2 \text{g}^{-1}$.

4.7.10 Summary

The hydrotalcite-like phase was formed after wet-impregnation. Increasing pH increased the potassium concentration. No correlation in potassium concentration was observed with lengthening ageing time, however, the copper dispersion, surface area and maximum surface reduction temperatures all decreased. All precursor and calcined samples showed similar XRD patterns, DTA and TPR profiles.

5 Microreactor Experiments

The results shown are a representative sample of the large quantity of experiments conducted. It was done in this way to give an overview of the work.

5.1 Treatment of Microreactor Results

From calibrations, the number of moles of each species can be calibrated. This can be compared with maximum number of moles present in the gas sample loop. This can be calculated by:-

$$n = \frac{PV}{RT}$$

where P = pressure (atm), V = volume (dm³), T = Temperature (K) and R = ideal gas constant (atm dm³ K⁻¹ mol⁻¹) and n = number of moles.

The yield can be calculated from

$$\text{Yield (\%)} = \frac{\text{moles of formed product}}{\text{number of moles in gas sample loop}} \times 100$$

Conversion is calculated from the yield equation by dividing the fraction of carbon atoms present in the gasfeed composition.

$$\text{Conversion (\%)} = \frac{\text{yield (\%)}}{\text{fraction of carbon atoms in gasfeed composition}} \times 100$$

The selectivity was calculated from the conversion by summing the total quantity of converted products.

$$\text{Selectivity (\%)} = \frac{\text{conversion (\%)}}{\text{sum of converted products}} \times 100$$

5.2 Cu/Cr₂O₃ (50/50) (Cu_{Cr})

The selectivity of the Cu_{Cr} catalyst under these conditions towards methanol increased from 82.9 % to 90.5 % through the duration of the experiment (Figure 5.2.1). DME selectivity varied with time. At the initial stages of the reaction, the selectivity was 11.0 % increasing to a maximum of 16.9 % and decreased to 9.1 % by completion of the experiment. Ethanol and propan-1-ol selectivities decreased after 8 hrs. The initial ethanol selectivity was 4.6 % decreasing to 0.3 %, while propan-1-ol decreased from 0.9 % to 0.1 %. This decrease in selectivity of DME, ethanol and propan-1-ol was due to the increase in selectivity of the catalyst for methanol.

Several different experiments were conducted varying one of the following parameters with selected products:- temperature, gas hourly space velocity and gasfeed composition.

5.2.1 Effect of changes in Temperature

Table 5.2.1. Product distribution for the Cu_{Cr} catalyst with variation in temperature (expressed as a conversion).

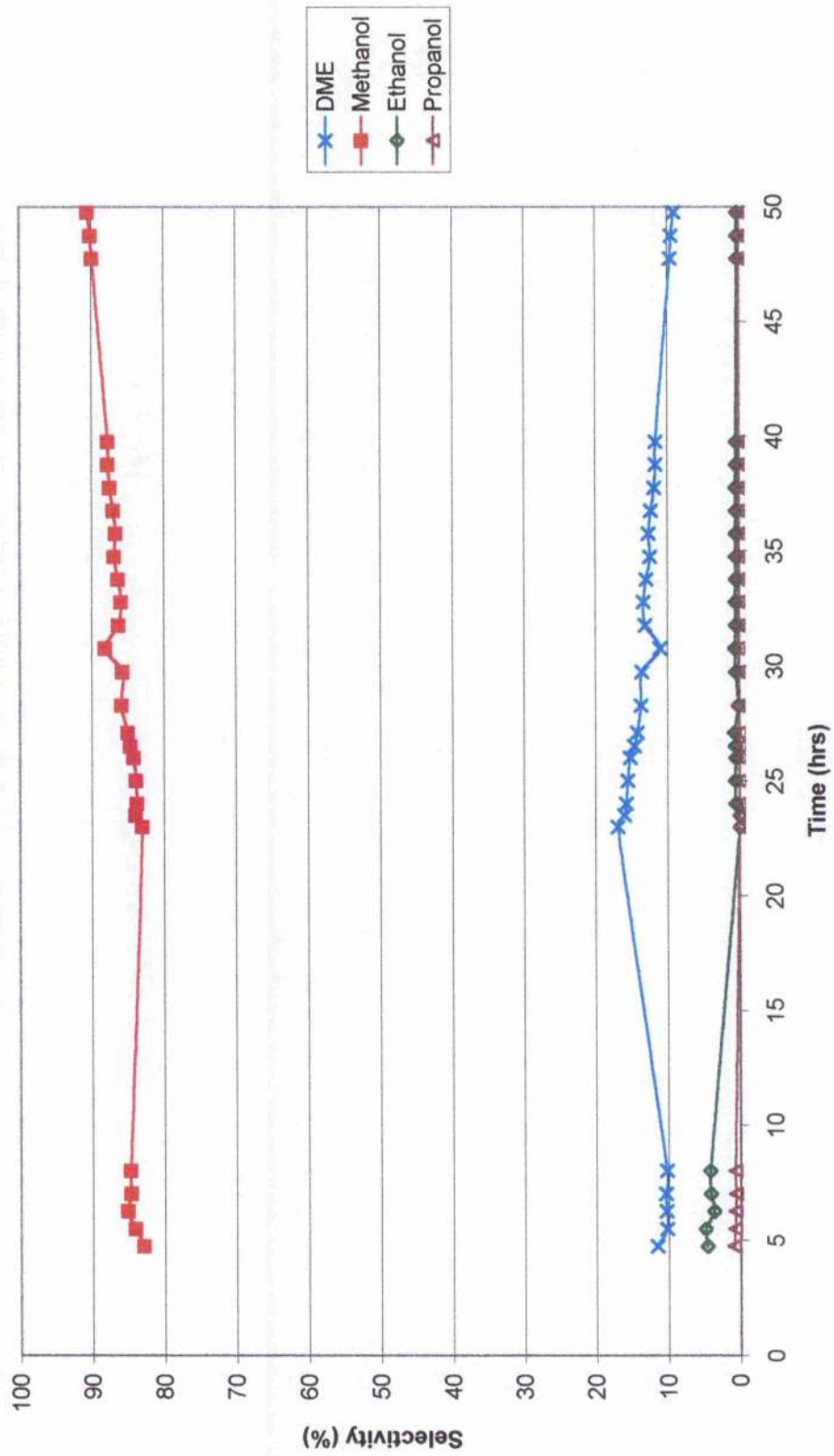
Temperature (K)	573	593
DME	0.26	0.17
Methanol	0.63	0.40
Propan-1-ol	0.02	0.022

Operating Conditions, P = 8 barg, GHSV = 1812 hr⁻¹, 65.3 % H₂, 32.7 % CO, 2 % CO₂.

Increasing the temperature of the reaction (Table 5.2.1) caused an increase in propan-1-ol formation but decreased the DME and methanol production. The increase in propan-1-ol production could partly explain the decrease in methanol production.

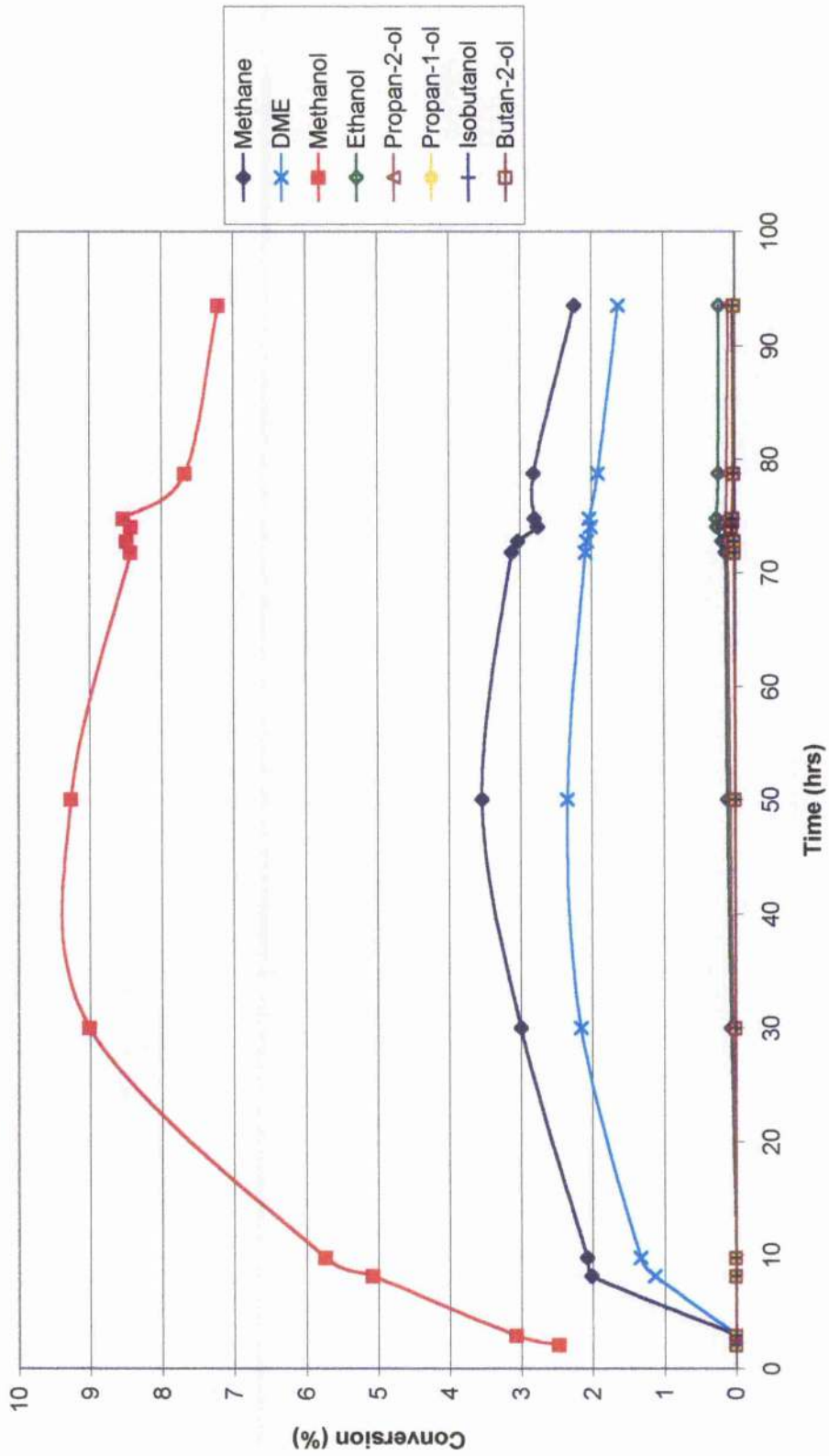
Methanol, DME and methane decreased in conversion after reaching a maximum at 50 hrs (Figure 5.2.2). At this point, methanol conversion was 9.3 %,

Figure 5.2.1. Product distribution for the Cu_{Cr} catalyst.



Operating Conditions, $T = 553\text{ K}$, $P = 8\text{ barg}$, $GHSV = 664\text{ hr}^{-1}$, $65.3\% \text{ H}_2$, $32.7\% \text{ CO}$, $2\% \text{ CO}_2$.

Figure 5.2.2. Product distribution for the Cu_{Cr} catalyst.



Operating Conditions, $T = 593 \text{ K}$, $P = 8 \text{ barg}$, $\text{GHSV} = 1000 \text{ hr}^{-1}$, 65.3 % H_2 , 32.7 % CO , 2 % CO_2 .

DME, 2.3 % and methane at 3.5 %. During this period, higher alcohols (ethanol, propan-2-ol, propan-1-ol, isobutanol and butan-2-ol) increased to a total maximum conversion of ca. 1 %. The increase in higher alcohol production and decrease in methane, DME and methanol production could be the result of carbon laydown on the catalyst (section 6.1.1).

A larger quantity of higher alcohols was produced as a consequence of the increase in temperature.

5.2.2 Effect of changes in Gas Hourly Space Velocity

Increasing the gas hourly space velocity (Table 5.2.2) caused a decrease in the concentration of methanol. The concentration of ethanol decreased from a conversion of 0.026 % to 0.008 % with a three-fold increase in gas hourly space velocity. The conversion of propan-1-ol decreased below detectable quantities when the gas hourly space velocity was increased.

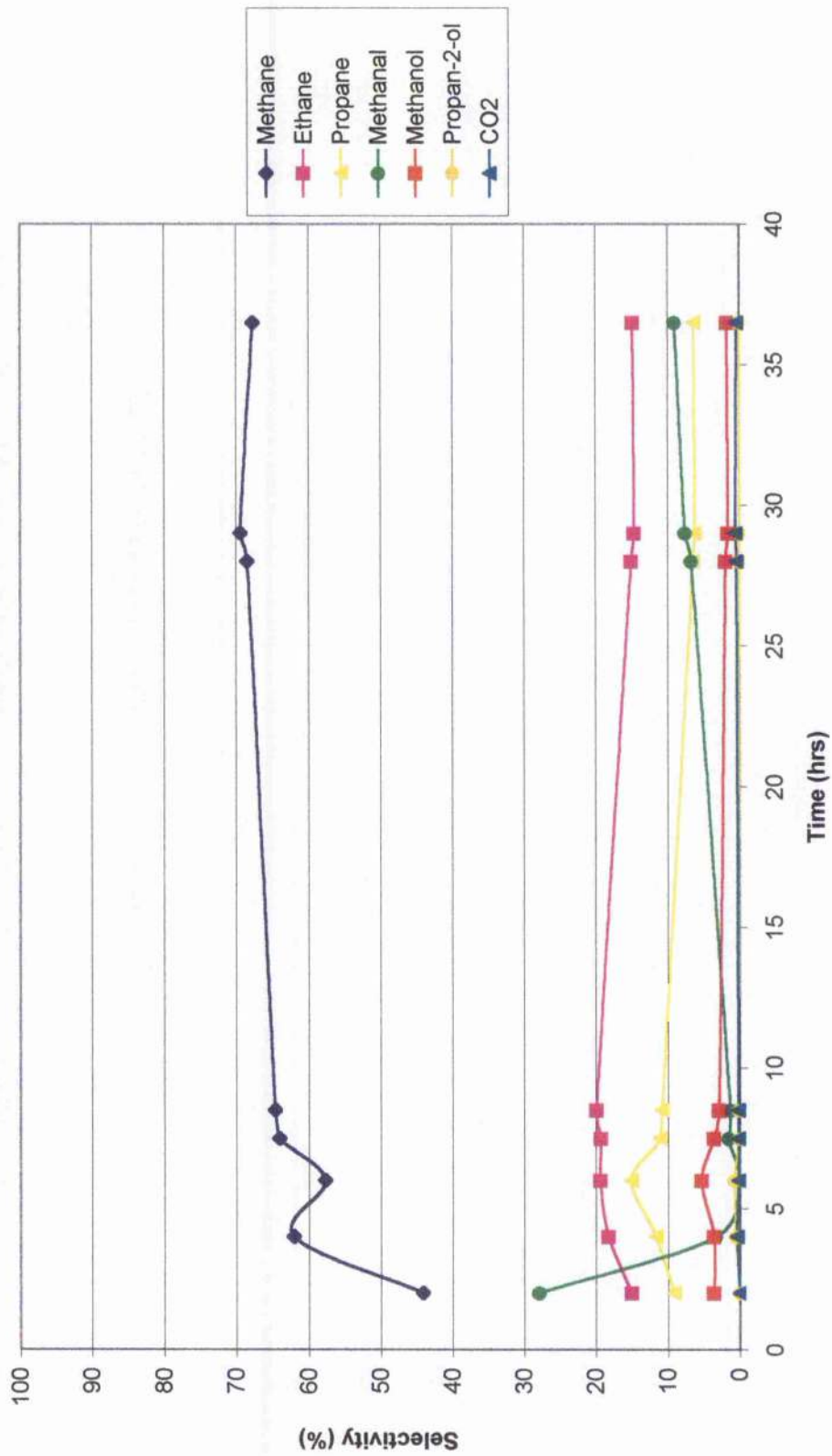
Table 5.2.2. Product distribution for the Cu_Cr catalyst with variation in gas hourly space velocity (expressed as a conversion).

Gas Hourly Space Velocity (hr^{-1})	665	1330	2000
Methanol	7.1	6.4	5.1
Ethanol	0.026	0.012	0.008
Propan-1-ol	0.01	-	-

Operating Conditions, $T = 573 \text{ K}$, $P = 8 \text{ barg}$, 65.3 % H_2 , 32.7 % CO , 2 % CO_2 .

The reaction was 65-70 % selective towards methane when the GHSV was increased to 4285 hr^{-1} (Figure 5.2.3); ethane constituted 15-20 % of the formed product. The third most selective product in this reaction is propane. Selectivity towards methanol increased through the duration of the experiment. On conclusion of the experiment, selectivity towards this product was almost 10 %. Methanol had a selectivity of only

Figure 5.2.3. Product Distribution for the Cu_{Cr} catalyst.



Operating Conditions, T = 573 K, P = 8 barg, GHSV = 4285 hr⁻¹, 56 % H₂, 42 % CO, 2 % CO₂.

3-5 %. Carbon dioxide and propan-2-ol constituted < 0.5 % of the total production.

5.2.3 Effect of changes in Gasfeed Composition

The maximum yield of all products stated occurred at the H₂:CO of 50:50 (Table 5.2.3). Carbon dioxide inclusion produced no higher alcohols, only methanol and DME. The lack of carbon dioxide did not appear to be detrimental to higher alcohol formation.

Table 5.2.3.

Product distribution for the Cu_C catalyst with variation in gasfeed composition (expressed as selectivity). The remainder is composed of methane.

H ₂	CO	CO ₂	Methanol	DME	Ethanol	Propan-1-ol
65.3	32.7	2	70.0	14.5	-	-
66.7	33.3	-	37.5	28.5	2.0	-
60	40	-	35.5	30.0	1.65	0.08
50	50	-	34.0	31.5	2.1	0.14

Operating Conditions, T = 573 K, P = 8 barg, GHSV = 1650 hr⁻¹.

5.2.4 Effect of changes in Methanol Addition

Table 5.2.4. Product distribution for the Cu_C catalyst with variation in gasfeed composition (expressed as selectivity).

Methanol in feed	Without	With
Methanol	76.0	50.0
Ethanol	4.0	14.2
Propan-1-ol	0.03	0.015

Operating Conditions, T = 573 K, P = 8 barg, GHSV = 3279 hr⁻¹, 55.8 % H₂, 43.2 % CO, 2 % CO₂ and 53 % H₂, 40 % CO, 2 % CO₂, 5 % Methanol.

Vapourised methanol was added to the synthesis gas (Table 5.2.4) as 5 % of the total gasfeed composition. This resulted in a large increase in selectivity for ethanol. Propan-1-ol increased by a factor of two. Therefore, the methanol addition primarily increased the chain growth by one carbon number.

The selectivity for hydrocarbons, methane and ethane, did not change with introduction of methanol. Therefore, hydrocarbon production was unaffected by methanol addition.

However, DME production and selectivity did increase, but not by the same magnitude as ethanol. This suggests that methanol introduction does not exclusively contribute to higher alcohol formation.

5.2.5 Summary

Methanol and higher alcohols were both formed, the former was the most selective product, the latter in small quantities. Higher alcohols increased with a lower GHSV, increased temperature, pressure, CO concentration and methanol introduction in the gasfeed composition. Unfortunately, hydrocarbons and DME were formed and catalytic deactivation was also observed.

5.3 Cu/MgO/Al₂O₃ (50/10/40) (Cu_{Mg(10)Al})

Several experiments were conducted on this series of catalyst to quantify the activity, both prepared at ⁷₃₀¹Cu_{Mg(10)Al} and ⁷₃₀²Cu_{Mg(10)Al} catalyst were attempted. The catalyst that was most active was the ⁷₃₀¹Cu_{Mg(10)Al} catalyst calcined at 623 K.

The pressure was varied between 8 and 15 barg, using differing reaction temperatures between 553 and 593 K. The gasfeed composition was varied from a H₂:CO ratio of 2:1 to 1:1 using gas hourly space velocities from 400-2400 hr⁻¹. Yet, the catalyst still proved to be inactive. The maximum observed conversion for methane was 0.98 %, ethane 0.18 %, propane 0.07 % and methanal 0.8 %. No methanol or carbon dioxide was formed during any of these reactions and as methanol was viewed as the initial starting point for activity and higher alcohol formation, experiments on this catalyst were soon stopped.

5.3.1 Effect of changes in Gas Hourly Space Velocity

The gas hourly space velocity was varied with methane being converted in larger quantities at higher gas hourly space velocities and methanal at lower (Table 5.3.1).

Table 5.3.1. Product distribution for the ⁷₃₀¹Cu_{Mg(10)Al} catalyst with variation in gas hourly space velocity (expressed as conversion).

Gas Hourly Space Velocity (hr ⁻¹)	400	800	1091
Methane	0.33	0.32	0.40
Methanal	0.48	0.53	0.42

Operating Conditions, T = 593 K, P = 12 barg, 50 % H₂, 50 % CO.

5.3.2 Summary

Very low activity was observed with only hydrocarbons and methanal being formed. No alcohols were formed.

5.4 Cu/MgO/Al₂O₃ (60/2/38) (Cu_{Mg(2)Al})

Under identical conditions, the ⁸₁₄₀Cu_{Mg(2)Al} catalyst produced the most amounts of hydrocarbons (methane, ethane and propane) (Table 5.4.1). The ⁸₇₀Cu_{Mg(2)Al} catalyst produced the most methanol. The ⁸₃₀Cu_{Mg(2)Al} catalyst produced CO₂ and DME in the largest proportions.

Table 5.4.1. Product distribution for the Cu_{Mg(2)Al} catalysts with variation in ageing time (expressed as a conversion).

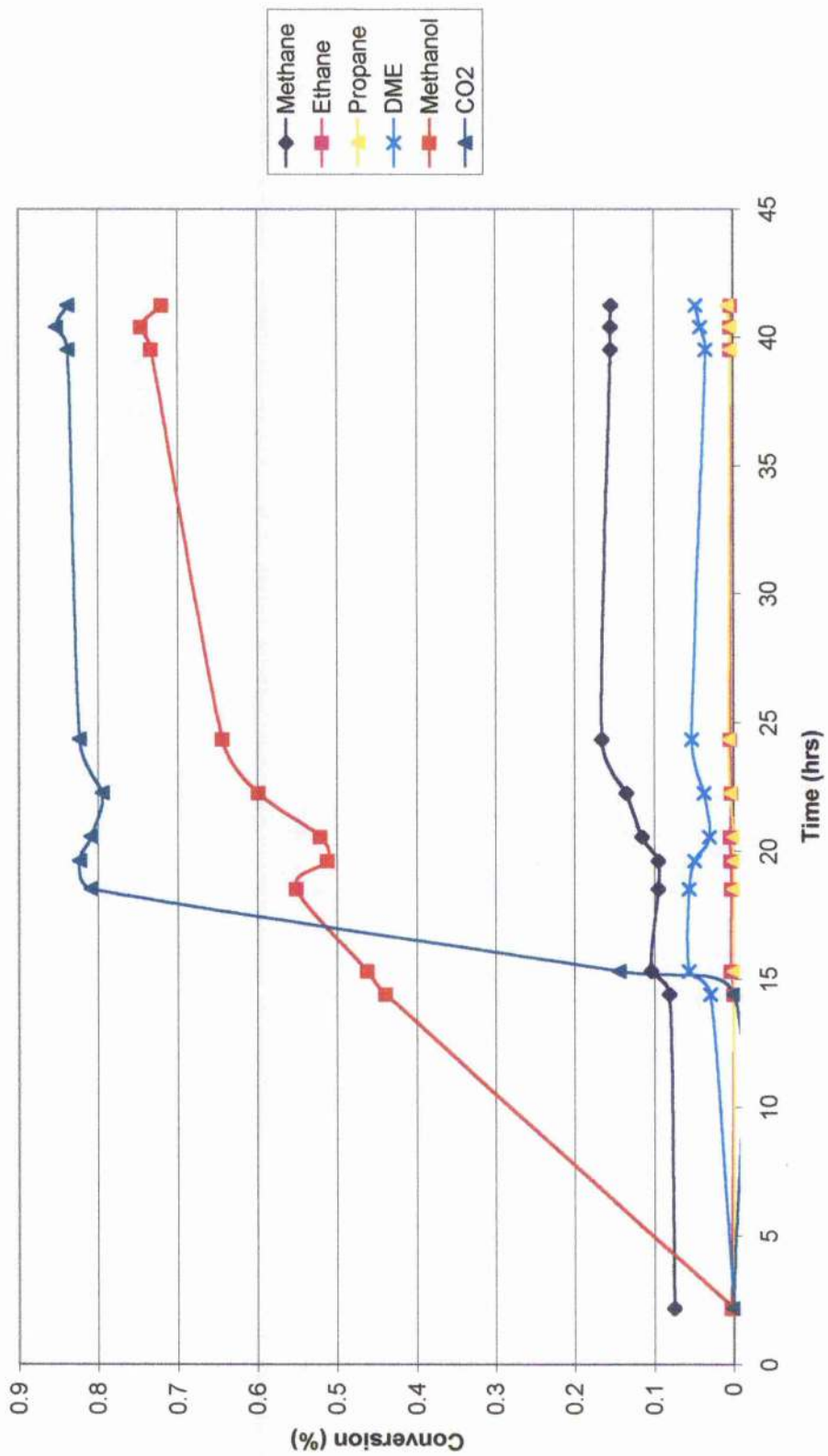
Ageing Time	⁸ ₃₀ Cu _{Mg(2)Al}	⁸ ₇₀ Cu _{Mg(2)Al}	⁸ ₁₄₀ Cu _{Mg(2)Al}
Methane	0.16	0.32	0.50
Ethane	0.04	0.11	0.12
Propane	0.04	0.09	0.20
DME	0.30	0.20	0.11
Methanol	0.72	1.2	0.90
Carbon Dioxide	0.80	0.40	0.65

Operating Conditions, T = 573 K, P = 10 barg, GHSV = 2550 hr⁻¹, 65.4 % H₂, 32.6 % CO, 2 % CO₂.

The graphical form of Table 5.4.1 for the ⁸₃₀Cu_{Mg(2)Al} catalyst (Figure 5.4.1) showed that the methanol production increased very slowly over a period of 40hrs until it reached a constant value. Methane was formed almost immediately and reached the maximum conversion after 25 hrs. Carbon dioxide was produced after an induction period of 15 hrs increasing to its steady state conditions conversion within a further 3 hrs and had the highest selectivity of any product formed. Propane and ethane were formed in barely detectable quantities. DME was first detected after 2 hrs and was the first of the many products to attain steady state conditions. DME achieved this within a reaction time of 15 hrs.

Due to the large CO₂ selectivity, no further microreactor experiments were conducted on the ⁸₃₀Cu_{Mg(2)Al} catalyst.

Figure 5.4.1. Product distribution for the $^{80}\text{Cu-Mg(2)Al}$ catalyst.



Operating Conditions, T = 573 K, P = 10 barg, GHSV = 2550 hr⁻¹, 65.4 % H₂, 32.6 % CO, 2 % CO₂.

Under identical reaction conditions as the previous reaction (Figure 5.4.2), the $^{87}\text{Cu}_{\text{Mg}(2)\text{Al}}$ catalyst was over 50 % selective towards methanol reaching maximum conversion within 7 hrs. Methane, DME and CO_2 were formed in similar selective amounts, reaching their respective maximum conversions within 7, 15, and 16 hrs. The selectivity towards ethane and propane had a cumulative value of 10 %.

5.4.1 Effect of changes in Temperature

Table 5.4.2. Product distribution for the $^{87}\text{Cu}_{\text{Mg}(2)\text{Al}}$ catalyst with variation in temperature (expressed as a conversion).

Temperature (K)	553	573	593
Methane	0.38	0.36	0.34
Ethane	0.06	0.07	0.06
Propane	0.04	0.06	0.06
DME	0.07	0.07	0.06
Methanol	2.5	1.4	1.1
Ethanol	0.11	0.4	0.62
Propan-2-ol	-	0.012	-
Propan-1-ol	-	0.01	0.013
Carbon Dioxide	0.4	0.5	0.45

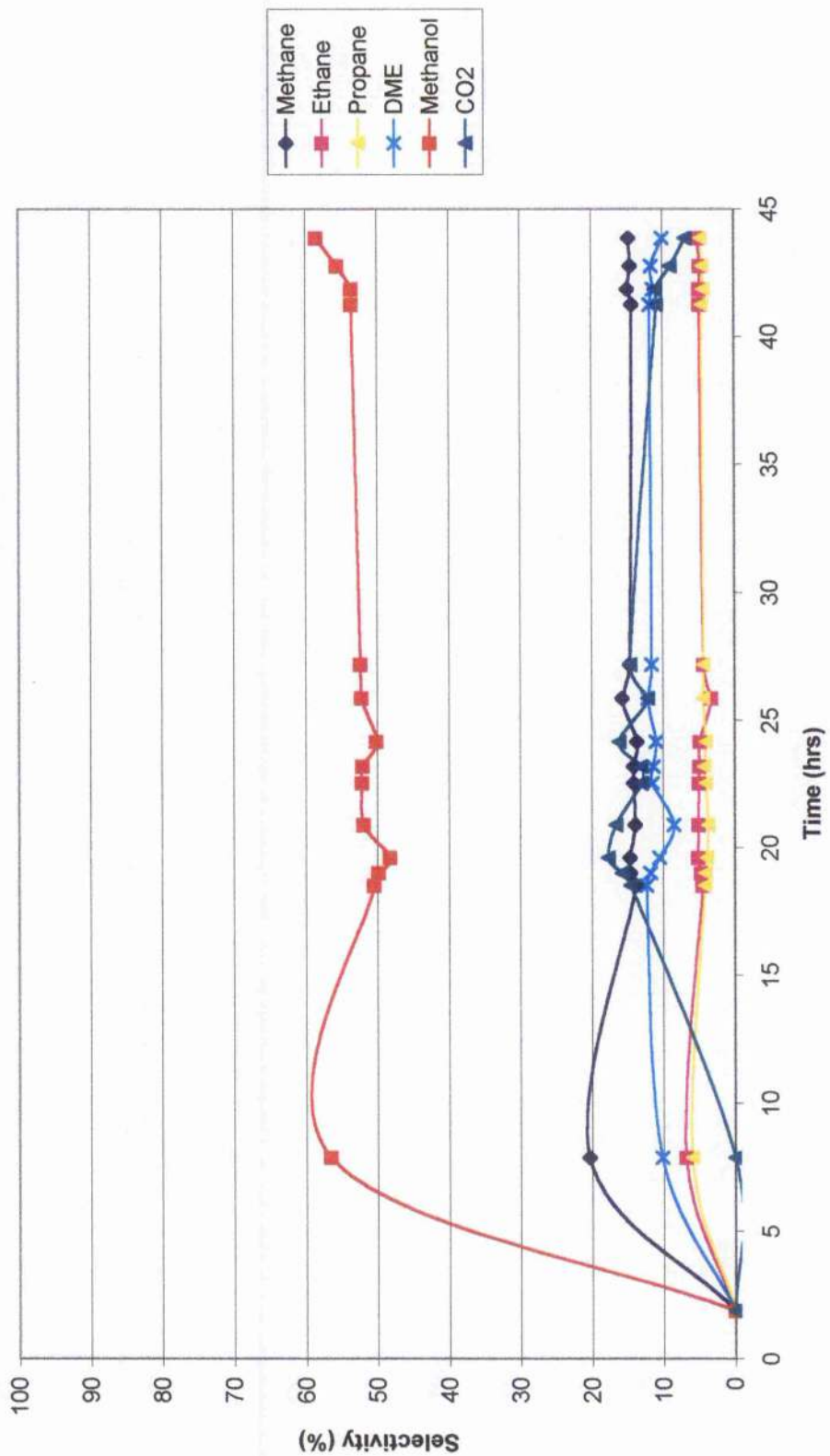
Operating Conditions, P = 20 barg, GHSV = 5000 hr^{-1} , 46.5 % H_2 , 46.5 % CO , 10 % Methanol.

Methane production decreased with increasing temperature (Table 5.4.2), ethane was virtually unaffected and propane increased slightly. DME was mainly unaffected by the variation in temperature.

Methanol production decreased with increasing temperature but the conversion towards higher alcohols, particularly ethanol and propan-1-ol increased to a maximum conversion of 0.62 % and 0.013 % respectively at 593 K. Propan-2-ol was only detected at a temperature of 573 K.

The CO_2 and propan-2-ol conversions proceed through a maximum at 573 K. Carbon dioxide was formed in the 2nd largest quantities regardless of temperature.

Figure 5.4.2. Product distribution for the $^{87}\text{Cu}_{\text{Mg}(2)\text{Al}}$ catalyst.



Operating Conditions, T = 573 K, P = 10 barg, GHSV = 2550 hr⁻¹, 65.4 % H₂, 32.6 % CO, 2 % CO₂.

5.4.2 Effect of changes in Gasfeed Composition

Variation in carbon dioxide concentration in the gasfeed composition resulted in hydrocarbon production, especially methane conversion decreasing with the introduction of CO₂ into the gasfeed composition (Table 5.4.3). The ethane and propane concentrations declined by a lesser amount. The change in CO₂ concentration resulted in only a minor decline in conversion to DME. The effect on methanol was more substantial than with methane; there was over a three-fold increase in conversion of methanol with CO₂ present. Carbon dioxide was only detected when itself was present in the synthesis gas composition.

Table 5.4.3. Product distribution for the ⁸₁₄₀Cu_{Mg(2)Al} catalyst with variation in gasfeed composition (expressed as a conversion).

Carbon Dioxide	Without	With
Methane	0.1	0.06
Ethane	0.03	0.02
Propane	0.01	-
DME	0.03	0.02
Methanol	0.06	0.20
Carbon Dioxide	-	1.0

Operating Conditions, T = 523 K, P = 10 barg, GHSV = 2550 hr⁻¹, H₂:CO 2:1, 2 % CO₂.

Carbon dioxide inclusion was addressed again with the same catalyst, this time at a more elevated temperature (Table 5.4.4). At the elevated temperature of 573 K, less effect on methane, methanol and CO₂ conversion with CO₂ inclusion was observed. Methane decreased only slightly and methanol production only increases two-fold instead of three. Carbon dioxide only increased from a non-detectable amount to 0.65 %. Ethane followed the same trend as methane, as the conversion decreased only

slightly with the change in gasfeed composition. Propane was produced more than ethane at this temperature.

It should be noted that the overall conversion of these products had increased considerably with the more elevated reaction temperature; an overall five-fold increase is observed with the two main FID detected products, methane and methanol. The change in temperature produced a greater affect with other products. Carbon dioxide was the only product that did not decrease with increasing reaction temperature.

Table 5.4.4. Product distribution for the $^8_{140}\text{Cu}_{\text{Mg}(2)\text{Al}}$ catalyst with variation in gasfeed composition (expressed as a conversion).

Carbon Dioxide	Without	With
Methane	0.55	0.50
Ethane	0.16	0.12
Propane	0.24	0.20
DME	0.12	0.11
Methanol	0.40	0.90
Carbon Dioxide	-	0.65

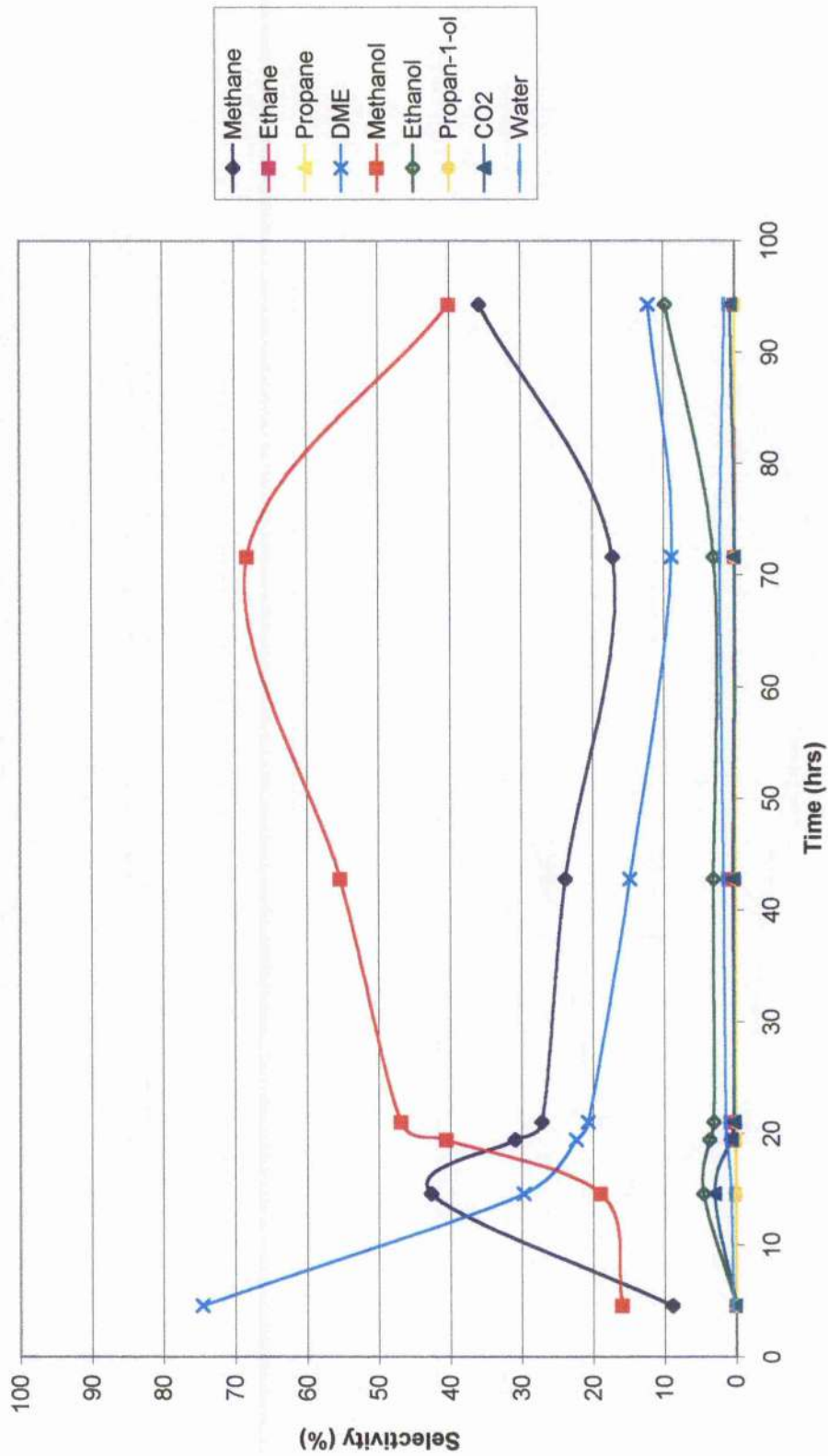
Operating Conditions, $T = 573 \text{ K}$, $P = 10 \text{ barg}$, $\text{GHSV} = 2550 \text{ hr}^{-1}$, $\text{H}_2:\text{CO} \text{ 2:1}$, $2\% \text{ CO}_2$.

5.4.3 Effect of changes in Methanol Addition

The introduction of methanol to a CO_2 -free synthesis gas resulted in methanol being the most produced product after 20 hrs reaction time (Figure 5.4.3) reaching a maximum selectivity of 70 % after 72 hrs, decreasing to 40 % after 95 hrs. DME was initially the most selective product before decreasing to 15 %.

Methane selectivity increased from 9 % after 4 hrs to stabilise at 28 % after 20 hrs and 75 hrs later, the selectivity increased further to 35 % after proceeding through a local minimum after 72 hrs.

Figure 5.4.3. Product distribution for the $^8\text{Cu}_{100\text{Mg}(2)\text{Al}}$ catalyst.



Operating Conditions, T = 553 K, P = 20 barg, GHSV = 5000 hr⁻¹, 36 % H₂, 54 % CO, 10 % Methanol.

Ethanol was also formed. It had a selectivity of between 5 and 8 %. After 94hrs reaction time an increase in selectivity to 10 % was observed; which corresponds to a decrease in methanol selectivity.

As titrometry was conducted on the collected sample (section 6.2.1, Reaction Reference 2B), the selectivity for water can be calculated. It was found that the maximum selectivity was 2 %.

Propane, propan-1-ol and CO₂ were formed in small quantities with only a cumulative selectivity of < 1 %.

5.4.4 Summary

Methanol was the most selective product for the ⁸₇₀Cu_{Mg(2)Al} and ⁸₁₄₀Cu_{Mg(2)Al} catalysts but required an induction period for formation. The ⁸₃₀Cu_{Mg(2)Al} catalyst selectively formed CO₂. Higher alcohols production increased with temperature with ethanol being the selective alcohol formed. None were formed without methanol introduction. Hydrocarbons and DME were formed in large quantities.

5.5 Cu/MgO/Al₂O₃ (60/5/35) (Cu_{Mg(5)Al})

The $^8_{70}\text{Cu}_{\text{Mg}(5)\text{Al}}$ catalyst had a high conversion to methanol from the H₂:CO synthesis gas (Table 5.5.1). Hydrocarbons were also formed in noticeable quantities with production decreasing with increasing chain length from C₁ to C₃, the larger decline between C₁ and C₂. DME was also formed.

Like the $^8_{70}\text{Cu}_{\text{Mg}(5)\text{Al}}$ catalyst, methanol was the main product of the $^8_{140}\text{Cu}_{\text{Mg}(5)\text{Al}}$ catalyst also, this time having a slightly higher conversion. A lesser amount of methane was produced at the expense of ethane and propane and therefore, increasing the overall C₂₊ yields. The $^8_{70}\text{Cu}_{\text{Mg}(5)\text{Al}}$ catalyst produced slightly more DME. No carbon dioxide or higher alcohols were formed in either of these reactions.

Table 5.5.1. Product distribution for the Cu_{Mg(5)Al} catalyst with variation in ageing time (expressed as a conversion).

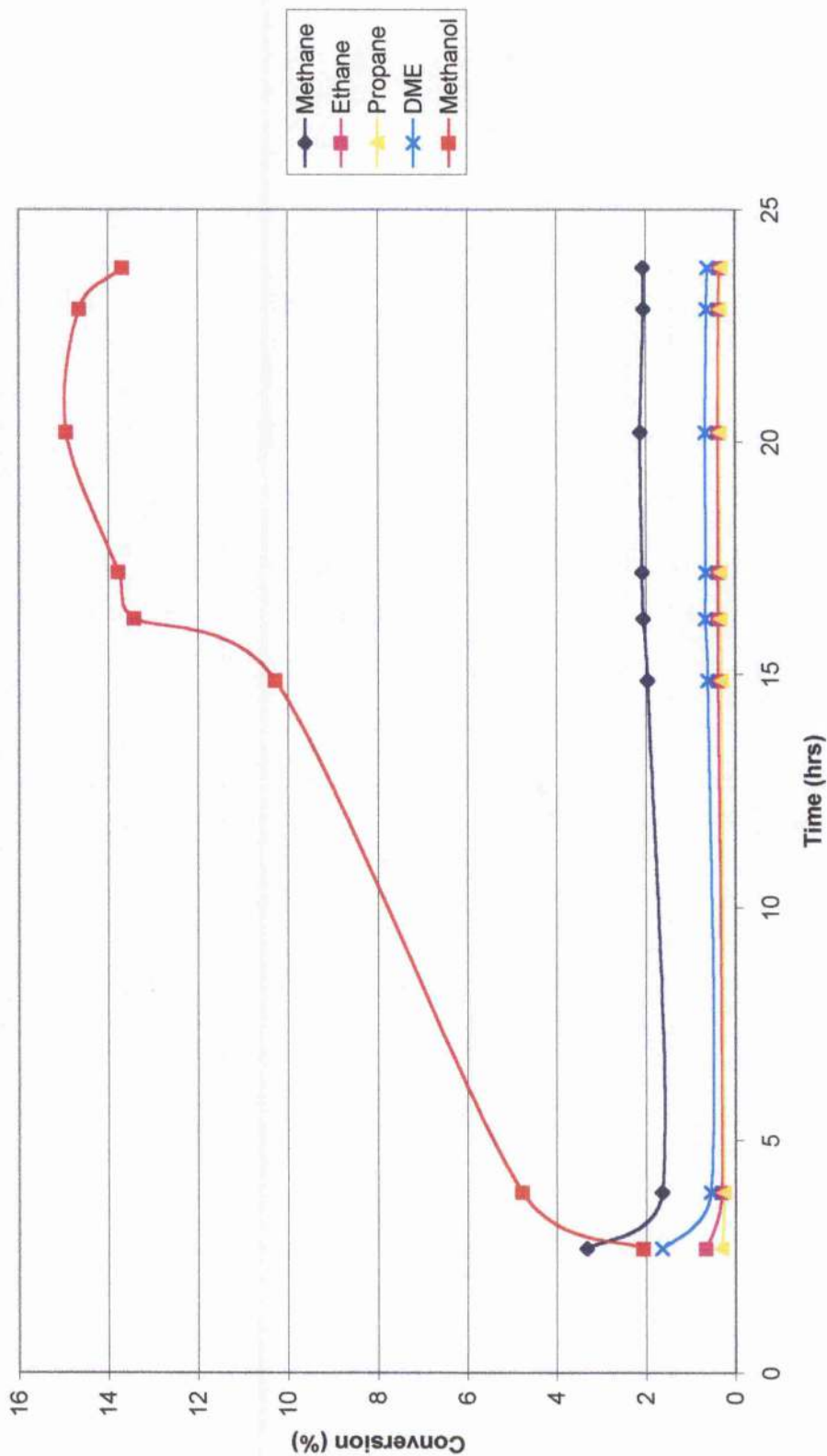
Ageing time	$^8_{70}\text{Cu}_{\text{Mg}(5)\text{Al}}$	$^8_{140}\text{Cu}_{\text{Mg}(5)\text{Al}}$
Methane	2.1	1.2
Ethane	0.39	0.8
Propane	0.34	0.5
DME	0.67	0.55
Methanol	14.9	18.3

Operating Conditions, T = 553 K, P = 20 barg, GHSV = 2000 hr⁻¹, 60 % H₂, 40 % CO.

The $^8_{70}\text{Cu}_{\text{Mg}(5)\text{Al}}$ catalyst showed (Figure 5.5.1) an induction time of 16hrs for methanol to attain steady state conditions. Methane required an induction period of only 3 hrs, decreasing in conversion after the initial sample similar effects were seen with ethane, propane and DME.

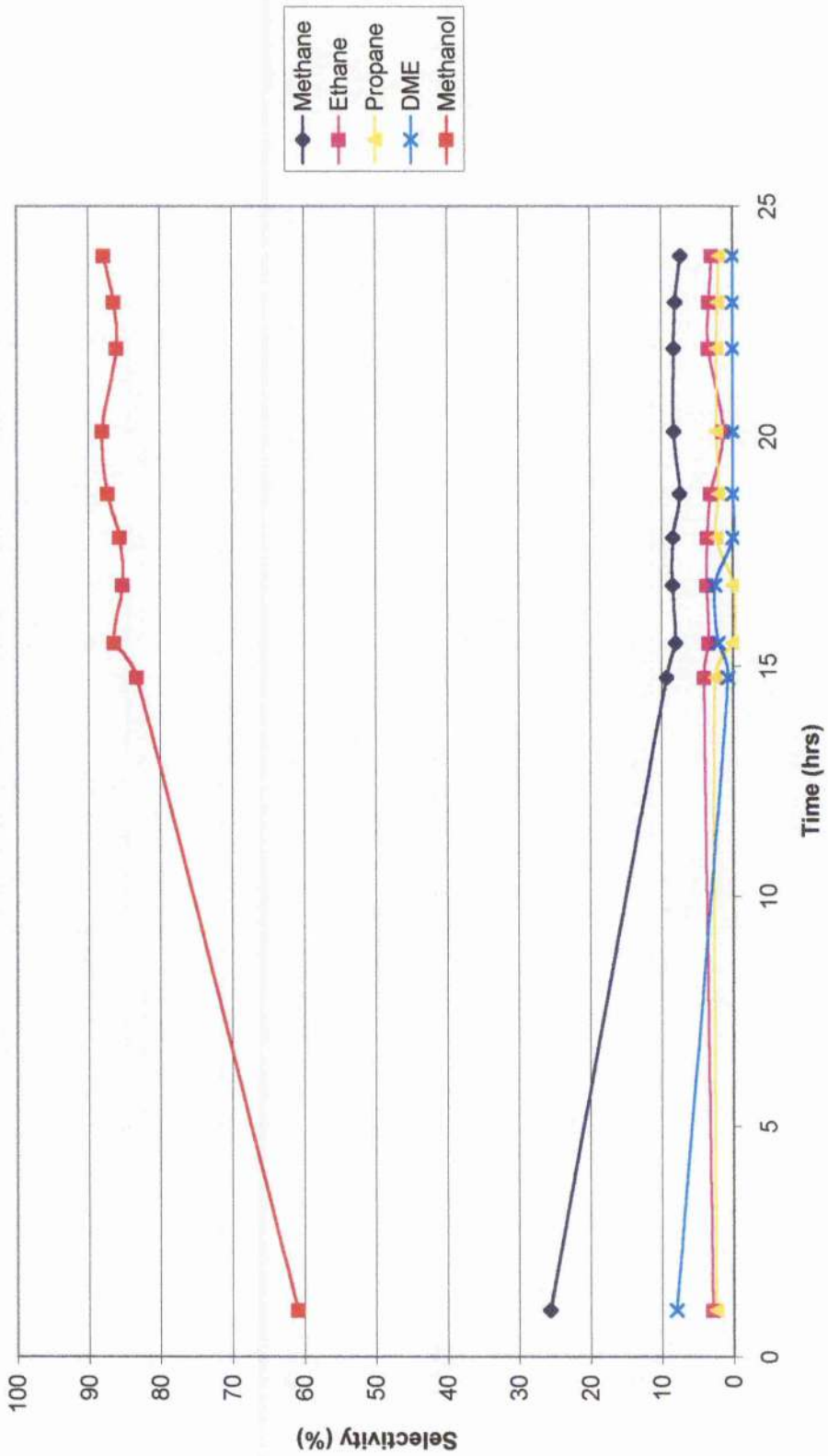
The selectivity of the $^8_{140}\text{Cu}_{\text{Mg}(5)\text{Al}}$ catalyst was observed in Figure 5.5.2 from the conversion results in Table 5.5.1. The methanol selectivity increased after 2 hrs from 60 to 80 % and remained with this selectivity until termination of the reaction.

Figure 5.5.1.1. Product distribution for the $^{80}\text{Cu}_{\text{Mg(5)Al}}$ catalyst.



Operating Conditions, $T = 553 \text{ K}$, $P = 20 \text{ barg}$, $\text{GHSV} = 2000 \text{ hr}^{-1}$, 60 % H_2 , 40 % CO .

Figure 5.5.2. Product distribution for the $^8_{140}\text{Cu}_{\text{Mg(5)Al}}$ catalyst.



Operating Conditions, T = 553 K, P = 20 barg, GHSV = 2000 hr⁻¹, 60 % H₂, 40 % CO.

The induction period was shorter for this catalyst than the ${}^8_{70}\text{Cu}_{\text{Mg}(5)\text{Al}}$ catalyst. The methane selectivity decreased from 26 to 9 % between 2 and 15 hrs reaction time. DME also decreased during this time period, however, the selectivity decreased from 9 to a lowly 1 %. Ethane and propane selectivities vary little throughout the duration of the reaction.

5.5.1 Effect of changes in Temperature

Table 5.5.2. Product distribution for the ${}^8_{30}\text{Cu}_{\text{Mg}(5)\text{Al}}$ catalyst with variation in temperature (expressed as a conversion).

Temperature (K)	553	573
Methane	1.3	3.4
Ethane	0.6	1.5
Methanal	0.7	1.7
DME	0.17	0.3
Methanol	1.4	3.0
Ethanol	0.24	2.1
Propan-2-ol	-	0.4
Propan-1-ol	-	0.3
Butan-2-ol	-	0.14
Isobutanol	-	0.08
Butan-1-ol	-	0.09
Carbon Dioxide	-	0.1

Operating Conditions, P = 20 barg, GHSV = 2000 hr⁻¹, 40 % H₂, 60 % CO.

The ${}^8_{30}\text{Cu}_{\text{Mg}(5)\text{Al}}$ catalyst formed ethanol at 553 K (Table 5.5.2). Increasing the temperature to 573 K resulted in significant increase in higher alcohol conversion with C₃ and C₄ alcohols being observed. Ethanol was formed with a conversion of 2.1 % having formed with 0.24 % conversion at 553 K. The C₃ alcohols had a total conversion of 0.7 % and the C₄ alcohols, 0.31 %. However, hydrocarbon conversion, methane and ethane, similarly increased. Methanal and DME were also formed and

both showed increased formation with higher temperature. Carbon dioxide was only formed at more elevated temperatures with a lower conversion of 0.1 %.

The catalyst and gasfeed composition were changed and again the temperature was varied (Table 5.5.3). The hydrocarbons, methane and ethane, were formed in larger quantities at 593 K rather than at 573 K, with the largest increase being observed with ethane. The propane production did not vary. DME, methanol and ethanol all increased with reaction temperature. However, propan-2-ol did not follow the same trend as the other alcohols, as the product was detected at only 573 K. The increase in production of the flammable products at the higher temperature resulted in a 5 % CO₂ conversion, none was formed at the lower temperature. Water was detected at the lower temperature but not at 593 K.

Table 5.5.3. Product distribution for the ${}^8_{70}\text{Cu}_{\text{Mg}(5)\text{Al}}$ catalyst with variation in temperature (expressed as a conversion).

Temperature (K)	573	593
Methane	2.3	2.9
Ethane	0.7	2.2
Propane	0.6	0.6
DME	8.5	10.0
Methanol	4.5	5.8
Ethanol	0.1	0.5
Propan-2-ol	0.015	-
Carbon Dioxide	-	5.0
Water	0.46	-

Operating Conditions, P = 20 barg, GHSV = 500 hr⁻¹, 36 % H₂, 54 % CO, 10 % Methanol.

5.5.2 Effect of changes in Gas Hourly Space Velocity

Quickening the gas hourly space velocity increased the production of hydrocarbons and DME (Table 5.5.4). The largest change being observed with ethane. Methanol was preferentially formed at the slower gas hourly space velocity, however, higher

alcohols were only detected at the higher gas hourly space velocity. The higher alcohols that were produced were ethanol, propan-2-ol, propan-1-ol and isobutanol, of which ethanol was converted in the largest quantities. More carbon dioxide was produced at 2000 than 500 hr⁻¹. Titrometry results detected water at the quicker gas hourly space velocity. Water was found to have a conversion of 0.23 %.

Table 5.5.4. Product distribution for the ⁸₃₀Cu_{Mg(5)Al} catalyst with variation in gas hourly space velocity (expressed as a conversion).

Gas Hourly Space Velocity (hr ⁻¹)	500	2000
Methane	1.3	2.3
Ethane	0.07	0.25
Propane	0.13	0.2
DME	1.5	1.7
Methanol	7.1	2.9
Ethanol	-	0.7
Propan-2-ol	-	0.03
Propan-1-ol	-	0.05
Isobutanol	-	0.006
Carbon Dioxide	0.2	4.5
Water	-	0.23

Operating Conditions, T = 573 K, P = 20 barg, 36 % H₂, 54 % CO, 10 % Methanol.

Table 5.5.5. Product distribution for the ⁸₁₄₀Cu_{Mg(5)Al} catalyst with variation in gas hourly space velocity (expressed as a conversion).

Gas Hourly Space Velocity (hr ⁻¹)	500	2000
Methane	1.6	5.5
Ethane	0.52	1.7
Propane	0.34	1.2
DME	1.2	1.0
Methanol	7.0	4.8
Ethanol	-	0.568
Propan-2-ol	0.5	-
Butan-2-ol	0.12	-
Isobutanol	0.02	-
Carbon Dioxide	3.5	-

Operating Conditions, T = 593 K, P = 20 barg, 36 % H₂, 54 % CO, 10 % Methanol.

Variation in products with different gas hourly space velocity was conducted at 593 K using the ${}^8_{140}\text{Cu}_{\text{Mg}(5)\text{Al}}$ catalyst (Table 5.5.5). Hydrocarbons were produced in greater quantities at 2000 rather than 500 hr^{-1} . Increased gas hourly space velocity resulted in only a slight decrease in DME production. More methanol was formed at 500 hr^{-1} , however, ethanol was only detected at 2000 hr^{-1} . Further higher alcohols were only produced at 500 hr^{-1} with propan-2-ol being formed in the largest quantities of the C_3 and C_4 oxygenates. Carbon dioxide was only formed at 500 hr^{-1} with a conversion of 3.5 %.

5.5.3 Effect of changes in Gasfeed Composition

Table 5.5.6. Product distribution for the ${}^8_{70}\text{Cu}_{\text{Mg}(5)\text{Al}}$ catalyst with variation in gasfeed composition (expressed as a conversion).

Gasfeed Composition	40 % H_2 , 60 % CO	36 % H_2 , 54 % CO , 10 % Methanol
Methane	0.8	0.95
Ethane	0.21	0.23
Propane	0.2	0.18
DME	0.41	0.22
Methanol	4.5	8.5
Ethanol	-	-
Propan-2-ol	0.06	-
Isobutanol	0.0134	-
Carbon Dioxide	0.34	2.0

Operating Conditions, $T = 573 \text{ K}$, $P = 20 \text{ barg}$, $\text{GHSV} = 2000 \text{ hr}^{-1}$.

Methane and ethane production increased slightly with the introduction of methanol into the gasfeed composition (Table 5.5.6), however, the production of propane decreased. The amount of DME was reduced by a factor of two when methanol was present in the synthesis gas. Methanol production doubled when itself was introduced into the gasfeed composition. Ethanol was not detected with either gasfeed composition. Propan-2-ol and isobutanol were only detected with the methanol-free

gasfeed composition. Carbon dioxide was formed in larger amounts when methanol was included in the gasfeed composition.

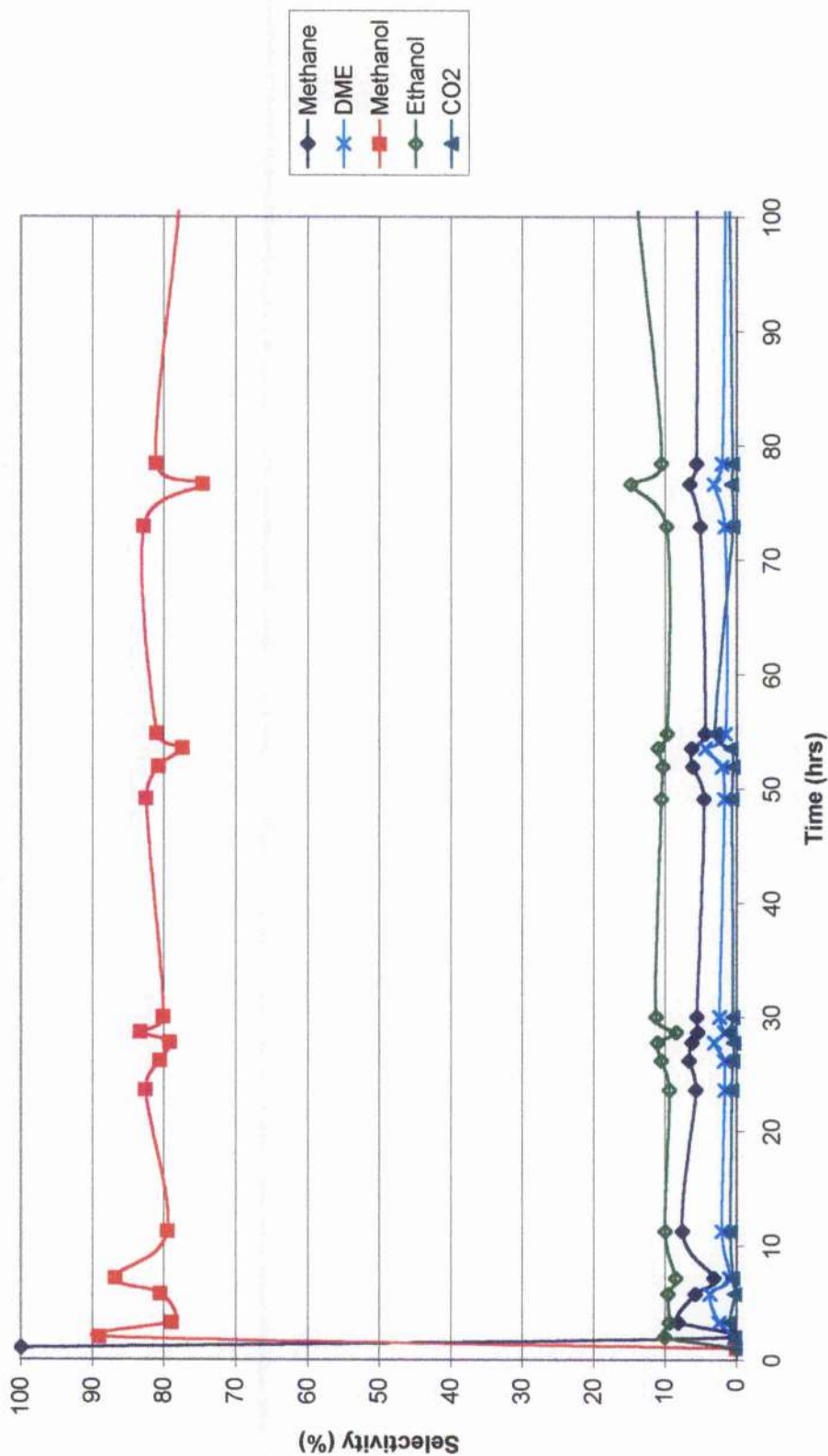
5.5.4 Effect of changes in Methanol Addition

The first sample taken from the ${}^8_{70}\text{Cu}_{\text{Mg}(5)\text{Al}}$ catalyst under the specified conditions showed 100 % selectivity towards methane, as it was the only product formed after this time period (Figure 5.5.3). This decreased to 7 %. Within 3 hrs of the microreactor experiment commencing, the catalyst was 80 % methanol selective, which remained constant throughout the remainder of the experiment. Ethanol had a selectivity of 10 %. DME and CO_2 were the remaining products formed with a selectivity of 2 and 1 % respectively.

5.5.5 Summary

Methanol was the most selective product but required an induction period. Higher alcohols were formed without methanol introduction and increased with reaction temperature. The optimum GHSV was catalyst dependent. DME and hydrocarbons were formed in excessive quantities than required.

Figure 5.5.3. Product distribution for the ${}^8\text{Cu}_{\text{Mg(5)Al}}$ catalyst.



Operating Conditions, $T = 593\text{ K}$, $P = 20\text{ barg}$, $\text{GHSV} = 2000\text{ hr}^{-1}$, 36 % H_2 , 54 % CO , 10 % Methanol.

5.6 Cu/MgO/Al₂O₃ (60/7/35) (Cu_{Mg(7)Al})

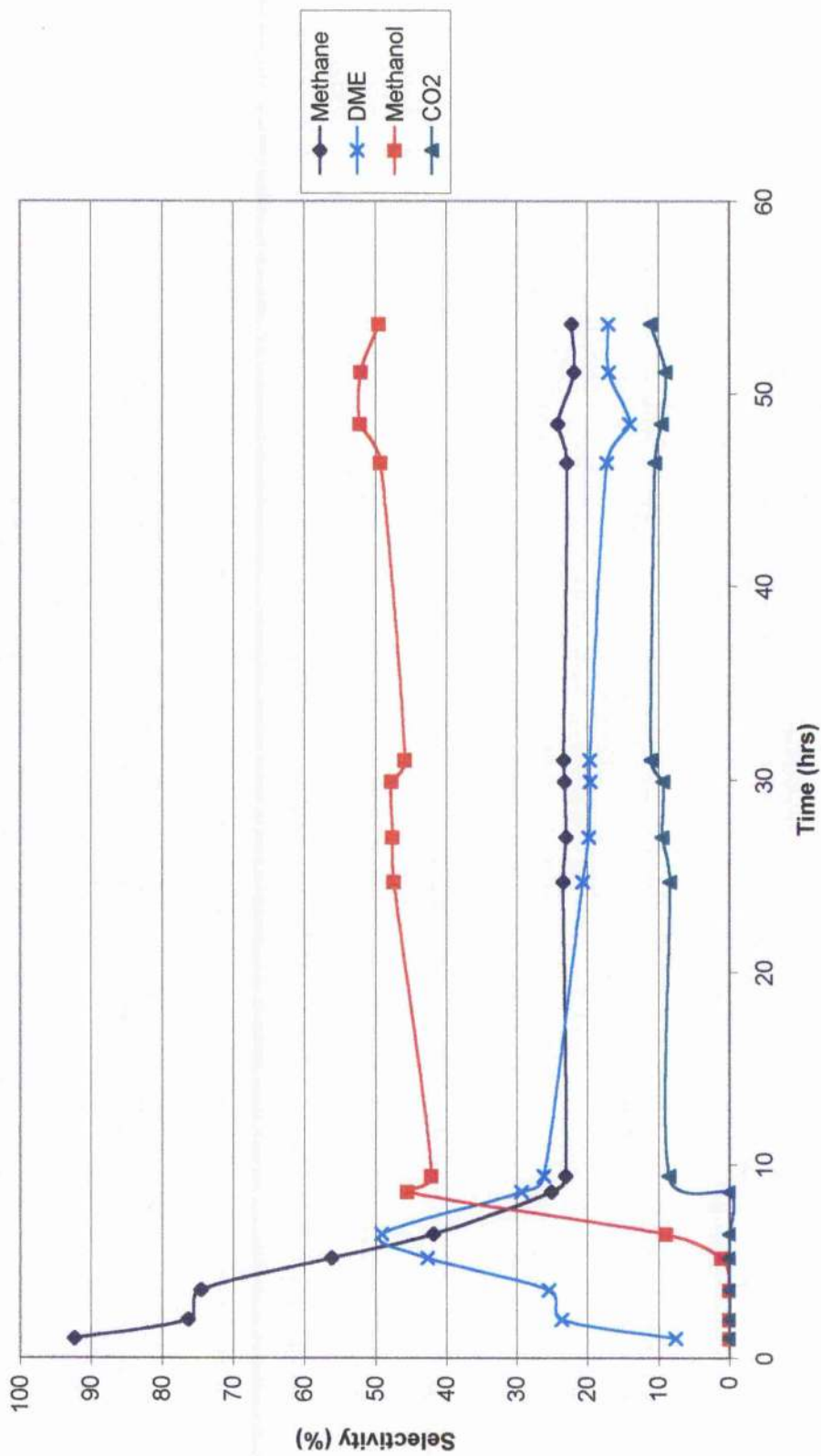
The ⁸₃₀Cu_{Mg(7)Al} catalyst showed that within the first 10hrs, the methane selectivity decreased from over 90 % to 22 % and remained there throughout the duration of the experiment (Figure 5.6.1). The DME selectivity increased steadily before reaching 49 % after 49 hrs before decreasing to 25 % after a further 10 hrs. After this time period, the selectivity gradually decreased to 18 %. Methanol selectivity had an induction period of 5hrs but within a further 5 hrs, it was the most selective product. The selectivity increased gradually from 42 % to a maximum 50 %. Carbon dioxide selectivity increased soon after the initial increase in methanol selectivity as it remained undetected before this time. The selectivity of CO₂ rose to a maximum of 9 %.

Under identical reaction conditions using the ⁸₇₀Cu_{Mg(7)Al} catalyst, methanol was also formed in the largest quantities (Figure 5.6.2). An induction period of 5 hrs was also observed. The methanol conversion increased rapidly to 5 % between 5 and 10 hrs reaction time and then increased more gradually to a maximum of 8 % after 25 hrs. Carbon dioxide had a longer induction time of 10hrs. The conversion initially increased rapidly and within 20 hrs reaction time, a maximum conversion of 5 % was achieved, which remained constant for the duration of the experiment.

Both methane and DME follow the same trend both were formed within the first hour of reaction, both increased in conversion at the same time to their maximum selectivities of 16-18 % within 8 hrs of reaction. However, the DME conversion decreased slightly over time and remained at 16 % selective, while methane increased to over 20 %.

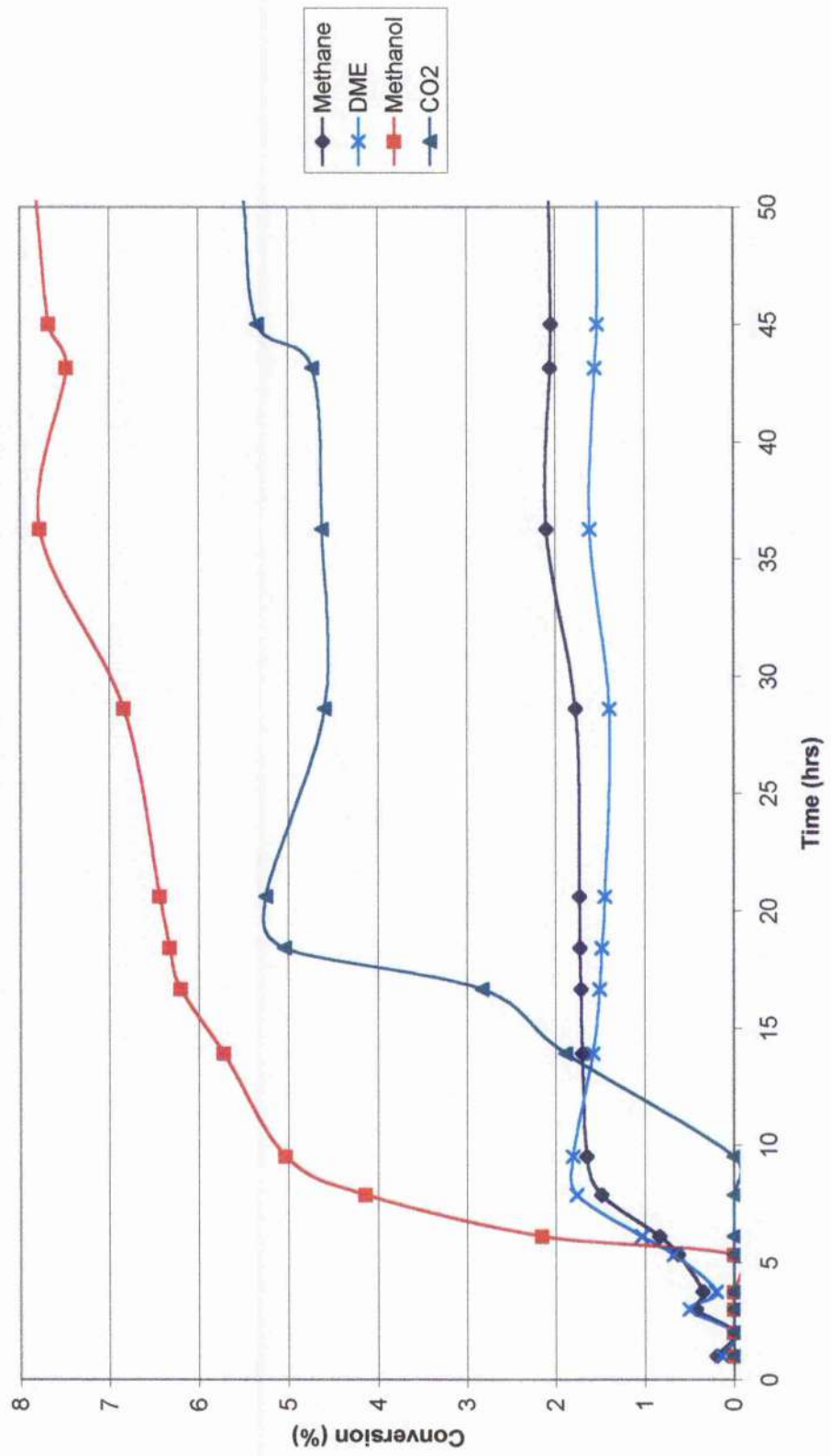
An experiment with the ⁸₁₄₀Cu_{Mg(7)Al} catalyst was conducted under the same reaction conditions (Figure 5.6.3). Methane and DME again form within the first hour of reaction but in this occasion, they only increased to maximum conversion of

Figure 5.6.1. Product distribution for the $^{8}_{30}\text{Cu}_{\text{Mg(7)Al}}$ catalyst.



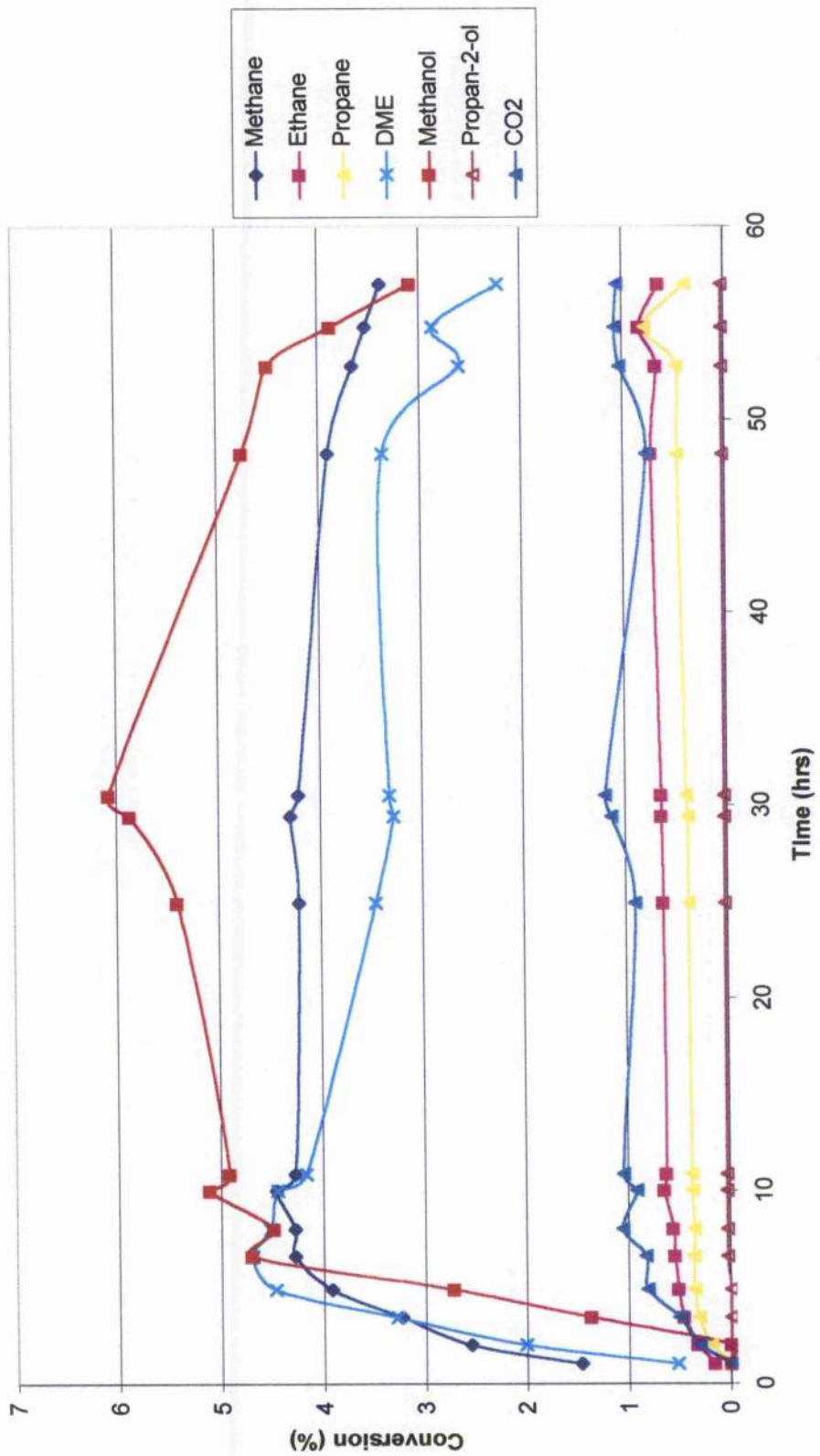
Operating Conditions, T = 573 K, P = 20 barg, GHSV = 2000 hr⁻¹, 40 % H₂, 60 % CO.

Figure 5.6.2. Product distribution for the $^{80}\text{Cu}_{\text{Mg}(7\text{Al})}$ catalyst.



Operating Conditions, T = 573 K, P = 20 barg, GHSV = 2000hr⁻¹, 40 % H₂, 60 % CO.

Figure 5.6.3. Product distribution for the $^{8}_{140}\text{Cu-Mg(7)Al}$ catalyst.

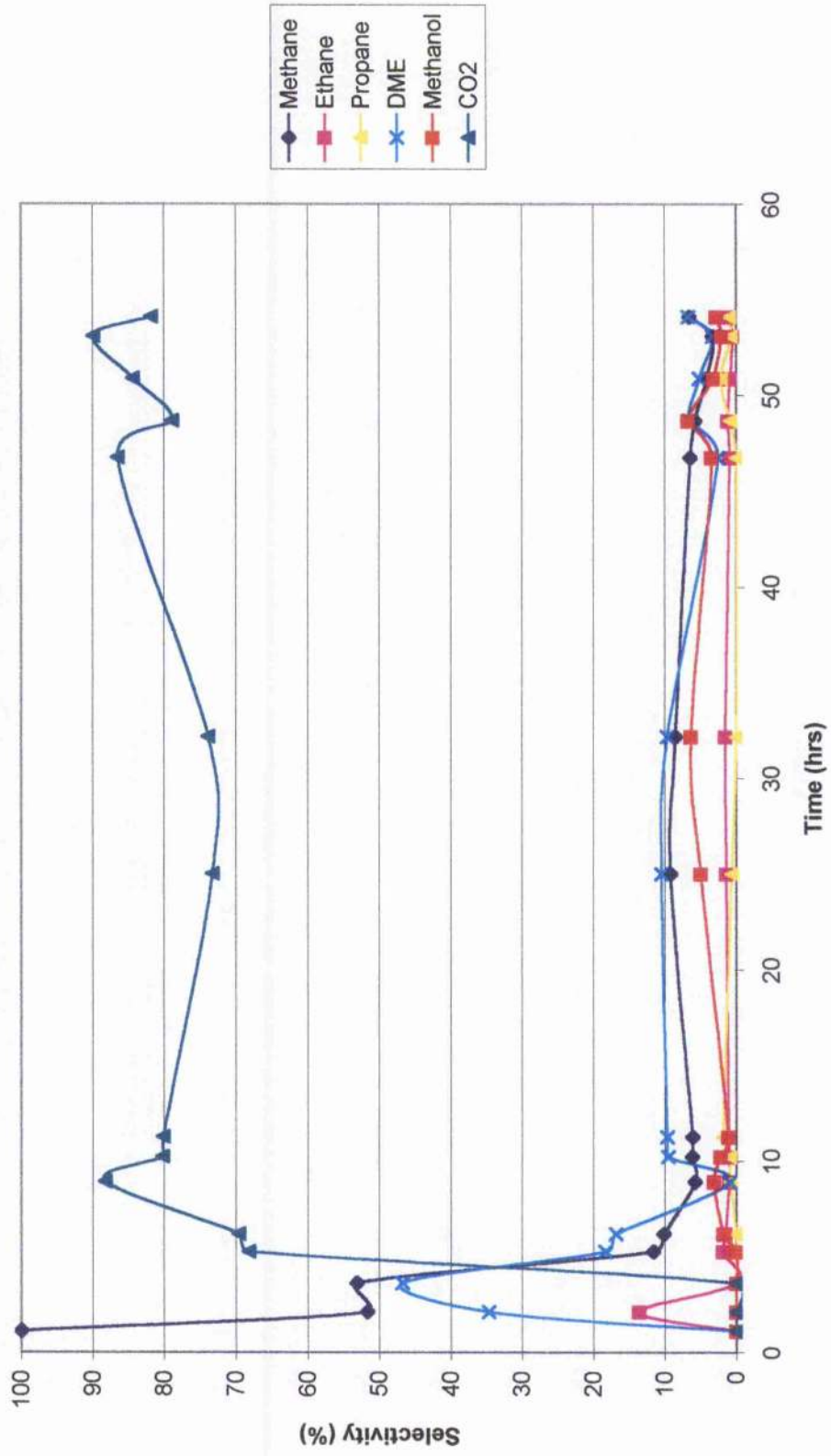


Operating Conditions, T = 573 K, P = 20 barg, GHSV = 2000 hr⁻¹, 40 % H₂, 60 % CO.

4-4.6 % within 9 hrs. After this time period, both products decrease in conversion, DME to 2.2 % and methane to 3.4 %. Methanol started being formed after 2 hrs and increased in conversion at the same rate as DME and methane. However, instead of decreasing after 9 hrs like DME and methane, the conversion continued to increase at a gradual rate to a maximum conversion of 6 % after 30 hrs duration. After this time period, the conversion decreased to 4.1 % after 57 hrs. Ethane and propane were formed within the first hour and increased to a conversion of 0.5 and 0.4 % respectively after 6 hrs reaction time. After this time, both increased slightly over time to conversions of 0.7 and 0.5 % respectively. Carbon dioxide conversion increased steadily to 1 % after 10 hrs reaction time and remained at this value for the duration of the reaction. Propan-2-ol was also formed but in minute quantities. Ethanol was undetected.

The same reaction conditions were used on the ${}^9\text{Cu}_{\text{Mg}(7)\text{Al}}$ catalyst (Figure 5.6.4). Methane was the first and only product formed, therefore, the catalyst initially had 100 % selectivity towards this product. The selectivity towards this product decreased to 8 % within 9 hrs reaction time. DME formation was a similar case to methane, as this product also formed early in the reaction and after an initial maximum selectivity of 47 % after 4 hrs decreased to between 10 and 7 % after 10 hrs. Ethane also formed early in the reaction and reached a maximum selectivity of 1 % within 4 hrs. Propane was only detected after 6hrs of reaction with a maximum selectivity of only 0.5 %. Carbon dioxide had an induction period of 4 hrs before quickly increasing to become the most selective product for the remainder of the reaction. The catalyst was 80 % selective. Methanol formation began very slowly after 5 hrs reaction time and reached a maximum selectivity of 6 % after 34 hrs reaction time before decreasing to 2 % at reaction termination.

Figure 5.6.4. Product distribution for the ${}^9\text{Cu}_{\text{Mg}(7)\text{Al}}$ catalyst.



Operating Conditions, T = 573 K, P = 20 barg, GHSV = 2000 hr⁻¹, 40 % H₂, 60 % CO.

5.6.1 Effect of changes in Temperature

Table 5.6.1. Product distribution for the ${}^8{}_{140}\text{Cu}_{\text{Mg}(7)\text{Al}}$ catalyst with variation in temperature (expressed as a conversion).

Temperature (K)	573	593	613
Methane	4.0	7.5	7.4
Ethane	0.8	1.2	1.3
Propane	0.5	0.8	0.9
DME	3.6	5.4	4.8
Methanol	4.75	4.3	1.4
Propan-2-ol	0.03	0.06	0.12
Carbon Dioxide	1.1	1.3	1.35

Operating conditions, $P = 20$ barg, $\text{GHSV} = 2000 \text{ hr}^{-1}$, 40 % H_2 , 60 % CO .

Hydrocarbons, methane, ethane and propane increased greatly from 573 to 593 K (Table 5.6.1) with a lesser effect on production being observed between 593 and 613 K. Methanol formation decreased from 4.75 to 1.4 % with the increase in temperature from 573 to 613 K, unlike the hydrocarbon production between 593 and 613 K, which saw the greater effect. DME production proceeded through a maximum conversion of 5.4 % at 593 K. Increasing the temperature increased the propan-2-ol conversion with the change in temperature resulting in a four-fold increase in production. Carbon dioxide conversion increased only slightly within the temperature range, a greater increase was observed between 573 and 593 K.

5.6.2 Effect of changes in Gas Hourly Space Velocity

The ${}^8{}_{70}\text{Cu}_{\text{Mg}(7)\text{Al}}$ catalyst was more selective towards methanol and ethanol at the lower gas hourly space velocity (Table 5.6.2), the greater increase being observed with methanol. Hydrocarbons were preferentially formed at the faster gas hourly space velocity, as both ethane and propane were not detected at 1000 hr^{-1} . The methane

selectivity increased three-fold when doubling the gas hourly space velocity. The gas hourly space velocity had also an affect on DME, as the selectivity towards this product was higher at the faster gas hourly space velocity.

The largest difference between selectivities was observed with CO₂, as at the lower gas hourly space velocity the selectivity was only 1.0 %, however, at twice the gas hourly space velocity, the selectivity had increased dramatically to 24 %. Water was detected at 2000 hr⁻¹ gas hourly space velocity with a catalyst selectivity of 1 %.

Table 5.6.2. Product Distribution for the ⁸₇₀Cu_{Mg(7)Al} catalyst with variation in gas hourly space velocity (expressed as selectivity).

Gas Hourly Space Velocity (hr ⁻¹)	1000	2000
Methane	5.5	13
Ethane	-	2.0
Propane	-	1.0
DME	2.5	9.0
Methanol	80	43
Ethanol	11	7.0
Carbon Dioxide	1.0	24
Water	-	1.0

Operating conditions, T = 573 K, P = 20 barg, 36 % H₂, 54 % CO, 10 % Methanol.

5.6.3 Effect of changes in Gasfeed Composition

The introduction of methanol into the gasfeed composition showed a large selectivity towards methanol and ethanol (Table 5.6.3). Ethanol was not detected in the methanol-free synthesis gas composition and methanol was not detected when the CO concentration was increased to 70 %. The selectivity of methane with 70 % CO was 33 %, this decreased to 26.5 % at 60 % CO and with methanol inclusion, decreased dramatically to 3 %. Ethane and propane were only formed with the gasfeed ratio 40:60 H₂:CO. DME selectivity was reduced with decreasing CO concentration from

34 % to 14 % to only 2 %. The CO₂ selectivity decreased in the same sequence as the DME production.

Table 5.6.3. Product Distribution for the ⁸₃₀Cu_{Mg(7)Al} catalyst with variation in gasfeed composition (expressed as selectivity).

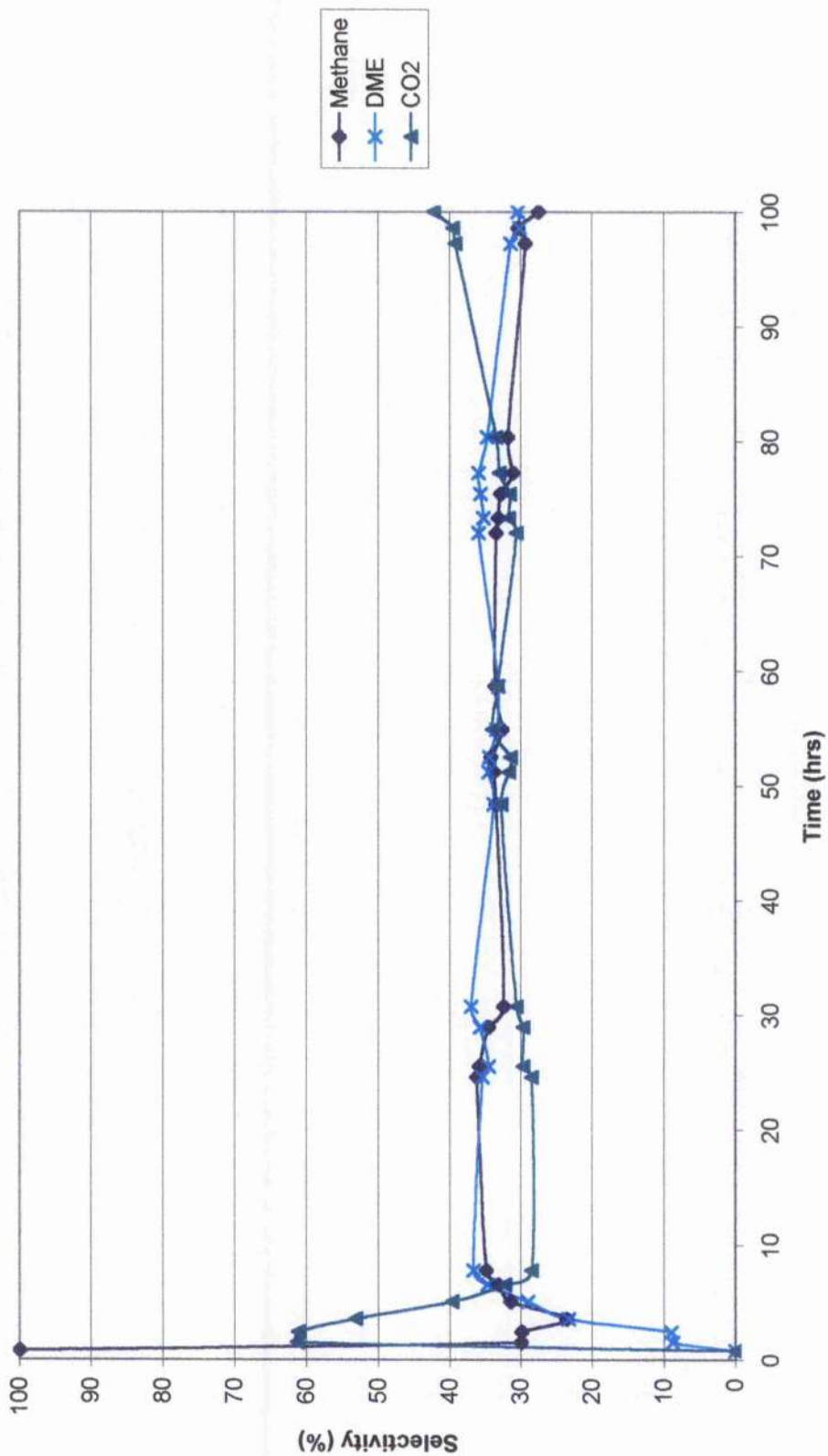
Gasfeed Composition	30 % H ₂ , 70 % CO	40 % H ₂ , 60 % CO	36 % H ₂ , 54 % CO, 10 % Methanol
Methane	33	26.5	3
Ethane	-	4	-
Propane	-	1.5	-
DME	34	14	2
Methanol	-	46	83
Ethanol	-	-	10
Carbon Dioxide	33	8	0.5

Operating Conditions, T = 593 K, P = 20 barg, GHSV = 2000 hr⁻¹.

The experiment involving the 30:70 H₂:CO gasfeed composition showed that methane was formed first having 100 % selectivity (Figure 5.6.5). The selectivity decreased after 2-3 hrs to 33 %. The selectivity decreased further to 30 % after 80 hrs. The DME selectivity increased the slowest of the three products formed. The product reached the maximum selectivity after 10hrs reaction time. Like methane, DME selectivity decreased after 80 hrs reaction time to 30 %. Carbon dioxide was the second product formed in this reaction. After reaching an early maximum selectivity of 61 % after 2 hrs, it went through a local minimum of 28 % before increasing steadily throughout the reaction to 40 % on completion.

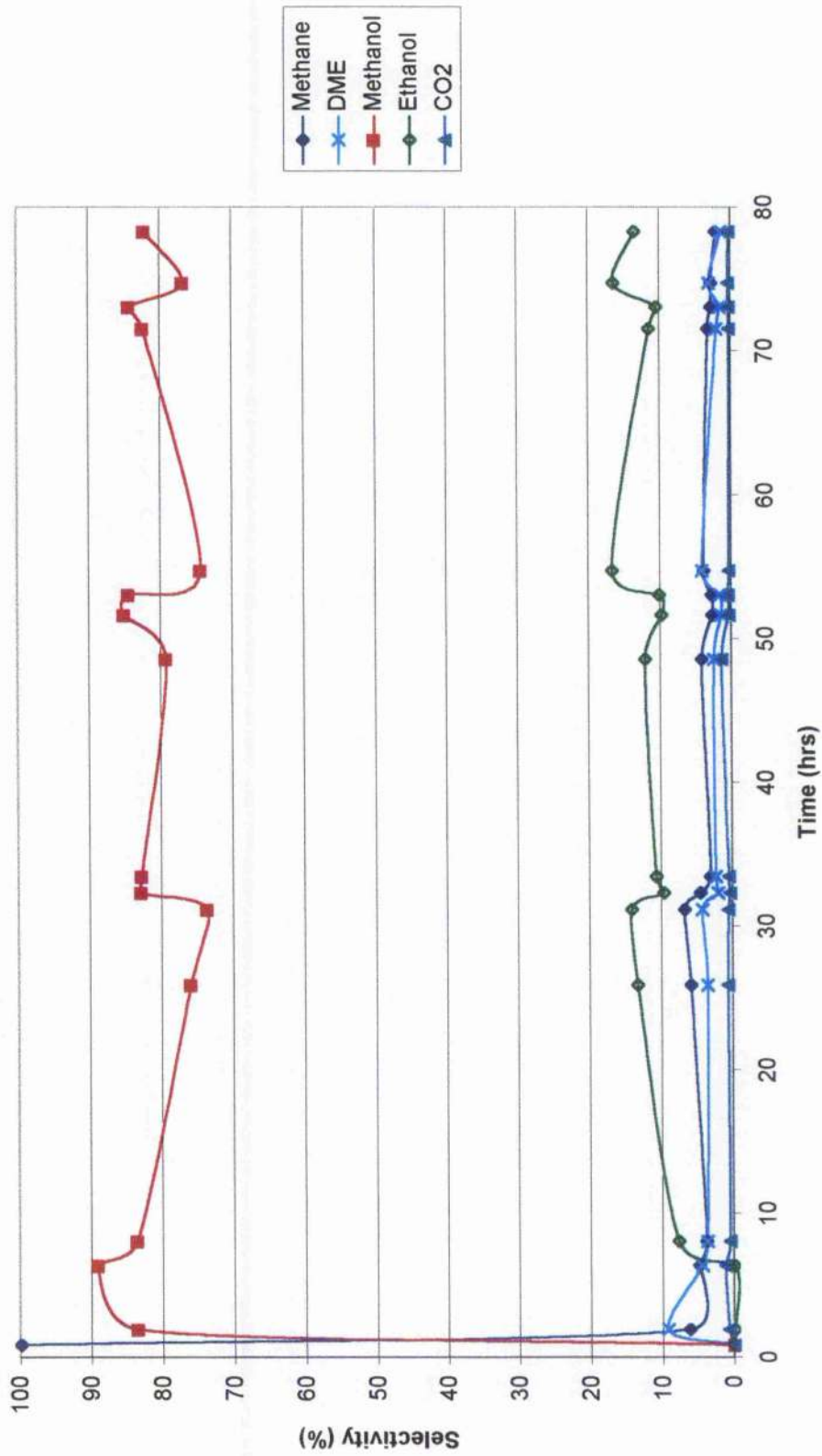
The methanol-included gasfeed composition from the results (Table 5.6.3), showed methane as the first product formed (Figure 5.6.6), thus having an initial selectivity of 100 %. This rapidly decreased to 3 % where it stayed for the remainder of the reaction. Little induction period was observed with methanol, as its selectivity increased within the initial 2 hrs to 83 %. DME had an initial maximum selectivity

Figure 5.6.5. Product distribution for the ${}^8_{30}\text{Cu}_{\text{Mg}(\gamma)\text{Al}}$ catalyst.



Operating Conditions, $T = 593 \text{ K}$, $P = 20 \text{ barg}$, $\text{GHSV} = 2000 \text{ hr}^{-1}$, 30 % H_2 , 70 % CO .

Figure 5.6.6. Product distribution for the ${}^8_{30}\text{Cu}_{(\text{Mg}(7)\text{Al})}$ catalyst.



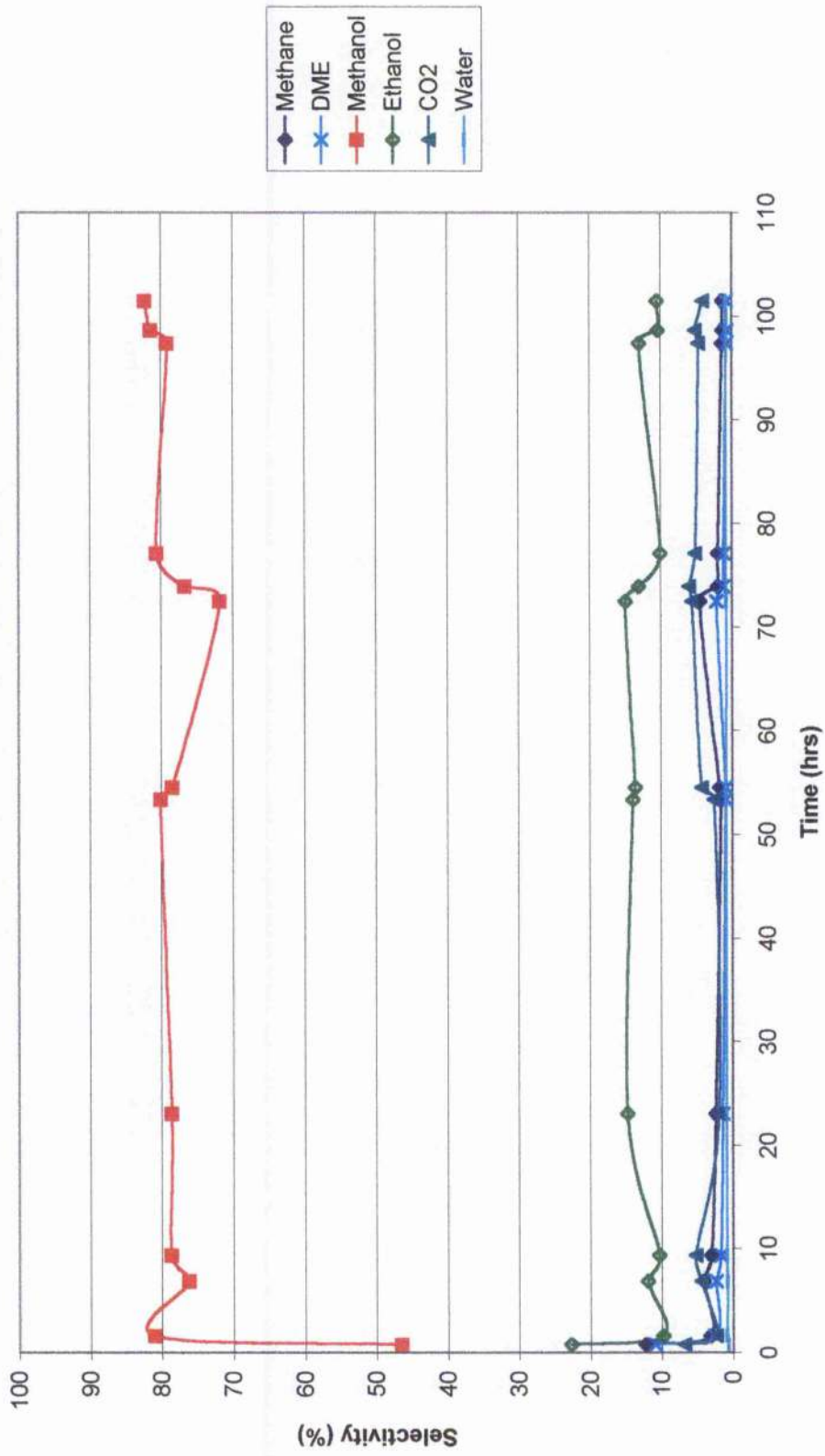
Operating Conditions, T = 593 K, P = 20 barg, GHSV = 2000 hr⁻¹, 36 % H₂, 54 % CO, 10 % Methanol.

after 2 hrs before decreasing to 2 %. Ethanol was the last product to start to form. The compound required 8hrs to be detected whereupon the selectivity increased to 8 % within a further hour. The selectivity increased to 10 % soon after this time period.

The same conditions as the previous reaction were conducted, this time using the $^{9}_{30}\text{Cu}_{\text{Mg}(7)\text{Al}}$ catalyst (Figure 5.6.7). Methanol was formed initially with a selectivity of 47 % before increasing to 80 % within 2 hrs. On this occasion, no induction period with ethanol was observed. The initial selectivity was 22 %, which decreased to 10 % within 2 hrs of reaction time. The selectivity then stabilised between 10-15 % for the remaining duration of the experiment. Methane, DME and CO_2 were all formed at the start of the reaction. Carbon dioxide had the largest selectivity of these products with a value of 5 %. DME and methane had values of 2-3 %. Water was also detected with a selectivity 0.9 %.

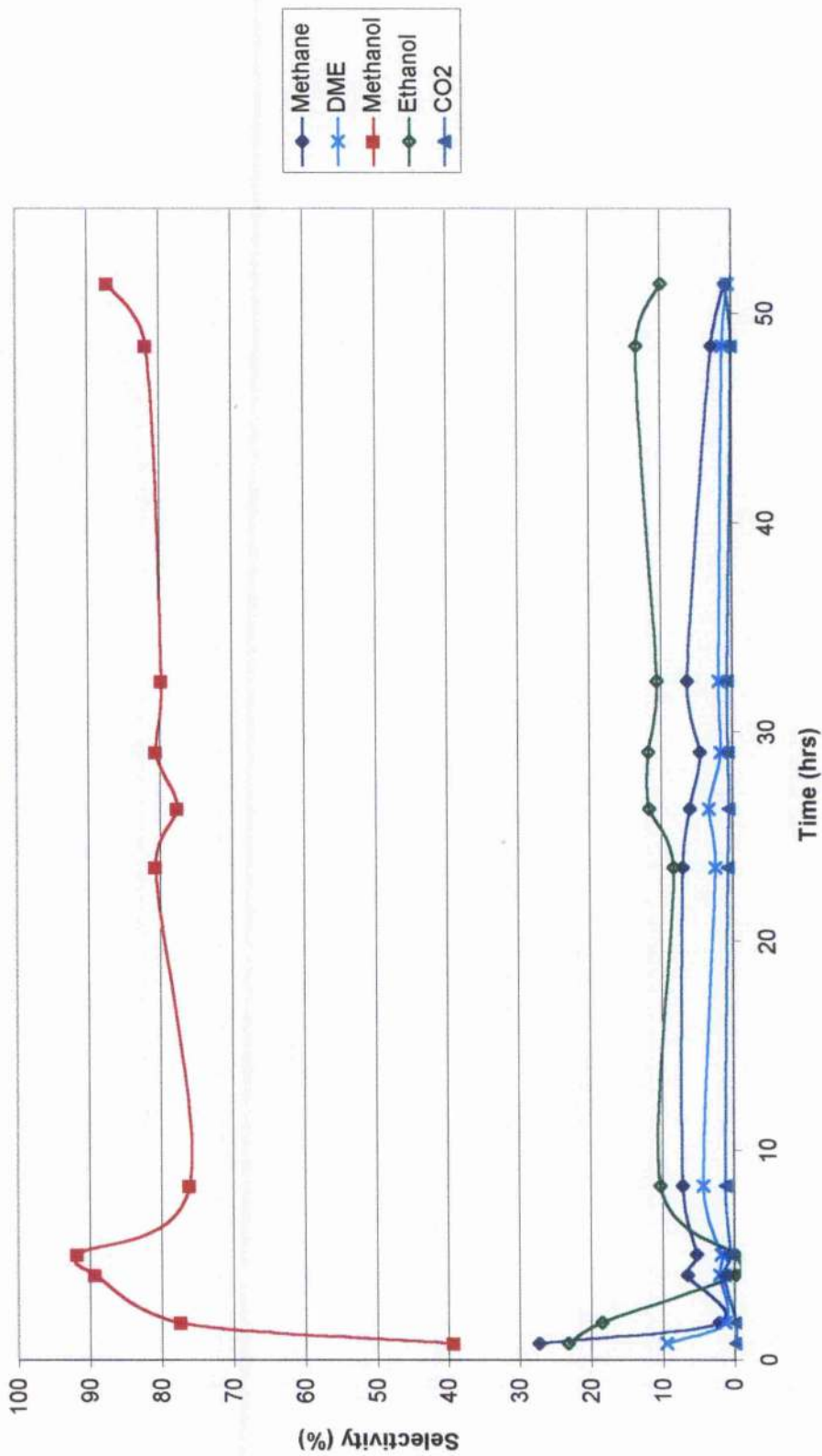
Similar reaction conditions (lower GHSV) were conducted on the $^{8}_{70}\text{Cu}_{\text{Mg}(7)\text{Al}}$ catalyst (Figure 5.6.8). Methanol was formed with an initial selectivity of 40 % before increasing to 80 % within 2 hrs reaction time. The selectivity remained at this value until completion of the reaction after 53 hrs. Ethanol was initially formed with a selectivity of 23 %, this decreasing to a non-detectable amount between 5 and 6 hrs reaction time. The selectivity stabilised soon after and remained at a value of 10 %. Methane was formed with an initial selectivity of 28 % before decreasing to 8 % between the reaction time of 8 and 24 hrs. After this time period, the selectivity of methane decreased to 1 % by the termination of the reaction. The initial DME selectivity was 10 % before decreasing to 4 % after 8 hrs, and by 53 hrs reaction time had further decreased to 1 %. Carbon dioxide was detected after 2-3 hrs, increasing to a maximum selectivity of 1 % after 8 hrs, before decreasing.

Figure 5.6.7. Product distribution for the ${}^9_{30}\text{Cu}_{\text{Mg}(7)\text{Al}}$ catalyst.



Operating Conditions, T = 593 K, P = 20 barg, GHSV = 2000 hr⁻¹, 36 % H₂, 54 % CO, 10 % Methanol.

Figure 5.6.8. Product distribution for the ${}^8_{70}\text{Cu}_{1\text{Mg}7\text{Al}}$ catalyst.



Operating Conditions, $T = 593 \text{ K}$, $P = 20 \text{ barg}$, $\text{GHSV} = 1000 \text{ hr}^{-1}$, 36 % H_2 , 54 % CO , 10 % Methanol.

5.6.4 Summary

Higher alcohols were formed without methanol introduction below 70 % CO. Higher alcohols with methanol in the gasfeed composition were all formed with a similar selectivity. Hydrocarbons, DME and CO₂ were all formed in large quantities.

5.7 K/Cu/MgO/Al₂O₃ (K60/7/35) (Cu_{MgAlK})

Table 5.7.1. Product distribution for the Cu_{MgAlK} catalyst with variation in preparation conditions (expressed as a conversion).

Catalyst	⁸ ₃₀ Cu _{MgAlK}	⁸ ₇₀ Cu _{MgAlK}	⁸ ₁₄₀ Cu _{MgAlK}	⁹ ₃₀ Cu _{MgAlK}
Methane	0.6	1.44	0.7	0.005
Ethane	0.07	0.26	0.06	-
Propane	0.045	0.13	0.02	-
Methanal	0.4	1.0	0.8	-
Ethanal	0.4	1.9	0.4	-
Methanol	-	-	0.05	-
Ethanol	-	0.02	0.4	-
Propanal	0.036	0.002	0.008	-
Propan-1-ol	0.038	0.001	-	-
Isobutanal	-	0.002	-	-
Butanal	0.002	0.001	0.001	-
Isobutanol	-	0.002	-	-
Carbon Dioxide	0.22	0.146	0.4	-

Operating Conditions, T = 573 K, P = 20 barg, GHSV = 1000 hr⁻¹, 40 % H₂, 60 % CO.

A very large product distribution was formed with the pH = 8 catalysts (Table 5.7.1). The ⁹₃₀Cu_{MgAlK} catalyst only formed small amounts of methane. The ⁸₇₀Cu_{MgAlK} catalyst was the most active catalyst especially for hydrocarbons, small aldehydes (methanal and ethanal) and C₄ alcohols. Ethanal was formed in largest quantities, followed by methane and methanal. No methanol was formed with the ⁸₃₀Cu_{MgAlK} and ⁸₇₀Cu_{MgAlK} catalysts, however, ethanol was produced with the ⁸₇₀Cu_{MgAlK} catalyst.

The ⁸₁₄₀Cu_{MgAlK} catalyst produced a large quantity of ethanol, however, this formed no C₃ or C₄ alcohols only aldehydes. The ⁸₃₀Cu_{MgAlK} catalyst formed the largest quantity of C₃'s oxygenates but the ⁸₇₀Cu_{MgAlK} catalyst produced a more variable selection. The ⁸₁₄₀Cu_{MgAlK} catalyst produced the most amount of carbon dioxide.

The results of the ⁸₃₀Cu_{MgAlK} catalyst (Table 5.7.1) are shown as catalyst

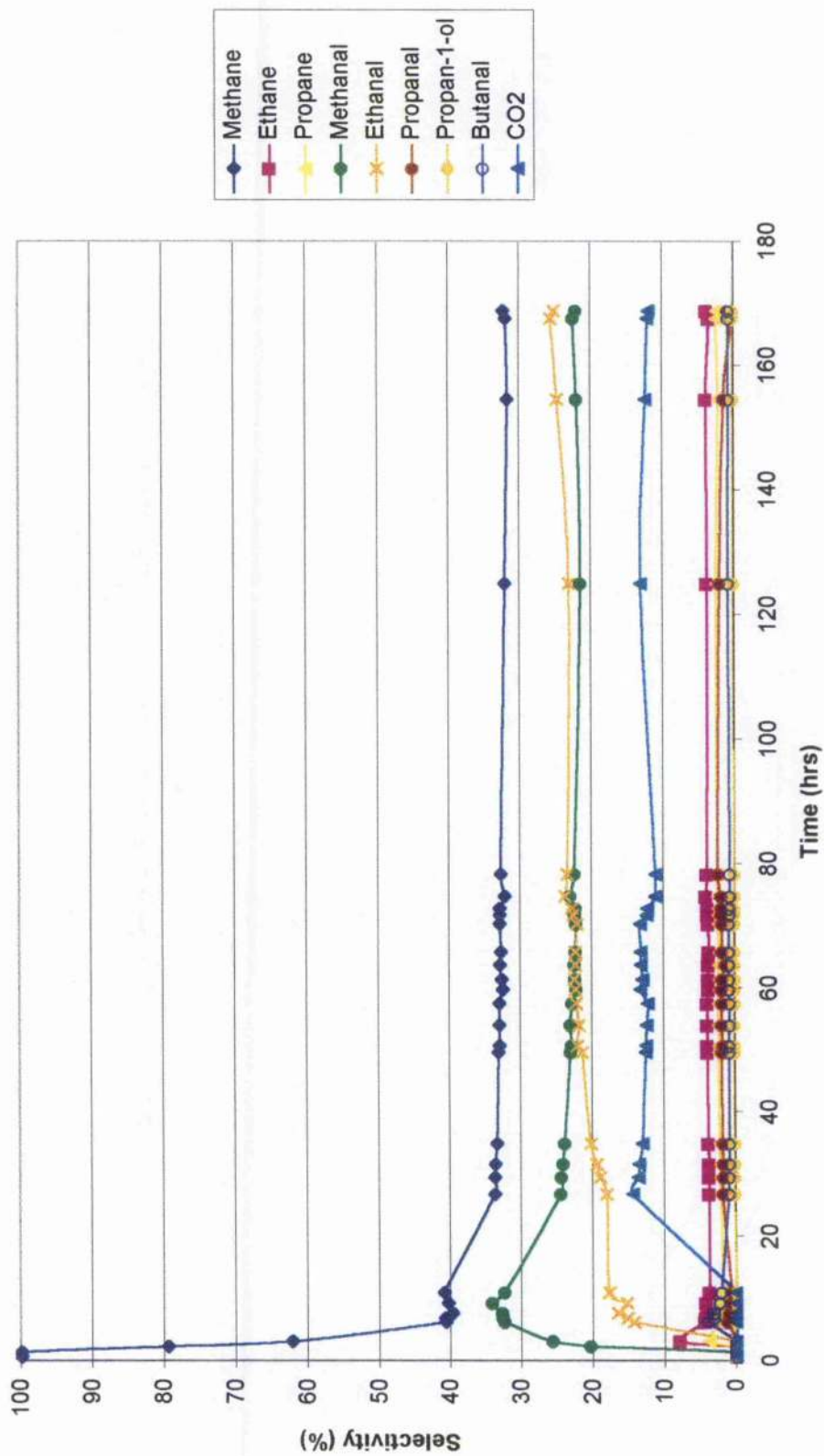
selectivity (Figure 5.7.1). The catalyst had an initial 100 % selectivity for methane, as it was the only product formed, this decreased to 34 % within 25 hrs, it remained at this value until termination of the reaction after 170 hrs. Methanal was also formed in large quantities, reaching an early selective maximum of 34 % before decreasing to 23 % after 26 hrs. The ethanal selectivity increased rapidly within the first 15hrs and to 26 % with 25 hrs. After 26 hrs, the catalyst was also 14 % selective towards CO₂. The other hydrocarbons formed, ethane and propane, had selectivities of 4 and 3 % respectively. The remaining products, higher aldehydes and alcohols, had smaller selectivities.

The same reaction conditions were used with the ⁸₇₀Cu_{MgAlK} catalyst (Figure 5.7.2). The catalyst initially had 100 % selectivity for methane, which decreased to 30 % within 8 hrs. The DME selectivity reached an early maximum of 36 % before decreasing steadily to 20 % for the remaining duration of the reaction. Ethanal increased steadily over 11 hrs to become the selective product at 35 to 40 %. Ethane and propane had selectivities of 4 % and 2 % respectively. Carbon dioxide was also formed and had a selectivity of 2 % after an earlier maximum of 7 %. Higher alcohols and aldehydes were also formed but in minute quantities.

5.7.1 Effect of changes in Temperature

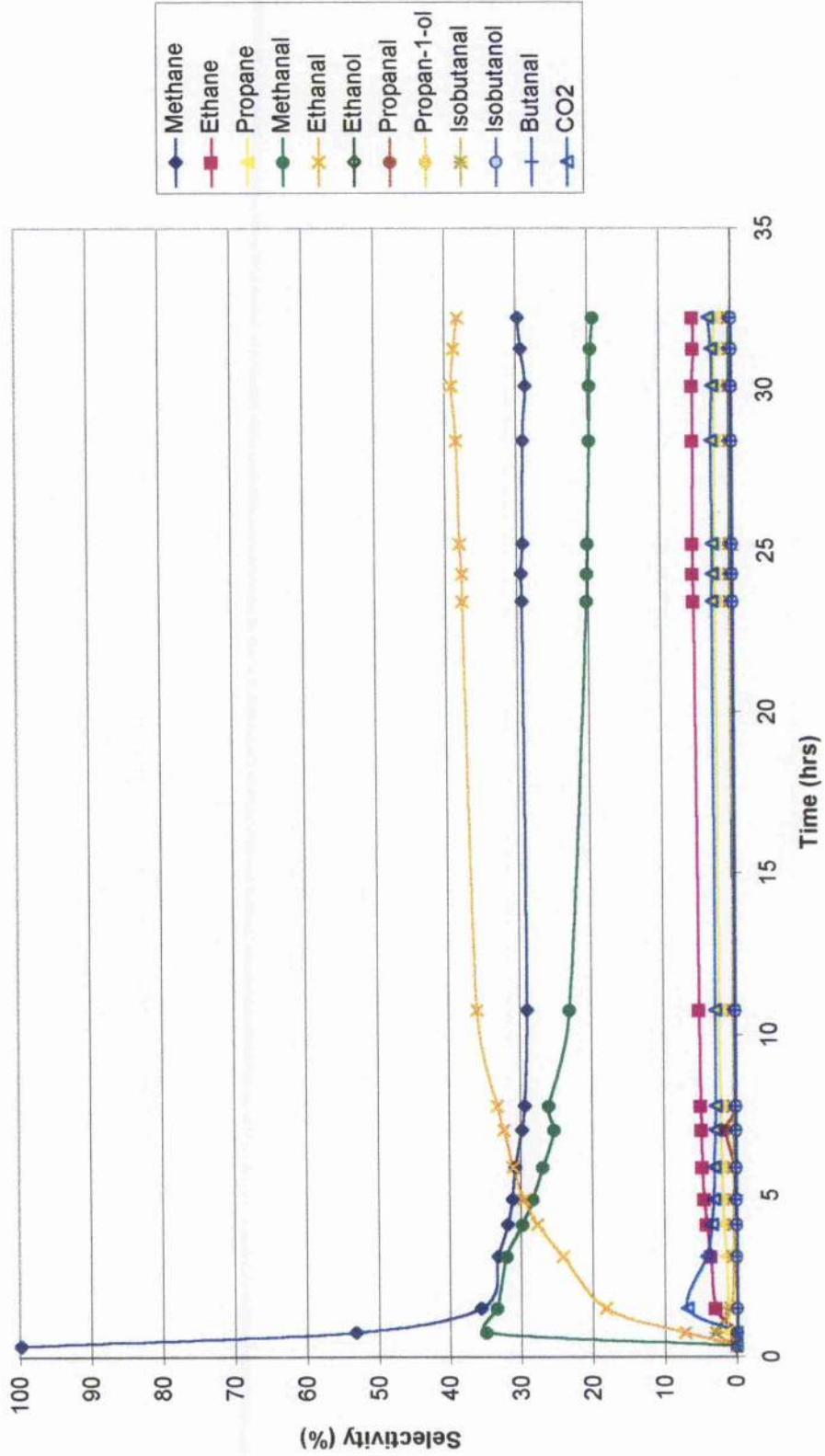
An increase in temperature for the ⁸₁₄₀Cu_{MgAlK} catalyst resulted in greater amounts of hydrocarbons being formed (Table 5.7.2). More aldehydes were formed at the higher temperature, especially methanal and propanal. No increase in ethanal or isobutanal was observed. Carbon dioxide showed no change in concentration with variation in temperature. No methanol was formed at either temperature. Propan-2-ol was formed in larger quantities than ethanol.

Figure 5.7.1.1. Product distribution for the $^{80}\text{Cu}_{\text{MgAlK}}$ catalyst.



Operating Conditions, T = 573 K, P = 20 barg, GHSV = 1000 hr⁻¹, 40 % H₂, 60 % CO.

Figure 5.7.2. Product distribution for the $^{80}\text{Cu}_{\text{MgAlK}}$ catalyst.



Operating Conditions, $T = 573 \text{ K}$, $P = 20 \text{ barg}$, $\text{GHSV} = 1000 \text{ hr}^{-1}$, 40 % H_2 , 60 % CO .

Table 5.7.2. Product distribution for the ${}^8_{140}\text{Cu}_{\text{MeAlK}}$ catalyst with variation in temperature (expressed as a conversion).

Temperature (K)	573	593
Methane	1.2	2.0
Ethane	0.13	0.25
Propane	0.05	0.11
Methanal	1.5	1.8
Ethanal	1.0	0.9
Ethanol	-	0.001
Propanal	0.008	0.06
Propan-2-ol	0.006	0.006
Isobutanal	0.002	0.002
Carbon Dioxide	0.2	0.2

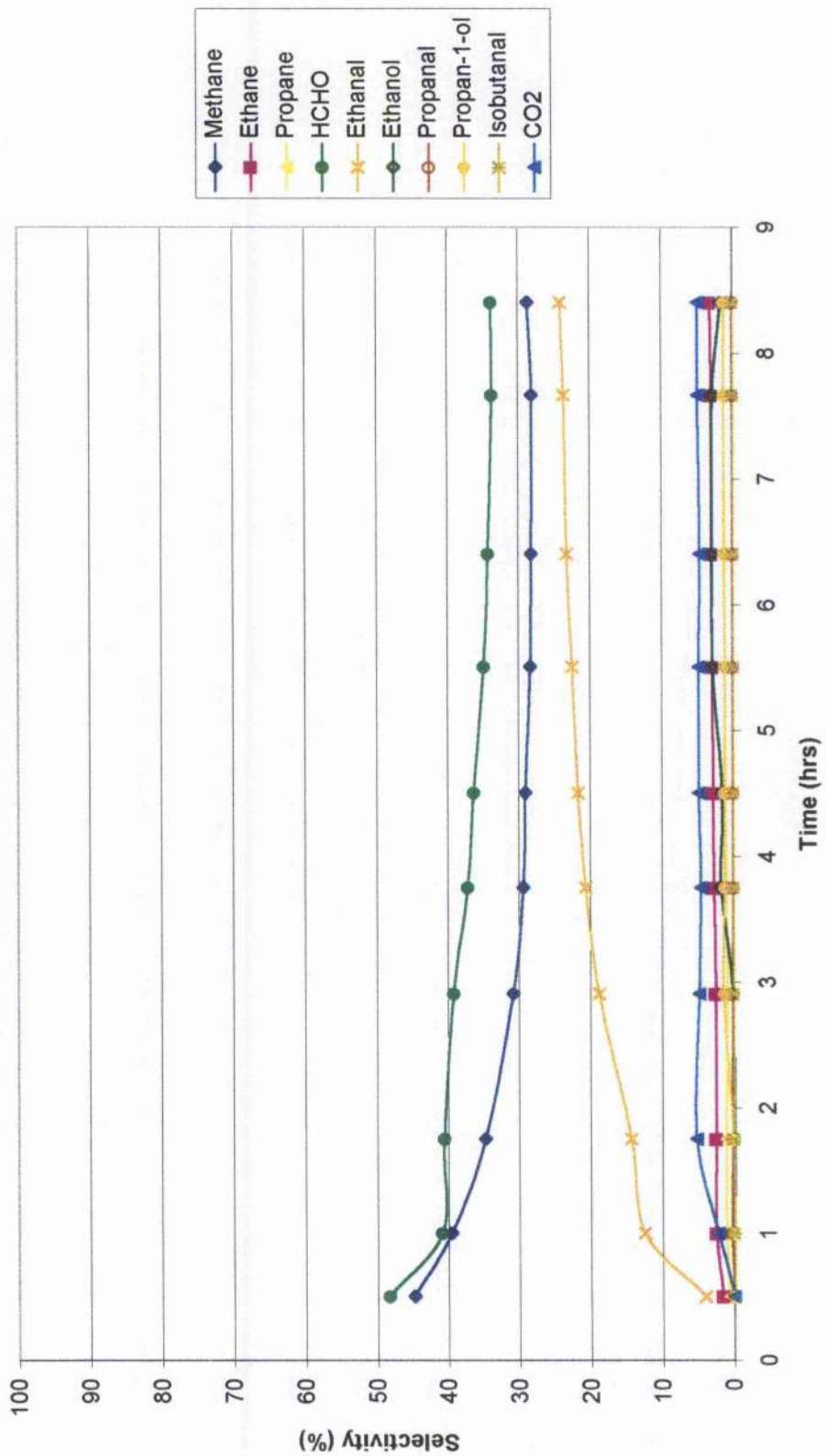
Operating Conditions, $P = 20$ barg, $\text{GHSV} = 3000 \text{ hr}^{-1}$, 40 % H_2 , 60 % CO .

The reaction conducted at 573 K (Table 5.7.2) is represented as a figure (Figure 5.7.3). Methanal was formed early in the reaction and remained the most selective product throughout the duration of the experiment. The catalyst was also selective towards methane, which decreased from an initial selectivity of 45 to 30 % in 4 hrs. Ethanal formed within the first hour with the selectivity increasing steadily over the duration of the experiment before reaching a value of 24 %. Carbon dioxide consisted of 5 % of the total products formed. Ethane and propane had selectivities of 3 and 2 % respectively. Ethanol had an induction period of 3 hrs, before increasing to a maximum selectivity of 3 % after 5.5 hrs. Propan-1-ol was detected an hour before ethanol with a selectivity of 1 %. The remaining products were selective in smaller quantities.

5.7.2 Effect of changes in Gas Hourly Space Velocity

Changing the gas hourly space velocity from 3000 to 10,000 hr^{-1} resulted in a decrease in hydrocarbon production, methane, ethane and propane (Table 5.7.3). Methanal,

Figure 5.7.3. Product distribution for the $^8_{140}\text{Cu}_{\text{MgAlK}}$ catalyst.



Operating Conditions, T = 573 K, P = 20 barg, GHSV = 3000 hr⁻¹, 40 % H₂, 60 % CO.

ethanal and isobutanal all decreased with increasing gas hourly space velocity, propanal and butanal were relatively unaffected. No methanol was formed in either case; however, ethanol showed a conversion of 0.01 % and only decreased slightly with increasing gas hourly space velocity. Carbon dioxide was unaffected by the change in gas hourly space velocity.

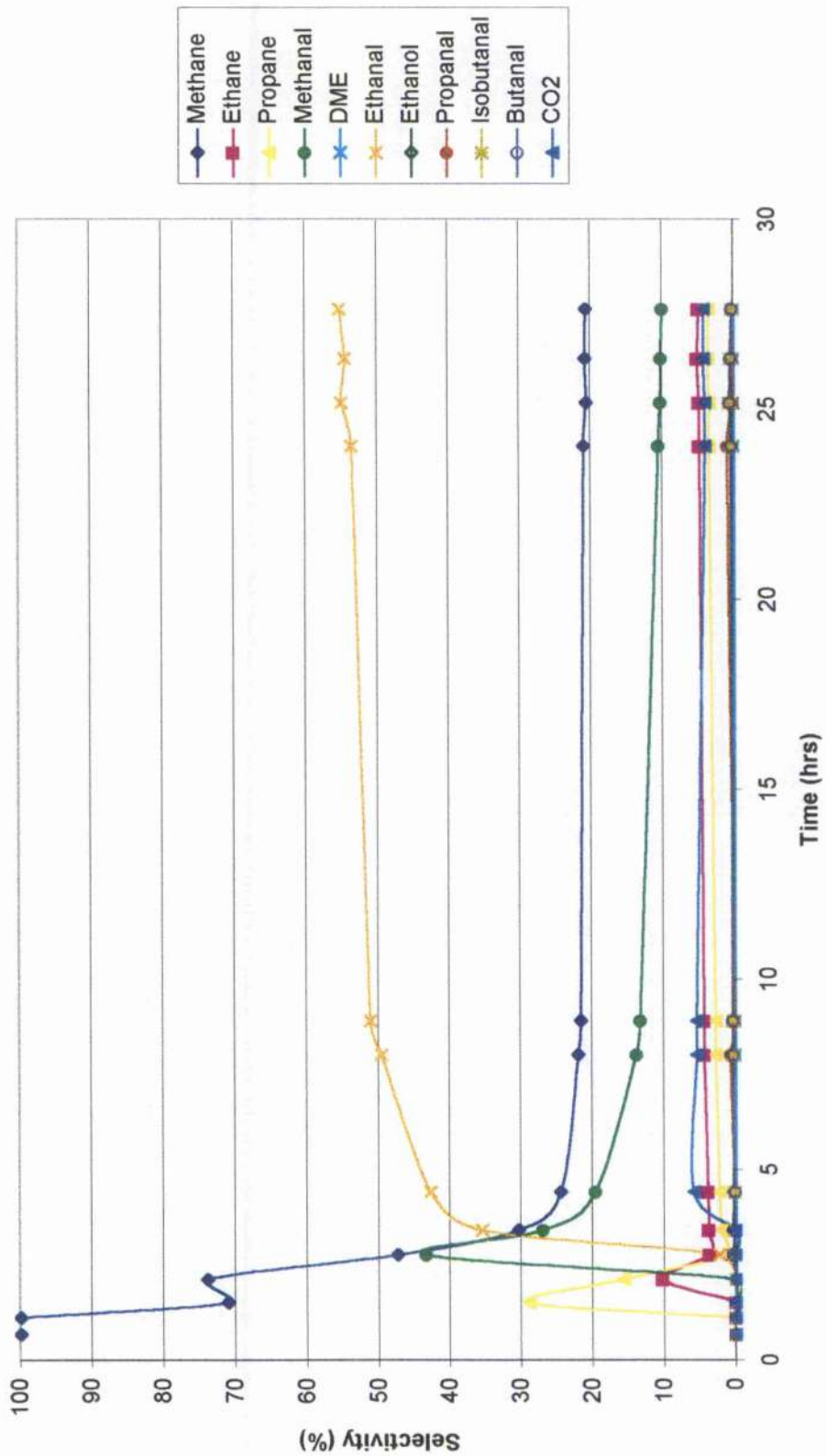
Table 5.7.3. Product distribution for the $^{87}\text{Cu}_{\text{MgAlK}}$ catalyst with variation in gas hourly space velocity (expressed as a conversion).

Gas Hourly Space Velocity (hr ⁻¹)	3000	10000
Methane	0.8	0.3
Ethane	0.13	0.06
Propane	0.1	0.08
Methanal	0.4	0.08
Ethanal	2.0	1.2
Ethanol	0.01	0.008
Propanal	0.008	0.009
Isobutanal	0.018	0.012
Butanal	0.011	0.012
Carbon Dioxide	0.16	0.16

Operating Conditions, T = 573 K, P = 20 barg, 40 % H₂, 60 % CO.

The GHSV=3000hr⁻¹ results (Table 5.7.3) are shown as selectivity (Figure 5.7.4). The ethanal selectivity increased to above 50 % within 10 hrs of reaction time after an initial induction period of 2 hrs. Methane decreased from 100 % to 21 % within 9 hrs and remained with this selectivity until completion of the experiment. The methanal selectivity proceeded through an early maximum of 43 % before decreasing to 10-11 %. Ethane and propane both went through early maxima before decreasing in selectivity to 3 and 4 % respectively. Carbon dioxide had an induction period of 3 hrs. This reached a maximum selectivity of 7 % after 4 hrs, which decreased to 5 % from 8hrs reaction time to completion. Higher aldehydes and alcohols consisted of the remaining products that were formed, all with selectivities < 1 %.

Figure 5.7.4. Product distribution for the $^{80}\text{Cu}_{\text{MgAlK}}$ catalyst.



Operating Conditions, $T = 573\text{ K}$, $P = 20\text{ barg}$, $\text{GHSV} = 3000\text{ hr}^{-1}$, $40\% \text{ H}_2$, $60\% \text{ CO}$.

Experiments on the ${}^8_{30}\text{Cu}_{\text{MgAlK}}$ catalyst at a GHSV of 3000 hr^{-1} were conducted (Figure 5.7.5), ethanal quickly became the main product formed within the first 10 hrs of reaction. The conversion had a value of 0.8 %. After this time period, the conversion increased only slightly to 0.85 %. The catalyst also converted a relatively large amount of CO_2 , 0.2 % after an induction period of 2 hrs. Hydrocarbons, methane, ethane and propane, were also formed, methane being formed in the largest of the three quantities with a conversion of 0.16 %. Ethane and propane were formed with conversions of 0.05 and 0.04 %, respectively. Methanal was also formed, reaching a maximum conversion of 0.08 %, decreasing to 0.06 % after 27 hrs. Higher aldehydes and ethanol are the remaining products formed, all with minute conversions.

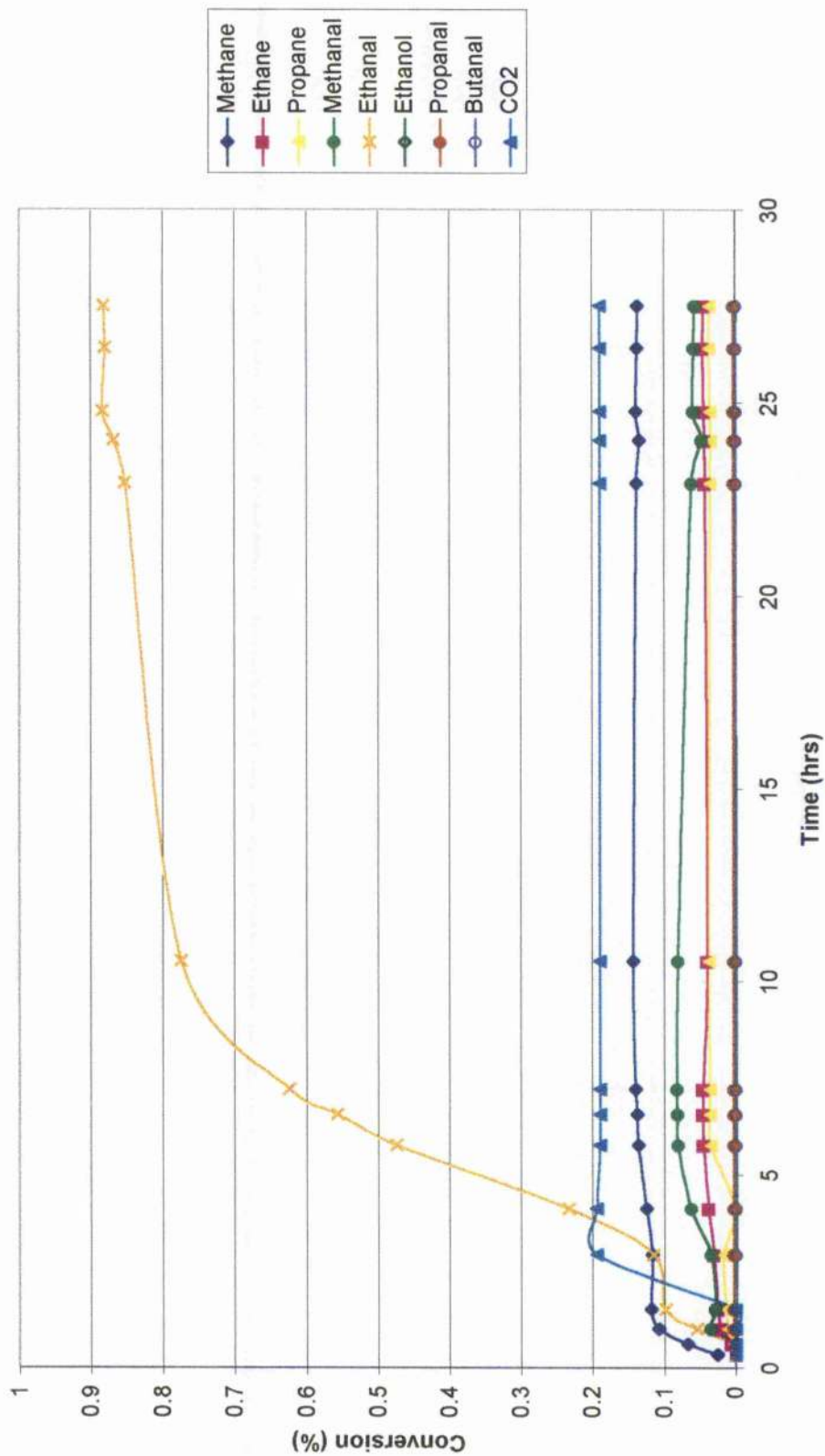
5.7.3 Effect of changes in Gasfeed Composition

Table 5.7.4. Product distribution for the ${}^8_{70}\text{Cu}_{\text{MgAlK}}$ catalyst with variation in gasfeed composition (expressed as a conversion).

Gasfeed Composition	38 % H_2 , 57 % CO , 5 % Methanol	31.7% H_2 , 63.3 % CO , 5 % Ethanol
Methane	2.1	1.2
Ethane	0.1	1.2
Propane	0.07	0.3
Methanal	1.2	0.01
Ethanal	0.06	6.0
Methanol	2.5	2.0
Ethanol	0.03	4.5
Propanal	0.03	0.13
Propan-2-ol	-	0.1
Isobutanal	0.04	-
Butan-2-ol	-	0.15
Butanal	0.04	-
Isobutanol	-	0.06
Carbon Dioxide	0.4	0.42

Operating Conditions, $T = 573 \text{ K}$, $P = 20 \text{ barg}$, $\text{GHSV} = 3000 \text{ hr}^{-1}$.

Figure 5.7.5. Product distribution for the ${}^8\text{Cu}_{10}\text{MgAlK}$ catalyst.



Operating Conditions, $T = 573\text{ K}$, $P = 20\text{ barg}$, $\text{GHSV} = 3000\text{ hr}^{-1}$, 40 % H_2 , 60 % CO .

Adding methanol or ethanol resulted in two different product distributions (Table 5.7.4). The longer chain of ethanol produced a significant quantity of ethane and ethanal with the methanol feed affecting methane and methane conversions. The propane conversion increased with ethanol in the gasfeed. Of the C₃ and C₄ products, methanol in the gasfeed produced primarily aldehydic oxygenates with the ethanol-included gasfeed converting products into alcohols. The higher alcohols were produced in larger quantities than the aldehydes. Carbon dioxide conversion was relatively unaffected.

5.7.4 Summary

Ethanal was the preferential product formed regardless of parameter variation. C₃ and C₄ aldehydes were also formed. Higher alcohols were formed without methanol being produced. The higher oxygenate formation increased with temperature and lower gas hourly space velocity. Ethanol introduction resulted in an increase in ethane and C₃₊ alcohols with methanol introduction increasing methane and C₃₊ aldehydes. Deactivation over 170 hrs was not observed.

6 Characterisation of Used Catalysts

6.1 Cu/Cr₂O₃ (50/50) (Cu_{Cr})

6.1.1 Elemental Analysis

After a microreactor reaction, the once conducted sample had a carbon content of 0.40 %, hydrogen of 0.36 %, and a non-detectable amount of nitrogen and sulfur (Table 6.1.1). On comparison to the calcined sample (Table 4.1.5), the concentration of carbon increased, whilst the remaining detectable elements decreased. The decrease in concentration of hydrogen, nitrogen and sulfur resulted from the reducing conditions used in either the catalyst reduction and/or reaction. The increase in carbon content was possibly due to carbon laydown on the catalytic surface.

Table 6.1.1.
Elemental Analysis result for the post-microreactor Cu_{Cr} catalyst.

Element	C	H	N	S
Post reaction	0.40	0.36	nda	nda

nda = non-detectable amount. Operating conditions, T = 553 K, P = 8 barg,
GHSV = 664 hr⁻¹, 65.4 % H₂, 32.6 % CO, 2 % CO₂.

6.1.2 Summary

The reaction conditions increased the carbon content but decreased the hydrogen, nitrogen and sulfur.

6.2 Cu/MgO/Al₂O₃ (60/2/38) (Cu_{Mg(2)Al})

6.2.1 Titrometry

Table 6.2.1. Conversion of reaction number to conditions for Karl Fischer Titrometry for the Cu_{Mg(2)Al} catalysts with variation in ageing time.

Catalyst Composition ageing time	Reaction Reference	Water concentration (%)
⁸ ₇₀ Cu _{Mg(2)Al}	2A	4.1
⁸ ₁₄₀ Cu _{Mg(2)Al}	2B	2.9

Operating Conditions, T = 553 K, P = 20 barg, GHSV = 5000 hr⁻¹, 36 % H₂, 54 % CO, 10 % Methanol.

Titrometry results showed that the ⁸₇₀Cu_{Mg(2)Al} catalyst produced more water than the ⁸₁₄₀Cu_{Mg(2)Al} under identical reaction conditions (Table 6.2.1). Water consisted of 4.1 % of liquid product for the former catalyst, with 2.9 % produced with the ⁸₁₄₀Cu_{Mg(2)Al} catalyst.

6.2.2 Summary

The ⁸₇₀Cu_{Mg(2)Al} catalyst produced more water than the ⁸₁₄₀Cu_{Mg(2)Al} catalyst.

6.3 Cu/MgO/Al₂O₃ (60/5/35) (Cu_{Mg(S)Al})

6.3.1 X-ray Fluorescence

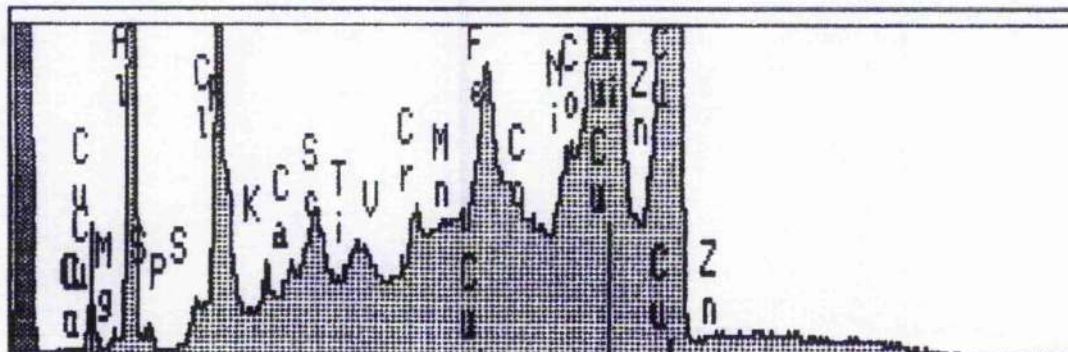
Copper K_α and K_β-line peaks and aluminium K_α-line peak are visible in Figure 6.3.1. This representative sample of a methanol-free gasfeed composition showed iron (K_α-line peak) as the main impurity. Potassium (K_α-line peak), calcium (K_α-line peak), chromium (K_α-line peak) and scandium (K_α-line peak) were also present in the sample. The magnesium K_α-line peak was very small.

The post reaction catalyst (Figure 6.3.2) gave an indication of the change in composition with methanol addition to the gasfeed. More peaks were present in the sample. Silicon was present but this was presumably from the silica wool that was used to pack the catalyst bed. The potassium, calcium, chromium and iron peaks had all increased in peak height. Manganese became visible. Iron, nickel, chromium and manganese could be from the stainless steel tube used as the catalyst bed. The calcium K_β-line peak (4.012 keV), which was almost identical to the scandium K_α-line peak so possible overlap may occur but the ratio, in this case was only about 2:1, instead of 5:1 suggests an external source.

6.3.2 Elemental Analysis

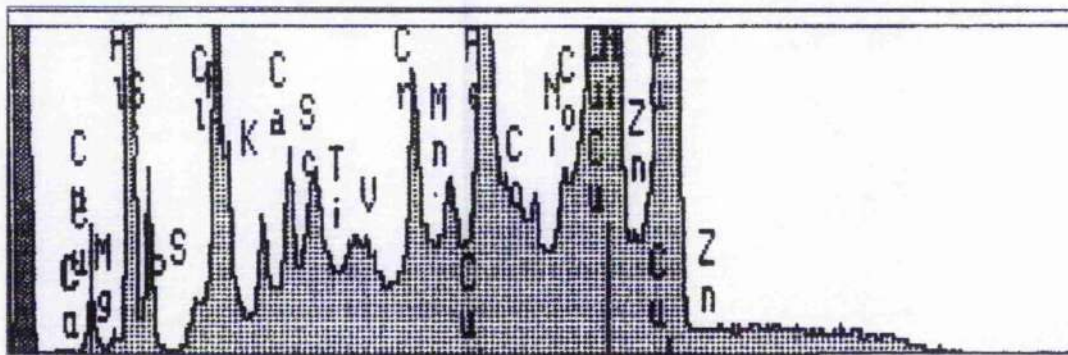
Elemental analysis experiments were conducted on the post reaction catalysts (Table 6.3.1) with operating conditions shown in Table 6.3.2. The difference in carbon content between the two ⁸₃₀Cu_{Mg(S)Al} samples, 3A and 3B, which had methanol-free and methanol gasfeed composition respectively, was considerable. The carbon in the methanol will either be adsorbed into the interlayer or on the surface in the form of carbon laydown. The hydrogen and sulfur concentrations also increased with methanol inclusion. Nitrogen was unaffected by the gasfeed composition.

Figure 6.3.1. XRF spectrum for a ${}^8{}_{70}\text{Cu}_{\text{Mg}(5)\text{Al}}$ post reaction catalyst.



Operating Conditions, P = 20 barg, T = 593 K, GHSV = 2000 hr⁻¹, 40 % H₂, 60 % CO, Reaction Duration 55 hrs.

Figure 6.3.2. XRF spectrum for a ${}^8{}_{70}\text{Cu}_{\text{Mg}(5)\text{Al}}$ post reaction catalyst.



Operating Conditions, P = 20 barg, T = 573 K, GHSV = 2000 hr⁻¹, 36 % H₂, 54 % CO, 10 % Methanol, Reaction Duration 66 hrs.

Table 6.3.1. Elemental Analysis results for the $\text{Cu}_{\text{Mg}(5)\text{Al}}$ post reaction catalysts with variation in ageing time.

Ageing Time	Reaction reference	C	H	N	S
$^8_{30}\text{Cu}_{\text{Mg}(5)\text{Al}}$	3A	2.1	0.85	0.05	nda
	3B	14.0	0.79	0.07	0.02
$^8_{70}\text{Cu}_{\text{Mg}(5)\text{Al}}$	3C	3.8	0.98	0.06	nda
	3D	2.4	1.6	0.07	nda
	3E	2.2	1.4	0.04	nda
$^8_{140}\text{Cu}_{\text{Mg}(5)\text{Al}}$	3F	4.5	1.4	0.07	nda
	3G	3.8	0.86	0.03	nda
	3H	4.9	0.61	0.02	0.09

nda = non-detectable amount, Operating Conditions - see Table 6.3.2.

Table 6.3.2. Conversion of reaction reference to conditions for the $\text{Cu}_{\text{Mg}(5)\text{Al}}$ catalysts.

Catalyst Composition (ageing time)	Reaction Reference	Gasfeed Composition $\text{H}_2:\text{CO}:\text{MeOH}$	GHSV (hr^{-1}): T (K)	Reaction duration (hrs)
$^8_{30}\text{Cu}_{\text{Mg}(5)\text{Al}}$	3A*	60:40:0	2000:*	47
	3B	36:54:10	2000:573	22
$^8_{70}\text{Cu}_{\text{Mg}(5)\text{Al}}$	3C	36:54:10	500:573	91
	3D*	*	2000:573	55
	3E	40:60:0	500:593	55
$^8_{140}\text{Cu}_{\text{Mg}(5)\text{Al}}$	3F*	60:40:0	*:553	69
	3G	36:54:10	500:593	50
	3H	36:54:10	2000:593	78

Operating Conditions, P = 20 barg, A*:- 24 hrs – 553 K, remainder 573 K, D*:- 36 % H_2 , 54 % CO, 10 % Methanol 33 hrs, remainder 40 % H_2 and 60 % CO, F* :- 24 hrs – 500 hr^{-1} , remainder 2000 hr^{-1} .

The elemental analysis results of the $^8_{70}\text{Cu}_{\text{Mg}(5)\text{Al}}$ post reaction catalysts (Table 6.3.1) showed that the carbon concentration decreased in quantity from 3C, 3D to 3E. The hydrogen concentration of 3D was greater than that of 3E and significantly greater than the 3C sample. This corresponded to the duration of which methanol was included into the gasfeed composition, sample reference 3C for 91 hrs, 3D for 20 hrs and with 3E, no methanol. Also 3D was conducted at 573 K and 3E at 593 K. Nitrogen and sulfur were unaffected by variation in the available parameters.

The $^8_{140}\text{Cu}_{\text{Mg}(5)\text{Al}}$ post reaction samples showed that the carbon concentration of 3G was considerably lower than the 3F and 3H samples but 3F had the largest hydrogen and nitrogen contents. Sulfur content of 3F and 3G was less than 3H. This was due to the increased gas hourly space velocity used in the 3G sample.

All samples were conducted only once.

6.3.3 BET surface area measurements

Table 6.3.3. BET surface area measurements for the $\text{Cu}_{\text{Mg}(5)\text{Al}}$ post reaction catalysts with variation in ageing time.

Catalyst	Reaction Reference	Single Point ($\text{m}^2 \text{g}^{-1}$)	BET surface area ($\text{m}^2 \text{g}^{-1}$)
$^8_{30}\text{Cu}_{\text{Mg}(5)\text{Al}}$	3A	46.4	48.6
	3B	34.7	44.9
$^8_{70}\text{Cu}_{\text{Mg}(5)\text{Al}}$	3C	60.7	66.5
	3E	75.2	79.4
$^8_{140}\text{Cu}_{\text{Mg}(5)\text{Al}}$	3G	57.5	65.2
	3H	47.8	51.8

Operating Conditions - see Table 6.3.2.

The BET surface area for sample 3A was greater than 3B (Table 6.3.3). In the case of 3B, this could be due to the inclusion of methanol in the gasfeed and resulting in methanol being retained on the catalyst surface. The $^8_{70}\text{Cu}_{\text{Mg}(5)\text{Al}}$ 3C sample was lower than the methanol-free sample 3E. The surface area of sample 3H was smaller than sample 3G with the gas hourly space velocity in 3H being greater.

6.3.4 Titrimetry

The water concentration of the $^8_{30}\text{Cu}_{\text{Mg}(5)\text{Al}}$ sample (3B) was same as the $^8_{70}\text{Cu}_{\text{Mg}(5)\text{Al}}$ samples, 3C and 3D (Table 6.3.4). The $^8_{140}\text{Cu}_{\text{Mg}(5)\text{Al}}$ 3G sample showed a dramatic increase in water concentration when compared to the previous samples, which could

be either the change in catalyst or the decrease in gas hourly space velocity from 2000 to 500 hr⁻¹ when compared to the previous samples.

Table 6.3.4.
Conversion of reaction number to conditions for Karl Fischer Titrometry for the Cu_{Mg(5)Al} catalysts with variation in ageing time.

Catalyst Composition (ageing time)	Reaction Reference	Water Concentration (%)
⁸ ₃₀ Cu _{Mg(5)Al}	3B	1.0
⁸ ₇₀ Cu _{Mg(5)Al}	3C	1.0
	3D	1.0
⁸ ₁₄₀ Cu _{Mg(5)Al}	3G	2.8

Operating Conditions - see Table 6.3.2.

6.3.5 Summary

More impurities visible in the XRF spectrum and an increase in the elemental analysis values with methanol introduction. It also reduced the BET surface area. Nitrogen and sulfur were unaffected with parameter variation.

6.4 Cu/MgO/Al₂O₃ (60/7/35) (Cu_{Mg(7)Al})

6.4.1 X-ray Fluorescence

The ⁸₃₀Cu_{Mg(7)Al} post reaction catalyst (Figure 6.4.1) showed copper K_α and K_β-line peaks and aluminium K_α-line peaks being easily visible, however, magnesium (K_α-line peak) cannot be observed. Iron (K_α-line peak) was present as the largest impurity concentration, calcium (K_α-line peak), chromium (K_α-line) and scandium (K_α-line) were also observed. These impurity peaks increased with ageing time and pH, which results in the ⁹₃₀Cu_{Mg(7)Al} post reaction catalyst spectrum (Figure 6.4.2). Silicon (K_α-line peak) was present in both of these spectra and will be from the silica wool used to pack the catalyst bed.

The addition of methanol into the gasfeed composition results in the representative sample (Figure 6.4.3). Copper (K_α and K_β-lines) and aluminium (K_α-line) peaks were both present. Iron (K_α-line), again, was the largest impurity. Other peaks that were present were chromium (K_α-line), scandium (K_α-line), potassium (K_α-line), calcium (K_α-line), manganese (K_α-line) and possibly nickel (K_α-line). The peak heights of the impurities in this sample were larger than the methanol-free synthesis gas spectra.

Addition of the chromium filter resulted in no chlorine being observed in these spectra.

6.4.2 Elemental Analysis

The carbon content for reaction references 4A and 4B increased in concentration with the mole fraction of carbon on the gasfeed composition (Table 6.4.1 and 6.4.2). However, increasing the concentration of carbon in the gasfeed composition further

Figure 6.4.1. XRF spectrum for a $^{80}\text{Cu}_{\text{Mg}(7)\text{Al}}$ post reaction catalyst.

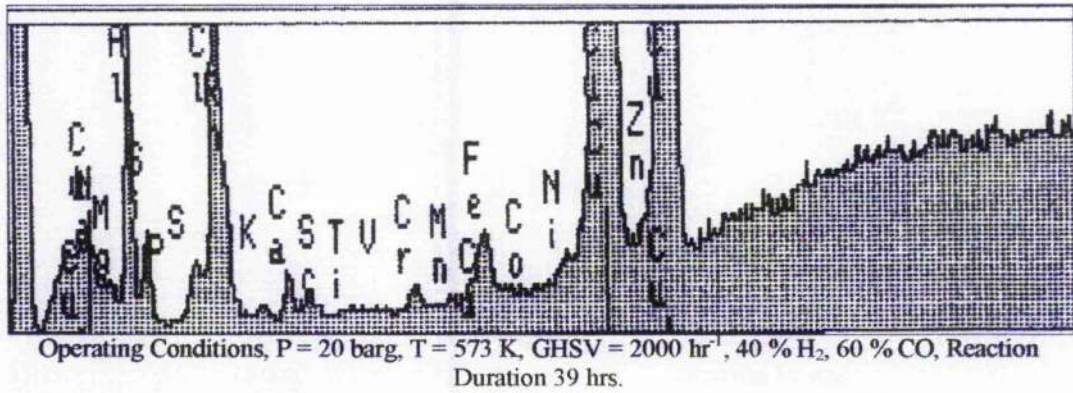


Figure 6.4.2. XRF spectrum for a $^{90}\text{Cu}_{\text{Mg}(7)\text{Al}}$ post reaction catalyst.

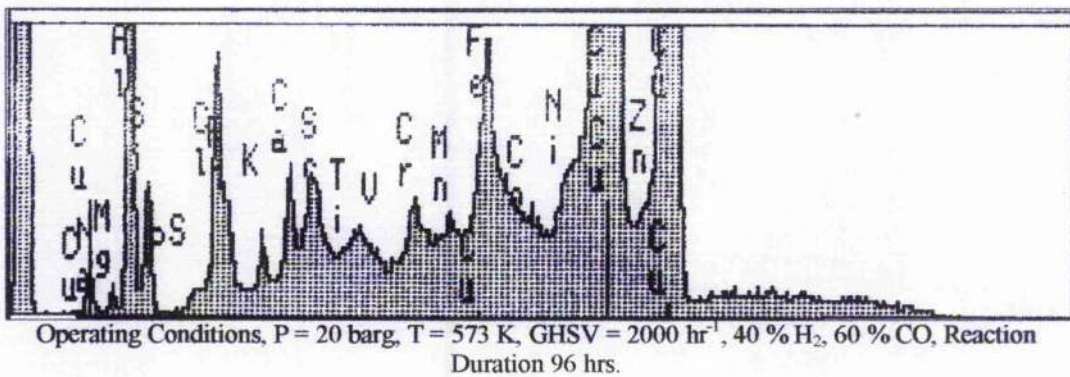
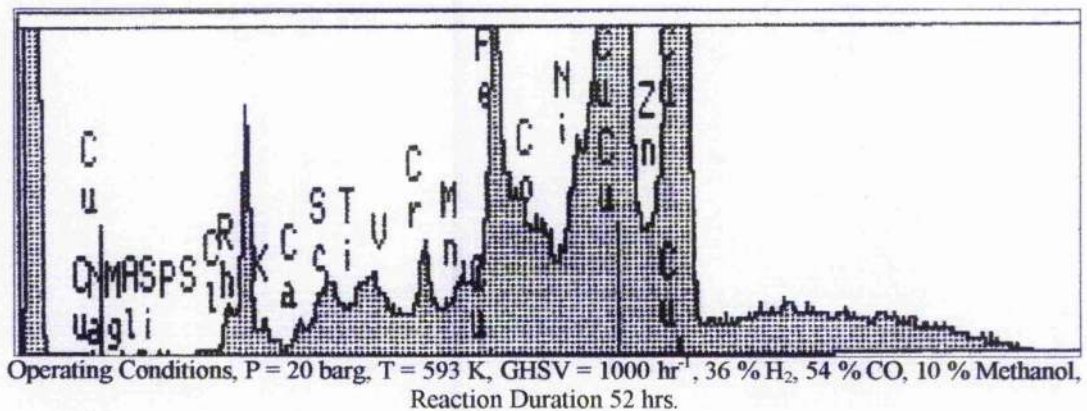


Figure 6.4.3. XRF spectrum for a $^{80}\text{Cu}_{\text{Mg}(7)\text{Al}}$ post reaction catalyst.



(Reaction Reference 4C) decreased the carbon content value. The hydrogen content increased with reaction temperature from 573 to 593 K, with the larger quantity of hydrogen being found when methanol was included in the gasfeed composition. The nitrogen concentration was greater at the lower reaction temperature. Little sulfur was detected.

Table 6.4.1. Elemental Analysis results for the $\text{Cu}_{\text{Mg}(7)\text{Al}}$ post reaction catalysts with variation in preparation conditions.

Ageing Time	Reaction Reference	C	H	N	S
$^{8}_{30}\text{Cu}_{\text{Mg}(7)\text{Al}}$	4A	2.7	0.15	0.16	0.01
	4B	3.0	0.91	0.03	nda
	4C	1.7	0.59	0.03	nda
$^{8}_{70}\text{Cu}_{\text{Mg}(7)\text{Al}}$	4D	2.2	0.95	0.03	0.01
	4E	3.6	1.1	0.05	nda
$^{8}_{140}\text{Cu}_{\text{Mg}(7)\text{Al}}$	4F	1.9	0.83	0.03	nda
	4G	1.9	0.78	0.03	nda
	4H	3.1	0.94	0.07	nda
	4I	2.2	0.86	0.07	nda
$^{9}_{30}\text{Cu}_{\text{Mg}(7)\text{Al}}$	4J	2.7	1.3	0.04	nda

nda = non-detectable amount, Operating Conditions - see Table 6.4.2.

The carbon content of the $^{8}_{70}\text{Cu}_{\text{Mg}(7)\text{Al}}$ catalysts, 4D and 4E, increased with methanol inclusion into the gasfeed and reaction temperature and duration. These changes in parameters had only a smaller effect on the hydrogen concentration. The nitrogen content increased and the sulfur decreased from reaction reference 4D to 4E.

The $^{8}_{140}\text{Cu}_{\text{Mg}(7)\text{Al}}$ post reaction catalysts, 4F and 4G gave a similar concentrations of carbon. Both the hydrogen and the nitrogen concentrations in 4F were larger than 4G, with sulfur being non-detectable. Although the reaction conditions for reaction references 4G and 4H were similar, the concentrations of carbon, hydrogen and nitrogen were considerably larger, especially for the carbon and nitrogen values but the durations of these reactions were different. Sulfur was non-

detectable.

The carbon and hydrogen concentrations increased from 4I to 4J with methanol included in reaction reference 4J. Nitrogen was unaffected. Sulfur was non-detectable. The post reaction samples were conducted only once.

Table 6.4.2. Conversion of reaction reference to conditions for the $\text{Cu}_{\text{Mg}(7)\text{Al}}$ catalysts.

Catalyst Composition (ageing time)	Reaction Reference	Gasfeed Composition $\text{H}_2:\text{CO}:\text{MeOH}$	GHSV (hr^{-1}) : T (K)	Reaction duration (hrs)
$^8_{30}\text{Cu}_{\text{Mg}(7)\text{Al}}$	4A	40:60:0	2000:573	39
	4B	36:54:10	2000:593	100
	4C	30:70:0	2000:593	100
$^8_{70}\text{Cu}_{\text{Mg}(7)\text{Al}}$	4D	40:60:10	2000:573	51
	4E	36:54:10	2000:593	74
$^8_{140}\text{Cu}_{\text{Mg}(7)\text{Al}}$	4F*	40:60:0	2000:*	100
	4G	36:54:10	2000:593	98
	4H	36:54:10	2000:573	97
$^9_{30}\text{Cu}_{\text{Mg}(7)\text{Al}}$	4I	40:60:0	2000:573	96
	4J	36:54:10	2000:593	101

Operating Conditions, P = 20 barg, F* :- 56 hrs at 573 K, 78 hrs at 593 K, remainder 613 K.

6.4.3 BET surface area measurements

Table 6.4.3. BET surface area measurements for the $\text{Cu}_{\text{Mg}(7)\text{Al}}$ post reaction catalysts with variation in preparation conditions.

Catalyst	Reaction Reference	Single Point ($\text{m}^2 \text{g}^{-1}$)	BET surface area ($\text{m}^2 \text{g}^{-1}$)
$^8_{30}\text{Cu}_{\text{Mg}(7)\text{Al}}$	4B	28.4	30.3
	4C	24.2	25.6
$^8_{70}\text{Cu}_{\text{Mg}(7)\text{Al}}$	4D	38.5	39.8
	4E	41.8	43.9
$^8_{140}\text{Cu}_{\text{Mg}(7)\text{Al}}$	4F	38.7	40.8
$^9_{30}\text{Cu}_{\text{Mg}(7)\text{Al}}$	4I	45.3	48.7
	4J	42.0	44.0

Operating Conditions - see Table 6.4.2.

The reaction reference 4B was greater than that of 4C (Table 6.4.3), which could be

due to the larger mole fraction of carbon in the gasfeed composition. The increased reaction temperature and methanol inclusion did not decrease the surface area in reaction references 4D and 4E. Reaction reference 4F had a BET surface area of $40.8 \text{ m}^2 \text{ g}^{-1}$. The BET surface area of 4H was larger than 4I, which could be due to the lower reaction temperature and methanol omission.

6.4.4 Titrimetry

Table 6.4.4. Conversion of reaction number to conditions for Karl Fischer Titrimetry for the $\text{Cu}_{\text{Mg}(7)\text{Al}}$ catalysts with variation in preparation conditions.

Catalyst Composition (ageing time)	Reaction Reference	Water Concentration (%)
$^8_{30}\text{Cu}_{\text{Mg}(7)\text{Al}}$	4B	1.0
$^8_{70}\text{Cu}_{\text{Mg}(7)\text{Al}}$	4E	0.3
$^8_{140}\text{Cu}_{\text{Mg}(7)\text{Al}}$	4H	0.4
$^9_{30}\text{Cu}_{\text{Mg}(7)\text{Al}}$	4J	1.0

Operating Conditions - see Table 6.4.2.

The pH = 8 and $^9_{30}\text{Cu}_{\text{Mg}(7)\text{Al}}$ catalysts produced similar water concentration in the exit gasfeed composition with a value of 1.0 % (Table 6.4.4). The two remaining catalysts, the $^8_{70}\text{Cu}_{\text{Mg}(7)\text{Al}}$ and $^8_{140}\text{Cu}_{\text{Mg}(7)\text{Al}}$ catalysts, showed water concentrations significantly lower than the two other samples, with the latter having a value of only 0.3 %. The reaction conditions were almost identical, reaction reference 4H was conducted at 573 K while the remainder were performed at 593 K.

6.4.5 Summary

More impurities present with increased ageing time. Elemental analysis results increased with methanol introduction and temperature, which decreased the BET surface area. Shorter ageing times produced more water.

6.5 K/Cu/MgO/Al₂O₃ (K60/7/35) (Cu_{MgAlK})

6.5.1 Elemental Analysis

Table 6.5.1. Elemental Analysis results for the Cu_{MgAlK} post reaction catalysts with variation in preparation conditions.

Ageing Time	Reaction Reference	C	H	N	S
⁸ ₃₀ Cu _{MgAlK}	5A	1.6	0.7	nda	nda
	5B	2.2	1.1	nda	0.01
⁸ ₇₀ Cu _{MgAlK}	5C	2.0	1.2	nda	0.01
	5D	2.7	1.5	nda	0.01
⁸ ₁₄₀ Cu _{MgAlK}	5E	1.9	1.0	nda	0.01
	5F	3.0	0.89	nda	0.01
⁹ ₃₀ Cu _{MgAlK}	5G	2.2	0.88	nda	0.01

nda = non-detectable amount, Operating Conditions - see Table 6.5.2.

Looking at the elemental analysis results for the ⁸₃₀Cu_{MgAlK} post reaction catalysts, reaction references 5A and 5B (Table 6.5.1), increasing the reaction duration (Table 6.5.2), increased the carbon and hydrogen content from 1.6 % to 2.2 % and 0.70 % to 1.1 % respectively. The sulfur concentration increased slightly.

The ⁸₇₀Cu_{MgAlK} post reaction catalysts results increased in carbon and hydrogen concentrations from 5C to 5D. This showed that on this occasion including methanol into the feedgas composition did not increase the carbon and hydrogen concentration. Nitrogen and sulfur were unaffected.

The inclusion of ethanol in the feedgas for reaction references, 5E and 5F, increased the carbon content. The hydrogen value decreased from 5E to 5F with sulfur being unaffected.

The ⁹₃₀Cu_{MgAlK} post reaction catalyst, reaction reference 5G had a carbon content of 2.2 %, a hydrogen concentration of 0.88 % and sulfur value of 0.01 %.

Nitrogen was not detected in any post reactions catalyst sample.

Table 6.5.2. Conversion of reaction reference to conditions for Cu_{MgAlK} catalysts.

Catalyst Composition (aging time)	Reaction Reference	Gasfeed Composition $\text{H}_2:\text{CO}:\text{MeOH}$	GHSV (hr^{-1}) : T (K)	Reaction duration (hrs)
$^8_{30}\text{Cu}_{\text{MgAlK}}$	5A	40:60:0	1000:573	29
	5B	40:60:0	1000:573	169
$^8_{70}\text{Cu}_{\text{MgAlK}}$	5C*	*	1000:573	27
	5D	40:60:0	1000:573	33
$^8_{140}\text{Cu}_{\text{MgAlK}}$	5E*	40:60:0	1000:*	98
	5F*	*	3000:573	25
$^9_{30}\text{Cu}_{\text{MgAlK}}$	5G	40:60:0	1000:573	25

Operating Conditions, P = 20 barg, C* :- 40 % H_2 , 60 % for 6 hrs remainder 36 % H_2 , 54 % CO, 10 % Methanol. E* :- 573 K for 79 hrs remainder 623 K, F* :- 31.7 % H_2 , 63.3 % CO, 5 % Ethanol.

6.5.2 BET surface area measurements

Table 6.5.3. BET surface area measurements for the Cu_{MgAlK} post reaction catalysts with variation in preparation conditions.

Catalyst	Reaction Reference	Single Point ($\text{m}^2 \text{g}^{-1}$)	BET surface area ($\text{m}^2 \text{g}^{-1}$)
$^8_{30}\text{Cu}_{\text{MgAlK}}$	5A	21.5	22.5
$^8_{70}\text{Cu}_{\text{MgAlK}}$	5C	58.8	30.0
	5D	32.9	34.3
$^8_{140}\text{Cu}_{\text{MgAlK}}$	5E	28.4	29.1
	5F	31.2	33.0
$^9_{30}\text{Cu}_{\text{MgAlK}}$	5G	21.3	21.6

Operating conditions - see Table 6.5.2.

The BET surface area measurement for reaction reference, 5A (Table 6.5.3) had a value of $22.5 \text{ m}^2 \text{g}^{-1}$.

Of the $^8_{70}\text{Cu}_{\text{MgAlK}}$ post reaction catalysts, 5C and 5D, 5C had methanol included into the gasfeed. Reaction reference 5D had the largest surface area of any sample of this series of catalyst. Reaction references, 5E and 5F, the former had the lower surface area, which could be due to the more elevated reaction temperature of 623 K.

The ${}^9_{30}\text{Cu}_{\text{MgAlK}}$ post reaction catalyst, 5G, had a BET surface area measurement of $21.6 \text{ m}^2 \text{ g}^{-1}$, which had the lowest value of any of the post reaction samples of this series of catalyst.

6.5.3 Summary

The carbon and hydrogen content increased with reaction duration and ethanol introduction. The nitrogen and sulfur contents were unaffected. A greater loss in BET surface area was observed with shorter ageing times.

7.1 Preparation and Characterisation of Catalyst Precursors

The chromium in the Cu_{Cr} catalyst gave completely different characterisation results when compared with those obtained with the tertiary Mg and Al-based catalysts. Whilst the latter catalysts showed an initial hydrotalcite-like phase, the Cu_{Cr} phase was structurally different, which is in agreement with the observations of Capece *et al* [231] and Cavani *et al* [175]. The calcined Cu_{Cr} sample formed a poorly crystalline $\text{CuCr}_2\text{O}_7 \cdot 2\text{H}_2\text{O}$ [219] phase. Capece *et al* [231] and Johansson and Lundin [232] found similar structures, CuCr_2O_4 and $\text{Cu}_2\text{Cr}_2\text{O}_4$ respectively. It is likely that the remaining copper atom required to ensure a Cu:Cr ratio of 1:1 was probably present as CuO. The TPR data indicated increased copper structural stability with the introduction of chromium, as the copper component reduced at a higher temperature than bulk CuO, which was also observed with Laine and Brito [233]. The copper surface area of the Cu_{Cr} catalyst was slightly smaller than the values of between 7 and $17 \text{ m}^2 \text{ g}^{-1}$ by Prasad [234].

For preparation of the Mg and Al included precursors, the extremes of the pH preparation range examined gave crystallographic phases, which were either heterophasic or the undesired phase. A pH = 8 proved optimum for the hydrotalcite-like phase, which was consistent with the findings of Auer *et al* [235]. The control of the pH is the most important factor since deviation from pH = 8 resulted in increased dissolution of the individual metal components during the ageing process. This dissolution problem is a reflection of the solubility products of the hydroxides, $\text{Al}(\text{OH})_3$ at pH = 5.8, $\text{Cu}(\text{OH})_2$ pH = 8.3 and $\text{Mg}(\text{OH})_2$ pH = 10.3. The inherently unstable nature of the copper hydroxycarbonate was also observed by the formation of

CuO, as previously reported by Cornthwaite [40]. During the preparation process, copper preferentially precipitates as malachite, which was observed on many occasions with this study, and the presence of magnesium forces it to enter into ternary precursors, which was observed elsewhere [236]. However, hydrotalcite-like structures were formed with the $^9\text{Cu}_{\text{Al}}$ and $^{10}\text{Cu}_{\text{Al}}$ catalysts, both of which are binary. The $\text{Cu}_6\text{Al}_2(\text{OH})_{16}\text{CO}_3 \cdot 4\text{H}_2\text{O}$ [227] phase was not ageing time dependent, indicating that the preparation conditions used in the present work were the crucial factor in forming this analogous structure.

Dissolution of the metal components also occurred with lengthening precursor ageing time, thus the shorter ageing times gave catalysts with a composition closer to the theoretically expected ratio. This is contrary to the observations of Villa and Lietti [52], who found the opposite occurred over the same time period when forming a $\text{ZnO}/\text{Cr}_2\text{O}_3$ catalyst, although different components from those used in the present study are involved. Nevertheless, this study and Villa and Lietti's work [52] concur with the concept that both temperature and pH influence the aluminium solubility [187].

The seemingly subtle difference of varying the ageing time usually resulted in large changes in structural characterisation and has been confirmed in work by Auer *et al* [235]. This was clearly observed in the TPR profiles as the reduction temperature of the copper varied by as much as 200-300 K from the start to the completion of reduction, however, this disparity makes the atomic structural arrangement of copper difficult to replicate. Auer *et al* [235], Pease and Taylor [237] and John [238] have also observed this variation in reduction temperature. Varying numbers of reduction peaks was also observed here and with work by Fornasari *et al* [239].

Magnesium introduction had a definite effect on the structural stability of the catalyst precursor. In general, increase in magnesium concentration resulted in an increase in the copper reduction temperature and greater crystallinity but no trend with these factors was observed with increasing ageing time. Baker *et al* [194] also found that increasing the concentration increased crystallinity, the addition of Mg^{2+} stabilising the hydrotalcite-type phase and stimulating its formation [199]. No change in the d-spacing values was observed between precursors. The increase in magnesium concentration also increased the calcination temperature required for decomposition and subsequent copper reduction temperature. Xu *et al* [87] found that the Mg^{2+} strengthened the Cu-O bonds, which may explain these observations. However, Xu *et al* [87] also concluded that it weakened the Cu-Cu bonds.

In general, the BET surface area of the ternary phase catalysts formed in this work decreased with increasing magnesium concentration, however, little difference was observed in copper surface area. Hence, the aluminium concentration is the more important contributor towards the surface area when compared to magnesium, which is apparent with the binary Cu_{Al} and Cu_{Mg} catalysts, even with the former having longer range order.

It is interesting to note that the $Cu_{Mg(10)Al}$ catalysts gave TPR profiles that were different in contour from those obtained with the other ternary catalyst precursors. A very large decrease in BET surface area with increasing calcination temperature from 623 K to 873 K was also found with the different precursor phase that was formed (Table 4.2.9), which on increasing calcination changed to a different Al_2O_3 phase [240]. This is contrary to the work of Auer *et al* [235], who found that the BET surface area of the sample calcined at 873 K was significantly higher than those

catalysts calcined at lower temperatures. However, this is almost certainly due to the different crystallite phases that were formed in the two studies.

The inclusion of the potassium resulted in a reformation of the hydrotalcite-type phase precursor. This was due to the incomplete decomposition of the hydroxycarbonate prior to doping as suggested by Nunan *et al* [241]. This effect, referred to as the "memory effect" by Sato *et al* [181], also resulted in a slight increase in crystallinity of the hydrotalcite-like phase, which has been also observed by Nunan *et al* [124]. No modification in the physical characteristics were revealed by the TPR profiles, therefore, it is unlikely that any structural rearrangement within the brucite-like layers had occurred during the wet-impregnation process. It may have been anticipated that these secondary preparation conditions would have resulted in a decrease in copper dispersion due to the recalcination process, as suggested by Xu *et al* [87] and Nunan *et al* [124]. However, the wet-impregnation and subsequent recalcination process resulted in a slight increase in copper dispersion and copper and BET surface areas. This is due to the continued decomposition of the hydrotalcite-type phase by possibly removing the remaining nitrogen present as nitrates, as suggested by Myers *et al* [242], as there was little or no loss in the carbon or hydrogen content observed in the elemental analysis. Also, surface potassium is known to hinder complete reduction to copper metal by retaining copper as Cu(I) present in the form of CuKCO_3 after calcination [243]. Measurement of the copper dispersion relies on surface copper to copper metal reduction. Therefore, this would naturally decrease the copper dispersion. An additional effect would be the potassium blocking surface copper sites. The potassium is definitely present on the surface as it is too large to be incorporated inside the hydrotalcite-like structure [244] but crystal phases of bulk $\text{K}_2\text{Cr}_2\text{O}_7$ have been detected on Cu/ZnO/Cr₂O₃ catalysts [245]. The alkali dispersion is

known to be sensitive to the details of the impregnation procedure [246], but as no appropriate analysis was conducted on these samples to determine the positioning of the potassium atoms, it is unrealistic to assume that the potassium was solely bonded to the copper or exists as potassium oxides or carbonate particles.

Robinson and Mol [247] found that their largest dispersion for a potassium-promoted-copper catalyst was obtained with a sample that was calcined at 1100 K, the potassium present in concentrations of between 4 and 8 wt %. This suggests that the removal of residual components or decomposition of the hydrotalcite-like structure determine the dispersion. It is fair to say, however, that no conglomeration of the inherently sintering copper particles in the hydrotalcite-type phase occurred, therefore, the structure was stable.

Overall, the pH was the single most important factor for the formation of the correct phase. However, the ageing time is important for the finer details. This is a different order to that suggested by Baker *et al* [194] whose work put ageing time as the most important factor.

7.2 Microreactor Experiments

It is evident from the results quoted in section 5 that varying the catalyst resulted in different product distributions. As expected, variations in microreactor conditions, for example, temperature, gas hourly space velocity, gas feed composition and pressure also led to different product distributions and conversions.

7.2.1 Cu/Cr₂O₃ (50/50) (Cu_{Cr})

Copper chromite was originally chosen as it has already proved to be an active for hydrogenation reactions on dienes and for CO oxidation [248]. The Cu_{Cr} catalyst showed that higher alcohol formation was possible under "methanol-preferential" conditions. These initial conditions formed ethanol and propan-1-ol but no propan-2-ol. As these operating conditions formed higher alcohols, they were initially used as the starting point to assess the activity of the rest of the catalysts.

Increasing the temperature above 553 K resulted in the formation of propan-2-ol and also increased the overall higher alcohol selectivity, in agreement with Forzatti *et al* [4]. Propan-2-ol was formed in larger quantities than propan-1-ol. Therefore, under these more elevated temperature conditions, the catalyst exhibited a product distribution preferential of a high temperature methanol synthesis catalyst [6]. An increase in temperature also resulted in a decrease in methanol selectivity, which is a thermodynamic effect, as the reaction tends towards equilibrium under the operating conditions used [89]. Methanol formation was dramatically reduced by a factor of two when CO₂ was removed from the input gasfeed.

Introduction of methanol into the input gasfeed resulted in an increase in ethanol selectivity, but little increase in the propan-1-ol yield suggesting that the mechanism for formation of higher alcohols is likely to be sequential with their

formation resulting from secondary reactions, which is in agreement with Nunan *et al* [124]. The formation of methanol being faster than the formation of alcohols, as an increase in higher alcohol selectivity was also observed with decreasing gas hourly space velocity due to the lower contact time. This effect was very apparent in the formation of propan-1-ol, the product not being detected above a GHSV of 1330 hr⁻¹ (Table 5.2.2).

Increase in the CO concentration to 40 % increased the higher alcohol formation (Table 5.2.3), concurring with Tronconi *et al* [49] and Smith *et al* [43]. This would be anticipated from the larger quantity of carbon present in the gasfeed causing a greater likelihood of chain growth. However, further increase in CO concentration to 50 % in the input gasfeed slightly decreased the methanol conversion but also resulted in an increase in DME formation. This may suggest that the methanol and DME may be mechanistically related with this catalyst. A possible DME mechanistic route is by dehydration of two methanol molecules, which is also in agreement with Matulewicz [171]. The increased CO concentration results in a greater quantity of carbon being available for conversion. Methane was also increased with the decrease in methanol conversion. Formation of DME and methane suggests that Brønsted acidity was present on the catalyst surface. The DME and methane were presumably formed on the chromium surface, as chromium is more acidic than copper. However, it is known [249] that metallic copper can dissociate CO on adsorption above 373 K.

At higher gas hourly space velocities (4000+ hr⁻¹), the alcohols selectivity decreased, which resulted in a great increase in hydrocarbons, which is in agreement with Chaumette *et al* [66]. The three main products formed with Figure 5.2.3 were all hydrocarbons, methane, ethane and propane, which suggests that hydrocarbon

formation is less affected by change in the GHSV than higher alcohols formation. Methanal was also formed during this reaction with 8-9 % selectivity, which suggests that its formation is favoured at increased GHSV as the compound was undetected at lower GHSV.

Carbon dioxide was detected in most reactions, which suggests an active WGS reaction. This would explain the low higher alcohol formation, as water is known to inhibit higher alcohol formation [92] because of its competitive adsorption with C_1 oxygenated intermediates for catalyst active sites [100], suggesting that different adsorption sites are being utilised with higher alcohols and hydrocarbons, as also suggested by Bardet *et al* [250]. Both copper or chromium are likely to be responsible for the WGS reaction, since the high temperature WGS reaction occurs on Cr_2O_3 -supported catalysts [153] and the low temperature WGS is catalysed by Cu-based systems [151].

As a partially defective spinel ($CuCr_2O_7 \cdot H_2O$) was formed during the catalyst preparation, rather than actual discrete CuO and Cr_2O_3 particles, intimate mixing of copper and chromium had occurred. However, it does not completely exclude CuO and Cr_2O_3 particle formation, as their size may be below XRD detection limits, which would explain nitrous oxide chemisorption results. Johansson and Lundin [232] ascribed the catalytically active sites as a combination of Cu and $Cu_2Cr_2O_4$, both of which are possible considering the stoichiometry of the catalyst and N_2O chemisorption results; the copper contributing a larger proportion than chromium towards the overall surface area due to the difference in BET and Cu results. Laine and Brito [233] proposed a Cu-surface enrichment phenomenon where Cu migrated from the bulk to the surface and copper preferentially generated oxygen vacancies rather than Cr. Another suggestion for the active site was speculated by Burch *et al*

[251], who suggested that it could be a cation of a support, for example, Cr^{3+} or the cation of the metallic element of the catalyst (Cu^+) and stabilised by the promoter or the support. Hydrogen would be supplied as H_{ads} by migration from the Cu^0 surface. Some authors [9,252] refer to the pair of active centres as a “bifunctional” mechanism, for example, $\text{Cu}^0\text{-Cu}^+$. Both suggestions for the active site are equally likely.

Deactivation of the catalytic activity with increased time online was observed, which may be attributed to either copper sintering or carbon laydown. Copper sintering is inherent at temperatures above 543 K [27] and post reaction elemental analysis confirmed an increase in carbon concentration, which in turn blocked active sites. The observation that the production of both methane and DME, which are likely to form on Cr, and methanol, which is likely to form on Cu, all decrease with time on stream suggesting that carbon laydown may be a more likely source of deactivation. Coke formation is known to increase at higher CO concentrations [6]. Deactivation of FT-based HAS catalysts is reported [65] to be caused by surface carbides. The Boudouard reaction has been found to occur on these catalysts with the formation of graphitic carbon, CO_2 , $-(\text{CH}_x)_n$ - and H_2O [253]. Poisoning by sulfur can be discounted as post-reaction elemental analysis confirmed its exclusion from the catalyst.

7.2.2 Cu/MgO/Al₂O₃ (50/10/40) ($\text{Cu}_{\text{Mg(10)Al}}$)

In order to reduce the hydrocarbon and DMF conversions, the $\text{Cu}_{\text{Mg(10)Al}}$ catalyst was investigated. This was to be done by increasing the basicity of the catalyst. However, the introduction of the basic and more stable magnesium and the change of chromium for aluminium resulted in an overall decrease in activity. The conversion to methane, ethane, propane and methanol were generally considerably lower than with the Cu_{Cr} catalyst. This inactivity occurred regardless of variation of reaction temperature,

pressure, GHSV, gasfeed and regardless of calcination temperature. The lower calcined catalyst of the $^{73}\text{Cu}_{\text{Mg}(10)\text{Al}}$ samples was the most active.

No methanol was formed in any of the reactions with this catalyst, which would suggest that the catalyst was inactive for subsequent higher alcohol formation, as methanol production was seen as the main starting point for their formation, this assumption proved to be correct. As methanol is most likely to be formed on the copper surface [35], it is not surprising that the catalyst was inactive towards methanol and subsequent higher alcohol production from the low copper percentage detected by AAS. Höppener *et al* [199] found that if the copper concentration increased, the overall alcohol production also increased.

The low copper concentration may also explain the low formation of methanol from hydrogenation of CO. No CO_2 was detected indicating that little or no condensation reactions occur or an inactive Cu-based WGS reaction [151].

Methane was the most selective product with all of the reactions conducted over the $^{73}\text{Cu}_{\text{Mg}(10)\text{Al}}$ catalysts (623 K and 873 K), ethane and propane were also formed. The hydrocarbon activity suggests that their formation occurred preferentially on the aluminium component [87] because of the large BET surface area ($641 \text{ m}^2 \text{ g}^{-1}$). The copper activity would be expected to be comparatively small, as the N_2O chemisorption results gave a very small Cu surface area and magnesium is known to be relatively inactive [199]. Clausen *et al* [254] indicated that aluminium addition leads to drastic changes in the local surroundings of the other atoms, which may partly explain the decrease in activity by reducing the number of active sites on the surface with the change in catalyst and calcination temperature. Other literature work [64] concluded that the formation of light hydrocarbons is not structure sensitive, however, this is not the case with this catalyst as the precursor that was calcined at a higher temperature

(873 K) had a considerably smaller BET surface area and subsequent lower activity. Methanal formation was also a structure-sensitive reaction as the conversion decreased with decrease in surface area. The precursor characterisation showed no differences between the two calcined samples.

The $^{730}Cu_{Mg(10)Al}$ catalyst was the most inactive from the $Cu_{Mg(10)Al}$ series. This was probably due to the preparation procedure, as the precursor formed was not homogenous with three different XRD crystallographic phases being detected in the precursor. Also, the $^{730}Cu_{Mg(10)Al}$ precursor had particle diameters that were visibly larger than the $^{730}Cu_{Mg(10)Al}$ samples. These points highlight the importance of the precipitation procedure.

The alcohol inactivity of this catalyst series may be due to several reasons, the main reason being the incomplete co-precipitation of the three metal components, which was determined by the preparation conditions of the precursor. This gave a different metal ratio than the theoretical, which probably resulted in the undesired crystallographic phase that was detected being formed. The low copper ratio gave small copper surface areas, which diminished the activity of the structure sensitive reactions.

7.2.3 Cu/MgO/Al₂O₃ (60/2/38) ($Cu_{Mg(2)Al}$)

Lowering the magnesium concentration and increasing the copper concentration resulted in an increase in the overall activity of all catalysts but still resulted in large amounts of hydrocarbons being formed. This was particularly evident for the $^{8140}Cu_{Mg(2)Al}$ catalyst as hydrocarbons constituted over a third of the products formed under the preferred methanol forming conditions [3]. The hydrocarbon selectivity was still lower than the $Cu_{Mg(10)Al}$ catalyst series.

The ${}^8_{70}\text{Cu}_{\text{Mg}(2)\text{Al}}$ catalyst was the most active for the formation of methanol and also produced the least quantity of CO_2 , which is advantageous considering CO_2 preferentially forms low molecular weight products [4]. Figure 5.4.2 showed 50 % selectivity towards methanol, which was a significant increase in compared to the $\text{Cu}_{\text{Mg}(10)\text{Al}}$ catalysts.

Addition of methanol to the input gasfeed produced higher alcohols. Ethanol and propan-1-ol were formed in largest quantities at 593 K, which was the highest temperature used. However, for propan-2-ol formation 573 K was the most productive temperature. Overall, propan-1-ol was produced in greater quantities than propan-2-ol, therefore, one can assume that straight chained alcohols are the preferential formation path for this catalyst series because the activation energy is lower to form primary rather than secondary alcohols [43].

Ethanol was formed in substantially greater quantities than any other higher alcohol, supporting the theory that chain growth is sequential, as C_n addition (methanol) increased C_{n+1} and some C_{n+2} yields, which is in agreement with work by Smith and Anderson [98]. This may also indicate that methanol and ethanol formation were from a common intermediate, agreeing with proposals by Elliott and Pennella [125]. Campos-Martín *et al* [46] suggested two primary homologation routes from methanol addition, reaction with H_2 and CO ($\text{CH}_3\text{OH} + \text{CO} + \text{H}_2 \rightleftharpoons \text{C}_2\text{H}_5\text{OH} + \text{H}_2\text{O}$) and coupling of two methanol molecules ($2\text{CH}_3\text{OH} \rightleftharpoons \text{C}_2\text{H}_5\text{OH} + \text{H}_2\text{O}$), both of which are possible with these catalysts. However, both proposed reactions produce water, which would inhibit the HAS [92], especially as the extent of the WGS reaction determines the apparent stoichiometry of the alcohol formation [88].

No overall correlation can be attached between Cu surface areas and alcohol productivities if their formation occurs solely on copper [35], as the ${}^8_{70}\text{Cu}_{\text{Mg}(2)\text{Al}}$

catalyst, the most active for alcohol formation, did not have the largest copper surface area when compared to the other two catalysts in the series, which was a similar observation as Robinson and Mol [247] and Robbins *et al* [255] but dissimilar to Denise *et al* [111,256]. The ${}^8_{70}\text{Cu}_{\text{Mg}(2)\text{Al}}$ catalyst did have the highest maximum surface reduction temperature, which might also be important.

The ${}^8_{70}\text{Cu}_{\text{Mg}(2)\text{Al}}$ catalyst contained the most carbon prior to reaction, which increased after reaction. This was probably present as a carbidic overlayer and may also aid the formation of higher alcohols. Lee *et al* [253] observed the Boudouard reaction over these catalysts with the formation of graphitic carbon, CO_2 , $-(\text{CH}_x)_n$ - and H_2O . However, this is in disagreement with Herman *et al* [36], who suggested that the surface of the working catalyst is free from carbon both in the presence or absence of CO_2 in the input gasfeed.

Hydrocarbon production increased dramatically when CO_2 was removed from the input gasfeed, which is in agreement with results of Tronconi *et al* [89]. This may be due to the CO_2 blocking active sites for hydrocarbon formation. The DME conversion only increased slightly, even though the methanol production decreased significantly, therefore, the DME and methanol mechanisms are not mutually exclusively related. Xiaoding *et al* [6] has observed that increasing the pressure or magnesium concentration could reduce the hydrocarbon and DME production, but this can be detrimental to the alcohol activity [199]. The magnesium content increases the basicity of the catalytic sites [87] by suppressing the acidity of the aluminium to reduce DME and hydrocarbon production in a manner similar to the effects of zinc in the industrial low temperature methanol synthesis catalyst [37].

Carbon dioxide was also formed in large quantities, with the ${}^8_{30}\text{Cu}_{\text{Mg}(2)\text{Al}}$ catalyst producing most from the series. The WGS reaction is the likely source of

CO₂, especially at the operating conditions used as the WGS reaction is nearing equilibrium [89]. As this catalyst produced more CO₂ than the ⁸₇₀Cu_{Mg(2)Al} catalyst, it can be concluded that the WGS reaction is not structure sensitive over this catalyst series, as the activity is independent of copper surface area, similar to the Cu/ZnO/Al₂O₃ catalyst formed by Chinchén *et al* [168].

Another possibility for the large production of CO₂ is from the dehydration of DME to form hydrocarbons [171], leaving an adsorbed oxygen atom, then reacting with CO to form CO₂. The industrial low temperature methanol catalyst is partially covered with lone oxygen during reaction [110]. It is observed in Figure 5.4.3, that CO₂ had an induction period of 15 hrs and from that point the selectivity increased rapidly to CO₂ maximum conversion. This suggests that surface restructuring probably occurs by the gradual increase of oxygen coverage until a sufficient coverage was reached before its formation commences. Jackson and Brandreth [114] found a considerable delay before methanol was detected and subsequent steady state was attained. The rate of formation of CO₂ paralleled with alcohol selectivity, especially methanol, as an induction period was observed also, which is in agreement with work elsewhere [4]. The WGS reaction is facilitated by adsorbed oxygen [167], however, oxygen coverage can inhibit HAS [86].

The large CO₂ selectivity was the main reason why the microreactor reactions were discontinued on the ⁸₃₀Cu_{Mg(2)Al} catalyst, as CO₂ is known to preferentially form low molecular weight alcohol products [4]. Another reason is the 40 hr period required for methanol production to reach steady state production from a H₂:CO:CO₂ gasfeed (Figure 5.4.1).

From a methanol-based input gasfeed, more water was produced over the ⁸₇₀Cu_{Mg(2)Al} catalyst than with the ⁸₁₄₀Cu_{Mg(2)Al} catalyst (Table 6.2.1) even though the

latter formed more CO₂, but this may be due to the increased overall activity over the ⁸₇₀Cu_{Mg(2)Al} catalyst.

The precursor characterisation produced results that made it appear that these catalysts were structurally homogeneous and crystalline, however, deactivation of the catalyst was observed after 70 hrs (Figure 5.4.3), which resulted in a large decrease in methanol selectivity and large increase in methane, as also observed with work by Chaumette *et al* [66]. This suggests that the activity decreased due to sintering of the copper particles and as methane is most likely to form over aluminium [87], its production would be unaffected by such copper sintering. Surface carbon may also block the surface active sites and diminish the activity, which is in agreement with work by Sheffer and King [69].

The reactions conducted over the ⁸Cu_{Mg(2)Al} catalysts were performed at the increased pressure of 20 barg rather than earlier reactions over the Cu_{Mg(10)Al} and Cu_{Cr} catalysts at 14 barg and below. The increased pressure may also explain the overall increase in activity of the ⁸Cu_{Mg(2)Al} catalysts. Initially, the pressure was maintained between 6-14 barg but as activity was not apparent, the pressure was increased. Higher pressure is beneficial for higher alcohol formation due to thermodynamic reasons [6] and also leads to a higher alcohol:hydrocarbon ratio in the products [44]. It was observed that no higher alcohols were formed unless methanol was included into the input gasfeed.

7.2.4 Cu/MgO/Al₂O₃ (60/5/35) (Cu_{Mg(5)Al})

Increasing the magnesium concentration from 2 % (Cu_{Mg(2)Al}) to 5 % (Cu_{Mg(5)Al} catalyst series), increased the overall alcohol activity and decreased the induction time for the formation of products despite a decrease in copper and BET surface areas. The

reactions over this catalyst series are, therefore, not structure sensitive, which is in agreement with Robinson and Mol [247] and Robbins *et al* [255] but conflicts with the results of Chinchon *et al* [168].

The decrease in induction time was especially noticeable for methanol production over the ${}^8{}_{140}\text{Cu}_{\text{Mg}(5)\text{Al}}$ catalyst, as it was reduced to only 2 hrs (Figure 5.5.2), compared with 40 hrs observed with the ${}^8{}_{30}\text{Cu}_{\text{Mg}(2)\text{Al}}$ catalyst. Methanol and higher alcohols were formed in larger quantities than with the earlier catalysts even without CO_2 in the input gasfeed. The most likely methanol mechanism with this catalyst series (${}^8\text{Cu}_{\text{Mg}(5)\text{Al}}$) is by direct CO hydrogenation via a formyl intermediate. The earlier ${}^8\text{Cu}_{\text{Mg}(2)\text{Al}}$ catalyst series would most likely proceed through a formate intermediate formed from CO_2 . Both mechanisms utilising different copper sites, which has been reported by McNeil *et al* [257], as this would explain the variation in methanol activity. However, evidence from an oxide-based mechanism is from Gopal *et al* [258], who found surface formates from the reaction of CO with alumina and magnesia and speculation [9,252] that formyl (-CHO) or formates can migrate from the oxide to Cu^0 , to be hydrogenated there. The ${}^8{}_{30}\text{Cu}_{\text{Mg}(5)\text{Al}}$ catalyst produced the least amount of methanol, it also contained the lowest quantity of copper when compared to the other two catalysts in the series and if methanol was formed only on copper, which was also proposed by Andrew [35], this might explain the low activity.

Higher alcohols were formed using a $\text{H}_2:\text{CO}$ gasfeed over the ${}^8{}_{30}\text{Cu}_{\text{Mg}(5)\text{Al}}$ catalyst (Table 5.5.2). Increasing the temperature increased higher alcohol production and chain length from C_2 to C_4 , as also observed by Xiaoding *et al* [6]. A mixture of straight and branched higher alcohols were formed, the branched C_3 - (propan-2-ol) and C_4 - alcohols (isobutanol and butan-2-ol) being produced in larger quantities. Therefore, branched alcohols are formed preferentially to straight-chained alcohols,

like the high temperature methanol synthesis catalysts [6], but is contrary to the $\text{Cu}_{\text{Mg}(2)\text{Al}}$ catalysts. Roberts *et al* [88] stated that isobutanol is the preferred species between about 473 and 773 K. However, ethanol was formed in the largest quantities with this study, suggesting kinetic rather than thermodynamic effects determine the alcohol distribution.

Higher alcohols were also formed from a H_2 and CO gas mixture with the $^8_{70}\text{Cu}_{\text{Mg}(5)\text{Al}}$ catalyst, however, no ethanol was detected, only propan-2-ol and isobutanol (Table 5.5.6). As only C_3 - and C_4 - alcohols were detected, this suggested that the C_2 - C_3 chain growth step was faster than the C_1 - C_2 chain growth step, which is in agreement with Nunan *et al* [122-124] and Elliott and Pennella [125]. Like the $^8_{30}\text{Cu}_{\text{Mg}(5)\text{Al}}$ catalyst, this catalyst preferentially formed branched alcohols, but is different than the earlier $\text{Cu}_{\text{Mg}(2)\text{Al}}$ catalysts, as this preferentially formed straight alcohols. This could be explained by any number of reasons, for example, increased basicity or crystallinity but a likely possibility is that different active sites were being formed or utilised due to the increased magnesium concentration. This hypothesis coincides with the contrast in the TPR profiles and in the methanol activities observed between these two catalyst series.

Addition of methanol to the input gasfeed, generally resulted in greater quantities of higher alcohols, including ethanol, being produced with one exception, which may be due to the high GHSV used with the $^8_{70}\text{Cu}_{\text{Mg}(5)\text{Al}}$ catalyst, as the $^8_{140}\text{Cu}_{\text{Mg}(5)\text{Al}}$ catalyst was the higher alcohol conversion decreased with increasing GHSV. Therefore, a longer contact time is better for chain growth with these two catalysts, which is in agreement with Xiaoding *et al* [6]. The $^8_{30}\text{Cu}_{\text{Mg}(5)\text{Al}}$ catalyst preferentially formed alcohols at 2000 hr^{-1} rather than at 500 hr^{-1} but also increased the hydrocarbon formation [66]. This was also recognised with the two other catalysts.

Ethanol was only formed when methanol was added to the input gasfeed and was the only product to increase significantly on methanol introduction. This suggests that C_1 addition increased C_{n+1} and some C_{n+2} yields, as previously reported by Smith and Anderson [43] and also that hydrocarbon and DMF formation are likely to be formed from a different intermediate than ethanol [122-124,142,171]. A likely ethanol mechanism is between one methanol-derived and one CO derived intermediate, which was also proposed by Calverley and Smith [259], as ethanol forms preferentially using a methanol and CO gasfeed rather than from CO alone. The mechanism proposed by Falter [149] (in which methanol reacts to ethanol via DME) can be discounted, as an increase in DME conversion would be observed with a methanol-based input gasfeed in producing ethanol. Therefore, ethanol is likely to be formed at sites different from those at synthesising DME, which is in agreement with Slaa *et al* [130].

For additional chain growth of alcohols, likely mechanistic routes are by either linear insertion or aldol condensation reactions. It is likely that over these catalysts that both mechanisms occur, with the preferential mechanism by aldol condensation mechanism, as this mechanism favourably forms branched alcohols and methanal cant undergo aldol condensation reactions, which was formed with the $^8_{30}\text{Cu}_{\text{Mg}(5)\text{Al}}$ catalyst. However, without conducting specific mechanistic studies, it is impossible to conclusively determine the mechanism or mechanisms present on the surface.

The $^8_{30}\text{Cu}_{\text{Mg}(5)\text{Al}}$ catalyst, which was the most active for higher alcohol formation of this series, did contain the largest percentage of carbon and hydrogen of the series prior to reaction (Table 4.5.6). The large carbon concentration may be partially responsible for the greater formation of higher alcohols. A high carbon and hydrogen concentration was also observed with the $^8_{70}\text{Cu}_{\text{Mg}(5)\text{Al}}$ catalyst, which was also active. The TPR profiles for the $^8_{30}\text{Cu}_{\text{Mg}(5)\text{Al}}$ and $^8_{70}\text{Cu}_{\text{Mg}(5)\text{Al}}$ catalysts were of

similar shape, therefore, the copper is likely to be in a similar structural form making the formation of higher alcohols structure dependent. The $^8_{140}\text{Cu}_{\text{Mg}(5)\text{Al}}$ sample, which formed a smaller amount of alcohols, showed a completely different TPR profile, reducing at a temperature 100 K greater than the other two catalyst precursors and contained the least amount of carbon prior to reaction. The XRD pattern showed a $\text{MgCO}_3 \cdot 2\text{H}_2\text{O}$ [222] phase (Figure 4.5.2), which was not observed in the $^8_{30}\text{Cu}_{\text{Mg}(5)\text{Al}}$ and $^8_{70}\text{Cu}_{\text{Mg}(5)\text{Al}}$ precursors or any other sample in this study. This high copper reduction temperature exceeds the reaction temperatures commonly used in the microreactor experiments in this study, therefore, it is possible that complete reduction of the $^8_{140}\text{Cu}_{\text{Mg}(5)\text{Al}}$ catalyst did not occur. This theory is confirmed by the increase in the BET surface area after completion of microreactor experiments, therefore, the reducing gases of H_2 and CO completed the reduction of this catalyst. This increase in BET surface area occurred even though an increase in carbon concentration after reaction was observed. The carbon concentration also increased for the $^8_{30}\text{Cu}_{\text{Mg}(5)\text{Al}}$ and $^8_{70}\text{Cu}_{\text{Mg}(5)\text{Al}}$ catalysts after reaction, which was probably present as carbon laydown on the surface, which is in agreement with Lee *et al* [253].

The $^8_{140}\text{Cu}_{\text{Mg}(5)\text{Al}}$ catalyst had the lowest copper dispersion from this series of catalysts (Table 4.5.3); this may be due to the higher reduction temperature required resulting in agglomeration of copper particles. The high copper reduction temperature might be stabilised by the $\text{MgCO}_3 \cdot 2\text{H}_2\text{O}$ [222] present in the sample, with the carbon bonded to the Mg and not present in the hydrotalcite-like interlayer as expected [175] but the overall concentration of carbon was low. The hydrotalcite-type phase was very poorly crystalline with comparison to the other $^8\text{Cu}_{\text{Mg}(5)\text{Al}}$ precursors, partial degradation was observed during preparation and elemental analysis showed nitrogen was present pre and post calcination, which suggests an alternative phase, compound

or anion may be present within the precursor but was undetectable by bulk characterisation techniques. A decrease in nitrogen concentration was observed post reaction, therefore, it is likely this alternate phase, compound or anion was removed on reduction of the catalyst. This "alternative phase" present may also explain the catalyst density, as it was 175 % more dense than the other two precursors. It is unlikely that the remaining nitrogen was present as nitrates, as suggested by Myers *et al* [242], as these should have been removed either on initial calcination or catalyst reduction. However, these differences did not really impede the catalyst's activity, as methanol induction period (2 hrs) was shorter than the other ${}^8_{30}\text{Cu}_{\text{Mg}(5)\text{Al}}$ and ${}^8_{70}\text{Cu}_{\text{Mg}(5)\text{Al}}$ catalysts.

Higher alcohol formation may have been aided by the slight presence of the basic K and Ca atoms, which was detected in the XRF spectra, as higher alcohols preferentially form on basic sites [87]. However, the XRF technique does not determine whether these two basic elements were present on the surface or the bulk.

Methane and the other hydrocarbons, ethane and propane were formed in almost all reactions performed over this catalyst series with no induction period being required with any hydrocarbon, however, the hydrocarbon conversion was greater than the earlier $\text{Cu}_{\text{Mg}(2)\text{Al}}$ catalyst series. Methane always being formed in largest quantities followed by ethane and propane respectively. Carbon dioxide removal from the input gasfeed prompted a further increase in production, therefore, CO_2 suppressed hydrocarbon activity, this occurred regardless of temperature or catalyst, ${}^8_{70}\text{Cu}_{\text{Mg}(5)\text{Al}}$ and ${}^8_{140}\text{Cu}_{\text{Mg}(5)\text{Al}}$ respectively. This is in contrast with work by Iglesia *et al* [58], who found that CO_2 had little influence over hydrocarbon activity. Carbon dioxide is known to suppress the HAS [92]. This suggests that, perhaps, similar active sites may be utilised for hydrocarbon and HAS, which suggests that the HAS could proceed

through a linear insertion mechanism, involving a carbene species [260], as well as aldol condensation reactions over this catalyst series. Hydrocarbons were relatively unaffected by the introduction of methanol into the input gasfeed, unlike the ethanol selectivity.

DME was also produced in greater quantities than the earlier catalyst series, again, no induction period was observed. However, if DME was formed on acidic sites, a decrease in conversion may have been anticipated because of the lower concentration of aluminium in the catalyst. Xu *et al* [87] also hypothesised that DME formation occurred on acidic sites. The increase is probably due to the overall greater activity observed with alcohols and hydrocarbons.

Carbon dioxide was again produced in largest quantities with the 30mins aged catalyst ($^8_{30}\text{Cu}_{\text{Mg}(5)\text{Al}}$) but on this occasion, with less conversion than the $^8_{30}\text{Cu}_{\text{Mg}(2)\text{Al}}$ catalyst. As water was produced in some cases, it is easy to assume that the likely CO_2 formation was from either condensation or the WGS reaction, the latter option being more probable due to its equilibrium with the reaction conditions in operation, which is in agreement with Tronconi *et al* [89] and Edwards and Schrader [261]. Carbon dioxide was produced in greater quantities when methanol was introduced into the input gasfeed, which in this case, was probably due to the formation of water from ethanol formation, then proceeding via the WGS reaction or the remaining oxygen from ethanol formation reacting directly with CO. It appears that the water and CO_2 are unavoidable by-products.

The reduction of hydrocarbon and CO_2 activity is not aided by the small quantity of iron visible in the XRF spectra prior to reaction, and iron is known to preferentially form hydrocarbons [57] and is an active WGS reaction catalyst [153].

The increase in magnesium concentration when compared with the previous $\text{Cu}_{\text{Mg}(2)\text{Al}}$ catalysts resulted in a crystalline hydrocalcite-type phase, which was able to form at $\text{pH} = 9$, ${}^9_{30}\text{Cu}_{\text{Mg}(5)\text{Al}}$. Preparation of the earlier ${}^9\text{Cu}_{\text{Mg}(2)\text{Al}}$ catalyst was unfavourable due to decomposition of the hydrocalcite-phase during ageing.

No or little deactivation was observed with any of the reactions conducted, which was contrary to the earlier catalyst. This increased stability is due to the increased magnesium concentration, which was also proposed by Höppener *et al* [199]. The lack of deactivation occurred regardless of an increase in carbon concentration, presence of water, which is detrimental [209] and increased impurities being detected in the XRF spectra. Fortunately, the impurities were present in only minute concentrations and, therefore, unlikely to have a large impact on the overall activity.

Impurity products such as DME, hydrocarbons, water and CO_2 were still being formed in quantities larger than desired, so the magnesium concentration was increased further with respect to the aluminium concentration. The copper concentration was maintained at 60 %.

7.2.5 $\text{Cu/MgO/Al}_2\text{O}_3$ (60/7/35) ($\text{Cu}_{\text{Mg}(7)\text{Al}}$)

Increasing the magnesium concentration to suppress the formation of hydrocarbons and DME resulted in changes in the product distribution and increased the methanol induction time. The latter was apparent with the ${}^8_{30}\text{Cu}_{\text{Mg}(7)\text{Al}}$ catalyst shown in Figure 5.6.1, as the induction time increased from 2 to 10 hrs when compared with the earlier ${}^8_{140}\text{Cu}_{\text{Mg}(5)\text{Al}}$ catalyst. This feature was also evident with the ${}^8_{70}\text{Cu}_{\text{Mg}(7)\text{Al}}$ and the ${}^8_{140}\text{Cu}_{\text{Mg}(7)\text{Al}}$ catalysts, again with methanol formation, the former sample required an initial 6hrs induction period but a further 29 hrs to achieve the maximum conversion.

The latter had a 2 hrs induction period but only a further 8 hrs for maximum conversion. After the maximum conversion had been accomplished, methanol was the most selective product with all three catalysts.

However, in all reactions, DME and the hydrocarbons (methane, ethane and propane) were formed prior to methanol and unaffected by induction times, therefore, lack of surface oxygen does inhibit methanol formation. This effect was also observed with the earlier ${}^8\text{Cu}_{\text{Mg}(5)\text{Al}}$ catalyst series, Jackson and Brandreth's [114] catalyst and the industrial low temperature methanol synthesis catalyst [111]. The adsorbed oxygen would be produced from CO bond scission. Wachs and Madix [262] observed that copper generally required the addition of surface oxygen atoms, as it facilitated the proton transfer to the basic surface oxygen. Hydrocarbon and DME formations occurred on the Al surface, therefore, were unaffected by the adsorbed oxygen on copper.

The overall production of methanol with this catalyst series had decreased by a factor of two with comparison with the earlier ${}^8\text{Cu}_{\text{Mg}(5)\text{Al}}$ catalysts. This may be related to the overall increase in magnesium concentration, as magnesium is known to inhibit methanol production [199]. The methanol conversion also decreased with increasing temperature, which is ascribed to thermodynamic factors, as the reaction approaches equilibrium conditions with increasing reaction operating conditions [85]. The methanol synthesis is thermodynamically limited [3,5] with a maximum conversion of 25 %.

Higher alcohols were formed with a $\text{H}_2:\text{CO}$ gasfeed over the ${}^8_{140}\text{Cu}_{\text{Mg}(7)\text{Al}}$ catalyst. The production of propan-2-ol increased with temperature and decreasing GHSV, as also reported by Xiaoding *et al* [6] and Chu *et al* [143] respectively. Again, no ethanol was detected from a $\text{H}_2:\text{CO}$ gasfeed, which further confirms that the slow

formation of ethanol is followed by fast addition to a C₃ alcohol, which is in agreement with observations of Nunan *et al* [121-124] and Elliott and Pennella [125]. The formation of propan-2-ol in preference to propan-1-ol suggests that these catalysts preferentially form secondary alcohols, which was observed with the ⁸Cu_{Mg(5)Al} catalyst series and the high temperature methanol synthesis catalyst [6]. The mechanism for the formation of C₃ alcohols is likely to follow the same trend as the earlier Cu_{Mg(5)Al} catalyst series, due to the similar alcohol product distribution. Therefore, these catalysts are likely to form C₃ alcohols preferentially through an aldol condensation reaction, which is in agreement with Nunan *et al* [124]. However, this is also contrary to Nunan *et al* [124], who stipulated that for the aldol condensation reactions to occur, the catalysts must be promoted.

Ethanol but no C₂-alcohols were detected with methanol addition to the input gasfeed, which was independent of reaction conditions with the ⁸Cu_{Mg(7)Al} catalysts. Little difference in ethanol selectivity was observed with these catalysts, as all values were in the range of 10-13 % with no indications of either poisoning or deactivation, making its formation ageing time and copper surface area independent, therefore, a structure-insensitive reaction. This hypothesis agrees with experiments conducted over the Cu_{Mg(5)Al} catalysts and by work elsewhere [247]. However, ethanol generally required a small induction period of ca. 2 hrs before detection, which was a longer time period than required for the other products. The effect of lower activity with these catalysts with comparison with the Cu_{Mg(5)Al} catalyst series, but increased induction periods and higher alcohol selectivity are all probably related to the overall increase in magnesium concentration, which is in agreement with Hilmen *et al* [86]. The mechanism for ethanol formation is likely to follow the same principles proposed with the Cu_{Mg(5)Al} catalyst, as it follows the same conversion trend.

No methanol, methanal or C_{2+} oxygenates were formed when the CO concentration was increased to 70 % (Figure 5.6.5). However, the reaction over the $^{87}_{30}Cu_{Mg(7)Al}$ catalyst formed, only methane, DME and CO_2 . All three products had similar selectivity, which varied little with reaction time online. Methanol was only formed when the CO concentration was decreased to 60 %, which is in agreement with the conclusion by Sheffer and King [69], who hypothesised that a high CO concentration can be detrimental to alcohol activity. The CO concentration rather than the H_2 controls the overall product distribution with reactions varying the $H_2:CO$ gasfeed. A possible reason for this could be that the lack of hydrogen reduces the probability of hydrogen activation on the copper surface, therefore, decreasing the likelihood of methanol formation. Another suggestion could be that the high CO concentration saturates the Cu surface area and hydrogen cannot be activated, as CO chemisorption is stronger than H_2 [263]. Both possibilities are plausible but as ethane and propane were only formed at the 60 % CO concentration level rather than the 70 %, this suggests that the former is more likely. Changing the input gasfeed to incorporate methanol changed the product distribution considerably, the methane selectivity decreased to 3 %, DME 2 % and CO_2 , 0.5 %. Changing the $^{87}_{70}Cu_{Mg(7)Al}$ catalyst, again changed the product distribution. Carbon dioxide consisted of almost a quarter of the total selectivity, which in turn considerably decreased the methanol and ethanol selectivity. The differences in the impurity (hydrocarbon, DME and CO_2) product distribution are best related to the ability of these catalysts to absorb oxygen, which is required for methanol formation.

The hydrocarbon (methane, ethane and propane) conversion increased with increasing temperature, which agrees with work by several authors [85,143,172]. Like the earlier $Cu_{Mg(5)Al}$ catalyst series, methane selectivity did not increase with methanol

addition in the gasfeed; DME and CO₂ did likewise. No ethane or propane was detected with the methanol-based input gasfeed. Therefore, it is unlikely that ethanol formation is mechanistically related to hydrocarbons, DME or CO₂. The syntheses of methanol and CO₂ have also been found to be mechanistically unrelated [106].

The CO₂ selectivity decreased significantly with increasing GHSV and temperature from a H₂:CO gasfeed, both of which could be due to the overall decrease in activity of this series of catalysts or ascribed as more unfavourable WGS reaction equilibrium conditions. The latter is more likely to be prominent under these reaction conditions, which has previously been reported [261]. The likely mechanism for the WGS reaction is by a regenerative mechanism due to the large likelihood of adsorbed oxygen being present on the catalyst surface required for methanol formation. This mechanism is in agreement with work by Chinchon *et al* [113] and Vanden Bussche and Froment [158].

DME conversion increased with GHSV but proceeded through a production maximum at 593 K with increasing temperature from a H₂:CO gasfeed. These effects may be partially ascribed to equilibrium effects from the decrease in methanol production over the same temperature range, assuming that its formation is by dehydration of methanol, as also proposed by Matulewicz [171]. However, this mechanism is not exclusive, as no increase in selectivity was observed with the methanol-based input gasfeed. An alternative mechanism is the reaction between CO and a surface carbide, as the post-reaction carbon analysis showed an increase. The mechanism would be then followed by subsequent hydrogenation, however, this would result in a larger ethanol conversion observed from a H₂:CO gasfeed. Another possible DME formation route is by the reaction between a methane intermediate (possibly a methyl group) and CO where it is followed by hydrogenation, as suggested by

Campos-Martín *et al* [46]. This mechanism is the most likely as the DME conversion mirrors that of methane.

Microreactor experiments over the ${}^9\text{Cu}_{\text{Mg}(7)\text{Al}}$ catalyst gave a product distribution that varied little with GHSV (Figure 5.6.4). Carbon dioxide was by far the most selective product after 10 hrs, with an average of 80 % selectivity. The methanol selectivity was only 12 % after 3 hrs before stabilising at around 6-8 % for the remainder of the reaction. This catalyst also formed hydrocarbons and DME. Overall, the ${}^9\text{Cu}_{\text{Mg}(7)\text{Al}}$ catalyst was also more inactive than any earlier catalyst conducted with this study. This inactivity can be related to the peptised precursor formed on ageing during the preparation process.

Methanol was still by far, the most selective product from this catalyst series but a large quantity of hydrocarbons, DME and CO_2 were still being formed and in larger quantities than the earlier $\text{Cu}_{\text{Mg}(5)\text{Al}}$ catalyst series. An increase in higher alcohol selectivity was also observed but the overall activity was lower.

Increasing the magnesium concentration did not have the desired effect of reducing the activity from the aluminium sites but did produce TPR and DTA profiles which were all of the similar shape unlike the earlier catalysts series of ${}^8\text{Cu}_{\text{Mg}(5)\text{Al}}$ and ${}^8\text{Cu}_{\text{Mg}(2)\text{Al}}$. The presence of iron visible in the XRF spectrum would not aid decrease the hydrocarbon conversion [57] or reduce the extent of the WGS reaction [153].

7.2.6 K/Cu/MgO/Al₂O₃ (K60/7/35) (Cu_{MgAlK})

The addition of potassium to the $\text{Cu}_{\text{Mg}(7)\text{Al}}$ catalysts resulted in aldehydes, especially methanal and ethanal, being the most selective products from a $\text{H}_2:\text{CO}$ gasfeed. The formation of ethanal is especially important, as the main recurring problem throughout this work has been the $\text{C}_1\text{-C}_2$ oxygenate chain growth and has appeared to be the rate

determining step in further chain growth, which is in agreement with work by Tronconi *et al* [144]. The $^8_{70}\text{Cu}_{\text{MgAlK}}$ and the $^8_{30}\text{Cu}_{\text{MgAlK}}$ catalysts produced the most amount of ethanal and C_3 aldehydes respectively. Propanal, isobutanal and butanal, like ethanal, were all formed in larger quantities than alcohols. This occurred regardless of temperature or GHSV variation with the $^8_{140}\text{Cu}_{\text{MgAlK}}$ and $^8_{70}\text{Cu}_{\text{MgAlK}}$ catalysts respectively. Little or no variation in aldehyde conversion was observed with increasing temperature but an optimum GHSV of 3000 hr^{-1} was observed with ethanal, the yield being less at 1000 and $10,000 \text{ hr}^{-1}$. However, no effect in selectivity of C_3 - and C_4 -aldehydes was observed with increasing GHSV. Hilmen *et al* [86] observed a similar occurrence with isobutanol and explained it as "strong inhibition effects". However, ethane and propane conversions decreased with increasing GHSV, therefore, this may be an anomalous result as methanal also decreased over the 3000 to $10,000 \text{ hr}^{-1}$ space velocity range.

Although the $^8_{70}\text{Cu}_{\text{MgAlK}}$ catalyst formed the most ethanal of the Cu_{MgAlK} series, 10 hrs were still required to reach the maximum selectivity. A shorter period was observed for methanal conversion, but both methanal and ethanal were formed with similar conversions, making this catalyst less selective for C_{2+} oxygenates than the $^8_{30}\text{Cu}_{\text{MgAlK}}$ catalyst. However, the $^8_{30}\text{Cu}_{\text{MgAlK}}$ catalyst required 15 hrs to achieve the maximum ethanal conversion but was more selective towards methane. The $^8_{140}\text{Cu}_{\text{MgAlK}}$ catalyst produced selectively methanal and methane, making this catalyst, preferentially forming C_1 products. The $^9_{30}\text{Cu}_{\text{MgAlK}}$ catalyst produced only a minute quantity of methane (Table 5.7.1), this inactivity is in agreement with the original template catalyst ($^9_{30}\text{Cu}_{\text{Mg(7)Al}}$).

Very little methanol was produced with this catalyst series, only the $^8_{140}\text{Cu}_{\text{MgAlK}}$ sample produced methanol from a $\text{H}_2:\text{CO}$ gasfeed, this occurred regardless of alkali

promotion favouring CO hydrogenation rather than CO₂ [44]. No methanol induction period was observed with this catalyst either, which is contrary to the earlier catalysts. Higher alcohols were still formed with other catalysts without methanol being present in the product distribution. The most amount of ethanol was formed over the ⁸₁₄₀Cu_{MgAlK} catalyst, probably as a direct result of hydrogenation of the large ethanal formation. The ⁸₃₀Cu_{MgAlK} and ⁸₇₀Cu_{MgAlK} catalysts formed both straight and branched-chained alcohols (propan-1-ol and isobutanol) respectively.

Substituting the usual methanol for ethanol into the input gasfeed resulted in a larger proportion of longer chained products (C₂₊ oxygenates) than from methanol addition (Table 5.7.4). Aside from ethanol, ethanal showed the largest increase in conversion, propanal and propan-2-ol increased also. C₄ alcohols were also formed but propan-1-ol was not. The methanol addition on the otherhand produced only C₃- and C₄- aldehydes. This suggests that hydrogenation of the C_{n+1} or C_{n+2} oxygenates to alcohols is more likely to occur with ethanol (C_n) in the input gasfeed.

Introduction of methanol also considerably decreased the concentration of ethanal but increased the methanal and methane conversions. This was also observed with ethane using the ethanol-based input gasfeed. Therefore, it is likely that dehydrogenation reactions occur over these copper-based catalysts with the dehydrogenation step occurring faster than chain growth, which is in agreement with work by Chinchén *et al* [14], Ginés *et al* [129] and Waugh [264] respectively.

Due to the large formation of aldehydes, a subtly different mechanism or mechanisms may occur over these promoted catalysts on comparison with the unpromoted catalysts. However, an aldol-type mechanism seems most likely, proceeding through sequential chain growth for the dual formation of alcohols and aldehydes, which is in agreement with Nunan *et al* [122-124] and Elliott and Pennella

[125]. Aldol reactions can be reversible on copper and form ketones [129]; however, reverse reactions are unlikely to occur as no ketones were detected. Therefore, a surface bound aldehydic species rather than a ketonic species is favoured over these catalysts, which is in agreement with work by Slaa *et al* [130]. Ginés *et al* [129] concluded that aldol type coupling reactions of alcohols requires both Cu and basic sites. Addition of potassium must increase the stability of the intermediate species, which is in agreement with Smith *et al* [127], and increase the density and strength of the basic sites, as previously reported by Hilmen *et al* [86]. Another theory was suggested Sheffer and King [69], who suggested that stabilisation was due to Cu^+ species, however, this is unlikely as copper is completely reduced under these conditions, as an increase in copper dispersion was observed over these catalysts when compared to the $\text{Cu}_{\text{Mg}(7)\text{Al}}$ catalysts.

Solids based on MgO and CaO can catalyse condensation reaction of alcohols, aldehydes or ketones with high selectivity [264]. Also, MgO is an active and selective catalyst for the Guerbet condensation reactions of primary $\text{C}_2\text{-C}_5$ alcohols with methanol [265]. However, the effect of MgO would have been observed over the unpromoted catalysts; therefore, can be discounted from any difference in the product distribution and reaction mechanism observed over these promoted catalysts.

No strict correspondence between aldehydes and alcohols was observed, which is contrary to work by Forzatti *et al* [4] even though only a small step hydrogenation step exists between them.

Hydrocarbon (methane, ethane and propane) conversion increased with increasing temperature and decreased with increasing GHSV, which is in agreement with authors Jager [57] and Slaa *et al* [130] respectively. Methane was formed in largest quantities followed by ethane and propane, which suggests that hydrocarbon

formation, is also sequential. The hydrocarbon conversion also varied with catalyst, the $^{87}\text{Cu}_{\text{MgAlK}}$ catalyst produced the most quantity, even though, it also formed the most C_{2+} oxygenates. This catalyst did have the largest BET surface areas; therefore, hydrocarbon formation is a structure sensitive reaction, which is in disagreement with work with Johnson *et al* [64].

Ethanol addition to the input gasfeed, saw a slight increase in propane conversion, which meant that chain growth occurred before desorption, which was dissimilar to methanol addition, as no such increase was observed with ethane when methanol was included. This further compounds the theory that the $\text{C}_1\text{-C}_2$ step is the rate-determining step when forming longer chained molecules and does not solely apply to higher oxygenate formation.

No DME was formed under any operating conditions over these promoted catalysts, which was different than with the other catalysts in this study. The addition of the potassium must have suppressed the active site/s for DME formation by possibly blocking the sites on wet-impregnation or decreased the surface acidity, as also reported by Forzatti *et al* [4], Hilmen *et al* [86] and Lietti *et al* [137]. Another possibility could be that the potassium restructured the surface in such a way that the DME active sites were removed, however, this is unlikely as no differences were detected in any of the characterisation techniques applied between these catalysts and the $\text{Cu}_{\text{Mg}(7)\text{Al}}$ catalysts.

The CO_2 conversion was between 0.14 and 0.42 % and was considerably lower than the earlier $\text{Cu}_{\text{Mg}(7)\text{Al}}$ catalyst series. The temperature, GHSV and gasfeed composition was varied but resulted in little change in the conversion. The lack of an effect with temperature variation is due to thermodynamic control with the WGS reaction, which is the most likely source of CO_2 and is in agreement with Courty *et al*

[5]. As no effect was observed with GHSV, this suggests that the turnover frequency is sufficiently high not to result in any detrimental effect on activity. Only varying the gasfeed and catalyst resulted in any subtle change in the conversion of CO₂, the former will be due to different thermodynamic effects, which is in agreement with conclusions by Courty *et al* [5]. This difference in the conversion of CO₂ between catalysts is due to different concentrations of active phases being present in the catalysts. Carbon dioxide was also relatively unaffected with either methanol or ethanol introduction to the input gasfeed, which suggests that its formation is not mechanistically related to either aldehyde or alcohol formation, in agreement with earlier work in this study and Chinchén *et al* [106].

No deactivation or decrease in activity over a 170 hrs period was observed with a reaction conducted over the ⁸₃₀Cu_{MgAlK} catalyst (Figure 5.7.1). No change in selectivity was observed after 80 hrs, even though an increase in carbon and hydrogen was observed using post reaction elemental analysis. Therefore, their concentration was sufficiently low to ensure inhibition did not occur. The lack of deactivation was due to either the magnesium concentration or the K-impregnation procedure, the former being most likely. The stability of the catalyst is more likely to be a bulk effect and the potassium was added to the surface and it is impossible to accommodate the large K⁺ ions within this structure [244]. However, K-impregnation cannot be completely excluded as no other microreactor experiments was conducted over such a long duration.

Overall, the ⁸₇₀Cu_{MgAlK} catalyst produced the largest conversion of C₂₊ oxygenates and hydrocarbons but contained the least amount of potassium of the Cu_{MgAlK} series, therefore, the low concentration did not hinder the oxygenate or

hydrocarbon activity. The ${}^9{}_{30}\text{Cu}_{\text{MgAlK}}$ catalyst had the highest potassium concentration and also the lowest activity but that is a preparation effect.

The highest selectivity of a C_{2+} oxygenated product (50-60 %) was shown in Figure 5.7.5 over the ${}^8{}_{30}\text{Cu}_{\text{MgAlK}}$ catalyst. However, the overall conversion of ethanal was only 0.8 % with 10 hrs induction time required to achieve this conversion. The addition of the potassium to each individual catalyst decreased the overall activity when compared to the $\text{Cu}_{\text{Mg}(7)\text{Al}}$ catalysts even with an increase in Cu and BET surface areas; therefore, the reactions on these catalysts are insensitive to structure variation. The change in activity and selectivity is definitely related to the potassium addition, as there is a significant change between these catalysts and with their original template catalysts, ${}^8{}_{30}\text{Cu}_{\text{Mg}(7)\text{Al}}$, ${}^8{}_{70}\text{Cu}_{\text{Mg}(7)\text{Al}}$, and ${}^8{}_{140}\text{Cu}_{\text{Mg}(7)\text{Al}}$. Also, no bulk structural changes were observed with the addition of the potassium. The peaks of DTA profiles all coincided and were all of the same magnitude, which was subtly different to their template catalysts. The TPR profiles were all similar and XRD patterns all showed the hydrotalcite-type precursor phase and on calcination, poorly crystalline CuO peaks. The recalcination resulted in a slight increase in copper dispersion and BET surface area, which was probably due to the continued loss of water and carbonate ions from the interlayer.

The main point must be stressed that selective formation higher oxygenates did occur over these catalysts. To have 50-60 % selectivity with over 50 possible products from a CO and H_2 gasfeed [144] highlights the complexity of the study.

8 Conclusions

The main reactions to occur were the higher oxygenate formation, the methanol synthesis and the WGS and FT reactions, the extent of which was catalyst dependent. Each catalyst showed a subtly different product distribution and selectivity, with product formation being primarily structurally insensitive. The pH = 8 30 mins and the 70 mins catalysts were generally the most active and the pH = 9 catalysts the least.

The higher alcohol production increased with increasing magnesium concentration in the catalysts using either a $H_2:CO$ or $H_2:CO:CO_2$ gasfeed. A higher proportion of which were branched alcohols, although little ethanol was formed. The optimum CO concentration was ca. 60 %, as a higher concentration resulted in no methanol or higher alcohols being formed. The addition of methanol (C_n) to the gasfeed resulted in increased C_{n+1} and a little C_{n+2} alcohols. The most likely mechanisms may involve either linear insertions or aldol condensations, with the latter becoming more prominent with increasing magnesium concentration. The $Cu_{Mg(7)Al}$ samples produced the most alcohols with an optimum GHSV of 2000 hr^{-1} .

Potassium promotion overcame the inhibiting C_1-C_2 step with a large production of ethanal, with an optimum GHSV of 3000 hr^{-1} . No induction period was required. Higher aldehydes and alcohols (C_2 , C_3 and C_4) were also formed without methanol. Only a small step exists between alcohols and aldehydes. Aldol condensation was the most likely route for higher oxygenates formation was by aldol coupling. However, the overall activity was lower than unpromoted catalysts, probably due to the potassium blocking active hydrogenation or chain growth sites. It is possible to recycle lower alcohol production to increase the overall chain length.

Methanol was formed from CO_2 and CO , the Cu_{Cr} and the $\text{Cu}_{\text{Mg}(2)\text{Al}}$ catalysts from the former and the remaining catalysts from CO . The $\text{Cu}_{\text{Mg}(5)\text{Al}}$ catalysts were the most active series, even though methanol formation was from CO not CO_2 . Oxygen coverage was generally required for methanol formation, with the induction time being variable with increasing magnesium concentration. The unpromoted Cu_{Cr} and $\text{Cu}/\text{MgO}/\text{Al}_2\text{O}_3$ series of catalysts behaved like either typical LT or HT methanol synthesis catalysts, for example, decreased in methanol production with increasing GHSV, pressure or temperature. Little connection was observed with FT behaviour for alcohol formation.

Hydrocarbon formation was likely to proceed by the typical FT reaction mechanism, with their formation probably occurring on different active sites than those involved in higher alcohol production. DME was formed either by dehydration of two methanol molecules or by CO insertion into a methyl group followed by hydrogenation. No DME was formed with the promoted catalyst. DME and hydrocarbon formation were unaffected by the extent of surface oxygen coverage. Carbon dioxide formation favoured a regenerative WGS reaction mechanism, as an oxygen coverage induction period was observed. Carbon dioxide suppressed hydrocarbon formation; however, it also decreased higher alcohol formation. Hydrocarbon and DME formation and the WGS reaction must be decreased to a minimum to increase higher alcohol selectivity; they can be decreased by promotion with potassium. However, that may be due to the overall decline in activity. In industrial higher alcohol formation, CO_2 is removed [4].

No ketones and esters were formed with any catalyst, even with the large formation of aldehydes by the promoted catalyst.

Increasing the magnesium concentration in the catalyst decreased the copper or BET surface areas. It also decreased deactivation due to copper sintering. Deactivation on the Cu_{Cr} catalyst was by carbon laydown. No poisoning from sulfur or chlorine was observed and the transition and alkali metal impurities were unlikely to affect the overall activity.

The Cu_{MgAlK} catalysts were by far the most promising samples for higher oxygenate selectivity, but at the expense of lowering the activity. Further work could be conducted with the promotion with potassium of the $\text{Cu}_{\text{Mg}(5)\text{Al}}$ catalysts, as these were more active than the $\text{Cu}_{\text{Mg}(7)\text{Al}}$ series. Introduction into the gasfeed with C_3 alcohols might be experimented with, as their production cost is lower than ethanol.

9 References

- [1] Berzelius, J.J., *Annl. Chim. Phys.*, 1836, **61**, 146.
- [2] Ostwald, W., *Z. Physik. Chem.*, 1894, **15**, 705.
- [3] Wender, I., *Fuel processing Technology*, 1996, **48** (3), 189.
- [4] Forzatti, P., Tronconi, E. and Pasquon I., *Catal. Rev.-Sci. Eng.*, 1991, **33** (1&2), 109.
- [5] Courty, Ph., Chaumette, P., Raimbault, C. and Travers, C., *Rev Inst. Fr. Pétrole*, 1990, **45** (4), 561.
- [6] Xiaoding, X., Doesburg, E.B.M. and Scholten, J.J.F., *Catal. Today*, 1987, **2**, 125.
- [7] Courty, Ph., Chaumette, P., Durand, D., Kawata, N., Obayashi, Y. and Uchiyama, S., *Ab. Papers Am. Chem. Soc.*, 1988, **196**, Sep, 39-I&EC.
- [8] Courty, Ph., Forestière, A., Kawata, N., Ohno, T., Raimbault, C. and Yoshimoto, M., *Am. Chem. Soc. Symp. Ser.*, 1987, **328**, 42.
- [9] Klier, K., *Adv. Catal.*, 1982, **31**, 243.
- [10] Natta, G., Colombo, U. and Pasquon, I., "Catalysis", (Ed. Emmett, P.H.), 1957, **5**, 131.
- [11] Pillai, G.C., Wei, T.C.J. and Stiles, A.B., "Synthesis of methanol and higher alcohols", Interim report, Dept. of Chem. Eng., University of Delaware, Newark, 1981.
- [12] Bridger, G.W. and Spencer, M.S., "Catalyst Handbook", Second Edition, (Ed. Twigg, M.V.), Wolfe Publishing Ltd., London, 1989, Chap. 9, p.441.
- [13] Farrauto, R.J. and Bartholomew, C.H., "Fundamentals of Industrial Catalytic Processes", Blackie Academic and Professional, London, 1997, Chap. 5, p.376.

- [14] Chinchen, G.C., Denny, P.J., Jennings, J.R., Spencer, M.S. and Waugh, K.C., *Appl. Catal.*, 1988, **36**, 1.
- [15] Fleisch, T.H. and Mieville, R.L., *J. Catal.*, 1984, **90**, 165.
- [16] Friedrich, J.B., Wainwright, M.S. and Young, D.J., *J. Catal.*, 1983, **80**, 1.
- [17] Yoshihara, J. and Campbell, C.T., *J. Catal.*, 1996, **161**, 776.
- [18] Muhler, M., Törnqvist, E., Nielsen, L.P., Clausen, B.S. and Töpsøe, H., *Catal. Lett.*, 1994, **25**, 1.
- [19] Askgaard, T.S., Nørskov, J.K., Ovesen, C.V. and Stoltze, P., *J. Catal.*, 1995, **156**, 229.
- [20] Nakamura, J., Nakamura, I., Uchijima, T., Watanabe, T. and Fujitani, T., *Stud. Surf. Sci. Catal.*, 1996, **101**, 1389.
- [21] Okamoto, Y., Fukino, K., Imanaka, T. and Terenishi, S., *J. Phys. Chem.*, 1983, **87**, 3740.
- [22] Chinchen, G.C., Waugh, K.C. and Whan, D.A., *Appl. Catal.*, 1986, **25**, 101.
- [23] Robinson, W.R.A.M. and Mol, J.C., *Appl. Catal.*, 1990, **60**, 73.
- [24] Burch, R., Golunski, S.E. and Spencer, M.S., *Catal. Lett.*, 1990, **5**, 55.
- [25] Joyner, R.W., *Catal. Lett.*, 1990, **6**, 151.
- [26] Bart, J.C.J. and Sneed, R.P.A., *Catal. Today*, 1987, **2**, 1.
- [27] Pan, W.X., Cao, R., Roberts, D.L. and Griffin, G.L., *J. Catal.*, 1988, **114**, 440.
- [28] Kiennemann, A., Idriss, H., Hindermann, J.P., Lavalley, J.C., Vallet, A., Chaumette, P. and Courty, Ph., *Appl. Catal.*, 1990, **59**, 165.
- [29] Le Peltier, F., Chaumette, P., Kiennemann, A., Saussey, J. and Lavalley, J.C., *J. Chim. Phys.*, 1996, **93** (7&8), 1376.
- [30] Spencer, M.S., *Nature*, 1986, **323**, 685.

- [31] Spencer, M.S., *Surf. Sci.*, 1987, **192** (2), 323.
- [32] Spencer, M.S., *Surf. Sci.*, 1987, **192** (2), 329.
- [33] Spencer, M.S., *Surf. Sci.*, 1987, **192** (2), 336.
- [34] Spencer, M.S., Burch, R. and Golunski, S.E., *J. Chem. Soc., Faraday Trans. I*, 1990, **86** (18), 3151.
- [35] Andrew, S.P.S., Plenary Lecture, Post Congress Symp., *7th Int. Congr. on Catalysis*, Osaka, 1980.
- [36] Herman, R.G., Klier, K., Simmons, G.W., Finn, B.P., Bulko, J.B. and Kobylinski, T.P., *J. Catal.*, 1979, **56**, 407.
- [37] Chinchén, G.C., Mansfield, K. and Spencer, M.S., *ChemTech*, 1990, **20** (11), 692.
- [38] Gallagher, J.T. and Kidd, J.M., U.K. Patent 1,159,035 (to ICI).
- [39] Fischer, A., Hosemann, R., Vogel, W., Koutecky, J. and Ralek, M., *Proc. 7th Int. Congr. on Catalysis* (Tokyo), 1980, 341.
- [40] Cornthwaite, D., U.K. Patent 1,296,212 (to ICI).
- [41] Elliott, D.J., *J. Catal.*, 1988, **111**, 445.
- [42] Calafat, A. and Laine, J., *J. Catal.*, 1994, **147**, 88.
- [43] Smith, K.J. and Anderson, R.B., *Can. J. Chem. Eng.*, 1983, **61**, 40.
- [44] Calverley, E.M. and Smith, K.J., *J. Catal.*, 1991, **130**, 616.
- [45] Campos-Martín, J.M., Guerrero-Ruiz, A. and Fierro, J.L.G., *J. Catal.*, 1995, **156**, 208.
- [46] Campos-Martín, J.M., Fierro, J.L.G., Guerrero-Ruiz, A., Herman, R.G. and Klier, K., *J. Catal.*, 1996, **163**, 418.
- [47] Fox, J.R., Pesa, F.A. and Curatolo, B.S., *J. Catal.*, 1984, **90**, 127.
- [48] Tronconi, E. and Forzatti P., *Chimica & L'Industria*, 1988, **70** (4), 66.

- [49] Tronconi, E., Ferlazzo, N., Forzatti, P. and Pasquon, I., *Ind. Eng. Chem. Res.*, 1987, **26**, 2122.
- [50] Hofstadt, C.E., Kochloeff, K. and Bock, O., European Patent-0034338-A2 (to Süd Chemie AG).
- [51] Keim, W. and Falter W., *Catal. Lett.*, 1989, **3**, 59.
- [52] Villa, P.L. and Lietti, L., *Stud. Surf. Sci. Catal.*, 1998, **118**, 395.
- [53] Fischer, F. and Tropsch, H., German Patent 411,216.
- [54] Fischer, F. and Tropsch, H., *Brennst.-Chem.*, 1926, **7**, 97.
- [55] Kummer, J.T. and Emmett, P.H., *J. Am. Chem. Soc.*, 1953, **75**, 5177.
- [56] Dry, M.E., *Appl. Catal. A: General*, 1996, **138**, 319.
- [57] Jager, B., *Stud. Surf. Sci. Catal.*, 1998, **119**, 25.
- [58] Iglesia, E., Reyes, S.C., Madon, R.J. and Soled, S.L., *Adv. Catal.*, 1993, **39**, 221.
- [59] Jager, B., Dry, M.E., Shingles, T. and Steynberg, A.P., *Catal. Lett.*, 1990, **7**, 293.
- [60] Jager, B., Kelfkens, R.K. and Steynberg, A.P., *Proc. 3rd Int. Nat. Gas Conversion*, Sydney, 1994, 419.
- [61] Fu, L. and Bartholomew, C.H., *J. Catal.*, 1985, **92**, 376.
- [62] Sie, S.T., Sended, M.M.G., and Van Wechem, H.M.H., *Catal. Today*, 1991, **8**, 371.
- [63] Anderson, R.B., "Catalysis", Volume 4, (Ed. Emmett, P.H.), Reinhold, 1956, Chap. 1-3.
- [64] Johnson, B.G., Bartholomew, C.H. and Goodman, D.W., *J. Catal.*, 1991, **128**, 231.

- [65] Courty, Ph., Durand, D., Freund, E. and Sugier, A., *J. Mol. Catal.*, 1982, **17**, 241.
- [66] Chaumette, P., Courty, Ph., Kiennemann, A., Kieffer, R., Boujana, S., Martin, G.A., Dalmon, J.A., Meriaudeau, P., Mirodatos, C., Holhein, B., Mausbeck, D., Hubert, A.J., Germain, A. and Noels, A., *Ind. Eng. Chem. Res.*, 1994, **33**, 1460.
- [67] Chaumette, P., Courty, Ph., Durand, D., Grandvallet, P. and Travers, C., U.K. Patent 2,158,730 (to IFP).
- [68] Rasines, I., *J. Appl. Cryst.*, 1972, **5**, 11.
- [69] Sheffer, G.R. and King, T.S., *Appl. Catal.*, 1988, **44**, 153.
- [70] Blanchard, M., Derule, H. and Canesson, P., *Catal. Lett.*, 1989, **2**, 319.
- [71] Huang, W., Yin, L. and Wang, C., *Energy Convers. Mgmt.*, 1995, **36** (6-9), 589.
- [72] Dalmon, J.A., Chaumette, P. and Mirodatos, C., *Catal. Today*, 1992, **15**, 101.
- [73] Baker, J.E., Burch, R. and Niu, Y., *Appl. Catal.*, 1991, **73**, 135.
- [74] Ohno, T., Yoshimoto, M., Asselineau, L., Courty, Ph. and Travers, Ph., 78th *AIChE Spring National Meeting*, New Orleans, 1986.
- [75] Courty, Ph., Durand, D., Sugier, A. and Freund, E., U.K. Patent 2,118,061 (to IFP).
- [76] Xiaoding, X., Scholten, J.J.F. and Mausbeck, D., *Appl. Catal. A: General*, 1992, **82**, 91.
- [77] Szymanski, R., Travers, C., Chaumette, P., Courty, Ph. and Durand, D., "Preparation of Catalysts IV", (Eds. Delmon, B., Grange, P., Jacobs, P.A. and Poncelet, G.), Elsevier, Amsterdam, 1987, p.738.

- [78] Ichikawa, M., Fukushima, T., Yokoyama, T., Kosugi, N. and Kuroda, H., *J. Phys. Chem.*, 1986, **90**, 1222.
- [79] Ichikawa, M., *Bull. Chem Soc. Japan*, 1978, **51** (8), 2268.
- [80] Bhasin, M.M., Bartley, W.J., Ellgen, P.C. and Wilson, T.P., *J. Catal.*, 1978, **54**, 120.
- [81] *Japan. Chem. Week*, November 1985, 21.
- [82] Yu-Hua, D., De-An, C. and Khi-Rui, T., *Appl. Catal.*, 1987, **35**, 77.
- [83] Quarderer, G.J. and Cochran, G.A., European Patent 0119609-A1 (to Dow Chemical Company).
- [84] Naumann, A.W. and Behan, A.S., U.S. Patent 4,243,553 (to Union Carbide Corporation).
- [85] Apesteguía, C.R., DeRites, B., Miseo, S. and Soled, S.L., *Catal. Lett.*, 1997, **44**, 1.
- [86] Hilmen, A.-M., Xu, M., Ginés, M.J.L. and Iglesia, E., *Appl. Catal. A: General*, 1998, **169**, 355.
- [87] Xu, M., Ginés, M.J.L., Hilmen, A.-M., Stephens, B.L. and Iglesia, E., *J. Catal.*, 1997, **171**, 130.
- [88] Roberts, G.W., Mawson, S., McCutcheon, M.S. and Lim, P.K., *Ab. Papers Am. Chem. Soc.*, 1992, **203**, Pt2, 83-PETR.
- [89] Tronconi, E., Forzatti, P., and Pasquon, I., *J. Catal.*, 1990, **124**, 376.
- [90] Courty, Ph., Arlie, J.P., Convers, A., Mikitenko, P. and Sugier, A., *Petrochemical Processing*, 1984, **63** (11), 105.
- [91] Supp, E., 78th *AIChE Spring National Meeting*, New Orleans, 1986.
- [92] Majocchi, L., Licetti, L., Beretta, A., Forzatti, P., Micheli, E. and Tagliabue, L., *Appl. Catal. A: General*, 1998, **166**, 395.

- [93] Quarderer, G.J., 78th AIChE Spring National Meeting, New Orleans, 1986.
- [94] Tronconi, E., Lietti, L., Forzatti, P. and Pasquon, I., *Appl. Catal.*, 1989, **47**, 317.
- [95] Schack, C.J., McNeil, M.A. and Rinker, R.G., *Appl. Catal.*, 1989, **50**, 247.
- [96] Liu, G., Willcox, D., Garland, M. and Kung, H.H., *J. Catal.*, 1985, **96**, 251.
- [97] Neophytides, S.G., Marchi, A.J. and Froment, G.F., *Appl. Catal. A: General*, 1992, **86**, 45.
- [98] Smith, K.J. and Anderson, R.B., *J. Catal.*, 1984, **85**, 428.
- [99] Sibilía, J.A., Dominguez, J.M., Herman, R.G. and Klier, K., *Prep. Fuel. Div. Amer. Chem. Soc.*, Philadelphia, 1984.
- [100] Frohlich, P.K. and Cryder, D.S., *Ind. Eng. Chem.*, 1930, **22**, 1051.
- [101] Graves, G.D., *Ind. Eng. Chem.*, 1931, **23**, 1381.
- [102] Morgan, G.T., Hardy, D.V.N. and Proctor, R.A., *J. Soc. Chem. Ind. Trans.*, 1932, **51**, 11.
- [103] Kung, H.H., *Catal. Rev.-Sci. Eng.*, 1980, **22** (2), 235.
- [104] Apai, G.R., Monnier, J.R. and Hanrahan, M.J., *J. Chem. Soc., Chem. Comm.*, 1984, 212.
- [105] Klier, K., Chatikavanij, V., Herman, R.G. and Simmons, G.W., *J. Catal.*, 1982, **74**, 343.
- [106] Chinchén, G.C., Denny, P.J., Parker, D.G., Spencer, M.S. and Whan, D.A., *Appl. Catal.*, 1987, **30**, 333.
- [107] Kagan, Yu.B., Rozowskii, A.Ya., Lin, G.I., Slivinskii, E.V., Loktev, S.M., Liberov, L.G. and Bashkirov, A.N., *Kinet. Katal.*, 1975, **16**, 810.

- [108] Kagan, Yu.B., Liberov, L.G., Slivinskii, E.V., Loktev, S.M., Lin, G.I., Rozovskii, A.Ya. and Bashkirov, A.N., *Dokl. Akad. Nauk. S.S.S.R., English Transl.*, 1975, **221**, 1093.
- [109] Kagan, Yu.B., Rozovskii, A.Ya., Liberov, L.G., Slivinskii, E.V., Lin, G.I., Loktev, S.M. and Bashkirov, A.N., *Dokl. Akad. Nauk. S.S.S.R., English Transl.*, 1975, **224**, 1081.
- [110] Chinchin, G.C. and Waugh, K.C., *J. Catal.*, 1986, **97**, 280.
- [111] Denise, B., Sneed, R.P.A., Beguin, B. and Cherifi, O., *Appl. Catal.*, 1987, **30**, 353.
- [112] Idriss, H., Hindermann, J.P., Kieffer, R., Kiennemann, A., Vallet, A., Chauvin, C., Lavalley, J.C. and Chaumette, P., *J. Mol. Catal.*, 1987, **42**, 205.
- [113] Chinchin, G.C., Spencer, M.S., Waugh, K.C. and Whan, D.A., *J. Chem. Soc., Faraday Trans. I*, 1987, **83** (7), 2193.
- [114] Jackson, S.D. and Brandreth, B.J., *J. Chem. Soc., Faraday Trans. I*, 1989, **85** (10), 3579.
- [115] Bowker, M., Hadden, R.A., Houghton, H., Hyland, J.N.K. and Waugh, K.C., *J. Catal.*, 1988, **109**, 263.
- [116] Bowker, M., Houghton, H. and Waugh, K.C., *J. Chem. Soc., Faraday Trans. I*, 1981, **77**, 3023.
- [117] Millar, G.J., Rochester, C.H., Howe, C. and Waugh, K.C., *Mol. Phys.*, 1992, **76** (4), 833.
- [118] Nakamura, I., Nakano, H., Fujitani, T., Uchijima, T. and Nakamura, J., *Surf. Sci.*, 1998, **402-404**, 92.
- [119] Waugh, K.C., *Catal. Today*, 1993, **18**, 147.

- [120] Rasmussen, P.B., Holmblad, P.M., Askgaard, T., Ovesen, C.V., Stoltze, P., Nørskov, J.K. and Chorkendorff, I., *Catal. Lett.*, 1994, **26**, 373.
- [121] Habraken, F.H.P.M., Mesters, C.M.A.M. and Bootsma, G.A., *Surf. Sci.*, 1980, **97**, 264.
- [122] Nunan, J.G., Bogdan, C.E., Klier, K., Smith, K.J., Young, C.-W. and Herman, R.G., *J. Catal.*, 1988, **113**, 410.
- [123] Nunan, J.G., Bogdan, C.E., Klier, K., Smith, K.J., Young, C.-W. and Herman, R.G., *J. Catal.*, 1989, **116**, 195.
- [124] Nunan, J.G., Herman, R.G. and Klier, K., *J. Catal.*, 1989, **116**, 222.
- [125] Elliott, D.J. and Pennella, F., *J. Catal.*, 1988, **114**, 90.
- [126] Calverley, E.M., PhD Dissertation, McMaster University, 1990.
- [127] Smith, K.J., Young, C.-W., Herman, R.G. and Klier, K., *Ind. Eng. Chem. Res.*, 1991, **30** (1), 61.
- [128] Klier, K., Herman, R.G., Himelfarb, P.B., Young, C.-W., Hou, S. and Marcos, J.A., *Stud. Surf. Sci. Catal.*, 1993, **75**, 1441.
- [129] Ginés, M.J.L. and Iglesia, E., *J. Catal.*, 1998, **176**, 155.
- [130] Slaa, J.C., van Ommen, J.G. and Ross, J.R.H., *Catal. Today*, 1992, **15**, 129.
- [131] Mazanec, T.J., *J. Catal.*, 1986, **98**, 115.
- [132] Riva, A., Trifirò, F., Vaccari, A., Busca, G., Mintchev, L., Sanfilippo, D. and Manzatti, W., *J. Chem. Soc., Faraday Trans. I*, 1987, **83** (21), 2213.
- [133] Beretta, A., Lietti, L., Tronconi, E., Forzatti, P. and Pasquon, I., *Ind. Eng. Chem. Res.*, 1996, **35**, 2154.
- [134] Lietti, L., Tronconi, E. and Forzatti, P., *J. Mol. Catal.*, 1988, **44**, 201.
- [135] Lietti, L., Botta, D., Forzatti, P., Mantica, E., Tronconi, E. and Pasquon, I., *J. Catal.*, 1988, **111**, 360.

- [136] Lietti, L., Tronconi, E. and Forzatti, P., *J. Mol. Catal.*, 1989, **55**, 43.
- [137] Lietti, L., Forzatti, P., Tronconi, E. and Pasquon, I., *J. Catal.*, 1990, **126**, 401.
- [138] Sachtler, J.W.A., Kool, J.M. and Ponec, V., *J. Catal.*, 1979, **56**, 284.
- [139] Bell, A.T., *Proc. 9th Int. Congr. on Catalysis* (Eds. Philips, M.J. and Ternan, M.), Calgary, 1988, **2**, 134.
- [140] Hindermann, J.P., Hutchings, G.J. and Kiennemann, A., *Catal. Rev.-Sci. Eng.*, 1993, **35** (1), 1.
- [141] Kobori, Y., Yamasaki, H., Naito, S., Onishi, T. and Tamaru, K., *J. Chem. Soc., Faraday Trans. I*, 1982, **78**, 1473.
- [142] Kiennemann, A., Diagne, C., Hindermann, J.P., Chaumette, P. and Courty, Ph., *Appl. Catal.*, 1989, **53**, 197.
- [143] Chu, W., Kieffer, R., Kiennemann, A. and Hindermann, J.P., *Appl. Catal. A: General*, 1995, **121**, 95.
- [144] Tronconi, E., Lietti, L., Groppi, G., Forzatti, P. and Pasquon, I., *J. Catal.*, 1992, **135**, 99.
- [145] Farrauto, R.J. and Bartholomew, C.H., "Fundamentals of Industrial Catalytic Processes", Blackie Academic and Professional, London, 1997, Chap. 5, p.383.
- [146] Ichikawa, M., Fukushima, T. and Shikakura, K., *Proc. 8th Int. Congr. on Catalysis*, Berlin, 1984, **2**, 69.
- [147] Santiesteban, J.G., Bogdan, C.E., Herman, R.G. and Klier, K., *Proc. 9th Int. Congr. on Catalysis* (Eds. Philips, M.J. and Ternan, M.), Calgary, 1988, **2**, 561.
- [148] Xu, M. and Iglesia, E., *Catal. Lett.*, 1998, **51**, 47.
- [149] Falter, W., PhD Dissertation, TH Aachen, Germany, 1988.
- [150] Fox, J.R., Pesa, F.A. and Curatolo, B.S., *J. Catal.*, 1984, **90**, 127.

- [151] Rhodes, C., Hutchings, G.J. and Ward, A.M., *Catal. Today*, 1995, **23**, 43.
- [152] Farrauto, R.J. and Bartholomew, C.H., "Fundamentals of Industrial Catalytic Processes", Blackie Academic and Professional, London, 1997, Chap.5, p.376.
- [153] Kung, M.C. and Kung, H.H., *Surf. Sci.*, 1981, **104**, 253.
- [154] Lloyd, L., Ridler, D.E. and Twigg, M.V., "Catalyst Handbook", Second Edition, (Ed. Twigg, M.V.), Wolfe Publishing Ltd., London, 1989, Chap. 6, p.293.
- [155] Farrauto, R.J. and Bartholomew, C.H., "Fundamentals of Industrial Catalytic Processes", Blackie Academic and Professional, London, 1997, Chap. 5, p.357.
- [156] Markina, M.I., Boreskov, G.K., Ivanoskii, F.P. and Lyudkovskaya, B.G., *Kinet. Katal.*, 1961, **2**, 867.
- [157] Tinkle, M. and Dumesic, J.A., *J. Catal.*, 1987, **103**, 65.
- [158] Vanden Bussche, K.M. and Froment, G.F., *J. Catal.*, 1996, **161**, 1.
- [159] Kul'kova, N.V. and Temkin, M.I., *Zh. Fiz. Chim.*, 1949, **23**, 695.
- [160] Boreskov, G.K., Yureva, T.M. and Sergeeva, A.S., *Kinet. Katal.*, 1970, **11**, 1476.
- [161] van Herwijnen, T. and de Jong, W.A., *J. Catal.*, 1980, **63**, 83.
- [162] van Herwijnen, T., Guzalski, R.T. and de Jong, W.A., *J. Catal.*, 1980, **63**, 94.
- [163] Goodman, D.R., "Catalyst Handbook", Second Edition, (Ed. Twigg, M.V.), Wolfe Publishing Ltd., London, 1989, Chap. 3, p.170.
- [164] Nakamura, J., Campbell, J.M. and Campbell, C.T., *J. Chem. Soc., Faraday Trans.*, 1990, **86** (15), 2725.
- [165] Nakamura, J., Rodriguez, J.A. and Campbell, C.T., *J. Phys. Condensed Matter*, 1989, **1** (B), SB149.

- [166] Ovesen, C.V., Stoltze, P., Nørskov, J.K. and Campbell, C.T., *J. Catal.*, 1992, **134**, 445.
- [167] Au, C.T. and Roberts, M.W., *J. Chim. Phys.*, 1981, **78**, 921.
- [168] Chinchén, G.C. and Spencer, M.S., *Catal. Today*, 1991, **10**, 293.
- [169] Ginés, M.J.L., Amadeo, N., Laborde, M. and Apesteguía, C.R., *Appl. Catal. A: General*, 1995, **131**, 283.
- [170] Dawood, T.A.K., Denise, B. and Sneed, R.P.A., *C₁ Mol. Chem.*, 1984, **1** (1), 49.
- [171] Matulewicz, E.R.A., PhD Dissertation, University of Amsterdam, 1984.
- [172] Lietti, L., Tronconi, E. and Forzatti, P., *J. Catal.*, 1992, **135**, 400.
- [173] Elliott, D.J. and Pennella, F., *J. Catal.*, 1989, **119**, 359.
- [174] Wells, A.F., "Structural Inorganic Chemistry", Third Edition, Oxford University Press, The Clarendon Press, 1962, p.548.
- [175] Cavani, F., Trifirò, F. and Vaccari, A., *Catal. Today*, 1991, **11**, 169.
- [176] Wells, A.F., "Structural Inorganic Chemistry", Third Edition, Oxford University Press, The Clarendon Press, 1962, p.551.
- [177] Miyata, S., Kumara, T., Hattori, H. and Tanabe, K., *Nippon Kagaku Zasshi.*, 1971, **92**, 514.
- [178] Pausch, I., Lohse H.H., Schürmann K. and Allmann R., *Clays and Clay minerals*, 1986, **34** (5), 507.
- [179] Aminoff, G. and Broomé, B., *Kungl. Sven. Vetensk. Handl.*, 1930, **9** (3), 5, 23.
- [180] Sato, T., Wakabayashi, T. and Shimada, M., *Ind. Eng. Chem., Prod. Des. Dev.*, 1986, **25**, 89.
- [181] Sato, T., Fujita, H., Endo, T., Shimada, M. and Tsunashima, A., *React. of Solids*, 1988, **5** (2&3), 219.

- [182] Brindley, G.W. and Kikkawa, S., *Clays and Clay Minerals*, 1980, **28**, 87.
- [183] Allmann, R., *Chimia*, 1970, **24**, 99.
- [184] Trifirò, F., Vaccari, A. and Del Piero, G., *Characterisation of Porous solids*, 1988, 571.
- [185] Brindley, G.W. and Kikkawa, S., *Amer. Min.*, 1979, **64**, 836.
- [186] Köckerling, M., Geismar, G., Henkel, G. and Nolting, H.-F., *J. Chem. Soc., Faraday Trans.*, 1997, **93** (3), 481.
- [187] Reichle, W.T., *Solid State Ionics*, 1986, **22**, 135.
- [188] Courty, Ph. and Marcilly, Ch., "Preparation of Catalysts III", (Eds. Poncelet, G., Grange, P. and Jacobs, J.A.), Elsevier, Amsterdam, 1983, p.485.
- [189] Taylor, H.F.W., *Miner. Mag.*, 1973, **39**, 377.
- [190] Drits, V.A., Sokolova, T.N., Sokolova, G.V. and Cherkashin, V.I., *Clays and Clay Minerals*, 1987, **35** (6), 401.
- [191] Bish, D.L., *Bull. Miner.*, 1980, **103**, 170.
- [192] Miyata, S., *Clays and Clay Minerals*, 1980, **28**, 50.
- [193] Miyata, S., *Clays and Clay Minerals*, 1983, **31**, 305.
- [194] Baker, J.E., Burch, R. and Golunski, S.E., *Appl. Catal.*, 1989, **53**, 279.
- [195] Reichle, W.T., Kang, S.Y. and Everhardt, D.S., *J. Catal.*, 1986, **101**, 352.
- [196] Miyata, S., *Clays and Clay Minerals*, 1975, **23**, 369.
- [197] Bish, D.L. and Livingstone, A., *Miner. Mag.*, 1981, **44**, 339.
- [198] Carlino, S., *Chemistry in Britain*, September 1997, p.59.
- [199] Höppener, R.H., Doesburg, E.B.M. and Scholten, J.J.F., *Appl. Catal.*, 1986, **25**, 109.
- [200] Herman, R.G., Bogdan, C.E., Kumler, P.L. and Nuzzkowski, D.M., *Mater. Chem. and Phys.*, 1993, **35**, 233.

- [201] Hutchings, G.J., King, F., Oboye, I.P. and Rochester, C.H., *Appl. Catal. A: General*, 1992, **83**, L7.
- [202] Bart, J.C.J. and Sneed, R.P.A., *Catal. Today*, 1987, **2**, 1.
- [203] Santiesteban, J.G., Bogdan, C.E., Herman, R.G. and Klier, K., "Catalysis", (Ed. Ward, J.W.), Elsevier Science, Amsterdam, 1988, p.745.
- [204] Farrauto, R.J. and Bartholomew, C.H., "Fundamentals of Industrial Catalytic Processes", Blackie Academic and Professional, London, 1997, p.266.
- [205] Carnell, P.J.H., "Catalyst Handbook", Second Edition, (Ed. Twigg, M.V.), Wolfe Publishing Ltd., London, 1989, Chap. 4, p.192.
- [206] Bridger, G.W. and Spencer, M.S., "Catalyst Handbook", Second Edition, (Ed. Twigg, M.V.), Wolfe Publishing Ltd., London, 1989, Chap. 9, p.461.
- [207] Stiles, A.B., Chen, F., Harrison, J.B., Hu, X.-D., Storm, D.A. and Yang, H.X., *Ind. Eng. Chem. Res.*, 1991, **30** (5), 811.
- [208] Richardson, J.T., "Principles of Catalytic Development", Plenum Press, New York, 1989, Chap. 8, p.185.
- [209] Farrauto, R.J. and Bartholomew, C.H., "Fundamentals of Industrial Catalytic Processes", Blackie Academic and Professional, London, 1997, Chap.5, p.283.
- [210] Dewing, J. and Davies, D.S., *Adv. Catal.*, 1975, **24**, 221.
- [211] Wrobel, G., Walter, P. and Beaufils, J.-P., *C. R. Acad. Sci., Series C*, 1976, **283**, 335.
- [212] Bond, G.C. and Namijo, S.N., *J. Catal.*, 1989, **118**, 507.
- [213] Sinfelt, J.H., Taylor, W.F. and Yates, D.J.C., *J. Phys. Chem.*, 1965, **69** (1), 95.
- [214] Narita, K., Takezawa, N., Kobayashi, H. and Toyoshima, I., *React. Kinet. Catal. Lett.*, 1982, **19**, 91.

- [215] Chinchén, G.C., Hay, C.M., Vandervell, H.D. and Waugh K.C., *J. Catal.*, 1987, **103**, 79.
- [216] Evans, J.W., Wainwright, M.S., Bridgewater, A.J. and Young, D.J., *Appl. Catal.*, 1983, **7**, 75.
- [217] Langmuir, I., *J. Am. Chem. Soc.*, 1918, **49**, 1631.
- [218] Brunauer, S., Emmett, P.H. and Teller, E.J., *J. Am. Chem. Soc.*, 1938, **60**, 309.
- [219] JCPDS Powder Diffraction File, File no. 01-0547, $\text{CuCr}_2\text{O}_7 \cdot 2\text{H}_2\text{O}$.
- [220] JCPDS Powder Diffraction File no. 29-0106, $(\text{NH}_4)_2\text{Al}(\text{OH})_2\text{CO}_3 \cdot y\text{H}_2\text{O}$.
- [221] JCPDS Powder Diffraction File no. 07-0324, $\text{Al}(\text{OH})_3$.
- [222] JCPDS Powder Diffraction File no. 18-0768, $\text{MgCO}_3 \cdot 2\text{H}_2\text{O}$.
- [223] JCPDS Powder Diffraction File no. 10-0399, $\text{Cu}_2\text{CO}_3(\text{OH})_2$.
- [224] JCPDS Powder Diffraction File no. 05-0661, CuO .
- [225] JCPDS Powder Diffraction File no. 22-1458, $\text{Na}_2\text{Cu}(\text{CO}_3)_2 \cdot 3\text{H}_2\text{O}$.
- [226] JCPDS Powder Diffraction File no. 36-0545, $\text{CuO} \cdot 3\text{H}_2\text{O}$.
- [227] JCPDS Powder Diffraction File no. 37-0630, $\text{Cu}_4\text{Al}_2(\text{OH})_{16}\text{CO}_3 \cdot 4\text{H}_2\text{O}$.
- [228] JCPDS Powder Diffraction File no. 19-1175, $\text{NaAlCO}_3(\text{OH})_2$.
- [229] JCPDS Powder Diffraction File no. 09-0185, CuAlO_2 .
- [230] JCPDS Powder Diffraction File no. 14-0191, $\text{Mg}_6\text{Al}_2\text{CO}_3(\text{OH})_{16}\text{CO}_3 \cdot 4\text{H}_2\text{O}$.
- [231] Capece, F.M., Di Castro, V., Furlani, C., Mattogno, G., Fragale, C., Gargano, M. and Rossi M., *J. Electron Spec. and Related Phenomena*, 1982, **27**, 19.
- [232] Johansson, L.E. and Lundin, S.T., *J. Am. Oil Chemists' Society*, 1979, **56**, 974.
- [233] Laine, J., Brito, J., Severino, F., Castro, G., Tacconi, P., Yunes, S. and Cruz, J., *Catal. Lett.*, 1990, **5**, 45.
- [234] Prasad, R., *Stud. Surf. Sci. Catal.*, 1993, **75**, 1747.

- [235] Auer, S.M., Gredig, S.V., Köppel, R.E. and Baiker, A., *J. Mol. Catal. A: Chemical*, 1999, **141**, 193.
- [236] Gusi, S., Pizzoli, F., Trifirò, F., Vaccari, A. and Del Piero, G., "Preparation of Catalysts IV", (Eds. Delmon, B., Grange, P., Jacobs, P.A. and Poncelet, G.), Elsevier, Amsterdam, 1987, p.753-763.
- [237] Pease, R.N. and Taylor, H.S., *Science*, 1921, **53**, 577.
- [238] John, J.L., *J. Phys. Chem.*, 1922, **33**, 1938.
- [239] Fornasari, G., Gusi, S., Trifirò, F., Vaccari, A. and Del Piero, G., *Het. Cat.*, 1987, **1**, 241.
- [240] Richardson, J.T., "Principles of Catalytic Development", Plenum Press, New York, 1989, Chap. 8, p.104.
- [241] Nunan, J.G., Himelfarb, P.B., Herman, R.G., Klier, K., Bogdan, C.E. and Simmons, G.W., *Inorg. Chem.*, 1989, **28**, 3868.
- [242] Meyn, M., Beneke, K. and Lagaly, C., *Inorg. Chem.*, 1990, **29**, 5201.
- [243] Sheffer, G.R. and King, T.S., *J. Catal.*, 1989, **116**, 488.
- [244] Villa, P.L., Del Piero, G., Cipelli, A., Lietti, L. and Pasquon, I., *Appl. Catal.*, 1986, **26**, 161.
- [245] Fornasari, G., Gusi, S., La Torretta, T.M.G., Trifirò, F. and Vaccari, A., "Catalysis and Automotive Pollution", (Eds. Crucq, A. And Frennet, A.), Elsevier, Amsterdam, 1987, p.469.
- [246] Chu, P.-J., Gerstein, B.C., Sheffer, G.R. and King, T.S., *J. Catal.*, 1989, **115**, 194.
- [247] Robinson, W.M.A. and Mol, J.C., *Appl. Catal.*, 1988, **44**, 165.
- [248] Khasin, A.V., Simentsova, I.I. and Yurieva, T.M., *React. Kinet. Catal. Lett.*, 1994, **52**, 113.

- [249] Barber, M., Vickerman, J.C. and Wolstenholme, J., *J. Chem. Soc., Faraday Disc.*, 1976, **72**, 40.
- [250] Bardet, R., Thivolle-Cazat, J. and Trambouze, Y., *C. R. Hebd. Seances Acad. Sci. Ser. 2*, 1984, **299** (8), 423.
- [251] Burch, R., Chappell, R.J. and Golunski, S.E., *J. Chem. Soc., Faraday Trans. I*, 1989, **85** (10), 3569.
- [252] Driessen, J.M., Poels, E.K., Hindermann, J.P. and Ponec, V., *J. Catal.*, 1988, **112**, 34.
- [253] Lee, J.S., Lee, K.H., Lee, S.Y. and Kim, Y.G., *J. Catal.*, 1993, **144**, 414.
- [254] Clausen, B.S., Lengeler, B. and Rasmussen, B.S., *J. Phys. Chem.*, 1985, **89** (11), 2319.
- [255] Robbins, J.L., Iglesia, E., Kelkar, C.P. and DeRites, B., *Catal. Lett.*, 1991, **10**, 1.
- [256] Denise, B., Sneed, R.P.A. and Hamon, C., *J. Mol. Catal.*, 1982, **17**, 359.
- [257] McNeil, M.A., Schack, C.J. and Rinker, R.G., *Appl. Catal.*, 1989, **50**, 265.
- [258] Gopal, P.G., Schneider, R.L. and Watters, K.L., *J. Catal.*, 1987, **105** (2), 366.
- [259] Calverley, E.M. and Smith, K.J., *Ind. Eng. Chem. Res.*, 1992, **31** (3), 792.
- [260] Kiennemann, A., Boujana, S., Diagne, C. and Chaumette, P., *Stud. Surf. Sci. Catal.*, 1993, **73**, 1479.
- [261] Edwards, J.F. and Schrader, G.L., *J. Catal.*, 1985, **94** (1), 175.
- [262] Wachs, I.E. and Madix, R.J., *Surf. Sci.*, 1978, **76**, 531.
- [263] Waugh, K.C., *Catal. Today*, 1992, **15**, 51.
- [264] Tsuji, H., Yagi, F., Hattori, H. and Kita, H., *J. Catal.*, 1994, **148** (2), 759.

- [265] Ueda, W., Ohshida, T., Kuwabara, T. and Morikawa, Y.J., *Catal., Lett.*, 1992, **12** (1-3), 97.

10 Appendix

10.1 Atomic Absorption Spectroscopy

The quantity of metal co-precipitation was calculated by the following manner. Assuming copper is present as Cu^{2+} , chromium, Cr^{3+} , aluminium, Al^{3+} and magnesium, Mg^{2+} .

e.g. CuO/MgO (60/40)

$$\text{m.w. CuO} = 0.6 \times (63.546 + 15.996) = 47.725 +$$

$$\text{m.w. MgO} = 0.5 \times (23.11 + 15.996) = \underline{15.642}$$

$$\text{m.w.} = \underline{63.367}$$

From the cumulative molecular weight, the weight percentage of each element can be calculated. The correct dilution from these values gives a concentration within the linear part of the element dependent calibration curve (see introduction section 3.4.4).

10.2 Nitrous Oxide Chemisorption (Derivation of Copper density constant)

The copper density constant is derived in the following manner.

$$N_s = \frac{\text{particles area } (\pi d^2)}{\text{area per Cu site } (0.068 \text{ nm}^2 \text{ per site})}$$

$$N_T = \text{Volume} \times \text{Density} \times \text{A.W.} \times N_A$$
$$N_T = \frac{1}{6} \pi d^3 (\text{nm}^3) \times \frac{8.96 \times 10^{-21} \text{ g}}{1 \text{ nm}^3} \times \frac{1 \text{ mole}}{63.546 \text{ g}} \times \frac{6.023 \times 10^{23} \text{ atoms}}{1 \text{ mole}} = 14.14 \pi d^3 \text{ atoms}$$

$$\% \text{ Dispersion} = \frac{N_s}{N_T} \times 100 = \frac{\pi d^2}{0.068} \times \frac{1}{14.14 \pi d^3} \times 100 = \frac{100 \pi d^2}{0.9629 \pi d^3} = \frac{104}{d}$$

10.3 Errors from Results

The Differential Thermogravimetric Analysis results have potential errors of $\pm 1\%$,

which is due to a heat lag when initially increasing the temperature. Atomic Absorption spectroscopy results are correct to within $\pm 2\%$ as the experiments were conducted in duplicate. The imposed error is due to the inherent problem of sensitivity from the detection component of the spectrometer. Temperature Programmed Reduction and Nitrous oxide chemisorption experiments have been conducted in triplicate, which increases the accuracy of the results presented to within $\pm 2\%$ and decreases the error in the temperature and hydrogen consumption values, dispersions, particle sizes and copper surface areas. This will be due to either unfinished reduction or incomplete nitrous oxide adsorption. Elemental analysis results were conducted twice unless otherwise stated, thus reducing the possible discrepancy to $\pm 2\%$, which will be from a heterogeneous sample. The Titrimetry results were conducted in triplicate, limiting the error to $\pm 2\%$ arising from errors with sample injection.

X-ray and BET surface area measurements were conducted once unless the sample was anomalous and gave an ambiguous result.

Microreactor experiments were conducted once only but the tabulated values represent 3 or more results under those specified conditions, enabling the error on these values to be reduced to $\pm 2\%$. The figures and tables shown represent only a proportion of the quantity of experiments conducted. The main problem with microreactor experiments is the inherent problem of GC detection.

10.4 Conversion of Units

Le Système International d' Unités (SI units) are used throughout, but other units are retained where appropriate for convenience. The conversion factors are listed below:-

$$1 \text{ eV} = 1.602 \times 10^{-19} \text{ J}$$

$$1 \text{ atm} = 101.325 \text{ kPa} = 14.696 \text{ lb in}^{-2}$$

$$n \text{ barg} = 100 \text{ kPa} + (n \times 100 \text{ kPa})$$

$$1 \text{ \AA} = 10^{-10} \text{ m}$$

$$1 \text{ ''} = 2.54 \text{ cm}$$